

# EMPIRE-3.2 Malta (rev.1)

## modular system for nuclear reaction calculations and nuclear data evaluation

### User's Manual

M. Herman<sup>1</sup>, R. Capote<sup>2</sup>, M. Sin<sup>3</sup>, A. Trkov<sup>4</sup>, B.V. Carlson<sup>5</sup>,  
P. Obložinský<sup>6</sup>, C.M. Mattoon<sup>7</sup>, H. Wienke<sup>†</sup>, S. Hoblit<sup>1</sup>,  
Young-Sik Cho<sup>8</sup>, G.P.A. Nobre<sup>1</sup>, V.A. Plujko<sup>9</sup>, V. Zerkín<sup>2</sup>

1) NNDC, Brookhaven National Laboratory, Upton, USA

e-mail: mwherman@bnl.gov

2) NAPC–Nuclear Data Section, International Atomic Energy Agency, Vienna, Austria

e-mail: r.capotenoy@iaea.org

3) University of Bucharest, Bucharest, Romania

4) Jožef Stefan Institute, Ljubljana, Slovenia

5) ITA/Centro Tecnico Aeroespacial, Sao Jose dos Campos, Brazil

6) Bratislava, Slovakia

7) Lawrence Livermore National Laboratory, Livermore, USA

8) Korea Atomic Energy Research Institute, Daejeon, South Korea

9) Taras Shevchenko National University, Kiev, Ukraine

*To Harm Wienke in memoriam*

August 18, 2015

EMPIRE is a modular system of nuclear reaction codes, comprising various nuclear models, and designed for calculations over a broad range of energies and incident particles. The system can be used for theoretical investigations of nuclear reactions as well as for nuclear data evaluation work. Photons, nucleons, deuterons, tritons, helions ( $^3\text{He}$ ),  $\alpha$ 's, and light or heavy ions can be selected as projectiles. The energy range starts just above the resonance region in the case of a neutron projectile, and extends up to few hundred MeV for heavy ion induced reactions. The code accounts for the major nuclear reaction models, such as optical model, Coupled Channels and DWBA (ECIS06 and OPTMAN), Multi-step Direct (ORION + TRISTAN), NVWY Multi-step Compound, exciton model (PCROSS), hybrid Monte Carlo simulation (DDHMS), and the full featured Hauser-Feshbach model including width fluctuations and the optical model for fission. Heavy ion fusion cross section can be calculated within the simplified coupled channels approach (CCFUS). A comprehensive library of input parameters based on the RIPL-3 library covers nuclear masses, optical model parameters, ground state deformations, discrete levels and decay schemes, level densities, fission barriers, and  $\gamma$ -ray strength functions. Effects of the dynamic deformation of a fast rotating nucleus can be taken into account in the calculations (BARFIT, MOMFIT).

The results can be converted into the ENDF-6 format using the accompanying EMPEND code. Modules of the ENDF Utility Codes and the ENDF Pre-Processing codes are applied for ENDF file verification. The package contains the full EXFOR library of experimental data in computational format C4 that are automatically retrieved during the calculations.

EMPIRE contains the resonance module that retrieves data from the electronic version of the Atlas of Neutron Resonances by Mughabghab (not provided with the EMPIRE distribution), to produce resonance section and related covariances for the ENDF-6 formatted files. EMPIRE can be used to determine covariances of the calculated data using either sensitivity matrices along with the KALMAN code or employing Monte Carlo approach to produce model generated covariances. In both cases experimental data can be taken into account, either directly (KALMAN) or by feeding the EMPIRE calculated Monte Carlo modelling covariance as a prior to the least square fitting GANDR system.

Publication quality graphs can be obtained using the powerful and flexible plotting package ZVView. Interactive plots with ZVView comparing experimental results with calculations can be produced with ENDVER modules.

The backbone of the EMPIRE system are bash-shell UNIX scripts that provide for seamless console operation of EMPIRE on Linux, Mac OS X, and Microsoft Windows with GNU gfortran compiler installed. Additionally, the graphical interface, provides for an easy operation of the system on Linux, Mac OS X and virtual Linux machines running on Microsoft Windows.

# Contents

<b>Introduction</b>	<b>7</b>
<b>I NUCLEAR REACTION MODELS</b>	<b>11</b>
<b>1 Direct reactions and fusion cross sections</b>	<b>13</b>
1.1 Fusion/reaction cross section . . . . .	13
1.2 Coupled-Channels Codes . . . . .	15
1.2.1 Coupled-Channels Code ECIS . . . . .	15
1.2.2 Coupled-Channels Code OPTMAN . . . . .	15
1.2.3 Input of coupled-channels Codes ECIS and OPTMAN . . . . .	16
1.3 Photoabsorption . . . . .	18
<b>2 Quantum-mechanical preequilibrium models</b>	<b>21</b>
2.1 Multi-step Direct . . . . .	21
2.1.1 Outline of the theory . . . . .	21
2.1.2 Notes on RPA-Description of Transition Strength Functions . . . .	26
2.1.3 Implementation of ORION and TRISTAN codes in EMPIRE . . . .	28
2.2 Multi-step Compound . . . . .	29
2.2.1 Conditional level densities . . . . .	31
2.2.2 Gamma-emission in Multi-step Compound . . . . .	32
2.3 Coupling between MSC and MSD . . . . .	35
<b>3 Phenomenological preequilibrium models</b>	<b>39</b>
3.1 Exciton model (PCROSS code) . . . . .	39
3.2 Monte Carlo Preequilibrium (DDHMS code) . . . . .	43
3.3 Compatibility of preequilibrium models . . . . .	47
<b>4 Compound nucleus model</b>	<b>51</b>
4.1 Compound Nucleus . . . . .	51
4.1.1 Width fluctuation correction . . . . .	52
4.2 Level densities . . . . .	53
4.2.1 Basic relations of Fermi-Gas Model . . . . .	54
4.2.2 Gilbert-Cameron Model . . . . .	55

4.2.3	Generalized Superfluid Model . . . . .	56
4.2.4	Enhanced Generalized Superfluid Model . . . . .	60
4.2.5	Microscopic combinatorial level densities (HFBM) . . . . .	66
4.3	Gamma-ray emission . . . . .	68
4.3.1	Gamma-ray strength function . . . . .	69
4.3.2	Giant Multipole Resonance parameters . . . . .	71
4.4	Fission . . . . .	73
4.4.1	Optical model for fission (FISSHI=0) . . . . .	74
4.4.2	Sierk model for fission (FISSHI=1) . . . . .	90
4.4.3	Prompt Fission Neutrons . . . . .	92
4.5	Nuclear astrophysics S-factor . . . . .	99
<b>II</b>	<b>NUCLEAR DATA EVALUATION</b>	<b>101</b>
<b>5</b>	<b>Resonance module</b>	<b>105</b>
5.1	Architecture of the module . . . . .	105
5.2	GUI control panel . . . . .	106
<b>6</b>	<b>Determination of covariances</b>	<b>111</b>
6.1	EMPIRE-KALMAN approach . . . . .	112
6.1.1	Sensitivity calculation . . . . .	112
6.2	EMPIRE-MC approach . . . . .	114
6.3	EMPIRE resonance covariance module . . . . .	115
6.4	Inclusion of experimental data . . . . .	116
6.5	Conclusions . . . . .	117
<b>7</b>	<b>ENDF formatting</b>	<b>119</b>
7.1	Spectra of recoils . . . . .	119
7.2	Exclusive spectra . . . . .	121
7.3	EMPEND code . . . . .	125
7.4	EMPEND Input instructions . . . . .	127
<b>III</b>	<b>STRUCTURE OF EMPIRE CODE</b>	<b>129</b>
<b>8</b>	<b>Code</b>	<b>131</b>
8.1	Directory structure . . . . .	131
8.2	Installation . . . . .	134
8.3	Array dimensions . . . . .	136
8.4	Parameter libraries . . . . .	137
8.5	List of EMPIRE modules . . . . .	139
8.6	Flow of calculations . . . . .	144
8.7	empy: python modules for EMPIRE . . . . .	146

8.8	Executing EMPIRE . . . . .	146
8.8.1	“runE” sequence (Run EMPIRE) . . . . .	147
8.8.2	“format” sequence . . . . .	147
8.8.3	“verify” sequence . . . . .	148
8.8.4	“process” sequence . . . . .	148
8.8.5	“run” sequence . . . . .	149
8.8.6	Script mode . . . . .	149
8.8.7	GUI mode . . . . .	157
8.9	Input/Output files . . . . .	163
8.9.1	*.inp (INPUT.DAT; main input) . . . . .	163
8.9.2	*-inp.fis (FISSION.INP) . . . . .	166
8.9.3	*.lst (LIST.DAT; lengthy output) . . . . .	174
8.9.4	*.out (OUTPUT.DAT) . . . . .	176
8.9.5	*.fus (FUSION) . . . . .	176
8.9.6	*.lev (LEVELS) . . . . .	176
8.9.7	*-lev.col (TARGET_COLL.DAT) . . . . .	176
8.9.8	*-fiss.out (FISSION.OUT) . . . . .	183
8.9.9	*.xcs (XS.OUT) . . . . .	183
8.9.10	*-preq.xcs (PREQ_XS.OUT) . . . . .	183
8.9.11	*-fiss.xcs (FISS_XS.OUT) . . . . .	183
8.9.12	*-omp.ripl (OMPAR.RIPL) . . . . .	184
8.9.13	*-omp.dir (OMPAR.DIR) . . . . .	184
8.9.14	*.endf (OUTPUT.ENDF) . . . . .	184
8.9.15	*-s.endf . . . . .	184
8.9.16	*-mat.sen (SENSITIVITY.MATRIX) . . . . .	184
8.9.17	*.exf (EXFOR.DAT) . . . . .	185
8.9.18	*.c4 (empire/util/x4toc4/c4.dat) . . . . .	186
8.9.19	*.ps (empire//util/plotc4/plot.ps) . . . . .	187
8.9.20	*-cum.ps . . . . .	187
8.9.21	*-ompfit.lst (FIT.OUT) . . . . .	187
8.9.22	*.x42c4.lst (empire/util/x4toc4/x4toc4.lst) . . . . .	187
8.9.23	*.x42c4_errs (empire/util/x4toc4/errors) . . . . .	187
8.9.24	Log files . . . . .	187
8.10	Plotting capabilities . . . . .	188
8.10.1	ZVView . . . . .	188
8.11	Plans for further development . . . . .	190

## IV WORKING NOTES 193

### 9 Avoiding problems 195

### 10 Fitting discrete levels 197

<b>11 Handling OM potentials</b>	<b>199</b>
11.1 DWBA with RIPL OMP . . . . .	200
11.2 Coupled-Channels with RIPL spherical OMP . . . . .	201
11.3 Coupled-Channels with RIPL CC OMP for inelastic scattering . . . . .	201
11.4 Complete Coupled-Channels with RIPL CC OMP for inelastic scattering . . . . .	202
<b>12 Effects of parameter modifications</b>	<b>203</b>
12.1 Fusion . . . . .	209
12.2 Coupled-Channels (ECIS) . . . . .	210
12.3 Multi-step Direct . . . . .	211
12.4 Multi-step Compound . . . . .	211
12.5 Level densities . . . . .	212
12.6 Fission . . . . .	214
12.7 GDR parameters ( $\gamma$ -ray strength functions) . . . . .	215
12.8 Avoiding unreasonably low uncertainties . . . . .	216
<b>13 Parameter fitting</b>	<b>219</b>
13.1 Fitting Optical Model Parameters . . . . .	219
13.2 Using Kalman filter for parameter fitting . . . . .	220
13.2.1 Calculation of sensitivity matrices . . . . .	221
13.2.2 Kalman script . . . . .	223
13.2.3 Fitting example: $^{235}\text{U}$ . . . . .	229
13.3 Fitting $\bar{\mu}$ and $\bar{\nu}$ in Empire with Kalman . . . . .	230
13.3.1 $\bar{\mu}$ (Mubar) . . . . .	231
13.3.2 $\bar{\nu}$ (Nubar) . . . . .	233
<b>Acknowledgments</b>	<b>245</b>
<b>A EMPIRE optional input keywords</b>	<b>255</b>
<b>B Description of test cases</b>	<b>279</b>
<b>C ChangeLog</b>	<b>281</b>

# Introduction

The first version of EMPIRE code was released in 1980. This code originally contained the Hauser-Feshbach theory and the classical HYBRID model to account for the preequilibrium effects. The width fluctuation correction was implemented in terms of the HRTW approach [1, 2]. Since that time, the code has been continuously developed. Adding the FKK Multi-step Compound mechanism [3] lead to the EMPIRE-MS version. Subsequently, the NVWY formulation of the Multi-step Compound mechanism [4] was implemented in the HMS-EMPIRE. This version also included combinatorial calculations of particle-hole level densities. In addition, a version for heavy ion induced reactions (EMPIRE HI) was developed.

EMPIRE-2 was a totally new release of the code. Contrary to the preceding developments, which largely consisted in adding new features without changing the structure of the code, this version was rewritten from scratch, using different programming concepts. Taking advantage of the relaxed memory limitations, all intermediate files were eliminated, which together with careful coding of the most crucial parts of the code, increased the speed of the program by a factor of 20. The new code is projected to be general and flexible, and can be applied to the calculation of neutron capture in the keV region, as well as for heavy ion (HI) induced reactions at several hundreds of MeV. All dimensions in the main code are set up through the parameter statements contained in the separate file, which is included wherever appropriate, making any adjustment of the code to the actual problem and/or computer straightforward. The code has a modular structure. Each module performs a well defined task and communicates with other modules through a set of global COMMONS which are included in most of the subroutines. This assures access to all the resources throughout the code, and facilitates adding new features and mechanisms.

The current version EMPIRE-3.2, named Malta after the Napoleon's capture of the island on the way to Egypt, follows the Rivoli version released in 2011. Although a minor release, it features a number of significant improvements such as: (i) prompt fission neutron spectra (PFNS) including automatic adjustment to experimental data, (ii) plotting of PFNS,  $\mu$ -bars, and  $\nu$ -bars, (iii) anisotropic angular distributions for compound elastic and inelastics, (iv) simulation of the Engelbrecht-Weidenmüller transformation, and (v) new IO subroutines for manipulating the ENDF-6 formatted files. In addition, this manual contains an extended description of parameter fitting and covariance generation using EMPIRE coupled with the KALMAN code. As usual, the stability of the code has been further improved and a number of deficiencies were fixed.

EMPIRE makes use of several codes, written by different authors, which were converted into subroutines and adapted for the present use. In most cases, the modifications concerned input/output interface and never affected the physical model contained in the original source. The following codes are incorporated in the present version of EMPIRE:

<b>ECIS06</b>	Coupled-Channels and DWBA code by J. Raynal [5, 6],
<b>OPTMAN</b>	Coupled-Channels code with soft-rotor capability by Soukhovitskii <i>et al.</i> [7, 8, 9]
<b>CCFUS</b>	simplified Coupled-Channels calculation of HI fusion cross section by C.H. Dasso and S. Landowne [10],
<b>ORION</b>	TUL [11] approach to Multi-step Direct by H. Lenske [12],
<b>TRISTAN</b>	TUL [11] approach to Multi-step Direct by H. Lenske [12],
<b>DDHMS</b>	Monte Carlo simulation of the preequilibrium decay by M.B. Chadwick [13]
<b>BARMOM</b>	fission barriers and moments of inertia by A. Sierk [14].

The reader is referred to the original papers for a more detailed description of these incorporated codes. Furthermore, the package includes the following stand-alone codes:

<b>EMPEND</b>	converts EMPIRE results into ENDF-6 format (written by A. Trkov),
<b>ENDRES</b>	merges existing resonance parameters into ENDF-6 formatted file produced by EMPEND (written by A. Trkov),
<b>X4TOC4</b>	converts experimental data retrieved from EXFOR into computational C4 format (written by D.E. Cullen) [15],
<b>C4SORT</b>	sorts experimental data in the computational C4 format file by MAT/MF/MT numbers and incident energy (written by A.Trkov) [16],
<b>FIXUP</b>	used to reconstruct redundant cross sections MT=4, 103, and 107 (Program of the Pre-Pro series, written by D.E. Cullen) [15],
<b>LEGEND</b>	reconstructs tabular linearly interpolable angular distributions from ENDF data in different format representations (Program of the Pre-Pro series, written by D.E. Cullen) [15],
<b>LSTTAB</b>	tabulates ENDF and EXFOR data in PLOTTAB format (module of ENDVER package, written by A.Trkov) [16],
<b>SIXTAB</b>	converts ENDF file MF6 to Law 7 representation (module of ENDVER package, written by A.Trkov) [16],



<b>PLOT4</b>	plots comparison between EMPIRE results and EXFOR data (written by D.E. Cullen and A. Trkov) [16],
<b>CHECKR</b>	performs format checking of the ENDF-6 formatted file (ENDF Utility codes, written by Ch. Dunford)
<b>FIZCON</b>	performs physics check of the ENDF-6 formatted file (ENDF Utility codes, written by Ch. Dunford)
<b>PSYCHE</b>	performs more physics checking of the ENDF-6 formatted file (ENDF Utility codes, written by Ch. Dunford)
<b>LINEAR</b>	converts MF=3 (cross sections) in an ENDF file into a linear-linear interpolable form (Program of the Pre-Pro series, written by D.E. Cullen) [15]
<b>PLTLST</b>	prepares a list of data types in the EXFOR data-base that can be compared to quantities in the ENDF files (module of ENDVER package, written by A.Trkov) [16],
<b>RECENT</b>	reconstructs the resonance contribution to the cross sections in an ENDF file into linearly interpolable form (Program of the Pre-Pro series, written by D.E. Cullen) [15]
<b>SIGMA1</b>	Doppler broadens neutron induced cross sections in an ENDF file (Program of the Pre-Pro series, written by D.E. Cullen) [15]
<b>STANEF</b>	Standardizes ENDF-6 formatted file (ENDF Utility codes, written by Ch. Dunford)
<b>zvvdxd</b>	Produces plots of angular distributions, spectra and double differential cross sections using ZVView package (written by V. Zerkin).
<b>c4zvd</b>	ZVView plotting package by V. Zerkin [17].
<b>Calc-Cov</b>	Codes and scripts for calculating cross section covariances using Monte Carlo (parameter uncertainties must be specified in the input file).
<b>cs2zvd</b>	Produces zvd plots of cross sections directly from EMPIRE output without ENDF-6 formatting.
<b>endf33zvd</b>	Produces three-dimensional zvd plots of covariances (written by V. Zerkin).
<b>IO</b>	Set of f90 modules for reading and writing ENDF-6 files (written by S. Hoblit).

<b>KALMAN</b>	KALMAN code for generating covariances and fitting experimental data (written by T. Kawano).
<b>KERCEN</b>	C++ code for generating covariances in the resonance region using kernel approximation method to be executed as a standalone code (written by Young-Sik Cho).
<b>MRGMAT</b>	Code for merging ENDF-6 files for different materials into a single file.
<b>PLTSENMAT</b>	Produces zvd plot of cross section sensitivity to model parameters (written by G. Nobre).
<b>RESONANCE</b>	Resonance module for extracting data from the Atlas of Neutron Resonances and producing ENDF-6 formatted resonance file with covariances (written by Young-Sik Cho).
<b>STAN</b>	Modern f90 replacement for STANEF (written by S. Hoblit).

This manual consists of three parts: (i) outline of the nuclear reaction models used in the calculations, (ii) description of the EMPIRE code structure, parameter libraries, input instructions and outputs, and (iii) working notes containing practical suggestions that should be helpful for judicious execution of the code, choosing proper reaction models, avoiding possible errors and correct interpretation of the results.

To facilitate further reading we anticipate our discussion by providing a brief description of the EMPIRE code operation and naming convention that will be used through the manual. The code depends on the naming scheme which has to be strictly preserved. The work is organized by projects; each project has a user assigned name (e.g., [Fe56-project](#)), which forms a root of all the project files (e.g., [Fe56-project.inp](#), [Fe56-project-lev.col](#), [Fe56-project.lst](#), ...). All project files are located in the same working directory selected by the user.

This manual is divided in four Parts. The Part **I** outlines nuclear reaction models and the corresponding physics covered by the code. Tools needed for nuclear data evaluation that include resonance evaluation and generation of covariance matrices are described in Part **II**. Both, the structure of the code and the input/output files are described in Part **III**. Use of the code, the role of input parameters, and a few typical examples of input files are discussed in Part **IV**. Finally, the input description is given in Appendix A.

**Part I**

**NUCLEAR REACTION MODELS**



# Chapter 1

## Direct reactions and fusion cross sections

### 1.1 Fusion/reaction cross section

The reaction cross section is calculated in terms of transmission coefficients  $T_l^a(\epsilon)$  using the expression

$$\sigma_a(U, J, \pi) = \frac{\pi}{k^2} \frac{(2J+1)}{(2I+1)(2i+1)} \sum_{S=|I-i|}^{I+i} \sum_{l=|J-S|}^{J+S} f(l, \pi) T_l^a(\epsilon), \quad (1.1)$$

where  $k$  is the wave number of relative motion,  $i, I, J$ , and  $S$  indicate projectile, target, compound nucleus, and channel spin, respectively, and  $l$  is the orbital angular momentum of the projectile  $a$ . The function  $f(l, \pi)$  ensures parity conservation. It is unity if  $p * P * (-1)^l = \pi$  and zero otherwise. Here  $p, P$ , and  $\pi$  are projectile, target, and compound nucleus parities and  $\epsilon$  and  $U$  stand for the projectile and compound nucleus energy.

For projectiles with mass numbers  $A < 5$  the transmission coefficients entering Eq. 1.1 are calculated using optical model routines ECIS06 [5, 6] and OPTMAN [7, 8] unless an external file FUSION exists. In the latter case, the spin distribution of the Compound Nucleus is constructed from this file.

The heavy ion fusion cross section is calculated using Eq. 1.1 with transmission coefficients determined according to one of the following methods:

- (i) Simplified Coupled-Channels approach [10] (CCFUS code). Inelastic excitations and transfer reaction channels are treated as independent modes which couple to the initial ground state. The corresponding wave equations are approximately uncoupled by diagonalizing the interaction at the barrier. The total transmission probability is then obtained by summing over the distribution of transmission probabilities for the eigenbarriers, with weights given by the overlap of the initial state with the eigenchannels. This is a default option. It takes into account coupling of the excited

collective states in the target and projectile. A detailed description of the method can be found in the original reference [10].

- (ii) Distributed fusion-barrier model [18]. This method accounts for the effective lowering of the one-dimensional fusion barrier by allowing for the additional dimension and assuming that the barrier distribution in the added dimension can be represented by a truncated Gaussian. Thus the fusion barrier distribution  $f(B')$  can be characterized by the mean energy  $B$ , the standard deviation  $\sigma_B$ , and the truncation parameter  $t$ , and is written as

$$f(B') = n_0 \exp\left(\frac{B - B'}{2\sigma_B^2}\right)^2 \quad (1.2)$$

for  $|B - B'| < t\sigma_B$  and  $f(B') = 0$  otherwise. The parameter  $t$  defines the lowest possible value of the fusion barrier and  $n_0$  is the normalization factor ensuring that the integral of Eq. 1.2 is 1. The fusion probability for a given angular momentum  $l$  is given by a convolution of the barrier distribution  $f(B')$  and the transmission coefficient  $T_l(E - B')$

$$p(E, l) = \int_{-\infty}^{\infty} f(B') T_l(E - B') dB'. \quad (1.3)$$

The transmission coefficient in the Hill-Wheeler approach [19] reads

$$T_l(E - B') = \{1 + \exp[-2\pi(E - B' - E_{rot})/(\hbar\omega)]\}^{-1}, \quad (1.4)$$

with  $E_{rot}$  being rotation energy at angular momentum  $l$ . The distributed fusion-barrier option in EMPIRE allows for the extra-push energy that can be specified in the input and added to the fusion barrier. The latter, if not specified in the input, is by default calculated using BAR subroutine of CCFUS (see above).

- (iii) Fusion cross sections for each  $l$  read from the external file *FUSION* (\*.fus). The code converts them into transmission coefficients to be used in Eq. 1.1. The existence of the *FUSION* (\*.fus) file overrides all input dispositions regarding fusion determination. NOTE: *FUSION* (\*.fus) file refers to a single incident energy, therefore only one energy at a time can be calculated.
- (iv) Total fusion cross section specified in input (single incident energy only).
- (v) Critical angular momentum  $l_{cr}$  for compound nucleus formation specified in input (single incident energy only).

In the latter two cases the transmission coefficients are assumed to be of the form

$$T_l^a(\epsilon) = \frac{1}{1 + \exp(-\frac{l_{cr} - l}{\delta l})}, \quad (1.5)$$

where  $\delta l$  is an input parameter. If the total fusion cross section is specified in the input, then the code adjusts  $l_{cr}$  in order to reproduce the requested value.

## 1.2 Coupled-Channels Codes

### 1.2.1 Coupled-Channels Code ECIS

ECIS [5, 6] is a well known and highly respected code for calculations within the generalized optical model and Coupled-Channels model (CC). These are important for modeling reactions on deformed nuclei and, in particular, for the correct description of a strong population of collective discrete levels in the inelastic scattering. ECIS-95 was added to EMPIRE as its new extensive module by R. Capote in February 2001 and replaced with the ECIS06 version in EMPIRE-3.1. Symmetric rotational, vibrational-rotational and harmonic-vibrational CC modes are available. The implementation features automatic preparation of the ECIS06 input. It uses the RIPL [20] optical model segment and resorts to the RIPL discrete level schemes and to the deformation parameters (quadrupole deformations  $\beta_2$ ) only if these are not included in the optical model parameter set available from RIPL. Since EMPIRE has no table of vibrational (dynamical) deformations, these are defined in a somewhat ad hoc manner as 0.15 for quadrupole and 0.05 for octupole vibrations.

Calculations can be performed for the majority of deformed nuclei including rotational and vibrational, even-even and even-A with integer spins, as well as odd-A with half-integer spins. Vibrational even-even nuclei and even-A are also covered. The only exceptions are vibrational odd-A nuclei. In these cases automatic construction of the file with collective levels is not possible and the user must prepare the corresponding file manually.

### 1.2.2 Coupled-Channels Code OPTMAN

For more than twenty years, an original coupled-channels optical model code OPTMAN has been developed at Joint Institute of Energy and Nuclear Research to investigate nucleon-nucleus interaction mechanisms and as a basic tool for nuclear data evaluation for reactor design and other applications [7, 8], being widely used in BROND-2 evaluations [21]. In addition to standard rigid rotator and harmonic vibrator coupling schemes encoded in widely-used ECIS [5, 6] code (which is already included in EMPIRE), level-coupling schemes based on a non-axial soft-rotator model are included for even-even nuclei in OPTMAN. This allows accounting of stretching of soft nuclei by rotations, which results in change of equilibrium deformations for excited collective states compared with that of the ground state.

Calculations with OPTMAN are now possible both for neutrons and protons as the projectile, and the upper incident nucleon energy is extended up to 200 MeV [22]. Current version of soft-rotator model of OPTMAN takes into account the non-axial quadrupole, octupole and hexadecapole deformations, and  $\beta_2$ ,  $\beta_3$  and  $\gamma$ -vibrations with account of nuclear volume conservation. With this option, OPTMAN is able to analyze the collective level structure, E2, E3, E4  $\gamma$ -transition probabilities and reaction data in a self-consistent manner. OPTMAN can be applied not only to heavy rotational nuclei [23, 24], but can be also applied very successfully even to a very light nucleus, namely  $^{12}\text{C}$  [25, 26] and light

one  $^{28}\text{Si}$  [27], and also to vibrational nuclei such as  $^{52}\text{Cr}$  [28],  $^{56}\text{Fe}$  [29, 30] and  $^{58}\text{Ni}$  [31]. Many of those soft-rotor potentials are available within the RIPL library, being therefore available for EMPIRE calculations, once OPTMAN was included.

Since 2005 the main efforts in the development of the OPTMAN code were devoted to the improvement of the optical model formalism. Dispersion relationships between imaginary and real parts of the optical potential were included [32, 33], allowing to decrease significantly the number of optical parameters used. We also extended the OPTMAN code allowing for calculations of the (p,n) cross sections with excitation of isobaric analog states and therefore, making possible to derive Lane consistent potentials including a new Lane-consistent Coulomb correction.

A complete OPTMAN code's manual [7, 8] and its newest extension [9] give details of the soft-rotator theory, physical ideas and computation algorithms developed and incorporated into OPTMAN code, and description of input and output files, allowing easy running, understanding and using of OPTMAN outputs. Interested readers may consult those documents. OPTMAN is called as an independent module by EMPIRE; EMPIRE automatically prepares OPTMAN input for the incident or the outgoing channels.

The latest version 12 of the code (Jan 2012, still unpublished) has been implemented within the EMPIRE system allowing the use of state-of-the-art optical model potentials based on soft-rotor couplings in EMPIRE theoretical modeling.

### 1.2.3 Input of coupled-channels Codes ECIS and OPTMAN

Once coupled-channels calculation is invoked, the EMPIRE system prepares two additional files to contain the input needed in those calculations:

**TARGET\_COLL.DAT** collective levels and their structure information to be used by the rotational, vibrational, soft-rotor and rotational-vibrational CC calculation. In the case of vibrational and rotational-vibrational models the phonon structure of the levels is included. For soft-rotor potentials the soft-rotor hamiltonian parameters are included into the file. Typical examples of collective levels' file for different models (both for ECIS and OPTMAN codes) are given in the Section 8.9.7 below.

**OMPAR.DIR** parameters of the Optical Model Potential (OMP) to be used in the inelastic channel (discrete collective levels). OMP parameters may be selected via a keyword DIRPOT (similar to OMPOT, but only for the inelastic channel). The coupling scheme is not stored in OMPAR files. This information is supplemented by the parameters read from the TARGET\_COLL.DAT (*\*-lev.col*) file.

Independently of the selected optical model, in the first EMPIRE run  $T_l$  values are calculated for the whole energy grid. These values are stored in the file *\*.tl* for further



use. Although the first run may take quite a lot of time (specially for  $\text{DIRECT} > 0$ ), all successive runs are much faster. It should be noted that files *\*.tl* can be used for successive runs only if no changes were made to the files *\*-lev.col* and *\*-omp.ripl*. For each incident energy in the input file, there is one set of *\*.tl* files stored in the *work* directory.

ECIS06/OPTMAN can be invoked by the EMPIRE in three different ways, using input directive **DIRECT**. The default value ( $\text{DIRECT}=0$ ) calls the spherical optical model and suppresses calculation of direct reactions (ECIS06 always used in this case). The remaining options have the following meaning:

**DIRECT 1.** Population of collective levels in the incident channel is calculated using the Coupled-Channels model for coupled levels and DWBA method for uncoupled discrete levels and levels embedded in the continuum. The coupled levels are defined by their level number  $N$  and the dimension parameter *LEVCC* (see description in the section 8.3). If  $N < NDLEVCC$  then the level is coupled; otherwise the level is uncoupled. The excitation energy of the collective level defines whether this is a discrete level, or is a level embedded in the continuum. In the later case the collective level number  $N$  is not used, as their scattering cross sections are spread among neighboring continuum energy bins using a gaussian function with the energy resolution defined by parameter *RESOLF*. However, the collective level number  $N$  is quite important for collective discrete levels as it determines the corresponding discrete level (e.g. if the collective level number is  $N = 5$ , then the calculated cross sections are assigned to the 5th discrete level). The latest remark is important as it will be a mistake to assign them sequential consecutive numbers without checking the discrete level numbering in the corresponding EMPIRE file (*\*.lev*).

For the **DIRECT 1** option, the direct cross sections are exact but spherical transmission coefficients  $T_l$  are used for subsequent preequilibrium and HF calculations in the whole energy grid with optical model potentials defined by *OMPOT* keywords. These results are re-normalized at the  $T_l$  level by taking into account direct component. The total, elastic, absorption and the inelastic cross sections are taken from the CC calculations if a true Coupled-Channel Optical Model Potential (CC-OMP) is being used (otherwise, in the case of the Spherical OMP (S-OMP), only inelastic cross sections are accepted).

The option  $\text{DIRECT}=1$  is fairly fast, though some accuracy may be lost compared to the  $\text{DIRECT}=2$  option described below. Differences to the exact (**DIRECT 2**) case are related to the use of approximated transmission coefficients in the outgoing channel. In general, the approximation should perform well for the weakly coupled levels. For strong coupling, such as in the highly deformed rotational bands in heavy nuclei, it should be used with caution. It is the recommended option if accuracy is not a critical issue and the appropriate CC-OMP is available.

**DIRECT 2.** Population of collective levels both in the incident and outgoing channels is calculated using the Coupled-Channels model for coupled levels and DWBA method for uncoupled discrete levels and levels embedded in the continuum. Importantly, the CC is used consistently, considering the ground state and the coupled levels, to calculate all necessary transmission coefficients for subsequent preequilibrium and HF calculations. These CC transmission coefficients define absorption cross section that is available for the preequilibrium and HF decay. The absorption cross section sums up with the direct cross sections to collective levels to the reaction cross section. DIRECT=2 is an exact option that considers flux decrease due to the collective excitations at the level of  $T_l$ . The DIRECT=2 is a recommended option for accurate calculations whenever an appropriate CC-OMP is available.

**DIRECT 3.** Population of discrete collective levels in the inelastic scattering is calculated using the DWBA method providing approximate direct cross sections. The spherical transmission coefficients  $T_l$  are used for the whole energy grid in subsequent preequilibrium and HF calculations. These results are re-normalized at the  $T_l$  level by taking into account DWBA calculated direct component.

This option is fairly fast, though some accuracy may be lost. In general, it should perform well for weakly coupled levels. For a strong coupling, such as in the highly deformed rotational bands in heavy nuclei, it should be used with caution. The DWBA option has an advantage if the suitable CC-OMP is not available. In such a case, one can use S-OMP parameters in the DWBA calculations tuning inelastic cross sections by adjusting dynamical deformations of collective levels in file *\*-lev.col*.

OPTMAN can be invoked by the EMPIRE for DIRECT=1 and 2 for those optical model potentials that use either soft-rotor for spherical nuclei, or rigid-rotor or deformed vibrational-rotational model for deformed nuclei.

## 1.3 Photoabsorption

A model of photonuclear reactions must account for the different reaction mechanisms involved in the initial photonuclear excitation process and the subsequent decay of the excited nucleus by particle and gamma-ray emission. At low energies, below about 30 MeV, the Giant Dipole Resonance (GDR) is the dominant excitation mechanism, where a collective bulk oscillation of the neutrons against the protons occurs. At higher energies, up to approximately 150 MeV, photoabsorption on a neutron-proton pair (a quasi-deuteron, QD), which has a large dipole moment, is the dominant mechanism.

In EMPIRE, the photoabsorption cross section is calculated as the sum of two compo-

nents [34],

$$\sigma_{abs}(E_\gamma) = \sigma_{GDR}(E_\gamma) + \sigma_{QD}(E_\gamma).$$

The GDR component,  $\sigma_{GDR}(E_\gamma)$ , is given by a Lorentzian shape, with parameters describing the total absorption of the giant dipole resonance. The expression used takes the basic form

$$\sigma_{GDR}(E_\gamma) = \sum_i \sigma_i \frac{(E_\gamma \Gamma_i)^2}{(E_\gamma^2 - E_i^2)^2 + (E_\gamma \Gamma_i)^2},$$

where  $\sigma_i$ ,  $E_i$  and  $\Gamma_i$  are the GDR peak cross section, energy and width, respectively. The summation is limited to  $i = 1$  for spherical nuclei, while for deformed nuclei the resonance is split and one uses  $i = 1, 2$ . As a rule, the parameters are derived from fits to experimental data or from systematics [35].

The QD component,  $\sigma_{QD}(E_\gamma)$ , is taken from the model of Chadwick *et al.* [36], which uses a Levinger-type theory. It relates the nuclear photoabsorption cross section to the experimental deuteron photodisintegration cross section,  $\sigma_d(E_\gamma)$ , as

$$\sigma_{QD}(E_\gamma) = L \frac{NZ}{A} \sigma_d(E_\gamma) f(E_\gamma).$$

Here, the Levinger parameter was derived as  $L = 6.5$  and  $f(E_\gamma)$  is the Pauli-blocking function, which reduces the free deuteron cross section  $\sigma_d(E_\gamma)$  to account for Pauli blocking of the excited neutron and proton by the nuclear medium. The experimental deuteron photodisintegration cross section was parametrized as

$$\sigma_d(E_\gamma) = 61.2 \frac{(E_\gamma - 2.24)^{3/2}}{E_\gamma^3},$$

with  $E_\gamma$  in MeV and  $\sigma_d$  in mb. The Pauli-blocking function was found by Chadwick *et al.* to be a multidimensional integral whose solution could be well approximated in the energy range 20 – 140 MeV by the polynomial expression

$$\begin{aligned} f(E_\gamma) = & 8.3714 \times 10^{-2} - 9.8343 \times 10^{-3} E_\gamma + 4.1222 \times 10^{-4} E_\gamma^2 \\ & - 3.4762 \times 10^{-6} E_\gamma^3 + 9.3537 \times 10^{-9} E_\gamma^4, \end{aligned}$$

with  $E_\gamma$  in MeV. In Ref. [36], the Pauli-blocking function was not parametrized below 20 MeV, where it tends to zero, or above 140 MeV, where it tends to unity. As the contribution needs to be defined at all energies considered, EMPIRE follows the example of Ref. [34] and uses an exponential shape,  $f(E_\gamma) = \exp(-D/E_\gamma)$ , for energies below 20 MeV and above 140 MeV, with  $D = 73.3$  MeV for  $E_\gamma < 20$  MeV and  $D = 24.2$  MeV for  $E_\gamma > 140$  MeV. This form has the correct behavior in that it tends to zero at  $E_\gamma = 0$  and to unity for large  $E_\gamma$ , and is continuous with the previous equation at 20 and 140 MeV.

Preequilibrium reaction mechanisms become important for incident photon energies above 10 to 15 MeV. In the photoabsorption mechanisms described above, the initial nuclear excitation can be understood in terms of particle-hole excitations ( $1p1h$  for the GDR;

$2p2h$  or  $2p1h$  for QD processes) and thus it is natural to use a preequilibrium theory of particle-hole processes to describe the preequilibrium emission and damping to equilibrium during the evolution of the reaction. Such models can be used to calculate photonuclear reactions for incident photons with energies up to about 140 MeV, which is the threshold for pion production. At present, EMPIRE permits the calculation of preequilibrium emission in photonuclear reactions using either the exciton model module PCROSS or the Hybrid Monte-Carlo Simulation module HMS. Both implementations of photoabsorption represent the GDR fraction as an initial  $1p1h$  excitation and the QD fraction as an initial  $2p2h$  excitation. The implementation of photoabsorption in PCROSS does not take into account the correlation of the two holes created through the QD mechanism, which would require an initial configuration closer to a  $2p1h$  one than to a  $2p2h$  one[34]. The implementation in HMS takes this correlation into account in a manner consistent with the model of Ref. [36].

Following the possible emission of preequilibrium particles, the remaining nuclear system reaches equilibrium, after which it decays by sequential particle or gamma-ray emission (or possibly fission) until the nuclear ground state is reached. In EMPIRE, the Hauser-Feshbach theory is used to calculate cross sections for these processes.

Much more information on photonuclear reactions can be found in Ref. [34], which served as the basis for this brief description of these processes.

# Chapter 2

## Quantum-mechanical preequilibrium models

### 2.1 Multi-step Direct

The approach to statistical Multi-step Direct reactions is based on the Multi-step Direct (MSD) theory of preequilibrium scattering to the continuum originally proposed by Tamura, Udagawa and Lenske [11]. Since then, the approach has been revised, especially the part related to statistical and dynamical treatment of nuclear structure.

The evolution of the projectile-target system from small to large energy losses in the open channel space is described in the MSD theory with a combination of direct reaction (DR), microscopic nuclear structure and statistical methods. As typical for the DR-approach, it is assumed that the closed channel space, i.e. the MSC contributions, have been projected out and can be treated separately within the Multi-step Compound mechanism.

#### 2.1.1 Outline of the theory

In the MSD theory the effective Hamiltonian in the open channel space is divided into an energy averaged optical model part  $H^{opt}$ , describing the relative motion of projectile  $a$  and target  $A$ , the intrinsic Hamiltonian  $H^{intr}$  of the asymptotically separated nuclei and the residual effective projectile-target interaction  $V^{res}$  leading to non-elastic processes

$$H = H^{opt} + H^{intr} + V^{res} \quad . \quad (2.1)$$

Both  $H^{opt}$  and  $V^{res}$  are non-hermitian operators. To a large extent the imaginary parts are related to the flux absorbed into the closed channels, but those open channels which are not treated explicitly are also contributing.

The ORION code solves the Lippmann-Schwinger equation for the open channel T-

matrix where the  $n^{th}$ -order term

$$T_{\gamma 0}^{(n)} = \langle \chi_E^{(-)} | (\gamma | V^{res} (G^{chan}(E) V^{res})^{n-1} | 0) | \chi_0^{(+)} \rangle \quad (2.2)$$

describes the  $n$ -step transition from the entrance channel with incoming scattering wave  $\chi_0^{(+)}$  and the ground state configuration  $|0\rangle = |aA\rangle$  to an exit channel  $\gamma$  with outgoing wave  $\chi_E^{(-)}$  at the energy  $E$  [37, 38].  $G^{chan}(E)$  is the Green's function for the channel. The scattering waves are optical model wave functions. They are weakly energy dependent on a scale much larger than the one on which the intrinsic states  $\gamma$  vary. The MSD approach treats the residual projectile-target interactions perturbatively. In this sense, MSD theory is a “weak coupling” description of continuum scattering.

In order to describe the statistical content of pre-equilibrium spectra the real states  $\gamma$  are expanded into  $n$ -particle and  $n$ -hole model states  $c$ . Explicitly,  $H^{intr}$  is chosen as

$$H^{intr} = H_0^{intr} + V^{intr} \quad . \quad (2.3)$$

The states  $c$  are eigenstates of  $H_0^{intr}$  and the residual interaction  $V^{intr}$  couples states from different particle-hole classes only. It is assumed that the configuration mixing between  $np$ - $nh$  classes is stochastic in nature and leads to a random distribution of amplitudes with mean value zero [38]. When the density matrix is averaged over a finite energy interval, e.g. with a Lorentzian or Gaussian  $g(x)$  of full width  $\Delta$  large compared to the mean level spacing,

$$\hat{\rho}(E) = \int dE' g(E - E') \hat{\rho}_{micro}(E) \quad (2.4)$$

the coherence of the basis states is lost. As a result, the density matrix becomes a statistical matrix

$$\hat{\rho}(E) = \sum_n \hat{\rho}_n(E). \quad (2.5)$$

The summation extends over the  $np - nh$  classes with

$$\hat{\rho}_n(E) = \sum_{c=[npnh]} |c\rangle P_c(E) \langle c| \quad (2.6)$$

and the probability per energy to find the system in the configuration  $c$  is given by the spectroscopic densities,

$$P_c(E) = -\frac{1}{\pi} \text{Im} \left[ \int dE' g(E - E') \langle c | G^{intr}(E') | c \rangle \right], \quad (2.7)$$

with  $G^{intr}(E)$  being the intrinsic Green's function.

The statistical operators carry further properties which are important for the physical content of the description. Integrating  $P_c(E)$  over an interval  $\Delta E$  one obtains the spectroscopic factor for the configuration  $c$  in  $\Delta E$ . Irrespective of the representation, i.e. in either the  $\gamma$  or the  $c$  basis, the trace of  $\hat{\rho}(E)$ , Eq. 2.4, gives the total level density at energy  $E$ . The partial level density of  $np - nh$  states is determined by  $\text{tr}(\hat{\rho}_n)$  (Eq. 2.6).

Similar to the chaining and never-come-back hypotheses of [3] the interference terms  $n \neq k$  are neglected by assuming that in each step the reaction is dominated by transitions into configurations with the highest level density at a given excitation energy. This means, that we neglect de-excitation and re-scattering processes which decrease or leave the  $ph$ -number unchanged, respectively. With this assumption the cross section becomes an incoherent super-position of  $n$ -step contributions

$$\frac{d^2\sigma}{d\Omega dE} = \sum_n \frac{d^2\sigma^{(n)}}{d\Omega dE}, \quad (2.8)$$

where the multi-step cross sections are defined as

$$\frac{d^2\sigma^{(n)}}{d\Omega dE} = \sum_{c=[npnh]} P_c(E) |T_{c0}^{(n)}|^2. \quad (2.9)$$

Expanding  $V^{res}$  into multi-poles  $V_\lambda$  and noting that only  $1p-1h$  configurations are directly excited in a one-step process the  $\sigma^{(1)}$  is determined by an average over transitions into the  $1p-1h$  states  $c$  around excitation energy  $E$  with form factors

$$F_\lambda^{c0} = (c|V_\lambda|0). \quad (2.10)$$

Rather than treating each transition separately it is sufficient to consider averages over the microscopic form factors. Thus,  $V^{res}$  is represented in terms of state independent multipole form factors  $F_\lambda$  and nuclear transition operators  $O_\lambda$

$$V^{res}(r, \xi) = \sum_\lambda F_\lambda(r) O_\lambda(\xi). \quad (2.11)$$

Here,  $r$  denotes the relative motion coordinate and  $\xi = (\xi_a, \xi_A)$  are the intrinsic coordinates including spin and isospin, respectively. The multipole form factors  $F_\lambda$  in turn are related to  $O_\lambda$ . In a self-consistent approach they are obtained by averaging  $V^{res}$  over  $O_\lambda$ :

$$F_\lambda(r) = (c|O_\lambda^\dagger \hat{\rho}(E) V^{res}|c)/S_\lambda(E, c). \quad (2.12)$$

Here, the general case of a transition starting from an arbitrary state  $c$  is considered which appears in the intermediate steps of higher order multi-step processes. For one-step reactions the initial state is the ground state  $c = 0$ . By normalization to the transition strength function  $S_\lambda$

$$(c|O_\lambda^\dagger \hat{\rho}(E) O_\lambda|c) = \delta_{\lambda\lambda'} S_\lambda(E, c) \quad (2.13)$$

the dependence of the form factor on the internal state is removed to a large extent.  $S_\lambda$  is the nuclear response function for the external operator  $O_\lambda$  describing the transition rate per unit energy from the state  $c$  into the ensemble of states  $c'$  centered at energy  $E$ .

The above relations are appropriate for one-step reactions where  $c$  is the ground state. However, in higher steps  $c$  is an arbitrary intermediate  $np-nh$  state which is summed

over in the cross section. Thus, for multi-step scattering the form factor, Eq.2.12 actually utilizes a too microscopic picture. The statistical aspects in multi-step transitions are taken fully into account by the average multipole form factors

$$F_\lambda = \frac{\text{tr}(\hat{\rho} O_\lambda^\dagger \hat{\rho} V^{res})}{\text{tr}(\hat{\rho} O_\lambda^\dagger \hat{\rho} O_\lambda)}, \quad (2.14)$$

which are independent of the initial state and the multi-step order, respectively. In the applications of the theory these global form factors together with the response functions of Eq.2.13 are used.

With the above results the one-step cross section is expressed as

$$\frac{d^2\sigma^{(1)}}{dEd\Omega} = \sum_\lambda S_\lambda(E) \overline{\frac{d\sigma^{(1)}}{d\Omega}}|_\lambda, \quad (2.15)$$

where  $\overline{\sigma^{(1)}}$  is a reduced DWBA cross section calculated with the average form factors (Eq.2.12).

The multi-step part of the theory is discussed here for two-step reactions only. The state-independent and slowly varying two-step amplitudes read

$$T_{\lambda_1, \lambda_2}^{(2)} = \langle \chi_E^{(-)} | F_{\lambda_2} G^{opt} F_{\lambda_1} | \chi_\alpha^{(+)} \rangle, \quad (2.16)$$

with  $G^{opt}$  being Green's function for the optical model potential. The nuclear structure information is now contained completely in

$$(0 | O_{\lambda_1'}^\dagger G^{(intr)\dagger}(E_1') O_{\lambda_2'}^\dagger \hat{\rho}(E) O_{\lambda_2} G^{(intr)}(E_1) O_{\lambda_1} | 0). \quad (2.17)$$

By definition, the exit channel configurations are  $2p - 2h$  states which are excited from  $1p - 1h$  states  $c_1$ . Also in the first step only  $1p - 1h$  states  $a$  are excited. Therefore, we only have to consider the  $1p - 1h$  reduced parts of the two Green functions.

To a good approximation the dependence of  $S_{\lambda_2}(E, c_1)$  on  $c_1$  can be replaced by a dependence on  $E_1$  by considering that the spectroscopic strength usually is located in the vicinity of the unperturbed energy. Theoretically, this is achieved by taking the average over the response functions belonging to states  $c_1$  at energy  $E_1$

$$\begin{aligned} S_\lambda(E, E_1) &= \frac{\sum_{c_1} P_{c_1}(E_1) S_\lambda(E, c_1)}{\sum_{c_1} P_{c_1}(E_1)} \\ &= \frac{\text{tr}(\hat{\rho}_1(E_1) O_\lambda^\dagger \hat{\rho}(E) O_\lambda)}{\text{tr}(\hat{\rho}_1(E_1))}. \end{aligned} \quad (2.18)$$

The final result for the two-step MSD cross section is of very intuitive structure

$$d^2\sigma^{(2)}/dEd\Omega = \sum_{\lambda_1 \lambda_2} \int dE_1 S_{\lambda_2}(E, E_1) S_{\lambda_1}(E_1, 0) \overline{\frac{d\sigma^{(2)}}{d\Omega}}(E, E_1) |_{\lambda_1 \lambda_2}. \quad (2.19)$$



$\overline{\sigma^{(2)}}$  is an averaged cross section defined in terms of the  $T^{(2)}$ -matrix elements (Eq. 2.16, which describes two-step scattering wave-mechanically as a coherent quantal process. The total response of the intrinsic system at energy loss  $E$  is contained in the first and second step transition strength functions. The folding accounts for the partitions of the total energy  $E$  into one- and two-step parts such that  $E$  is conserved.

In the present version of the code only one- and two-step MSD contributions are considered. In most cases it is a good approximation to use the ground state response functions also for the second step but at an energy shifted by the amount of total energy loss in the first step. This corresponds to the assumption that the structure of excited nuclei is close to the structure of the ground state as far as single particle occupancies and other mean-field properties are concerned.

Summarizing this section, the statistical properties of pre-equilibrium spectra are used to eliminate interference contributions at various places. Physically, this corresponds to the neglect of certain intrinsic correlation functions which only would be observable at an energy resolution of the order of the average level spacing. This leads to a representation of pre-equilibrium cross sections as an incoherent super-position of multi-step contributions. The statistical treatment is introduced in a minimal way, namely referring only to the intrinsic systems while multi-step scattering is described quantum-mechanically as a coherent process at all steps.

## Updated formalism in TRISTAN

In the previous version of the EMPIRE nuclear single-particle energies and wave functions used in TRISTAN were obtained from a spherical Nilsson Hamiltonian with standard parameters. Pairing correlations were accounted for by the BCS method in the constant gap approximation. The resulting two-quasi-particle (2qp) excitation energies and wave functions determine the uncorrelated 2qp multipole nuclear Green functions  $G_L^{2qp}(\varepsilon)$ . The uncorrelated  $2qp$  response function for an external one-body multipole field  $U_L = v(r)Y_L$  is then  $\chi_L^{2qp}(\varepsilon) = \langle c | U_L^\dagger G_L^{2qp}(\varepsilon) U_L | c \rangle$ ,  $|c\rangle$  being an initial reference state. In the RPA schematic model a separable residual particle-hole interaction is assumed of the form  $V^{sep}(1, 2) = \sum_L \kappa_L U_L(1)U_L(2)$ . Then the quasi-particle RPA (QRPA) correlated response function for the operator  $U_L$  is obtained from the Bethe-Salpeter (B-S) equation [39]:

$$\chi_L^{QRPA}(\varepsilon) = \chi_L^{2qp}(\varepsilon) + \kappa_L \chi_L^{2qp}(\varepsilon) \chi_L^{QRPA}(\varepsilon) \quad (2.20)$$

The multipole spectroscopic strength function of multipolarity  $L$  is  $S_L(\varepsilon) = -Im\chi_L^{QRPA}(\varepsilon + i\Gamma/2)/\pi$ ,  $\Gamma$  being the spreading width. In the current version of EMPIRE we use the TRISTAN module modified according to Ref. [40]. A quadrupole deformation term, taken from the EMPIRE input, has been added to the nuclear Hamiltonian. As the nuclear Hamiltonian is now non-diagonal in the spherical Nilsson basis the  $2qp$  wave functions are, in contrast with the degenerate case, not eigenfunctions of the angular momentum squared  $L^2$ . Consequently the uncorrelated  $2qp$  multipole nuclear Green functions are not diagonal with respect to  $L$ . However, because of the symmetry with respect to the deformation axis both

parity  $\pi$  and angular momentum projection  $K$  onto this axis are still conserved. The uncorrelated  $2qp$  multipole response function for the external one-body field  $U_{L,K} = v_{L,K}(r)Y_L^K$  then becomes:

$$\chi_{L,K}^{2qp}(\varepsilon) = \langle c | \sum_{L'} U_{L,K}^\dagger G_{L,L',K}^{2qp}(\varepsilon) U_{L,K} | c \rangle = \langle c | U_{L,K}^\dagger G_{L,L,K}^{2qp}(\varepsilon) U_{L,K} | c \rangle \quad (2.21)$$

The QRPA correlated response function is obtained in the schematic RPA from the B-S equation for each  $K$  [41]:

$$\chi_{L,K}^{QRPA}(\varepsilon) = \chi_{L,K}^{2qp}(\varepsilon) + \kappa_{L,K} \chi_{L,K}^{2qp}(\varepsilon) \chi_{L,K}^{QRPA}(\varepsilon) + [off - diagonal terms in L] \quad (2.22)$$

The calculation of the multipole spectroscopic strength function  $S_L$  now involves a summation over  $K$  of  $Im\chi_{L,K}^{QRPA}$ . It can be shown that the contributions of the off-diagonal terms in the B-S equation to the spectroscopic strength function are negligibly small compared to the diagonal terms.

Calculations accounting for nuclear deformation in MSD nicely reproduce the data in the direct continuum region while the “spherical” calculations underpredict the same data. It should be stressed that, except for adjustment of dynamic deformations used in the coupled-channel calculations and the fission input, these results were obtained without any adjustment of the MSD part of the calculations. In the IAEA evaluation for  $^{232}\text{Th}$  the missing strength in the continuum region of the neutron spectrum was filled up with a large number of fictitious collective levels embedded in the continuum. Similar approach has also been used in other ENDF/B-VII evaluations for important actinides, such as  $^{235,238}\text{U}$  and  $^{239}\text{Pu}$ . The “deformed” MSD approach allows to achieve similar result on a physically more sound basis. The method is computationally faster and has been implemented as a default in the current version of the EMPIRE code.

### 2.1.2 Notes on RPA-Description of Transition Strength Functions

In the MSD approach continuum scattering is considered as a sequence of  $1p-1h$  transitions and the transition strength functions, Eq. 2.13, correspond to response functions of an external one-body operator acting repeatedly on a nucleus. A reliable description of one-body response functions is provided by the Random Phase Approximation theory [42, 43] (RPA). In RPA the whole series of  $1p-1h$  interaction diagrams is summed exactly. Thus, an essential contribution to the intrinsic correlations is treated explicitly. In the notation of Section 2.1.1 they are part of  $H_0^{intr}$ . Thus, the  $ph$ -classes are built from correlated basis states. This justifies also the *ansatz* of Eq. 2.3 where  $V^{intr}$  was defined as to act only between  $ph$ -classes.

An important advantage for a reliable description of pre-equilibrium spectra is that RPA accounts for collective and non-collective features on the same theoretical footing

[43, 44, 38, 37, 45]. The approach describes at the same time the large amount of weakly excited background states and the strongly excited giant resonances (*GR*) in the continuum together with low-lying surface vibrations. It is clear that the response functions do not suffer from double counting of transition strength which appears if collective states are treated separately. Important quantities like energy weighted sum rules are known to be conserved by RPA. Also the enhancement of the response due to ground state correlations is included.

In view of a large number of  $p - h$  configurations which are needed in order to describe nuclear spectra over a range of excitation energies of several tens of *MeV* a fully microscopic calculation is of little use. In accordance with the statistical description of cross section statistical considerations are also incorporated into the structure calculations. Instead of solving the RPA-eigenvalue problem by direct diagonalization it is more appropriate to consider the average properties of excitations. The Green function approach to RPA [43, 38] provides the proper theoretical basis for such a description.

For a general formulation, applicable also to open shell nuclei, the quasi-particle RPA (QRPA) is used. Thus, a BCS ground state and a canonical transformation to quasi-particles is assumed [46]. The excitations are then given in terms of two quasi-particle ( $2qp$ ) rather than by  $1p - 1h$  configurations. Furthermore, in order to account for the self-energies the  $2qp$  energies are taken to be complex by adding a state dependent damping width  $\Gamma_\alpha^\downarrow$ . The response functions include inelastic events only and are calculated in linear response theory. Formally, the response functions entering into the MSD-calculation are expressed through the RPA polarization propagator  $\chi^{RPA}(E)$

$$S_\lambda(E, 0) = -\frac{1}{\pi} \text{Im}[\chi^{RPA}(E)]. \quad (2.23)$$

In higher steps, where the transition starts from a state  $c \neq 0$ , the  $1p1h$  densities and response functions on the background of an already excited nucleus are required. At excitation energies per particle which are well below the Fermi energy the structure remains close to the ground state. Since this is the region of main interest for pre-equilibrium scattering Eq.2.23 is used also in two-step and higher order reactions at the appropriate excitation energy. The average response functions, Eq.2.18, are approximated by

$$S_\lambda(E, E_1) \simeq S_\lambda(E - E_1, 0), \quad (2.24)$$

where it is assumed that  $S_\lambda$  depends only on energy difference  $E - E_1$  which corresponds to the relative excitation energy. The form factors of Eq.2.14 are found to be given by folding  $V^{res}$  with  $\overline{\rho}_\lambda$ . Thus, the theory leads to a transparent and consistent description of nuclear structure and reaction dynamics which accounts for the microscopic and the statistical aspects of pre-equilibrium reactions.

The code TRISTAN assumes  $O_\lambda = \kappa_\lambda U_\lambda$ , where the radial part of  $U_\lambda$  is chosen as the derivative of the ground state potential and the coupling constants  $\kappa_\lambda$  are treated as empirical parameters. This phenomenological approach to RPA is widely used in structure calculations and has been found to give reliable results for response functions [44, 47].

The MSD response functions are calculated with single particle levels from a spherical Nilsson Hamiltonian with standard parameters. The ground state is obtained from a BCS calculation in the “fixed gap approximation” with  $\Delta_p = \Delta_n = 12.0/\sqrt{A}$  MeV for protons and neutrons. This also allows a realistic description of open-shell nuclei. Correspondingly, the response functions are calculated with quasi-particle RPA (QRPA).

Multipole fields with a radial shape  $\sim r^\lambda$  are taken. The coupling constants  $\kappa_\lambda$  are determined such that excitation energies of low-lying surface oscillations and of the Giant Dipole Resonance are reproduced.

The  $2qp$ -spreading width  $\Gamma_\alpha^\downarrow$  which describes in a global way the internal nuclear dissipation of the model states is parametrized as

$$\Gamma_\alpha^\downarrow = \Gamma_0 \left( \frac{1}{1 + \exp((E_\alpha - E_{thr})/a)} - \frac{1}{1 + \exp((-E_\alpha - E_{thr})/a)} \right) \quad (2.25)$$

an odd function of  $E_\alpha$ . The parameters  $\Gamma_0$ ,  $E_{thr}$ ,  $a$  are taken equal to the width and energy of the giant dipole resonance. The maximum  $l$ -transfer  $\lambda$  is internally set between 1 and 4 depending on the maximum  $l$  contributing to the reaction cross section.

In EMPIRE-3.1 fitting of the coupling constants  $\kappa_\lambda$  has been improved to minimize their fluctuations with changing incident energy.

### 2.1.3 Implementation of ORION and TRISTAN codes in EMPIRE

Implementation of ORION and TRISTAN codes in EMPIRE involves a few modifications that facilitate operation of the codes. The common input parameters (such as incident channel configuration and optical model parameters) are passed to ORION and TRISTAN directly from the EMPIRE. The parameters that are specific to ORION and TRISTAN are set to default values in EMPIRE and transmitted when ORION and TRISTAN are called. The latter parameters can be modified by the user in the optional input to EMPIRE. However, a default MSD calculation can be performed without any additional input.

EMPIRE takes care of multiple calls of ORION with appropriate energy losses (Q-triangle). In the first set of calls, a standard averaged form factor is used. Then EMPIRE calls ORION calculations with the compressional form factor, which is more appropriate for  $\lambda = 0$  momentum transfer. The tables resulting from both sets of calculations are merged in such a way that all  $\lambda = 0$  momentum transfers are calculated with the compressional form factor while the remaining ones are determined with the standard form factor. The extension of the original version of ORION to the compressional form factor for  $\lambda = 0$  was performed according to the suggestions by H. Lenske).

The TRISTAN code has been modified to automate blocking of the shell model orbital by the unpaired nucleon. In the stand alone version of the code this orbital must be specified in the input. Since the orbitals are reordered during the calculations two runs are necessary (the first one without blocking to identify a correct orbital). In the version of TRISTAN that is included in EMPIRE this preliminary calculation is performed internally, whenever necessary, and the blocking is set up.

Results of the MSD calculations are sensitive to the coupling constants  $\kappa_\lambda$ . By default, these are determined such that excitation energies of low-lying  $2^+$ ,  $3^-$ , and  $4^+$  collective levels be reproduced. The code identifies the lowest discrete levels with the above spins and uses them for fitting coupling constants  $\kappa_\lambda$ . However, not always the lowest levels are the collective ones. If this happens, the user has to fix the energies of these levels in the input file. The energy of the Giant Dipole Resonance is used to determine the  $\kappa_1$  parameter. For  $\lambda = 0$  transitions the self-consistent coupling constant is used by default. Also in  $\lambda = 0$  and  $\lambda = 1$  cases user may choose to provide the respective energies in the input. Each of the coupling constants can also be set to the self-consistent value.

It should be noted that actual implementation of the TRISTAN code does not allow for treatment of the charge exchange channels. Therefore, the MSD cross sections and double-differential spectra can only be calculated for the inelastic scattering. It should be stressed, however, that due to the collective nature of the MSD approach, its contribution to the inelastic scattering is much bigger than to the charge-exchange channels and thus the latter ones can be calculated with the exciton model PCROSS (see Section 3.1) or Monte Carlo approach (see Section 3.2) with reasonable accuracy.

## 2.2 Multi-step Compound

The modeling of Multi-step Compound (MSC) processes follows the approach of Nishioka et al. (NVWY) [4]. Like most of the precompound models, the NVWY theory describes the equilibration of the composite nucleus as a series of transitions along the chain of classes of closed channels of increasing complexity. In the present context, we define the classes in terms of the number of excited particle-hole pairs ( $n$ ) plus the incoming nucleon, i.e. excitons. Thus the exciton number is  $N = 2n + 1$  for nucleon induced reactions. Assuming that the residual interaction is a two-body force only neighboring classes are coupled ( $\Delta n = \pm 1$ ).

According to NVWY, the average MSC cross-section leading from the incident channel  $a$  to the exit channel  $b$  is given by

$$\frac{d\sigma_{ab}}{dE} = (1 + \delta_{ab}) \sum_{n,m} T_n^a \Pi_{n,m} T_m^b, \quad (2.26)$$

which also has to be summed over spins and parities of the intermediate states and where we have omitted kinematic and angular-momentum dependent factors. The summation includes all classes  $n$  and  $m$ . The transmission coefficients  $T_n^a$  describing the coupling between channel  $a$  and class  $n$  are given as

$$T_n^a = \frac{4\pi^2 U_n^a}{(1 + \pi^2 \sum_m U_m^a)^2}, \quad (2.27)$$

where  $U_n^a = \rho_n^b < W_{n,a} >$  is microscopically defined in terms of the average bound level density  $\rho_n^b$  of class  $n$ , and in terms of the average matrix elements  $W_{n,a}$  connecting channel

$a$  with the states in class  $n$ . The probability transport matrix  $\Pi_{mn}$  is defined via its inverse,

$$(\Pi^{-1})_{nm} = \delta_{nm}(2\pi\rho_n^b)(\Gamma_n^\downarrow + \Gamma_n^{ext}) - (1 - \delta_{nm})2\pi\rho_n^b\overline{V_{n,m}^2}2\pi\rho_m^b. \quad (2.28)$$

in terms of the mean squared matrix element  $\overline{V_{n,m}^2}$  coupling states in classes  $n$  and  $m$ , the average spreading width  $\Gamma_n^\downarrow$  of states in class  $n$ , and the average total decay width  $\Gamma_n^{ext}$  in class  $n$ . The spreading width  $\Gamma_n^\downarrow$  is again related to the mean squared matrix element  $\overline{V_{n,m}^2}$

$$\Gamma_n^\downarrow = 2\pi \sum_m \overline{V_{n,m}^2} \rho_m^b. \quad (2.29)$$

Under the chaining hypothesis  $\overline{V_{n,m}^2}$  couples only neighboring classes ( $\overline{V_{n,m}^2} = 0$  unless  $|n-m| = 1$ ). The decay width  $\Gamma_n^{ext}$  is determined by the sum of the transmission coefficients  $T_n^a$  over all open channels

$$\Gamma_n^{ext} = (2\pi\rho_n^b)^{-1} \sum_a T_n^a. \quad (2.30)$$

More explicitly  $\Gamma_n^{ext}$  may be expressed through the energy integral of the product of transmission coefficients and level densities

$$\Gamma_n^{ext} = (2\pi\rho_n^b)^{-1} \sum_\alpha \sum_{m=n-1}^{m=n+1} \int T_{n \rightarrow m}^\alpha(\varepsilon) \rho_m^b(E - Q_p - \varepsilon) d\varepsilon. \quad (2.31)$$

Here,  $\varepsilon$  stands for the ejectile  $p$  energy,  $Q_p$  for its binding in a composite system, and  $\alpha$  symbolically accounts for the angular momentum coupling of the residual nucleus spin, ejectile spin and orbital angular momentum to the composite nucleus spin. Again, due to the chaining hypothesis, only those emissions which change class number by  $|n-m| \leq 1$  are allowed. We note that, unlike the FKK[3] formulation, in the NVWY theory transmission coefficients  $T_{n \rightarrow m}$  carry two class indexes.

Following Ref. [48] the microscopic quantities  $\langle W_{n,a} \rangle$  and  $\overline{V_{n,m}^2}$  are expressed in terms of the macroscopic ones. To define  $\langle W_{n,a} \rangle$  EMPIRE uses Eq. 2.27 and equates it to the optical model transmission coefficient. The matrix element  $\overline{V_{n,m}^2}$  is related to the imaginary part of the optical model potential  $W(\epsilon)$  using Eq. 2.29 with  $\Gamma_n^\downarrow = 2W(\epsilon)$ . To evaluate  $\Gamma_n^\downarrow$ ,  $W(\epsilon)$  has to be averaged over the probability distribution of particles and holes. Once the matrix  $\Pi^{-1}$  is determined it is inverted numerically and used in Eq. 2.26 to calculate MSC emission spectra.

EMPIRE decides whether the MSC calculation should be followed by the Hauser-Feshbach one or not. If the number of MSC classes considered is high enough so that the equilibrium class is included in the MSC chain the code restricts calculations to the MSC mechanism only. To this end, the matrix element  $\overline{V_{n,n+1}^2}$  of Eq. 2.28, responsible for the transition to a next higher class, is set to zero for the highest class. This closes the “leakage” of flux from the MSC, which normally would be treated in the frame of the Hauser-Feshbach model. Thus, the whole flux entering the composite nucleus is consistently treated within the MSC mechanism. This approach is certainly attractive from the

theoretical point of view. On the practical side, however, there are severe drawbacks. The most important is that, so far, the discrete levels in a residual nucleus are not treated in the MSC formalism. In fact, EMPIRE, when using MSC mechanism, totally ignores the discrete level region. In addition, the particle-hole level densities, as used in the MSC, are less realistic than their counterparts used in the Hauser-Feshbach model. The latter ones have been carefully adjusted to the experimental data, especially in the low energy region, while the particle-hole level densities, in most cases, make use of an equidistant spacing model with  $g=A/13$ . Therefore, it is recommended to use a few (3 to 5) MSC classes, which are generally sufficient to grasp the most important part of the MSC spectrum and to delegate the rest of the decay to the Hauser-Feshbach model.

### 2.2.1 Conditional level densities

Following Ref. [49], the conditional density of states having all  $p$  particles bound (i.e. below the binding energy  $B$ ) reads

$$\rho_{ph}^B(E) = \frac{g^{p+h}}{p!h!} \sum_{i=0}^I \binom{p}{i} (-1)^i \frac{(E - iB)^{p+h-1}}{(p+h-1)!} \quad (2.32)$$

for  $IB < E \leq (I+1)B$ , with  $I = 0, 1, \dots, (p-1)$ , and

$$\rho_{ph}^B(E) = \frac{g^{p+h}}{p!h!} \sum_{i=0}^{p-1} \sum_{m=0}^{h-1} \binom{p}{i} (-1)^i \frac{[(p-i)B]^{p+m}}{(p+m)!(h-1-m)!} (E - pB)^{h-1-m} \quad (2.33)$$

for  $E > pB$ . The superscript  $B$  indicates that quantity refers to the bound states embedded in the continuum. For excitation energies lower than the Fermi energy, which is approximately 40 MeV, it is not necessary to consider any additional limitations for the energies of the hole states. For the higher energies, the depth of the potential well has to be taken into account. Relevant formulas were reported in Ref. [50], but for the time being these were not implemented in the EMPIRE code.

Using Eqs. 2.32 and 2.33 one can calculate energy dependence of the average escape width and of the damping width, which both depend on  $\rho_{ph}^B(U)$ . These factors were originally introduced by Feshbach, Kerman, and Koonin as the  $Y$ -functions (see p.462 of Ref.[3]). These functions define the density of final states accessible to different transition modes compatible with two-body interaction ( $\Delta n = -1, 0, +1$ ). For the  $\Delta = -1$  transition one obtains:

$$Y_n^{n-1} = \frac{\rho_{21}^B(E - U) \rho_{p-2, h-2}^B(U)}{\rho_{ph}^B(E)}. \quad (2.34)$$

The accessible state density for the  $\Delta = 0$  transition reads



$$\begin{aligned}
Y_n^n &= Bg^2h \frac{\rho_{p-1,h}^B(U)}{\rho_{ph}^B(E)} \\
&+ \alpha \frac{1}{2}(h+1)(h+2) \frac{g}{\rho_{ph}^B} \left[ \frac{U-E+2B}{h+2} g\rho_{p-2,h+1}^B(U) \right. \\
&\left. + \beta \rho_{p-2,h+2}^B(E-2B) - \rho_{p-2,h+2}^B(U) \right], \tag{2.35}
\end{aligned}$$

with  $\alpha = 1$  for  $E \leq 2B + U$ ,  $\beta = 1$  for  $E > 2B$ , and both equal to 0 elsewhere. The density of states available for the creation of the particle-hole pair is

$$Y_n^{n+1} = g \frac{1}{2} h(h+1) \frac{\rho_{p,h+1}^B(U)}{\rho_{ph}^B(E)} \tag{2.36}$$

The most complicated expression describes damping width

$$\begin{aligned}
Y_n^{n+1} \downarrow &= g \frac{(h+1)(h+2)}{\rho_{ph}^B(E)} \left\{ \frac{1}{2} h \rho_{p,h+2}^B(E) - \alpha \frac{1}{2} h \rho_{p,h+2}^B(E-B) \right. \\
&+ (h+3) \frac{1}{2} \rho_{p-1,h+3}^B(E) - \frac{1}{2} \alpha \left[ (h+3) \rho_{p-1,h+3}^B(E-B) \right. \\
&\left. \left. + \frac{B^2 g^2}{2(h+2)} \rho_{p-1,h+1}^B(E-B) + Bg \rho_{p-1,h+2}^B(E-B) \right] \right\}, \tag{2.37}
\end{aligned}$$

with  $\alpha$  equal 1 for  $E > B$  and 0 for  $E \leq B$ .

### 2.2.2 Gamma-emission in Multi-step Compound

The emission of  $\gamma$  in the Multi-step Compound mechanism is treated in terms of the model proposed by Hoering and Weidenmueller [51]. Application follows the paper by Herman *et al.* [52]. The model assumes that  $\gamma$  emission occurs through the deexcitation of the Giant Dipole Resonance (GDR) built within MSC classes. Following Brink-Axel hypothesis [53, 54, 55] each nuclear state serves as the basis of a GDR excitation with identical properties. Moreover, the Tamm-Dancoff approximation is used and GDR is represented as a linear combination of correlated 1p-1h states. Each MSC class  $M$ , now characterized also by its spin  $J$ , splits into four sub-classes  $M_n$ . The states in subclasses  $M_n$ , with  $n=1, 2$  and  $3$  contain GDR built on states in class  $M-1$  with spins  $J-1$ ,  $J$ , and  $J+1$ , respectively, and opposite parity. The states in class  $M_4$  are pure single particle excitations and contain no GDR.

The pure MSC-contribution to the cross section is obtained while neglecting the GDR built on the ground state, which leads to the non-statistical direct-semidirect process. The theory [51] allows for the inclusion of direct-semidirect in the formalism. However,



the implementation of direct-semidirect in the EMPIRE is oversimplified and has been disabled. On the other hand, an option is provided to start MSC calculations right from the first class. This approach lacks formal justification but brings the model closer to the treatment of  $\gamma$  emission in the classical preequilibrium models.

The average MSC cross section is given by

$$\overline{\sigma}_{a,\gamma}^{MSC} = T_{a,Mm} \Pi_{Mm,Nn} T_{Nn,\gamma}, \quad (2.38)$$

where

$$\begin{aligned} (\Pi^{-1})_{Mm,Nn} &= 2\pi\rho_{Mm}v_{Mm,Nn}2\pi\rho_{Nn} \\ &\quad + \delta_{M,N}\delta_{m,n}2\pi\rho_{Mm}(\Gamma_{Mm}^{\uparrow} + \Gamma_{Mm}^{\downarrow}) \end{aligned} \quad (2.39)$$

and  $T_a = \sum_{Mm} T_{aMm}$  are the optical model transmission coefficients.

The transmission coefficients for the  $E1$ - $\gamma$  channel are defined, as for the particle channel, in terms of the unitarity deficit of the average  $S$ -matrix.

$$T_{\gamma} = 1 - \left| \overline{S}_{\gamma\gamma} \right|^2. \quad (2.40)$$

This is directly proportional to the strength function  $f(E)$ , which can be written as a function of the absorption cross section, yielding

$$T_{\gamma}^{E_1} = \frac{1}{2\pi} \sigma_{abs}(E_{\gamma}^{E_1}) \frac{(E_{\gamma}^{E_1})^2}{(\hbar c)^2}. \quad (2.41)$$

The absorption cross section has a Lorentzian form and is given by

$$\sigma_{abs}(E_{\gamma}^{E_1}) = \sigma_{res} \frac{(E_{\gamma}^{E_1})^2 \Gamma_{res}^2}{((E_{\gamma}^{E_1})^2 - E_{res}^2)^2 + (E_{\gamma}^{E_1})^2 \Gamma_{res}^2}. \quad (2.42)$$

For the resonance energy  $E_{res}$ , the resonance width  $\Gamma_{res}$ , and the peak cross section  $\sigma_{res}$ , the experimental or systematics data are used as input parameters. As in the case of particle emission, the average matrix element  $v_{Mm,Nn}$  coupling non-collective states of two exciton classes is determined from the imaginary part of the optical model potential.

Next, we will analyze the individual matrix elements  $(\Pi^{-1})_{Mm,Nn}$ . We begin by investigating the non-diagonal block  $(\Pi^{-1})_{Mm,(M+1)n} = 2\pi\rho_{Mm}v_{Mm,(M+1)n}^2 2\pi\rho_{(M+1)n}$ , i. e., the transition from a state in exciton class  $M$  to a state in the next higher exciton class  $(M+1)$ . There are four different types of matrix elements:

- decay of a GDR,
- the single particle transitions leaving the GDR unchanged,
- transitions among non-collective states,
- GDR creation.

Computation of these four types of matrix elements is discussed below.

(i) The matrix element  $(\Pi^{-1})_{Mm,(M+1)4}$ ,  $m = 1, 2$  or  $3$  describes the decay of a GDR via coupling to the next higher exciton class. This process is responsible for the spreading width of the GDR. In colliding with a bound particle the GDR loses its coherence and the bound particle is excited into an excited state thus creating another particle-hole state. This matrix element can be written as

$$2\pi\rho_{Mm}v_{Mm,(M+1)4}^2 2\pi\rho_{(M+1)4} = 2\pi\rho_{Mm}\Gamma_{GDR}^\downarrow. \quad (2.43)$$

For the width of the GDR the experimental value is used. Unfortunately, there is little literature on how this width is separated into spreading and decay width. It is known that for heavy nuclei the spreading width is dominant, whereas for light nuclei the reverse is true. For  $^{208}\text{Pb}$  approximately 90% of the width is due to the spreading width. For  $^{16}\text{O}$ , on the other hand, 90% of the width is due to the decay width [56]. This separation can be entered into the calculations as an input parameter. The result depends only weakly on this coefficient. The level densities  $\rho_{Mm}^{J,\pi}(E)$  for  $m = 1, 2, 3$  are given by the exciton level densities  $\rho_{M-1}^{(J-1),-\pi}(E - E_{GDR})$ ,  $\rho_{M-1}^{J,-\pi}(E - E_{GDR})$  and  $\rho_{M-1}^{(J+1),-\pi}(E - E_{GDR})$ , respectively. These correspond to the level densities of the non-collective states on which GDR is built. Implicitly, all of them are for bound configurations.

(ii) The matrix element  $(\Pi^{-1})_{Mm,(M+1)n}$ ,  $m, n=1, 2, 3$  describes the transition of a GDR-state in class  $M$  to a GDR-state in class  $(M+1)$ . In such a transition the GDR is not affected and is just a “spectator”. This is again a consequence of the two-body nature of the residual interaction. The subclasses 1, 2, 3 differ only in the angular momenta of the non-collective states the GDR is built on. Since a transition among these states must not change the angular momentum this part is diagonal in the subclass indices, i. e.  $(\Pi^{-1})_{Mm,(M+1)m} \neq 0$ , only. Thus, these matrix elements are given by

$$(\Pi^{-1})_{Mm,(M+1)m} = 2\pi\rho_{Mm}v_{n.c.}^2 2\pi\rho_{Mm \rightarrow (M+1)m}^{acc}, \quad (2.44)$$

where  $\rho_{Mm}^J(E)$ ,  $m = 1, 2, 3$ , is the exciton level density  $\rho_{M-1}^{(J',-\pi)}(E - E_{GDR})$  with  $J' = (J-1), J, (J+1)$ ,  $\rho_{Mm \rightarrow (M+1)m}^{acc}(E)$ ,  $m = 1, 2, 3$  are the accessible state densities  $\rho_{(M-1),J \rightarrow M,J'}^{acc}(E - E_{GDR})$  with  $J' = (J-1), J, (J+1)$ , respectively.  $v_{n.c.}$  stands for the average transition matrix element between two non-collective states of neighboring exciton classes.

(iii) The matrix element  $(\Pi^{-1})_{M4,(M+1)4}$  describes transitions between non-collective states only. The matrix element is again expressed through the average transition strength  $v_{n.c.}$  between two non-collective states

$$(\Pi^{-1})_{M4,(M+1)4} = 2\pi\rho_{M4}(E)v_{n.c.}^2 2\pi\rho_{M4 \rightarrow (M+1)4}^{acc}(E). \quad (2.45)$$

(iv) The matrix element  $(\Pi^{-1})_{M4,(M+1)m}$  with  $m = 1, 2$ , and  $3$  describes the creation of a GDR in the next higher exciton class. In the current version of EMPIRE the total GDR width is taken to describe this process<sup>1</sup>. However, the creation of a GDR is possible only if a

<sup>1</sup>This may overestimate creation rate of the GDR. Other approaches are to use non-collective matrix element or the GDR width split among the neighboring classes. To activate these possibilities the user has to edit MSC-NVWY.f file and uncomment adequate lines in both of the following ranges 1028-1036 and 1093-1106.

particle or a hole has enough energy to create the GDR state. This is another consequence of the two-body nature of the residual interaction. A particle with the excitation energy of the GDR resonance is generally unbound. Thus, only a hole can contribute. The probability for a hole to have the required energy  $\epsilon$  within the configuration with the total exciton number  $(p + h)$  is given by

$$P(\epsilon) = N \frac{\rho(p, h - 1, E - \epsilon)}{\rho(p, h, E)}, \quad (2.46)$$

where  $\rho(p, h - 1, E - \epsilon)$  is the level density of the remaining excitons after removing a hole of the energy  $\epsilon$  and  $\rho(p, h, E)$  is the total level density at energy  $E$  for  $(p + h)$  excitons.  $N$  is the normalization constant.

$$\frac{1}{N} = \int_0^E \frac{\rho(p, h - 1, E - \epsilon)}{\rho(p, h, E)} d\epsilon = \frac{\rho(p, h - 1, E)}{\rho(p, h, E)(p + h - 1)}. \quad (2.47)$$

Hence, the probability for a hole to have the energy  $E \geq E_{GDR}$  is given by

$$\begin{aligned} \int_{E_{GDR}}^E P(\epsilon) d\epsilon &= \frac{(p + h - 1)}{\rho(p, h - 1, E)} \int_{E_{GDR}}^E \rho(p, h - 1, E - \epsilon) d\epsilon \\ &= \frac{\rho(p, h - 1, E - E_{GDR})}{\rho(p, h, E)}. \end{aligned} \quad (2.48)$$

Collecting everything yields

$$(\Pi^{-1})_{M4, (M+1)m} = 2\pi \rho_{M4}(E) \Gamma_{GDR}^\downarrow \frac{\rho(p, h - 1, E - E_{GDR})}{\rho(p, h, E)}. \quad (2.49)$$

Thus, all four types of matrix elements within the block  $(M, M + 1)$  have been determined. The matrix element  $(\Pi^{-1})_{(M+1)m, Mn}$  is obtained using the symmetry properties of the matrix  $\Pi^{-1}$ . The diagonal elements of this matrix are then obtained by summation:

$$(\Pi^{-1})_{Mm, Mm} = \sum_{n=1}^4 (\Pi^{-1})_{Mm, (M+1)n} + \sum_{n=1}^4 (\Pi^{-1})_{Mm, (M-1)n} + \sum_c T_{Mm, c}. \quad (2.50)$$

The matrix  $\Pi^{-1}$  is inverted numerically and used in Eq. 2.38 to calculate  $\gamma$ -emission spectra.

## 2.3 Coupling between MSC and MSD

The NVWY theory includes a possibility of feeding higher MSC classes directly from the MSD chain, in addition to the normal transitions between bound states of increasing complexity. This process is taken in to account by a double sum over classes in the cross section formula (Eq. 2.26). The second sum over  $n$  refers to the contribution of different classes to the particle emission, while the first one (over  $m$ ) corresponds precisely to the

population of various classes directly from the open channel space rather than through the transitions along the MSC chain. This effect is included in the EMPIRE code by distributing the incoming channel transmission coefficient over different MSC classes. For the time being, it is done according to phase space and global coupling arguments requiring that the incoming flux splits between the first MSD and MSC classes in proportion to the respective state densities and to the average value of the squared matrix elements coupling unbound to unbound ( $\langle V_{uu}^2 \rangle$ ) and unbound to bound states ( $\langle V_{ub}^2 \rangle$ ). Introducing  $R = \langle V_{ub}^2 \rangle / \langle V_{uu}^2 \rangle$ , denoting the optical model transmission coefficient by  $T_{om}$ , the density of bound and unbound states in class  $n$  by  $\rho_n^b$  and  $\rho_n^u$  respectively, and their sum by  $\rho$ , the transmission coefficient populating the first MSC class may be written as

$$T_1 = T_{om} \frac{\langle V_{ub}^2 \rangle \rho_1^b(E)}{\langle V_{ub}^2 \rangle \rho_1^b(E) + \langle V_{uu}^2 \rangle \rho_1^u(E)} = T_{om} \frac{R}{(R-1) + \frac{\rho_1^u(E)}{\rho_1^b(E)}} \quad (2.51)$$

The same reasoning may be applied to the flux remaining in the open space, which may enter the MSC chain in subsequent steps of the reaction. Assuming  $R$  to be independent of the class number the transmission coefficient  $T_n$  populating the  $n^{th}$  MSC class is written as

$$T_n = \left( T_{om} - \sum_{i=1}^{n-1} T_i \right) \frac{R}{(R-1) + \frac{\rho_n^u(E)}{\rho_n^b(E)}} \quad (2.52)$$

If the MSD option is selected the absorption cross section available to MSC ( $\sigma_{abs}$ ) is reduced by the total MSD emission cross section ( $\sigma_{MSD}$ ) in order to ensure flux conservation and becomes:

$$\sigma_{abs}(J) = \sigma_{OM}(J) \left( 1 - \frac{\sigma_{MSD}}{\sigma_{OM}} \right), \quad (2.53)$$

where  $\sigma_{OM}$  is optical model reaction cross section and  $J$  stands for the compound nucleus spin.

The MSD emission populates residual nucleus continuum. Spin distribution of this population is assumed to be proportional to the spin distribution of  $1p-1h$  states shifted by the spin of the target ground state. This approximation is imposed by the current structure of the ORION code which performs summations over angular momentum in the incident channel, thus making exact angular momentum coupling impossible. Choice of the  $1p-1h$  spin distribution reflects dominant contribution of the first step of the MSD, which leaves the residual nucleus in the 2-exciton state.

The MSD cross section to the discrete states is calculated if the keyword MSD is equal 2 (default MSD=1). In that case the MSD cross section to discrete levels is distributed arbitrarily among 2+, 3-, and 4+ states with relative weights 4:2:1 respectively and inversely proportional to the squared distance between the energy of the populated level and the energy of the level to which field parameters in the response functions were fitted. In the case of an odd nucleus all levels with spins that differ from 2+, 3-, and 4+ by 1/2

are assumed to belong to the respective spin multiplet. There was no attempt to treat MSD population of discrete levels more accurately as this kludge can be removed by using strict Coupled-Channels calculations that include explicitly both vibrational and rotational levels with a proper momentum coupling.



# Chapter 3

## Phenomenological preequilibrium models

Two preequilibrium models are described in this section, the classical exciton model including nucleon, cluster and gamma emissions, and the Monte Carlo DDHMS inspired by Blann's Hybrid model that is limited to nucleon emission. The former includes only the first pre equilibrium emitted particle and is therefore valid up to about 50 MeV. The latter also includes multiple preequilibrium emission, which extends its applicability to much higher energies. The exciton model code DEGAS implementing full angular momentum coupling in pre equilibrium emission of nucleons and gammas has been temporarily disabled due to incompatibilities with the current system.

### 3.1 Exciton model (PCROSS code)

The module PCROSS includes the pre-equilibrium mechanism as defined in the exciton model [57], as based on the solution of the master equation [58] in the form proposed by Cline [59] and Ribansky [60]

$$\begin{aligned} -q_{t=0}(n) = & \lambda_+(E, n+2)\tau(n+2) + \\ & \lambda_-(E, n-2)\tau(n-2) - \\ & [\lambda_+(E, n) + \lambda_-(E, n) + L(E, n)] \\ & \tau(n), \end{aligned} \tag{3.1}$$

where  $q_t(n)$  is the initial occupation probability of the composite nucleus in the state with the exciton number  $n$ ,  $\lambda_+(E, n)$  and  $\lambda_-(E, n)$  are the transition rates for decay to neighboring states, and  $L(n, E)$  is the total emission rate integrated over emission energy for particles (protons  $\pi$ , neutrons  $\nu$  and clusters) and  $\gamma$ -rays. Note that no spin is included in the PCROSS formulation, which is the main difference from the DEGAS treatment. To obtain the numerical solution of the system of algebraic equations for  $\tau(n)$ , given in Eq. (3.1), the algorithm proposed by Akkermans, Gruppelaar and Reffo [61] is used.

This produces the exact result for any initial condition of the problem. As PCROSS calculates only the pre-equilibrium contribution to the reaction, it uses the *never-come-back* assumption, meaning that only transitions that increase the complexity of the system (and therefore the exciton number) are allowed, an approximation valid when  $\lambda_+(E, n) \gg \lambda_-(E, n)$ . Integrating the master equation over time, one obtains the solution  $\tau(n)$ , which represents the time during which the system remains in the state characterized by  $n$  excitons. The pre-equilibrium spectra can be calculated as

$$\frac{d\sigma_{a,b}}{d\epsilon_b}(\epsilon_b) = \sigma_{a,b}^r(E_{inc}) D_{a,b}(E_{inc}) \times \sum_n W_b(E, n, \epsilon_b) \tau(n), \quad (3.2)$$

where  $\sigma_{a,b}^r(E_{inc})$  is the cross section of the reaction  $(a, b)$ ,  $W_b(E, n, \epsilon_b)$  is the probability of emission of a particle of type  $b$  (or gamma ray) with energy  $\epsilon_b$  from a state with  $n$  excitons and excitation energy  $E$  of the CN, and  $D_{a,b}(E_{inc})$  is the depletion factor, which takes into account the flux loss as a result of the direct reaction processes. Using the direct reaction cross section  $\sigma_{a,b}^{dir}(E_{inc})$ , the depletion factor can be calculated in the following manner,

$$D_{a,b}(E_{inc}) = 1 - \frac{\sigma_{a,b}^{dir}(E_{inc})}{\sigma_{a,b}^r(E_{inc})}. \quad (3.3)$$

A brief description of the main components of the exciton model as coded in the PCROSS module is given below.

**Particle/hole state densities** The equidistant spacing model has been used extensively to derive closed analytical formulae for partial state densities  $\omega(p, h, U)$  employed in pre-equilibrium models (for a review see Ref.[35]). At present, the PCROSS code uses the Williams formula [62], where the Pauli correction  $A(p, h)$  is calculated in accordance with Kalbach's method [63].

$$\omega(p, h, E) = g \frac{(g(E - D) - A(p, h))^{p+h-1}}{p!h!(p+h-1)!} \quad (3.4)$$

$$A(p, h) = \frac{1}{4} [p(p-1) + h(h-1)].$$

The state density  $\omega(p, h, U)$  is set to zero when the excitation energy  $E$  is less than the Pauli energy  $\frac{1}{4g} [p^2 + h^2]$  [64]. It was pointed out by Blann [65] that the state density should be corrected by the depth of the potential well. The potential depth corrections formulated by Betak and Dobes [66] are used in PCROSS employing the simplified expressions obtained by Kalbach [67, 63].



**Internal transition rates.** In the PCROSS code, the parametrization of transition rate proposed by Blann and Mignerey [68] is used. This is based on experimental data of nucleon scattering and considers the Pauli principle in an approximate way. Using this parametrization and the particle-hole state densities from the Williams formula, one obtains the expressions for the internal transition rates found by Machner [69]

$$\lambda_+(E, n) = \frac{1}{K_{mfp}} \left[ 1.4 \times 10^{21} E' - \frac{2}{n+1} 6 \times 10^{18} E'^2 \right]. \quad (3.5)$$

In the PCROSS code, the additional 3/8 factor introduced by Gupta [70] is taken into account on the r.h.s. of Eq. (3.5). This factor results from the reduction of a two-component master equation (i.e. with the neutron-proton distinction) to an effective one-component equation [70]. Taking also into account the direct reaction contribution, as mentioned above, one usually obtains a value of 1.1-1.6 for the mean free path parameter  $K_{mfp}$ . The increase of this parameter above unity could be expected, as effects such as parity and angular momentum conservation are not considered in the Blann parameterization [68]. These effects taken together would produce an increase of the nucleon mean free path in the nuclear matter. The assumed default value of 1.3 for this parameter is in good agreement with the one employed in typical hybrid model calculations.

**Probability of nucleon emission** Kalbach's method [58, 59, 67] was implemented for the calculation of the nucleon emission rate. The expression for the nucleon emission probability is derived applying the principle of detailed balance in a way similar to what is done in the evaporation model. The probability of emission  $W_b(E, n, \epsilon_b)$  of a nucleon  $b$  with spin  $s_b$ , reduced mass  $\mu_b$  and energy  $\epsilon_b$  from a state with  $n$  excitons is given by,

$$W_b(E, n, \epsilon_b) = \frac{2s_b + 1}{\pi^2 \hbar^3} \mu_b \epsilon_b \sigma_b^{inv}(\epsilon_b) \times \frac{\omega_{res}(p - b, h, U)}{\omega_{CN}(p, h, E)} Q_b(p, h), \quad (3.6)$$

where  $E(U)$  is the excitation energy of the CN (residual nucleus),  $\omega(p, h, U)$  is the particle-hole state density, and  $\sigma_b^{inv}(\epsilon_b)$  is the inverse channel reaction cross section. The factor  $Q_b(p, h)$  takes into account the fraction of  $b$  nucleons in the  $n$ -th stage of the reaction and is calculated as discussed by Gupta [70].

**Probability of cluster emission.** The module PCROSS includes a pre-equilibrium mechanism for clusters in the incoming and outgoing channels by including the Iwamoto-Harada model [71] parametrized and improved in [72, 73, 74]. In this model, the formation probability of a cluster takes into account excitons below and above the Fermi surface and avoids free parameters. In the Iwamoto-Harada model the probability of emission of the cluster  $\beta$  with spin  $s_\beta$ , reduced mass  $\mu_\beta$  and energy  $\epsilon_\beta$  from a state with  $n$  excitons is given

by

$$W_\beta(E, n, \epsilon_\beta) = \frac{2s_\beta + 1}{\pi^2 \hbar^3} \mu_\beta \epsilon_\beta \sigma_\beta^{inv}(\epsilon_\beta) \times \frac{\sum_{l+m=\beta} F_{lm}^\beta(\epsilon_\beta) Q_{lm}^\beta(p, h) \omega_{res}(p-l, h, U)}{\omega_{CN}(p, h, E)}, \quad (3.7)$$

where the factor  $Q_{lm}^\beta(p, h)$  is the generalization of the factor  $Q_b(p, h)$  which takes into account the probability of the outgoing cluster  $\beta$  being formed with  $l$  particles situated above and  $m$  below the Fermi surface ( $\beta = l + m$ ) [74] and the factor  $F_{lm}^\beta(\epsilon_\beta)$  gives the probability of formation of the cluster  $\beta$  as a function of its energy. This last factor is calculated in PCROSS following the unpublished parametrization based on the original calculations of the cluster formation probability by Iwamoto and Harada [71].

Fig. 3.1 illustrates the essential improvement brought by the Iwamoto-Harada model to the interpretation of  $\alpha$ -particle emission in the  $^{197}\text{Au}(n, \alpha)$  reaction.



Figure 3.1: Improvement in the description of the  $^{197}\text{Au}(n, \alpha)$  reaction achieved by employing the Iwamoto-Harada model for pre-equilibrium emission of  $\alpha$ -particles.

**Probability of gamma emission** The probability of emission of gamma radiation (without spin selection rules) is derived in a way similar to the nucleon emission prob-

ability by applying the principle of detailed balance [75, 76, 77] and can be expressed as

$$W_\gamma(E, n, \epsilon_\gamma) = \frac{1}{\pi^2 \hbar^3 c^2} \epsilon_\gamma^2 \sigma_\gamma^{inv}(\epsilon_\gamma) \times \frac{\sum_k b(k \rightarrow n, \epsilon_\gamma) \omega_{res}(p, h, U)}{\omega_{CN}(p, h, E)}. \quad (3.8)$$

Coefficients  $b(k \rightarrow n, \epsilon_\gamma)$  are the branching ratios derived by Gruppelaar and Akkermans [77]. The inverse reaction cross section  $\sigma_\gamma^{inv}(\epsilon_\gamma)$  in the gamma channel is calculated taking into account only the contribution of the GDR.

**Initial and equilibrium number of excitons** Calculations in the PCROSS module start with exciton number  $n = 1$ , thus taking into account the direct gamma emission. The equilibrium exciton number is taken equal to  $\sqrt{1.4gE}$  [73, 74].

The exciton model, as implemented in the PCROSS code, has been extensively used in recent evaluations. Combined with the direct contributions described in terms of the CC+DWBA models, it gave an excellent description of the forward inelastic scattering of neutrons on  $^{232}\text{Th}$  in the energy range from 6.1 MeV up to 18 MeV, as can be seen in Fig. 3.2.

The 18-MeV emission spectra at 60 degrees extracted from the recent IAEA evaluation included in the ENDF/B-VII library is compared to previous evaluations in Fig. 3.3. The advanced modeling resulted in a dramatic improvement of the high energy part of the spectrum compared to the previous evaluations.

## 3.2 Monte Carlo Preequilibrium (DDHMS code)

The Hybrid Monte-Carlo Simulation (HMS) approach to the pre-equilibrium emission of nucleons has been formulated by M. Blann [79] as a hybrid-model [80, 81, 82, 83] inspired version of the intranuclear cascade approach. Contrary to other classical pre-equilibrium models, this approach avoids multi-exciton level densities, which were shown by Bisplinghoff [84] to be used inconsistently in the exciton and in the hybrid formulations. The HMS model has a number of attractive features. First of all, there are no physical limits on the number of pre-equilibrium emissions (apart from energy conservation). With the addition of linear momentum conservation by M. Chadwick and P. Obložinský (DDHMS), the model provides a nearly complete set of observables. These include cross sections for the production of residuals, light-particle double-differential spectra and spectra of recoils. Spin and excitation-energy dependent populations of residual nuclei can also be obtained, an essential feature for coupling the pre-equilibrium mechanism to the subsequent compound nucleus decay. The binding energies in the HMS model are thermodynamically correct. The DDHMS model proved to perform very well up to at least 250 MeV. The calculation flow in the DDHMS model can be summarized in terms of the following steps:

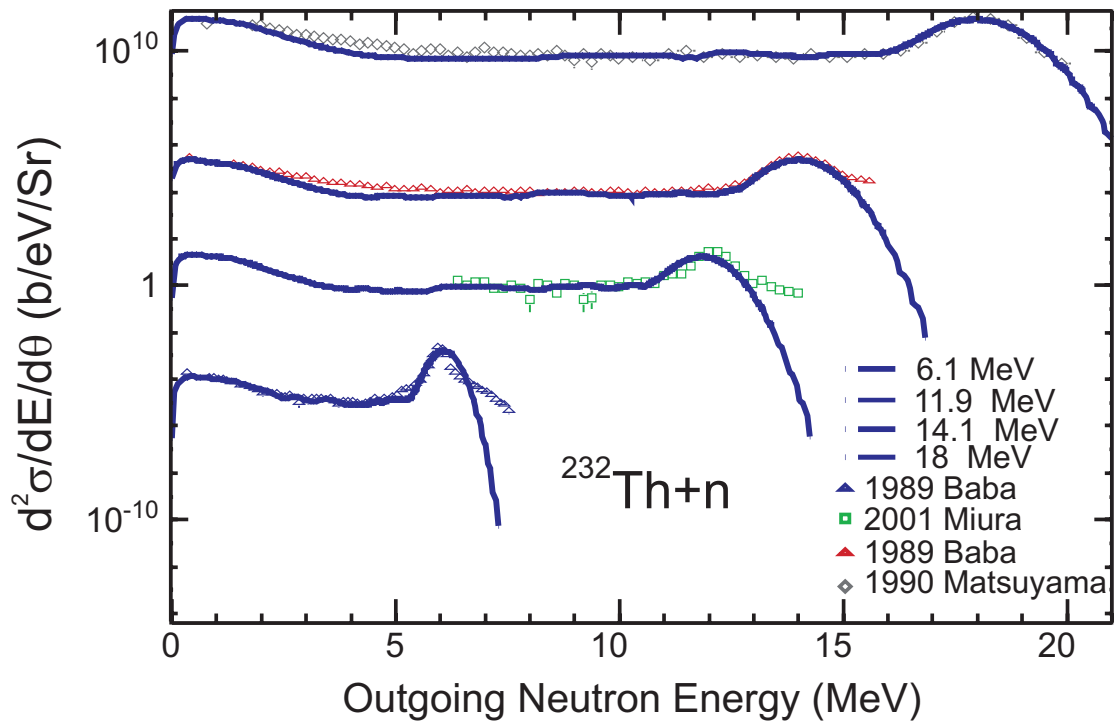


Figure 3.2: EMPIRE calculations of the spectra of neutrons emitted at 30 degrees for 6.1, 11.9, 14.1 and 18 MeV neutrons incident on  $^{232}\text{Th}$  (scaled by 1,  $10^3$ ,  $10^6$  and  $10^9$  respectively). Fission neutrons are not included.

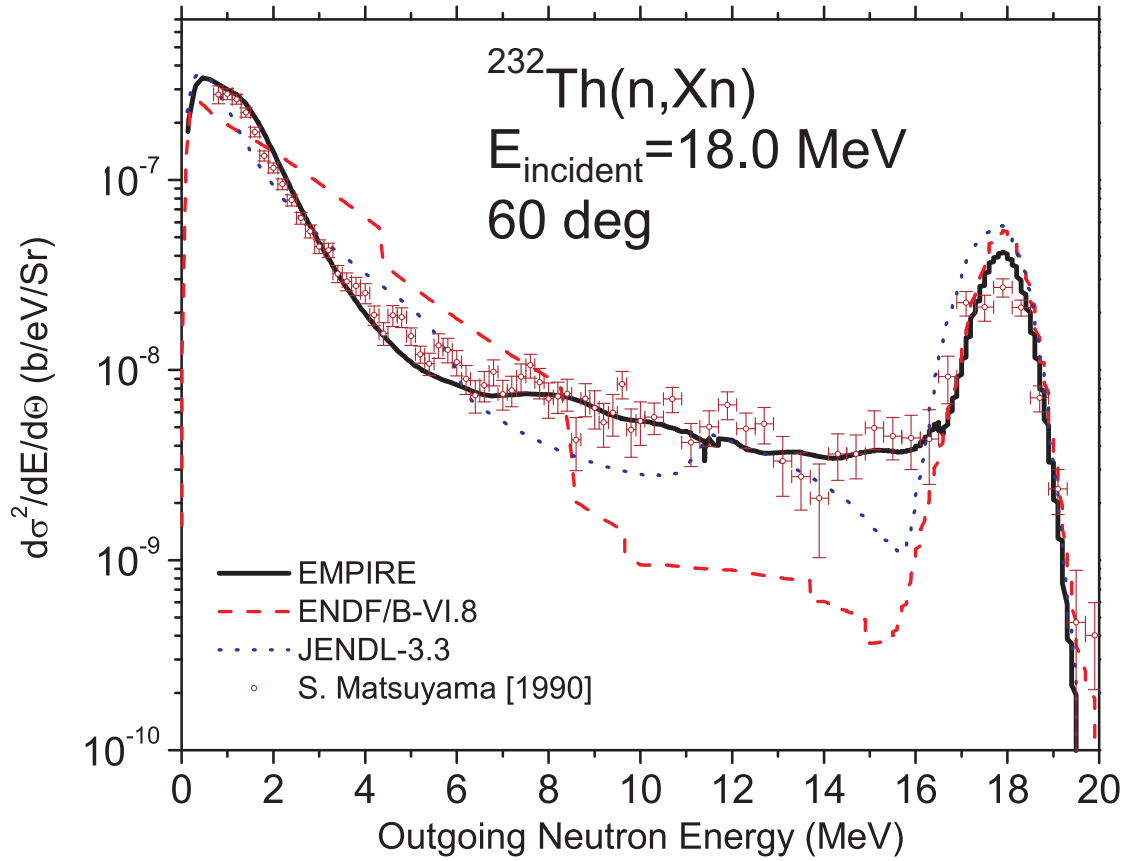


Figure 3.3: EMPIRE calculation for the neutron emission spectrum at 60 degrees for an incident neutron energy of 18.0 MeV on  $^{232}\text{Th}$ , compared to experimental data [78] and the ENDF/B-VI.8 and JENDL-3.3 libraries.

1. draw a collision partner for the incoming nucleon (2p-1h state created)
2. draw the energy ( $\varepsilon$ ) of the scattered nucleon (if bound go to step 5)
3. draw scattering angles for both particles
4. decide whether the scattered nucleon will be emitted, re-scattered or trapped
  - (a) if emitted, the appropriate cross section is augmented
  - (b) if re-scattered, an additional particle-hole is created and one returns to step 2
  - (c) if trapped, go to step 5
5. draw the excitation energy of a particle in the remaining 1p-1h configurations (between 0 and  $(U-\varepsilon)$ ), if unbound go to step 3, if bound choose another existing 1p-1h pair and repeat step 5.

All excitons (including holes) are treated on an equal footing and each of them is given a chance to interact or be emitted with *a priori* equal probability. The cascade ends when all excitons are bound. Below, we summarize various probability distributions which are used in concert with a random number generator. For choosing a collision partner, it is assumed that the unlike interaction is 3 times more probable than the like one ( $\sigma_{np} = 3\sigma_{nn}$ ). Thus, for an incident neutron we have  $P_{nn}$  and  $P_{np}$  for the probability of exciting neutron and proton respectively

$$P_{nn} = \frac{(A - Z)}{(A - Z) + 3Z}, \quad (3.9)$$

$$P_{np} = 1 - P_{nn} \quad (3.10)$$

and similarly for an incident proton

$$P_{pp} = \frac{Z}{Z + 3(A - Z)}, \quad (3.11)$$

$$P_{pn} = 1 - P_{pp}. \quad (3.12)$$

The energy distribution of the scattered particles  $P(\varepsilon)$  is given by the ratio of the  $(n-1)$ - and  $n$ -exciton level densities  $\rho_n$

$$P(\varepsilon)d\varepsilon = \frac{\rho_{n-1}(E - \varepsilon)g}{\rho_n(E)}d\varepsilon, \quad (3.13)$$

with  $n = 2$  or  $3$  and

$$\rho_2(E) = \frac{g(gV)}{2} \text{ if } E > V, \quad (3.14)$$

$$\rho_2(E) = \frac{g(gE)}{2} \text{ if } E \leq V, \quad (3.15)$$

$$\rho_3(E) = \frac{g^3 [V(2E - V)]}{4} \text{ if } E \geq V. \quad (3.16)$$

Here,  $V$  is the potential well depth. The emission probability is calculated as

$$P_\nu(\varepsilon - Q) = \frac{\lambda_c(\varepsilon - Q)}{\lambda_c(\varepsilon - Q) + \lambda_+(\varepsilon)}, \quad (3.17)$$

with the emission rate being

$$\lambda_c(\varepsilon - Q) \sim \frac{\sigma_\nu(\varepsilon - Q)(\varepsilon - Q)(2S + 1)\mu_\nu}{g}. \quad (3.18)$$

Here,  $\sigma_\nu$  is the inverse reaction cross section,  $Q$  is the binding energy,  $g$  is the single-particle density,  $S$  denotes nucleon spin, and  $\mu_\nu$  stands for the reduced nucleon mass. Following the hybrid model,  $\lambda_+(\varepsilon)$  is calculated from the mean free path of a nucleon in nuclear matter. The version which is actually implemented in EMPIRE was coded by M. Chadwick and extended to double-differential cross sections in collaboration with P. Obložinský [13].

Figure 3.4 presents the effect of the HMS contribution on spectrum of neutrons emitted from  $^{208}\text{Pb}$  bombarded with 14.6 MeV neutrons. The compound nucleus emission underestimates the experimental data starting at  $\sim 5$  MeV, and at higher emission energies it is practically negligible. The HMS model contribution is of the right order of magnitude to bring the calculations into reasonable agreement with the measurements. One notes, however, that the model still fall short of the experimental data above 8 MeV. This deficiency could be counteracted by adjusting the HMS input parameters (e.g., single-particle level densities) but such an intervention would be unphysical. The real reason for the discrepancy is the lack of a direct reaction contribution in the calculations reported in Fig. 3.4.

### 3.3 Compatibility of preequilibrium models

Possible inclusions of different preequilibrium models in a single calculation run rises a problem of double-counting. The current version of EMPIRE has 4 modules for preequilibrium decay: MSD, MSC, HMS and PCROSS. While MSD and MSC describe different reaction mechanisms and are complementary, neither of them is compatible with HMS or PCROSS. Therefore, neither of the latter two can be used together with MSD or MSC in the same exit channel. Also HMS and PCROSS mutually exclude each other. However, these models can be combined if used in different exit channels, e.g., neutron inelastic scattering may be calculated using MSD&MSC while the emission of protons can be treated within the exciton model using PCROSS. We also note that summing  $\gamma$ -emission spectra from more than one of the two possible mechanisms (MSC (GST=1 option) or PCROSS) would be obvious multiple-counting and must be avoided.

An additional complication is introduced by the possibility of using ECIS06 or OPTMAN code, which calculate Coupled-Channel contributions to the collective discrete levels. In general, these contributions are so strong that adding those provided by the exciton

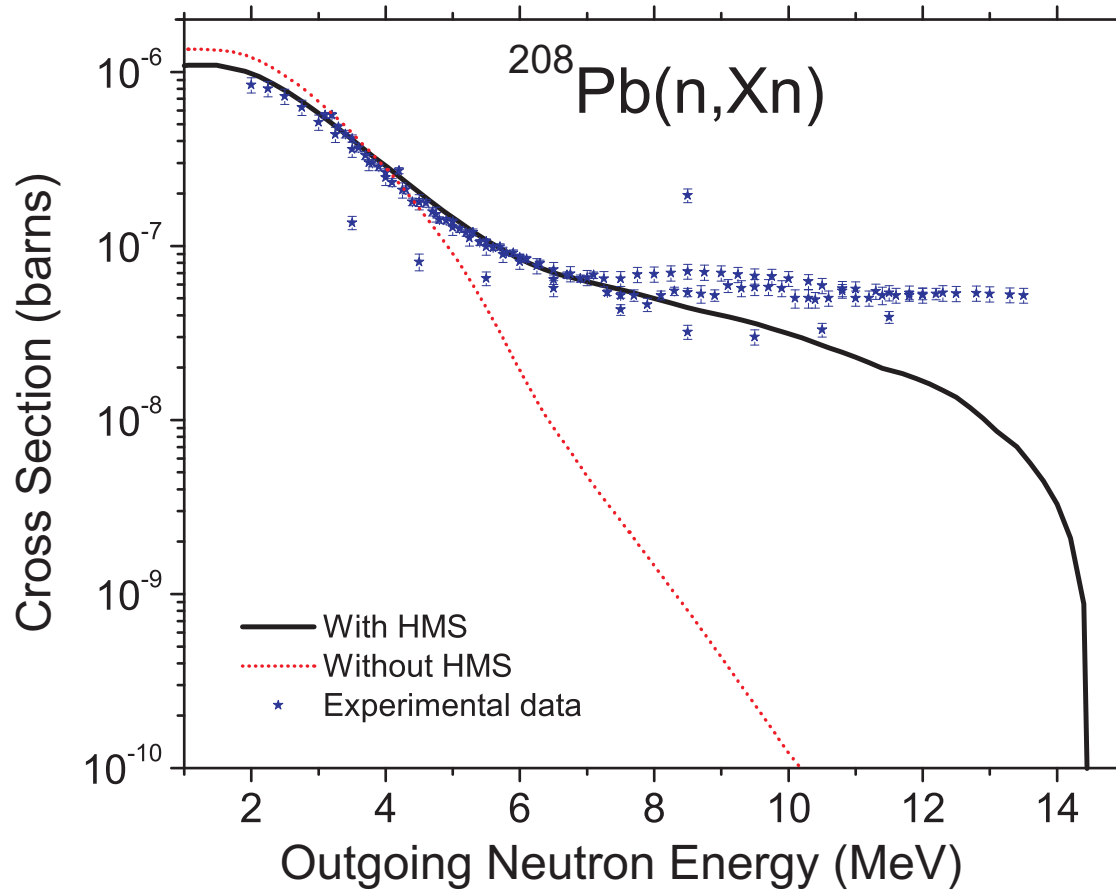


Figure 3.4: Contribution of the pre-equilibrium processes, modeled using Monte Carlo simulation, to neutron spectrum from the  $^{208}\text{Pb}(n, xn)$  reaction at 14.6 MeV.



model leave the results practically unchanged. Thus, ECIS06/OPTMAN can be considered compatible with HMS since the latter does not include collective excitations. By the same token ECIS06/OPTMAN codes are not compatible with MSD as both include collectivity of discrete levels. However, ECIS06/OPTMAN and MSD can be combined providing that only the continuum contribution from the MSD is retained.

To avoid double-counting when combining different models EMPIRE applies the following priorities:

**ECIS06 or OPTMAN** provides inelastic scattering to collective levels independently of the settings for the remaining models.

**MSD** provides inelastic continuum independently of other settings. Inelastic to the discrete levels is suppressed if ECIS06 is active. Note the provision for the second-chance preequilibrium emission after MSD.

**MSC** results are taken for the inelastic to the continuum. Charge-exchange to the continuum is accepted if not suppressed by use of HMS or PCROSS.

**HMS** provides inelastic and charge-exchange to the continuum and to discrete levels if MSD and MSC are not active. Otherwise only the charge-exchange contribution is used. Suppresses PCROSS results for particle emission if such was calculated. HMS does not provide  $\gamma$ -rays, thus PCROSS or MSC results are adopted.

**PCROSS** provides inelastic and charge-exchange to the continuum if these are not provided by any of the above listed models. Provides  $\gamma$ -emission if not suppressed by  $\gamma$ -emission from MSC. Provides preequilibrium emission of clusters independently of settings for other models.

This scheme allows the user to activate any combination of reaction mechanisms while the code ensures the internal consistency of calculations. Overlapping contributions from various models are summed up and the Compound Nucleus contribution is added in all cases. A concise summary explaining use of the models is printed as a table at the beginning of the lengthy output *\*.lst*. An example is reproduced below:

#### Use of direct and preequilibrium models

Exit channel	ECIS	MSD	MSC	HMS	PCROSS
neut. disc.	0	1	0	0	0
neut. cont.	0	1	1	0	0
prot. disc.	0	0	0	0	0
prot. cont.	0	0	0	0	1
gammas	0	0	0	0	1
alpha cont.	0	0	0	0	1

1 indicates that the contribution of the model is included, and 0 means that it is not calculated or ignored. In the above example, MSD, MSC and PCROSS were invoked, and priority rules caused PCROSS neutron contribution to be suppressed leaving emission of protons and clusters.

Selecting DIRECT =1 (or 2 or 3), MSD=1, MSC=1, PCROSS=1.5 is supposed to give the best results at low incident nucleon energies (say up to 50 MeV). At higher incident energies the preference should be given to the HMS model, which is the only one that accounts for the multiple preequilibrium emission. When selecting appropriate models the user should take into account that not all of them provide the same set of observables. For example, preequilibrium  $\gamma$ -emission can be obtained from PCROSS or MSC but not from HMS.

# Chapter 4

## Compound nucleus model

### 4.1 Compound Nucleus

The statistical model used in the EMPIRE is an advanced implementation of the Hauser-Feshbach theory. The exact angular momentum and parity coupling is observed. The emission of neutrons, protons,  $\alpha$ -particles, deuterons, tritons, and He-3 is taken into account along with the competing fission channel. The full  $\gamma$ -cascade in the residual nuclei is considered.

To account for the correlation between incident and exit channels in elastic scattering (width fluctuation correction) the model proposed by Hofmann, Richert, Tepel and Weidenmueller (HRTW) [1] is used. This model is briefly reviewed in the next subsection. Particular attention is dedicated to the determination of the level densities, which can be calculated in the non-adiabatic approach allowing for the rotational and vibrational enhancements (see Section 4.2).

In the Hauser-Feshbach model the  $(a, b)$  reaction cross section is written as:

$$\sigma_{a,b}(E) = \sum_{J\pi} \sigma_a^{CN}(E, J\pi) P_b(E, J\pi) \quad (4.1)$$

where  $\sigma_a^{CN}(E, J\pi)$  is the cross section of the compound nucleus formation in a state of spin and parity  $J\pi$  associated to the incident channel  $a$  and  $P_b(E, J\pi)$  represents the decay probability of the compound nucleus with the excitation energy  $E_x$  in  $b$  channel. The decay probability is defined in terms of transmission coefficients

$$P_b(E, J\pi) = \frac{T_b(E_x, J\pi)}{\sum_c T_c(E_x, J\pi)} \quad (4.2)$$

associated to the reaction channels which might be particles emission, photon emission or fission.

The transmission coefficient for the  $p$  particle emission has the expression

$$T_p(E, J\pi) = \sum_{I=|J-j|}^{I=J+j} \int_0^{E_x-B_p} \sum_{lj} T_{p,lj}(E_x - B_p + \varepsilon) \rho(\varepsilon, I\pi_I) \delta(\pi\pi_I, (-1)^l) d\varepsilon \quad (4.3)$$

where  $B_p$  is the separation energy of particle  $p$  in the compound nucleus,  $\rho(\varepsilon, I\pi_I)$  is the density of levels in the residual nucleus with the spin and parity  $I, \pi_I$  and the excitation energy  $\varepsilon$ , and  $T_{p,lj}$  stands for the transmission coefficient (discussed in Chapter ...) having channel energy  $E_x - B_p - \varepsilon$  and orbital angular momentum  $l$ , which together with the particle spin  $s$  couples to the channel angular momentum  $j$  used to select in the residual nucleus spins  $I$  populated for a given compound nucleus spin  $J$ . The factor  $\delta(\pi\pi_I, (-1)^l)$  stands for parity conservation. For the discrete levels (characterized by the energy  $E_i$ , spin  $I_i$ , and parity  $\pi_{I_i}$ ) the level density  $\rho(\varepsilon, I, \pi_I)$  reduces to  $\delta(\varepsilon - E_i)\delta(I, I_i)\delta(\pi_I, \pi_{I_i})$ . A similar expression is used for the gamma-decay coefficient

$$T_\gamma(E_x, J\pi) = \sum_{XL} \sum_{J'=|J-L|}^{|J+L|} \int_0^{E_x} f_{XL}(\varepsilon_\gamma) \rho(E_x - \varepsilon_\gamma, J', \pi') \delta(\pi\pi', (-1)^L) d\varepsilon_\gamma \quad (4.4)$$

where  $XL$  represents the photon type and multipole,  $J'\pi'$  are the spin and parity of the final states and  $f_{XL}(\varepsilon_\gamma)$  is the  $\gamma$ -ray strength function discussed in more detail in Section 4.3. The fission coefficients are presented in Section 4.4.

It should be mentioned that the above equations also hold for secondary CNs that are formed due to subsequent emissions of particles. The only difference is that while the first CN is initially excited to the unique (incident channel compatible) energy, the secondary CNs are created with excitation energies which spread over the available energy interval.

### 4.1.1 Width fluctuation correction

To account for the correlation between incident and exit channels in elastic scattering we use model proposed by Hofmann, Richert, Tepel and Weidenmueller (HRTW) [1]. In the case of no direct reaction contribution, the averaged  $S$ -matrix element connecting channels  $a$  and  $b$  can be written as

$$\langle S \rangle_{ab} = \delta_{ab} e^{i\zeta_{ab}} (1 - T_a)^{1/2}, \quad (4.5)$$

where

$$T_a = 1 - |\langle S \rangle_{aa}|^2 \quad (4.6)$$

is an optical model transmission coefficient. The HRTW model assumes that the Compound Nucleus (CN) cross sections factorize and can be expressed through a product of the channel dependent quantities  $\xi$ . This would be the famous Bohr's assumption if not

for the elastic enhancement factor  $W_a$ , which has been introduced by HRTW in order to account for the elastic channel correlation

$$\langle \sigma_{ab}^{fl} \rangle = \xi_a \xi_b \quad a \neq b \quad \text{and} \quad \langle \sigma_a^{fl} \rangle = W_a \xi_a^2. \quad (4.7)$$

Setting

$$\xi_a = \frac{V_a}{\sqrt{\sum_c V_c}} \quad (4.8)$$

we get for the CN cross section

$$\sigma_{ab}^{CN} \equiv \langle \sigma_{ab}^{fl} \rangle = V_a V_b \left( \sum_c V_c \right)^{-1} [1 + \delta_{ab} (W_a - 1)]. \quad (4.9)$$

Taking into account that the incoming flux has to be conserved (unitary condition) we find the relation between  $V$ s, the elastic enhancement factor ( $W_a$ ), and the transmission coefficient ( $T_a$ )

$$V_a = T_a \left[ 1 + \frac{V_a}{(\sum_c V_c)} (W_a - 1) \right]^{-1}. \quad (4.10)$$

This equation can be solved for  $V_a$  by iteration once all  $W_a$  are known. The current version of EMPIRE uses  $W_a$  derived from the analysis of numerically generated sets of  $S$ -matrices [2]. The resulting formula for the elastic enhancement factor is

$$W_a = 1 + 2 [1 + T_a^F]^{-1} + 87 \left( \frac{T_a - T_{ave}}{\sum_c T_c} \right)^2 \left( \frac{T_a}{\sum_c T_c} \right)^5, \quad (4.11)$$

with

$$F = 4 \frac{T_{ave}}{\sum_c T_c} \left( 1 + \frac{T_a}{\sum_c T_c} \right) \left( 1 + 3 \frac{T_{ave}}{\sum_c T_c} \right)^{-1}, \quad (4.12)$$

which completes formulation of the model.

## 4.2 Level densities

In EMPIRE the level densities are described by several models with the corresponding parametrizations. Three of them are phenomenological (Gilbert-Cameron Model (GCM), Generalized Superfluid Model (GSM), Enhanced Generalized Superfluid Model (EGSM)) and one is based on Hartree-Fock-Bogoliubov microscopic model (HFBM). All of them are included also in RIPL. Another common feature is that they are parametrized or normalized to reproduce the average parameters of the neutron resonances and the data on the cumulative number of low-lying nuclear levels. Choice of the proper representation depends on a case being considered.

The best known and used level density analytical expression was derived within Fermi-Gas Model (FGM), therefore the basic relations of FGM are presented in subsection 4.2.1. The following subsections are dedicated to each of the above four models.

### 4.2.1 Basic relations of Fermi-Gas Model

The density of intrinsic levels with spin  $J$ , parity  $\pi$  and excitation energy  $E_x$  is factorised in terms of state density and spin and parity dependence as

$$\rho(E_x, J, \pi) = \rho(E_x)\rho(J, \pi). \quad (4.13)$$

The energy dependence reads

$$\rho(E_x) = \frac{\exp S}{\sqrt{Det}} \quad (4.14)$$

where  $S$  is the entropy and  $Det$  is defined by Eq.4.16.

The spin and parity dependence is given by

$$\rho(J, \pi) = \frac{1}{2} \frac{(2J+1)}{\sqrt{8\pi\sigma^3}} \exp \left[ -\frac{(J+1/2)^2}{2\sigma^2} \right] \quad (4.15)$$

where  $\sigma^2$  is the spin cut-off parameter and equal parity distribution is assumed.

For the Fermi-Gas model the state equations determining the dependence of the excitation energy, entropy and other thermodynamic functions of a nucleus on its temperature  $T$  are

$$E_x = aT^2; \quad S = 2aT; \quad \sigma^2 = \Im T; \quad Det = 144a^3T^5/\pi \quad (4.16)$$

where  $a$  is the level density parameter and  $\Im$  is the nuclear moment of inertia.

To account for the odd-even effects in nuclei, the excitation energy is replaced in calculations with the effective energy  $U$

$$U = E_x - \Delta \quad (4.17)$$

where  $\Delta$  is equal or closely related to the pairing energy.

Introducing Eqs.4.16, 4.17 in Eq.4.14 the well known expression for the state density is obtained

$$\rho^{FG}(E_x) = \frac{\sqrt{\pi}}{12a^{1/4}U^{5/4}} \exp(2\sqrt{aU}) \quad (4.18)$$

and the level density becomes

$$\rho^{FG}(E_x, J, \pi) = \frac{2J+1}{48\sqrt{2}\sigma^{3/2}a^{1/4}U^{5/4}} \exp \left[ 2\sqrt{aU} - \frac{(J+1/2)^2}{2\sigma^2} \right]. \quad (4.19)$$

These equations show that nuclear level densities in Fermi-Gas model depend on three parameters:  $a$ ,  $\sigma$  and  $\Delta$ . Some general features about the energy and mass dependence of  $a$  parameter are outlined here, more details about these parameters being discussed in the subsections on various specific level density models.

The correlation between the  $a$ -parameter values deduced from the neutron resonance spacing and the shell correction and the fade-out of the shell effects with increasing the excitation energy imply energy dependence of the  $a$  parameter. The general form of this dependence was proposed by Ignatyuk [85]

$$a(E_x) = \tilde{a} \left[ 1 + f(U) \frac{\delta W}{U} \right], \quad (4.20)$$

where  $\delta W$  is the shell correction,  $\tilde{a}$  is the asymptotic value of the  $a$ -parameter and

$$f(U) = 1 - \exp(-\gamma U) \quad (4.21)$$

with  $\gamma$  being the shell effects damping parameter.

### 4.2.2 Gilbert-Cameron Model

The Gilbert-Cameron approach [86] splits excitation energy in two regions. Different functional forms of level densities are applied in each of them. The constant temperature formula applies at low excitation energies (below the matching point  $U_x$ ) and the Fermi Gas formula is used above  $U_x$

$$\rho^{GC}(E_x) = \begin{cases} \rho^{CT}(E_x) & E_x \leq U_x \\ \rho^{FG}(E_x) & E_x > U_x \end{cases} \quad (4.22)$$

The constant temperature level density reads

$$\rho^{GC}(E_x, J, \pi) = \rho^{GC}(E_x) \rho(J, \pi) \quad (4.23)$$

with  $\rho(J, \pi)$  from Eq. 4.15.

In the constant temperature region the state density is

$$\rho^{CT}(E_x) = \frac{1}{T} \exp\left(\frac{E_x - E_0}{T}\right) \quad (4.24)$$

where  $T$  is the nuclear temperature and  $E_0$  is a free parameter. The three model parameters,  $T$ ,  $U_x$ , and  $E_0$  are determined by the requirement that the level density and its derivative are continuous at the matching point  $U_x$ , and by fitting cumulative number of discrete levels with the integral of Eq. 4.22.

The Fermi Gas state density  $\rho^{FG}(E_x)$  is given by Eq. 4.18 where the effective excitation energy is  $U = E_x - \Delta$ . The pairing energy is calculated as

$$\Delta = n \frac{12}{\sqrt{A}} \quad (4.25)$$

where  $n=0,1$  and 2 for odd-odd, odd-A and even-even nuclei respectively.

The calculation can be performed using constant or energy dependent  $a$ -parameter. The constant  $a$ -parameter is read from input (GCROA). Alternatively can be used the general form given by Eq. 4.20 which accounts for the shell effects, and their fade-out with increasing energy. The three relevant systematics available in EMPIRE are:

**Ignatyuk *et al.* [85]** :  $\tilde{a} = 0.154A + 6.3 \cdot 10^{-5}A^2$  and  $\gamma = -0.054$

**Arthur [87]** :  $\tilde{a} = 0.1375A - 8.36 \cdot 10^{-5}A^2$  and  $\gamma = -0.054$

**Iljinov *et al.* [88]** :  $\tilde{a} = 0.114A + 9.80 \cdot 10^{-2}A^{2/3}$  and  $\gamma = -0.051$

The spin cut-off factor  $\sigma(E_x)$  is given by

$$\sigma^2(E_x) = 0.146A^{2/3}\sqrt{aU}. \quad (4.26)$$

We stress that Gilbert-Cameron approach does not account explicitly for the collective enhancements of the level densities. These are included implicitly in the  $\tilde{a}$  when fitting neutron resonance spacings. Such an approach leads to the over-estimation of the level densities above, say, 20 MeV.

For the nucleon induced reactions, with CN excited up to about 20 MeV, the Gilbert-Cameron approach is recommended. It assures an accurate description of level densities in the energy range up to the neutron binding energy. The collective effects are included in the level density parameter  $a$ , providing reasonable estimate of the level densities as long as damping of the collective effects is irrelevant. The relatively low angular momentum introduced by the incident projectile justifies neglect of dynamical effects.

### 4.2.3 Generalized Superfluid Model

The phenomenological version of the Generalized Superfluid Model (GSM) is characterized by a phase transition from superfluid behaviour at low energy [85, 89], where pairing correlations strongly influence the level density, to a high energy region which is described by the FGM. Thus, the GSM resembles the GC to the extent that the model distinguishes between a low energy and a high energy region, although for the GSM this distinction follows naturally from the theory and does not depend on specific discrete levels that determine a matching energy.

The influence of the superconducting pairing correlations on nuclear properties can be characterized by the value of the correlation function  $\Delta_0$ , which determines directly the even-odd differences in the nuclear binding energies and the energy gap of  $2\Delta_0$  in the spectrum of quasi-particle excitations in even-even nuclei. The critical temperature  $T_c$  of the phase transition from a superfluid to a normal state is connected with the correlation function through the relation

$$T_c = 0.567\Delta_0. \quad (4.27)$$

The excitation energy corresponding to the critical temperature, i.e., the critical energy  $U_c$ , may be expressed as

$$U_c = a_c T_c^2 + E_{cond}, \quad (4.28)$$

where  $E_{cond}$  is the condensation energy for the even-even nucleus that determines a reduction of the nuclear ground state energy due to the pairing correlations

$$E_{cond} = \frac{3}{2\pi^2} a_c \Delta_0^2. \quad (4.29)$$

The critical value of the determinant  $Det_c$ , and the critical entropy  $S_c$  are defined by the following expressions

$$Det_c = \left( \frac{12}{\sqrt{\pi}} \right)^2 a_c^3 T_c^5, \quad (4.30)$$



$$S_c = 2a_c T_c. \quad (4.31)$$

The parallel and perpendicular moments of inertia at the critical energy are calculated in terms of deformation as

$$\mathfrak{S}_{\parallel c} = \frac{6}{\pi^2} a_c \langle m^2 \rangle (1 - \frac{2}{3}\beta_2) \quad (4.32)$$

$$\mathfrak{S}_{\perp c} = \frac{6}{\pi^2} a_c \langle m^2 \rangle (1 + \frac{1}{3}\beta_2) \quad (4.33)$$

where  $a_c$  is the critical value of the level density  $a$ -parameter and  $\langle m^2 \rangle$  is the average value of the square of the projection of angular momentum for single-particle states on the Fermi surface parametrized as  $\langle m^2 \rangle = 0.24A^{2/3}$ .

One can notice that all the critical values described above are expressed in terms of the correlation function  $\Delta_0$  estimated as  $\Delta_0 = 12/\sqrt{A}$  and the critical  $a_c$ -parameter determined by the iteration procedure

$$a_c^{(0)} = \tilde{a} (1 + \gamma \delta_W) \quad (4.34)$$

$$U^{(n)} = a_c^{(n)} T_c^2 \quad (4.35)$$

$$a_c^{(n+1)} = \tilde{a} \left[ 1 + \frac{\delta_W}{U^{(n)}} (1 - \exp(-\gamma U^{(n)})) \right]. \quad (4.36)$$

where  $\tilde{a}$  is the asymptotic value of the level density parameter. Eqs. 4.35 and 4.36 are iterated until the condition

$$\frac{|a^{(n+1)} - a^{(n)}|}{a^{(n+1)}} < 0.001 \quad (4.37)$$

is fulfilled.

Both below and above the critical energy the quasi-particle level density has the same expression given by Eqs. 4.13, 4.14, 4.15

$$\rho_{qp}(E_x, J, \pi) = \frac{\exp S}{\sqrt{Det}} \frac{1}{2} \frac{(2J+1)}{\sqrt{8\pi\sigma_{eff}^3}} \exp \left[ -\frac{(J+1/2)^2}{2\sigma_{eff}^2} \right] \quad (4.38)$$

but with the thermodynamic quantities defined differently.

The calculations are performed for the effective excitation energy

$$U = E_x + n\Delta_0 + \delta_{shift} \quad (4.39)$$

where  $\Delta_0 = 12/\sqrt{A}$  and  $n=0, 1$  and  $2$  for even-even, odd-A and odd-odd nuclei, respectively. The energy shift  $\delta_{shift}$  was introduced to account for possible shortcomings of the global systematics.

At effective excitation energies below  $U_c$ , in the energy range where the superconductivity model BCS [90] applies, the function  $\varphi$  is introduced

$$\varphi = \sqrt{1 - U/U_c}, \quad (4.40)$$

which allows to express all thermodynamical quantities in terms of their critical values. Above  $U_c$  the condensation energy is subtracted from the effective excitation energy

$$U^* = U - E_{cond}. \quad (4.41)$$

The quantities entering GSM formulation are calculated with the following expressions

$$a = \begin{cases} a_c & U \leq U_c \\ \tilde{a}[1 + \delta W(1 - \exp(-\gamma U^*))/U^*] & U > U_c \end{cases} \quad (4.42)$$

$$T = \begin{cases} 2\varphi T_c / \ln \frac{\varphi+1}{1-\varphi} & U \leq U_c \\ \sqrt{\frac{U^*}{a}} & U > U_c \end{cases} \quad (4.43)$$

$$S = \begin{cases} S_c T_c (1 - \varphi^2)/T & U \leq U_c \\ 2aT & U > U_c \end{cases} \quad (4.44)$$

$$\text{Det} = \begin{cases} \text{Det}_c (1 - \varphi^2)(1 + \varphi^2)^2 & U \leq U_c \\ 144a^3 T^5 / \pi & U > U_c \end{cases} \quad (4.45)$$

$$\mathfrak{S}_{\parallel} = \begin{cases} \mathfrak{S}_{\parallel c} T_c (1 - \varphi^2)/T & U \leq U_c \\ \mathfrak{S}_{\parallel c} & U > U_c \end{cases} \quad (4.46)$$

$$\mathfrak{S}_{\perp} = \begin{cases} \frac{1}{3}\mathfrak{S}_{\perp} + \frac{2}{3}\mathfrak{S}_{\perp} T_{crit} (1 - \varphi^2)/T & U \leq U_c \\ \mathfrak{S}_{\perp c} & U > U_c \end{cases} \quad (4.47)$$

Squares of the effective spin cut-off parameters are defined as

$$\begin{aligned} \sigma_{eff}^2 &= \mathfrak{S}_{\parallel} T & \text{for } \beta_2 < 0.005, \\ \sigma_{eff}^2 &= (\mathfrak{S}_{\parallel})^{1/3} (\mathfrak{S}_{\perp}^{BCS})^{2/3} T & \text{for } \beta_2 > 0.005, \end{aligned} \quad (4.48)$$

with  $\beta_2$  being ground state deformation.

The final expression of the GSM level density is obtained by adding to Eq. 4.38 in an adiabatic mode the rotational and vibrational enhancements ( $K_{rot}$ ,  $K_{vib}$ ) and their damping with increasing energy ( $Q_{rot}$ ,  $Q_{vib}$ ) that results in

$$\rho(E_x, J, \pi) = \rho_{qp}(E_x, J, \pi) K_{rot} Q_{rot} K_{vib} Q_{vib}. \quad (4.49)$$

**Rotational enhancement.** In the adiabatic approximation, the rotational enhancement of the level density depends on the nuclear shape symmetry and can be written as [44]

$$K_{rot} = \begin{cases} 1 & \text{for spherical nuclei,} \\ \mathfrak{S}_{\perp} T & \text{for deformed nuclei.} \end{cases} \quad (4.50)$$

This formula is valid if the mirror and axial symmetry of a deformed nuclei is assumed. The most stable nuclei of the rare-earth elements ( $150 \leq A \leq 190$ ) and the actinides  $A \geq 230$  are of this shape. For non-axial forms the rotational enhancement of the level density becomes greater [44] (see fission level densities in Section 4.4).

Over the previous twenty years, some microscopic models have been developed to consider collective effects in highly excited nuclei. The results of all these models demonstrate the damping of level density enhancement factors with increase of excitation energy. On the basis of the level density calculations within the SU(3) model (oscillator mean field with quadrupole-quadrupole interaction between particles), Hansen and Jensen [91] obtained the following empirical function for the rotational damping factor

$$Q_{rot} = q_r \left[ 1 - \frac{1}{\mathfrak{S}_\perp T} \right] + \frac{1}{\mathfrak{S}_\perp T} \quad (4.51)$$

with

$$q_r = \frac{1}{1 + \exp[(U - U_r)/d_r]} , \quad (4.52)$$

Originally it was supposed that the damping parameters could strongly depend upon nuclear deformations. However, the analysis of heavy nuclei fissilities [92, 93] shows that damping is independent of deformation with the corresponding parameters  $U_r = 40$  MeV and  $d_r = 10$  MeV. Of course, uncertainties of these parameters are rather large and additional confirmations are required. Nevertheless, it seems that the damping of the rotational enhancement is comparable with the damping of the shell effects in magic nuclei. The two terms in Eq. 4.71 ensure that  $Q_{rot} = 0$  at  $U = 0$  and tends to 1 for  $U \rightarrow \infty$ . We note that  $1/\mathfrak{S}_\perp t$  is approximately equal to the rotational enhancement and therefore multiplication of the level densities by Eq. 4.70 actually removes rotational enhancement when  $Q_{rot} = 1$ .

$$U \rightarrow 0 \quad q_r \rightarrow 1 \quad Q_{rot} \rightarrow 1 \quad (4.53)$$

$$U \rightarrow \infty \quad q_r \rightarrow 0 \quad Q_{rot} \rightarrow 1/K_{rot} \quad (4.54)$$

**Vibrational enhancement.** The vibrational enhancement of the level density can be approximated by the equation

$$K_{vib} = \exp[\delta S - (\delta U/T)] , \quad (4.55)$$

where  $\delta S$  and  $\delta U$  are changes in the entropy and excitation energy, respectively, that result from the vibrational modes. These changes are described by the Bose gas relationships:

$$\begin{aligned} \delta S &= \sum_i (2\lambda_i + 1) [(1 + n_i) \ln(1 + n_i) - n_i \ln n_i] , \\ \delta U &= \sum_i (2\lambda_i + 1) \omega_i n_i , \end{aligned} \quad (4.56)$$

where  $\omega_i$  are the energies,  $\lambda_i$  are the multipolarities, and  $n_i$  are the occupation numbers for vibrational excitations at a given temperature. The disappearance of collective enhancement of the level density at high temperatures can be taken into account by defining the occupation numbers in terms of the equation:

$$n_i = \frac{\exp(-\gamma_i/2\omega_i)}{\exp(\omega_i/T) - 1} , \quad (4.57)$$

where  $\gamma_i$  are the spreading widths of the vibrational excitations. This spreading of collective excitations in nuclei should be similar to the zero-sound damping in a Fermi liquid, and the corresponding width can be written as

$$\gamma_i = C(\omega_i^2 + 4\pi^2 T^2) . \quad (4.58)$$

A value of  $C = 0.0075A^{1/3} \text{ MeV}^{-1}$  was obtained from the systematics of the neutron resonance densities of medium-weight nuclei [94]. This analysis adopted experimental values for the  $\omega_2$  energies of the first  $2^+$  excitation when available, otherwise the parametrizations  $\omega_2 = 30A^{-2/3} \text{ MeV}$  was used. Energies  $\omega_3 = 50A^{-2/3} \text{ MeV}$  were adopted for the octupole excitations. Due to the higher energies, the influence of the octupole enhancement is much weaker than for the quadrupole excitations.

For selected nuclei for which experimental information exist the precalculated asymptotic value of  $a$ -parameter,  $\omega_2$ , and  $\Delta_0$  from RIPL-3 were included in `/data/level-densities-par.dat` and used by EMPIRE. For the other nuclei the asymptotic  $a$ -parameter is parametrized as:

$$\tilde{a} = \alpha A + \beta A^{2/3} \quad \gamma = \gamma_0 A^{1/3} \quad (4.59)$$

with the global parameters from RIPL-2 TECDOC obtained using Myers-Swiiatecki shell correction (including the deformation term) are

$$\alpha = 0.103 \quad \beta = -0.105 \quad \gamma_0 = 0.375. \quad (4.60)$$

The energy shift (in MeV) is approximated by the relationship:

$$\delta = 0.61700 - 0.00164A. \quad (4.61)$$

#### 4.2.4 Enhanced Generalized Superfluid Model

The properly parametrized Enhanced Generalized Superfluid Model (EGSM) [95] (including adjustment to discrete levels) is the default level density formulation in the EMPIRE code; therefore, it is also referred as 'Empire Global Specific Model'.

The EGSM uses, as GSM, the super-fluid model below critical excitation energy and the Fermi Gas model above. Enhancement compared to GSM relates mainly to the spin distribution in the Fermi Gas model. It includes a more accurate treatment of high angular momenta which are important for the heavy-ion induced reactions.

The rotational energy in EGSM is subtracted from the intrinsic excitation energy. This contrasts with the treatment in the models discussed before, in which the spin dependence

is treated as a separate factor characterized by a spin cutoff parameter. The collective enhancement of the level density arising from nuclear rotation is taken into account in non-adiabatic form. Level densities acquire dynamic features through the dependence of the rotational enhancement on the shape of a nucleus. The deformation enters level densities formulas through moments of inertia and through the level density parameter  $a$  that increases with increase in the surface of the nucleus.

The effective excitation energy in EGSM is related to the excitation energy by the relationship

$$U = E_x + n\Delta_0, \quad (4.62)$$

where  $\Delta_0 = 12\sqrt{A}$  is taken as the average correlation function of the ground state  $n=0, 1$  and 2 for even-even, odd-A and odd-odd nuclei, respectively.

Below the critical energy  $U_c$ , the quasi-particle excitations' density  $\rho_{qp}(E_x, J, \pi)$  is calculated according to Eq.4.38. The nuclear level density in this low energy region reads

$$\rho(E_x, J, \pi) = \rho_{qp}(E_x, J, \pi) K_{rot} Q_{rot} K_{vib} Q_{vib} \quad U \leq U_c \quad (4.63)$$

with the collective enhancements and their damping coefficients defined by Eqs.4.69-4.77.

Above the critical energy, an energy shift equal to the condensation energy is introduced

$$U^* = U - E_{cond}. \quad (4.64)$$

In EGSM and in this energy range the level densities calculation implies the subtraction of the rotational energy from the intrinsic excitation energy. This contrasts with the treatment in the models discussed before, in which the spin dependence is treated as a separate factor characterized by a spin cutoff parameter. The collective enhancement of the level density arising from nuclear rotation is taken into account in non-adiabatic form. Level densities acquire dynamic features through the dependence of the rotational enhancement on the shape of a nucleus. The deformation enters level densities formulas through moments of inertia and through the level density parameter  $a$  that increases with increase in the surface of the nucleus.

Assuming that the prolate nuclei rotate along the axis perpendicular to the symmetry axis the explicit level density formulas reads

$$\begin{aligned} \rho(E_x, J, \pi) = & \frac{1}{16\sqrt{6}\pi} \left( \frac{\hbar^2}{\mathfrak{I}_{\parallel}} \right)^{\frac{1}{2}} a^{-1/4} \sum_{K=-J}^J \left( U^* - \frac{\hbar^2 K^2}{2\mathfrak{I}_{eff}} \right)^{-\frac{5}{4}} \\ & \exp \left\{ 2 \left[ a \left( U^* - \frac{\hbar^2 K^2}{2\mathfrak{I}_{eff}} \right) \right]^{\frac{1}{2}} \right\} Q_{rot} K_{vib} Q_{vib}. \end{aligned} \quad (4.65)$$

In the case of the oblate nuclei which are assumed to rotate parallel to the symmetry axis

we have

$$\begin{aligned} \rho(E_x, J, \pi) = & \frac{1}{16\sqrt{6}\pi} \left( \frac{\hbar^2}{\mathfrak{S}_{\parallel}} \right)^{\frac{1}{2}} a^{-1/4} \\ & \sum_{K=-J}^J \left( U^* - \frac{\hbar^2 [J(J+1) - K^2]}{2|\mathfrak{S}_{eff}|} \right)^{-\frac{5}{4}} \\ & \exp \left\{ 2 \left[ a \left( U^* - \frac{\hbar^2 [J(J+1) - K^2]}{2|\mathfrak{S}_{eff}|} \right) \right]^{\frac{1}{2}} \right\} Q_{rot} K_{vib} Q_{vib}. \end{aligned} \quad (4.66)$$

The effective moment of inertia  $\mathfrak{S}_{eff}$  is defined in terms of the perpendicular  $\mathfrak{S}_{\parallel}$  and parallel  $\mathfrak{S}_{\perp}$  moments through the difference of their inverses

$$\frac{1}{\mathfrak{S}_{eff}} = \frac{1}{\mathfrak{S}_{\parallel}} - \frac{1}{\mathfrak{S}_{\perp}}. \quad (4.67)$$

. The parallel and perpendicular moments of inertia are calculated according to Eqs. 4.85 and 4.86.

It should be stressed that Eqs. 4.65 and 4.66 include summation over projection of the angular momentum  $K$  and thus automatically account for the rotational enhancement. The yrast line is obtained, setting level densities to 0 whenever the rotational energy becomes larger than  $U$ .

In the limit of  $J \gg K$  Eqs. 4.65 and 4.66 are equivalent to

$$\rho(E_x, J, \pi) = \frac{\exp S}{\sqrt{Det}} \cdot \frac{1}{2} \cdot \frac{(2J+1)}{\sqrt{8\pi\sigma_{eff}^3}} \exp \left[ -\frac{(J+1/2)^2}{2\sigma_{eff}^2} \right] K_{rot} Q_{rot} K_{vib} Q_{vib}. \quad (4.68)$$

**Rotational enhancement.** As mentioned, the rotational enhancement is accounted for above  $U_c$ , but has to be considered explicitly for energies lower than the critical energy or in the limit of  $J \gg K$ . As in GSM, the rotational enhancement entering Eqs. 4.63 and 4.68 reads

$$K_{rot} = \mathfrak{S}_{\perp} T. \quad (4.69)$$

The damping of the rotational enhancement is

$$Q_{rot} = 1 - q_r \left( 1 - \frac{1}{\mathfrak{S}_{\perp} T} \right). \quad (4.70)$$

where  $q_r$  is a damping function which, following Junghans *et al.* [96], is assumed to be deformation independent

$$q_r = \frac{1}{1 + \exp \left( -\frac{E_{cr}}{d_{cr}} \right)} - \frac{1}{1 + \exp \left( \frac{U - E_{cr}}{d_{cr}} \right)} \quad (4.71)$$

with  $E_{cr} = 40$  MeV and  $d_{cr} = 10$  MeV. The two terms in Eq. 4.71 ensure that  $q_r = 0$  at  $U = 0$  and tends to 1 for  $U \rightarrow \infty$ . We note that  $\mathfrak{S}_\perp T$  is equal to the rotational enhancement and therefore multiplication of the level densities by Eq. 4.70 actually removes rotational enhancement when  $Q_{rot} = 1$ .

$$U \rightarrow 0 \quad q_r \rightarrow 0 \quad Q_{rot} \rightarrow 1 \quad (4.72)$$

$$U \rightarrow \infty \quad q_r \rightarrow 1 \quad Q_{rot} \rightarrow 1/K_{rot} \quad (4.73)$$

**Vibrational enhancement.** In EGSM the vibrational enhancement is simulated on the basis of the liquid drop parametrizations of vibrational modes [89]

$$K_{vib} = \exp \left[ C \left( \frac{\rho_0 R^3}{4\pi \hbar^2 \alpha} \right)^{2/3} T^{4/3} \right] \quad (4.74)$$

where the nuclear matter density, the nuclear radius and the coefficient of the surface tension are given by

$$\rho_0 = \frac{3m_0}{4\pi r_0^3}; \quad R = r_0 A^{1/3}; \quad \alpha = \frac{a_s}{4\pi r_0^2} \quad (4.75)$$

with the nucleon mass  $m_0 = 939$  MeV, the reduced nuclear radius  $r_0 = 1.26$  Fm, the phenomenological surface parameter  $a_s = 17$  MeV and  $C = 1.7$ .

As nuclear temperature  $T$  increases the vibrational enhancement is damped by the factor

$$Q_{vib} = 1 - q_v \left( 1 - \frac{1}{K_{vib}} \right) \quad (4.76)$$

with

$$q_v = \frac{1}{\exp \left( 1 - \frac{T - T_{1/2}}{DT} \right)}. \quad (4.77)$$

and  $T_{1/2} = 1$  MeV,  $DT = 0.1$  MeV taken as default. These constants are to certain extent arbitrary, since there are no reliable global estimates deduced from experiments or theory. The above liquid drop expressions were preferred over the seemingly more advanced formulations, such as Eqs. (4.55) -(4.58), since the liquid drop approach, after including damping of the vibrational enhancement, provides lower values supported by physically sound microscopic calculations.

The parameters  $\alpha, \beta$  and  $\gamma_0$  defining  $\tilde{a}$  and therefore the level density parameter at the neutron separation energy  $a(B_n)$ , were obtained by fitting average S-wave neutron resonance spacings  $D_{obs}$  compiled in RIPL-3. The original Myers-Swiiatecki shell-corrections listed in */RIPL/density/shellcorr-ms.dat* file were adopted.

The CERNLIB code MINUIT was employed to minimize  $f_{rms}$  quantity defined by

$$f_{rms} = \exp \left[ \frac{1}{N_e} \sum_{i=1}^{N_e} \ln^2 \frac{D_{th}^i}{D_{exp}^i} \right]^{1/2}, \quad (4.78)$$

where  $N_e$  is the number of nuclei considered. We prefer  $f_{\text{rms}}$  over the typical  $\chi^2$  minimization since the latter tends to be oversensitive to the outliers. The resulting global EGSM systematics is represented by the following set of parameters:

$$\begin{aligned}\alpha &= 0.0748 \\ \beta &= 0.0 \\ \gamma_0 &= 0.5609\end{aligned}\tag{4.79}$$

These parameters yield  $f_{\text{rms}} = 1.7$ . The corresponding value of  $\chi^2$  is 27.2 per degree of freedom and could be reduced by a factor of two if  $\chi^2$  were minimized instead of  $f_{\text{rms}}$ . In the latter case, however, the resulting  $D_{\text{obs}}$ , driven by a few reportedly very accurate measurements, would be considerably higher. Minimizing  $f_{\text{rms}}$ , we choose to rely on the bulk of experiments rather than on a few with very small uncertainties.

Notable feature of the EGSM parametrization is the vanishing role of the nuclear surface term and the linear dependence of “experimental” asymptotic  $\tilde{a}$  values on  $A$ . In particular, we note complete absence of the shell effects - a strong argument in favour of the collective enhancements and shell corrections adopted in the EGSM.

Contrary to other level density models, the EGSM global systematics does not account for discrete levels. Instead, the adjustment is performed automatically when level densities are calculated. The shift is applied to the excitation energy to reproduce cumulative number of levels at the energy corresponding to the highest level considered in the calculations. This shift is linearly decreased with increasing energy in such a way to reach zero at the neutron binding. Therefore, adjustment to discrete levels never changes level densities at, and above, neutron binding energy ensuring that the global EGSM systematics is independent from the number of adopted discrete levels. We stress, however, that level densities below neutron binding energy strongly depend on the selection of discrete levels, thus the user advised to inspect carefully cumulative plots generated by the EGSM code to ensure that a proper number of levels be included in the calculations.

### Nuclear deformation and moments of inertia

The shape of each nucleus affects such parameters as the Giant Dipole Resonance, level density parameters  $a$  and rotational enhancement of the level densities. This shape is estimated by the code by summing up ground state deformation and dynamic deformation induced by the rotation of the nucleus. The ground state deformation is taken from Nix & Moller [97], and the dynamic deformation is taken to be proportional to the square of the angular momentum  $I$ . Ground state deformation  $\alpha_{g.s.}$  is damped with the increasing nuclear temperature, since nuclei are known to become spherical at high excitation energies. The dynamic deformation  $\alpha_{2dyn}$  is calculated following Vigdor and Karwowski [98]

$$\alpha_{2dyn} \approx b(-1.25y/(1-x)),\tag{4.80}$$



where  $b$  is treated as an adjustable parameter. The angular momentum parameter  $y$  is given by

$$y = 1.9249I(I+1)\frac{I(I+1)}{\eta A^{7/3}} \quad (4.81)$$

and the fissility parameter is given by

$$x = 0.01965\frac{Z^2}{\eta A}, \quad (4.82)$$

where  $\eta$  is the neutron-proton difference term

$$\eta = 1 - 1.7826(N - Z)^2 A^{-2}. \quad (4.83)$$

Accordingly, the deformation is parametrized as

$$\alpha_2(T, I) = \alpha_{g.s.} h(T) + \alpha_{2dyn} \quad (4.84)$$

where  $h(T) = 1/\{1 + \exp[(T-2)/0.5]\}$  damps the ground state deformation with increasing excitation and reduces the value by 50 % at temperature  $T = 2$  MeV. This value seems a reasonable estimate corresponding to about 50 MeV of excitation energy. Obviously, such a procedure is an approximation, but a more rigorous approach (e.g. using Cranking Model to determine potential surface minima at different spins and temperatures) would require prohibitive calculation times, due to the large number of intermediate nuclei involved. However, we believe that the approximation used is sufficient to provide the leading term of the effect. We note that when using this prescription, a nucleus that is deformed in the ground state will tend (at low spins) to become spherical with increasing energy. This is because of the temperature damping of the ground state and negligible contribution of the dynamic deformation at low spins. On the other hand, for  $b > 0$ , a prolate nucleus will tend to become spherical and eventually oblate with increasing angular momentum. Qualitatively, such behavior agrees with the results of the more rigorous calculations [99]. Moments of inertia for the yrast states (not the saddle-point) are calculated for deformation  $\alpha_2(T, I)$  using expressions proposed by Vigdor and Karwowski [98]

$$\begin{aligned} \mathfrak{I}_{\parallel} = \mathfrak{I}_0 & (1 - \alpha_2 + 0.429\alpha_2^2 + 0.268\alpha_2^3 - 0.212\alpha_2^4 \\ & - 1.143\alpha_2\alpha_4 + 0.494\alpha_2^2\alpha_4 + 0.266\alpha_4^2) \end{aligned} \quad (4.85)$$

$$\begin{aligned} \mathfrak{I}_{\perp} = \mathfrak{I}_0 & (1 + 0.5\alpha_2 + 1.286\alpha_2^2 + 0.581\alpha_2^3 - 0.451\alpha_2^4 \\ & + 0.571\alpha_2\alpha_4 + 1.897\alpha_2^2\alpha_4 + 0.700\alpha_4^2) \end{aligned} \quad (4.86)$$

with the rigid-sphere moment of inertia

$$\mathfrak{I}_0/\hbar^2 = 0.01448A^{5/3} \text{ MeV}^{-1}, \quad (4.87)$$

and

$$\alpha_4 = \frac{\alpha_2^2(0.057 + 0.17x + c_2y) + c_3\alpha_2y}{1 - 0.37x - c_1y}. \quad (4.88)$$

The coefficients  $c$  are

$$\begin{array}{ll} c_1 = -0.266 & c_1 = -0.70 \\ c_2 = -0.896 & \text{for } \alpha_2 < 0 \quad c_2 = 0.663 \quad \text{for } \alpha_2 > 0. \\ c_3 = -0.571 & c_3 = 0.286 \end{array} \quad (4.89)$$

The three principal-axis moments of inertia for the saddle-point are calculated with the routine MOMFIT [14] by Sierk. MOMFIT is a fit to moments of inertia calculated in 1983-1985 by Sierk at Los Alamos National Laboratory, using Yukawa-plus-exponential double-folded nuclear energy, exact Coulomb diffuseness corrections, and diffuse-matter moments of inertia. The parameters of the model are those derived by Moller and Nix in 1979:  $r_0 = 1.16$  fm,  $a_s = 21.13$  MeV,  $\kappa_s = 2.3$ , and  $a = 0.68$  fm. The diffuseness of matter and charge distributions used correspond to a surface diffuseness parameter of 0.99 fm. It should be stressed that the above mentioned computations of moments of inertia are valid up to the liquid drop stability limit. Both calculation methods (MOMFIT and expressions proposed by Vigdor and Karwowski [98]) will provide this limit. As a default, the code will restrict calculations to the partial waves below the liquid drop stability limit (even if the fusion cross section extends above this value). The user can increase this limit to the  $l$ -value at which the fission barrier disappears (including shell correction) or to specify a value in the input. In both cases, the rigid sphere moments of inertia will be taken above the liquid drop stability limit.

#### 4.2.5 Microscopic combinatorial level densities (HFBM)

Another option (LEV DEN=3) to describe the nuclear level density implemented in EMPIRE is the microscopic combinatorial approach developed during the RIPL-3 project. The method consists in using single-particle level schemes obtained from constrained axially symmetric Hartree-Fock-Bogoliubov method (HFBM) based on the BSk14 Skyrme force [100] to construct incoherent particle-hole (ph) state densities  $\omega_{ph}(E_x, M, \pi)$  as functions of the excitation energy  $E_x$ , the spin projection  $M$  (on the intrinsic symmetry axis of the nucleus) and the parity  $\pi$ . It is worth mentioning that this  $HFB + BSk14$  method is also used to provide the fission barriers and fission level densities presented in Section 4.4, thus ensuring a global coherence for the microscopic ingredients employed for nuclear reaction calculations.

The collective effects are accounted for by introducing the boson partition function described in ref. [101]. This boson partition function provides a vibrational state density  $\rho_{vib}(E_x, M, \pi)$  which depends on the various phonon's energies accounted for. Three analytical expressions based on sets of experimentally tabulated vibrational levels which systematically provide the boson partition function with quadrupole, octupole, as well as hexadecapole phonons' energies. These expressions are

$$\omega_2[\text{MeV}] = 65A^{-5/6}/(1 + 0.05E_{shell}), \quad (4.90)$$

for the quadrupole vibrations,

$$\omega_3[\text{MeV}] = 100A^{-5/6}/(1 + 0.05E_{shell}), \quad (4.91)$$

for the octupole excitations. The hexadecapole mode can be expressed relative to the quadrupole mode, leading to a similar expression, i.e.,

$$\omega_4[\text{MeV}] = 160A^{-5/6}/(1 + 0.05E_{shell}) . \quad (4.92)$$

In all these expressions, the shell correction energy  $E_{shell}$  is determined as in [102], i.e.  $E_{shell} = E_{tot} - E_{LDM}$  where  $E_{tot}$  is the experimental total binding energy [103] (or theory [100] if not available experimentally) and  $E_{LDM}$  is the phenomenological binding energy of the spherical liquid drop given by

$$E_{LDM} = a_v A + a_s A^{2/3} + (a_{sym} + a_{ss} A^{1/3}) A I^2 + a_c Z^2 A^{1/3} \quad (4.93)$$

where  $I = (N - Z)/A$ . An optimized fit to the  $N, Z \geq 8$  experimental masses of Audi et al. [103] leads to a final rms deviation of 3 MeV with the liquid drop parameters (expressed in MeV)  $a_v = -15.6428$ ,  $a_s = 17.5418$ ,  $a_{sym} = 27.9418$ ,  $a_{ss} = -25.3440$  and  $a_c = 0.70$ .

The vibrational state density  $\omega_{vib}(E_x, M, \pi)$  is then folded in with the incoherent particle-hole state density  $\omega_{ph}(E_x, M, \pi)$  as was suggested in [104]. This folding procedure corresponds to the well known adiabatic approximation and implies that no coupling occurs between the vibrational excitations and the incoherent particle-hole excitations. It also present the advantage of enabling the introduction of purely vibrational states in the pairing gap of even-even nuclei (i.e. between the nucleus ground-state and the first particle-hole excitation), a feature which cannot be obtained with a simple enhancement factor. To deal with the known damping of the vibrational enhancement, the previously mentioned folding is restricted to p-h configurations having a total number of particle-holes lower than an arbitrary value. Also, the maximum number of phonons that can be coupled one with another is restricted. Several tests have been performed to optimise the reproduction of experimental mean s-wave resonance spacing  $D_0$ , and it has been found that a maximum number of 3 coupled phonons folded in with p-h configurations having a total number of particles lower than 3 yields fairly good reproduction of  $D_0(B_n)$ .

If the nucleus under consideration displays spherical symmetry, the level density is trivially obtained through the relation

$$\rho_{sph}(E_x, J, \pi) = \omega_{int}(E_x, M = J, \pi) - \omega_{int}(E_x, M = J + 1, \pi) \quad (4.94)$$

where  $\omega_{int}$  is the state density obtained after performing the folding. For deformed nuclei, rotational motion has to be explicitly treated. For an axially mirror symmetric nucleus, rotation takes place around an axis perpendicular to the nucleus symmetry axis. In this case, any intrinsic state of specified spin projection  $K$  and parity  $\pi$  is the band head of a set of levels having the same parity and spins  $J = K, K + 1, K + 2, \dots$  if  $K \neq 0$ , and  $J = 0, 2, 4, \dots$  or  $1, 3, 5, \dots$  if  $K^P = 0^+$  or  $0^-$ , respectively. These sequences of levels form rotational bands in which each member's energy can be deduced from the band-head energy provided the difference  $E_{rot}^{J,K}$  between the energy of the level  $J^\pi$  and that of the band-head

state  $K^\pi$  is known. The level density for deformed nuclei then reads

$$\begin{aligned}\rho_{def}(E_x, J, \pi) &= \frac{1}{2} \sum_{K=-J, K \neq 0}^J \omega_{int}(E_x - E_{rot}^{J,K}, K, \pi) \\ &+ \delta_{J=even} \delta_{\pi=+} \omega_{int}(E_x - E_{rot}^{J,0}, 0, \pi) \\ &+ \delta_{J=odd} \delta_{\pi=-} \omega_{int}(E_x - E_{rot}^{J,0}, 0, \pi)\end{aligned}\quad (4.95)$$

In the right hand side term of Eq.(4.95), the factor  $1/2$  accounts for the fact that in mirror axially symmetric nuclei, the intrinsic states with spin projections  $+K$  or  $-K$  give rise to the same rotational levels. Moreover, in the second and third terms of the summation, the symbol  $\delta_x$  (defined by  $\delta_x = 1$  if  $x$  holds true and 0 otherwise) restricts the rotational bands built on intrinsic states with spin projection  $K = 0$  and parity  $\pi$  to the levels sequences  $0, 2, 4, \dots$  for  $\pi = +$  and  $1, 3, 5, \dots$  for  $\pi = -$ . Finally, the rotational energy is obtained with the well-known expression

$$E_{rot}^{J,K} = \frac{J(J+1) - K^2}{2\mathcal{J}_\perp}, \quad (4.96)$$

where  $\mathcal{J}_\perp$  is the moment of inertia of a nucleus rotating around an axis perpendicular to the symmetry axis. In the present approach,  $\mathcal{J}_\perp$  is approximated by the rigid-body value  $\mathcal{J}_\perp^{rigid}$  which reads

$$\mathcal{J}_\perp^{rigid} = \frac{2}{5}mR^2 \left( 1 + \sqrt{\frac{5}{16\pi}}\beta_2 \right)$$

for an ellipsoidal shape with axial quadrupole deformation parameter  $\beta_2$ .

Globally, the  $D_0$  values are predicted within a factor about 2. The value of the factor Eq.(4.78) found with the present approach is  $f_{rms} = 2.3$  for both the s- and p-wave data. The HFB plus combinatorial model also gives satisfactory extrapolations to low energies. However the results were re-normalized to the experimental  $s$ -wave neutron resonance spacings and adjusted to the cumulative number of discrete levels using the scaling function

$$\rho(E_x, J\pi) = \exp\left(c\sqrt{E_x - p}\right) \rho^{HFB}(E_x - p, J\pi). \quad (4.97)$$

The HFB combinatorial level density tables are provided in *RIPL/densities/total/level-densities-hfb* directory for about 8000 nuclei with  $8 \leq Z \leq 110$ . They are contained in *zXXX.tab* files and the normalization  $c$  and  $p$  parameters are listed in the corresponding *zXXX.cor* files. Each table in *zXXX.tab* files includes the spin-dependent level densities at energies up to  $U=200$  MeV and spins up to  $J=29(59/2)$  for each isotope considered. The nuclear temperature, cumulative number of levels and total level and state densities are also included.

### 4.3 Gamma-ray emission

Gamma emission is one of the most important channels for nuclear de-excitation in the low incident energy range. In EMPIRE code, the transmission coefficients  $T_{XL}(E_\gamma)$  of

gamma-ray emission are expressed as an arbitrary mixture of the Weisskopf single-particle model [105] and of the Giant Multipole Resonance model (Brink-Axel hypothesis [53, 54, 55])

$$T_{XL} = (1 - t)T_{XL}^{Weiss} + tT_{XL}^{GMR}, \quad (4.98)$$

where  $XL$  denotes different multipolarities and the input  $t$ -parameter which weights the relative contributions of both approaches adopts values between 0 and 1. However, the default value  $t = 1$  (i.e., pure GMR) is normally used. Considering that the E1, E2, and M1 transitions are usually taken into account in the statistical model (Hauser-Feshbach) calculations, the Weisskopf estimates for the corresponding  $T_{XL}^{Weiss}$  are defined by the equations:

$$T_{E1}^{Weiss} = C_{E1} 4.599^{-7} A^{2/3} E_\gamma^3 [\text{MeV}^{-3}], \quad (4.99)$$

$$T_{M1}^{Weiss} = C_{M1} 1.3^{-7} E_\gamma^3 [\text{MeV}^{-3}], \quad (4.100)$$

$$T_{E2}^{Weiss} = C_{E2} 3.54^{-13} A^{4/3} E_\gamma^5 [\text{MeV}^{-5}], \quad (4.101)$$

where  $E_\gamma$  denotes the  $\gamma$ -ray energy and  $A$  is the nuclear mass. The coefficients  $C_{XL}$  can be used to adjust theoretical estimates to the experimental data.

The GMR contribution, based on Brink-Axel hypothesis to equate the cross section for photoabsorption by an excited state with that of the ground state, can be written as

$$T_{XL}^{GMR}(E_\gamma) = 2\pi E_\gamma^{2L+1} f_{XL}(E_\gamma), \quad (4.102)$$

where  $f_{XL}(E_\gamma)$  represent the  $\gamma$ -ray strength functions. Gamma-ray strength functions are important constituents of the compound nucleus model calculations of capture cross sections,  $\gamma$ -ray production spectra, isomeric state populations, and competition between  $\gamma$ -ray and particle emission. The  $\gamma$ -ray strength functions include information on nuclear structure, and are widely used to study the mechanisms of nuclear reactions as well as nuclear structure.

### 4.3.1 Gamma-ray strength function

The  $\gamma$ -decay strength function for a  $\gamma$ -ray emission of multipole type  $XL$  is defined as the average reduced partial radiation width  $E_\gamma^{-(2L+1)} \langle \Gamma_{XL}(E_\gamma) \rangle$  divided by the average level spacing  $D_l$

$$f_{XL}(E_\gamma) = E_\gamma^{-(2L+1)} \langle \Gamma_{XL}(E_\gamma) \rangle / D_l. \quad (4.103)$$

**Experimental  $\gamma$ -ray strength functions** Experimental gamma strength functions are based on the measurement of the partial radiative widths  $\Gamma_\gamma$  in experiments studying: discrete-resonance capture, thermal neutron capture and photo-nuclear reactions. EMPIRE uses for normalization the strength functions from `/data/Ggamma.dat` representing the Spline fit of the experimental data provided by Kopecky for RIPL-1. They are given as function of mass number for  $40 < A < 260$ .

**Closed-form models for E1 strength function** The absorption and emission of dipole  $\gamma$ -rays up to energies  $\approx 20$  MeV are mainly governed by excitation of the giant isovector dipole resonance (GDR). At energies around GDR, the imaginary part of the nuclear response function has a Lorentzian-like shape, therefore the realistic phenomenological models of the dipole strength function assume Lorentzian-like shapes. The scaling parameter (or “width”  $\Gamma_\gamma(E_\gamma, T)$ ) of such shapes in a heated nucleus at the temperature  $T$  is given by different expressions. It is governed by the damping of the collective states and its expression depends on the assumptions on the damping mechanism for the collective states (see [106] for details and references).

For example, the most used expression to describe the Giant Dipole Resonance (GDR) shape, known as Enhanced Generalize Lorentzian (EGLO), is sum of two Lorentzians

$$f_{E1}(E_\gamma) = \sum_{i=1}^2 \sigma_i \Gamma_{\gamma,i} \left[ \frac{E_\gamma \Gamma_i(E_\gamma, T)}{(E_\gamma^2 - E_i^2)^2 + E_\gamma^2 \Gamma_i(E_\gamma)^2} \right] + \sum_{i=1}^2 \sigma_i \Gamma_i \left[ \frac{0.7 \Gamma_i 4\pi^2 T^2}{E^5} \right] \quad (4.104)$$

where  $\sigma_i$ ,  $\Gamma_i$ , and  $E_i$  are the peak cross section, the width, and the energy of the  $i$ -th hump of the GDR, and the energy dependent width is given by

$$\Gamma_i(E_\gamma, T) = \Gamma_{\gamma,i} \frac{E_\gamma^2 + 4\pi T^2}{E_i^2}. \quad (4.105)$$

EMPIRE code includes six closed-forms for E1 strength function (selected by key-word GSTRFN)

- EGLO: Enhanced Generalized Lorentzian [107]
- MLO1, MLO2, ML03: Modified Lorentzian [108, 109, 110]
- GFL: Generalized Fermi Liquid Model [111]
- SLO: Standard Lorentzian [112]

We refer to the RIPL-2 TECDOC available at [www-nds.iaea.org/RIPL-2/handbook/ripl2.pdf](http://www-nds.iaea.org/RIPL-2/handbook/ripl2.pdf) for detailed description of these advanced approaches.

Depending on the formalism chosen, the shape of  $f_{XL}(E_\gamma)$  is modified, especially at low  $\gamma$  emission energies that are mostly responsible for the capture cross sections. Different  $\gamma$ -ray strength functions produce capture cross sections that differ by as much as a factor of two. On the other hand, all  $\gamma$ -ray strength functions tend to provide similar results in the vicinity of the GDR, since differences among the formalisms regard primarily low  $\gamma$ -emission energies. By using experimental  $\Gamma_\gamma$  for normalization these differences would be drastically reduced. This would, however, come at the price of losing the consistency among the calculations in the GDR energy range. As a consequence, the naturally imposed agreement with the experimental GDR cross sections would be compromised. Therefore, the user has an option to turn off the otherwise automatic normalization of the  $\gamma$ -ray strength function to the  $\Gamma_\gamma$ .

**Gamma-ray strength functions for other multipolarities** The user may increase the maximum multipolarity from the default value of 2 (E1, M1 and E2 transitions only) up to the maximal value of 10. This change affects the calculation of  $\gamma$ -transitions between states in the continuum as well as from the continuum to discrete levels. The radiative strength functions for higher multipole orders ( $f_{EL}$ ,  $f_{ML}$ ) are calculated using the relationships between single-particle radiative strength functions expressed in the Weisskopf form. For the electric transitions we have

$$f_{E(L+1)}/f_{E(L)} = CE_\gamma^2[(3+L)/(5+L)]^2, \quad (4.106)$$

where  $C = [R/(\hbar c)]^2 = 3.7 \cdot 10^{-5} A^{2/3}$ , if a nuclear radius  $R = 1.2A^{2/3}$  Fm is assumed. For the magnetic transitions, we use

$$f_{M(L+1)}/f_{E(L+1)} = 10[\hbar/(mcR)]^2 = 0.307A^{-2/3}. \quad (4.107)$$

### 4.3.2 Giant Multipole Resonance parameters

As mentioned before, the commonly used transitions are E1, M1 and E2, therefore most of systematics and parametrizations refers to them.

**E1 transitions** The source of GDR parameters is selected by the input key-word GDRGFL.

By default (GDRGFL=1) the GDR-parameters are retrieved from RIPL either from */RIPL/gamma/gdr-parameters-exp.dat* or, if they don't exist in this file, from */RIPL/gamma/gdr-parameters-theor.dat*. The experimental GDR parameters were obtained based on the analysis of the photoabsorption cross sections for 121 nuclides ranging from 12-C to 239-Pu. The *gdr-parameters-theor.dat* file contains predictions of the GDR energies and widths using Goldhaber-Teller model for about 6000 nuclei with  $14 \leq Z \leq 110$  lying between the proton and the neutron driplines.

IF GDRGFL=0 the GDR parameters are estimated from the systematics based on the Dietrich and Berman compilation [113], containing 150 experimental data for nuclei ranging from mass  $A = 51$  up to  $A = 239$ . The deformation parameter  $\delta=0.064$  is the

limit for considering a nucleus to be “nearly spherical”. GDR parameters for the deformed nuclei ( $\delta > 0.064$ ), are given by the following expressions:

$$E_2 = 50A^{-0.232} [MeV] \quad (4.108)$$

$$\ln(E_2/E_1) = 0.946\delta \quad (4.109)$$

$$\Gamma_1 = (0.283 - 0.263\delta)E_1 [MeV] \quad (4.110)$$

$$\Gamma_2 = (0.35 - 0.14\delta)E_2 [MeV] \quad (4.111)$$

$$\sigma_1 = 3.48A/\Gamma_1 [mb] \quad (4.112)$$

$$\sigma_2 = 1.464A^{4/3}/\Gamma_2 [mb] \quad (4.113)$$

where  $\Gamma$  and  $\sigma$  are the GDR width and peak cross section respectively, while subscripts 1 and 2 refer to the lower- and higher-energy GDR humps. The particular feature of the present systematics is the deformation independent energy of the second GDR hump ( $E_{2GDR}$ ).

Separate systematics was performed for the “nearly spherical” nuclei, because “deformed nuclei systematics” in the  $\delta = 0$  limit does not adequately describe the GDR parameters for spherical and slightly deformed nuclei. The following expressions were proposed for nuclei with  $\delta \leq 0.064$ :

$$E_{GDR} = (49.336 + 7.34\delta)A^{-0.2409} [MeV] \quad (4.114)$$

$$\Gamma_{GDR} = 0.3E_{GDR} [MeV] \quad (4.115)$$

$$\sigma_{GDR} = 10.6A/\Gamma_{GDR} [mb] \quad (4.116)$$

By default, the deformation is spin dependent as is the shape of GDR. An input option is provided to suppress this dependence and use ground state deformation.

It is also assumed that the systematics holds for the GDR built on the highly excited states with large angular momentum, like those produced in the HI reactions. However, the code allows for an additional increase of the GDR width with the excitation energy [114]. This increase cannot be deduced from the analysis of the database [113] containing GDRs built on the ground state but has to be added on top of the derived systematics giving

$$\Gamma = \Gamma_{syst} + c E_x^{1.6}, \quad (4.117)$$



where the index *syst* stands for the result of the systematics, and  $E_x$  is the excitation energy of the excited nucleus. This dependence (with  $c = 0.0026$ ) was obtained for Sn isotopes [114] and has been accepted in the code.

**M1 and E2 transitions** The following default parameters have been adopted for the Giant Quadrupole Resonance (GQR):

$$E_{GQR} = 63A^{-1/3} [MeV] \quad (4.118)$$

$$\Gamma_{GQR} = 6.11 - 0.012A [MeV] \quad (4.119)$$

$$\sigma_{GQR} = 0.00015 \frac{Z^2 E_{GQR}^2}{A^{1/3} \Gamma_{GQR}} [mb] \quad (4.120)$$

The GQR energy is taken after Ref. [115] while the GQR width and peak cross section are taken from Ref. [116].

The default parametrization of the spin-flip Giant Monopole Resonance follows Bohr and Mottelson [44]

$$E_{GMR} = 41A^{-1/3} [MeV] \quad (4.121)$$

$$\Gamma_{GMR} = 4.0 [MeV] \quad (4.122)$$

$$\sigma_{GMR} = 1.0 [mb] \quad (4.123)$$

## 4.4 Fission

The relation used in the statistical model for the fission cross section calculation is

$$\sigma_{a,f}(E) = \sum_{J\pi} \sigma_a(E_x J\pi) P_f(E_x J\pi), \quad (4.124)$$

where  $\sigma_a(E_x J\pi)$  is the population of the fissioning nucleus in the state  $E_x J\pi$  and  $P_f(E_x J\pi)$  represents the fission probability

$$P_f(E_x J\pi) = \frac{T_f(E_x J\pi)}{\sum_p T_p(E_x J\pi) + T_\gamma(E_x J\pi) + T_f(E_x J\pi)} \quad (4.125)$$

Depending on the projectile type EMPIRE offers two formalisms for the fission coefficient calculation selected by the directive input FISSHI. The default value (FISSHI = 0) selects the optical model for fission (or its simplified version) to calculate fission induced by light

particles or photons,  $\text{FISSHI} = 1$  selects the Sierk model adequate for heavy ion induced fission, and  $\text{FISSHI} = 2$  turns off any fission calculation.

For  $\text{FISSHI} = 0$  the fissility condition is somehow arbitrary and related to the availability of barrier parameters. In this case fission is considered an opened reaction channel for nuclei with  $Z > 78$  and  $A > 200$ . For  $\text{FISSHI}=1$  the fissility condition is  $0.0205Z^2/A > 0.3$ .

#### 4.4.1 Optical model for fission ( $\text{FISSHI}=0$ )

This fission formalism implemented in EMPIRE has been continuously updated by incorporating fundamental features of the fission process confirmed or revealed by the recent large scale experimental and theoretical studies. It has several unique features which make the code suitable for being used both in basic research and data evaluation for applications:

- is applicable to multi-chance fission induced by light particles and photons starting from sub-barrier excitation energies up to about 200 MeV;
- describes transmission through multi-humped fission barriers parameterized analytically or defined numerically;
- makes use of the optical model for fission concepts to account for the fission mechanisms associated to the different degrees of damping of the vibrational states within the minima of the fission path and can reproduce the resonant structure of the fission cross section in the sub-threshold region due to the coupling among these vibrational states;
- treats multi-modal fission, providing a coherent quantitative description of the relation between the pre-scission shapes and fission fragment properties.

All these features are valid for barriers with any number of humps. The fission coefficients for  $N$ -humped barriers are expressed recursively in terms of fission coefficients for the double-humped, barrier. Further details about the general formula are included in [117]. Because for practical applications the maximum number of humps is three, EMPIRE is dimensioned accordingly and explicit relations for the double- and triple-humped barriers are given in this paper. An exception is the multi-modal fission which is implemented only for double-humped barrier.

#### Fission barriers

Unlike the majority reaction codes which rely on multiple-humped fission barrier described by independent inverted parabolas, EMPIRE has two options to define the fission path as function of the quadrupole deformation:

- (i) parameterized by smoothly-joined parabolas, or
- (ii) described numerically.

**(i) Parabolic parametrization.** The barriers associated to the discrete transition states are parameterized as function of the quadrupole deformation by smoothly joined parabolas:

$$\begin{aligned} V_h(\beta) &= E_{fh} - \frac{1}{2}\mu\omega_h^2(\beta - \beta_h)^2 \quad h = 1, N_h \\ V_w(\beta) &= E_{fw} + \frac{1}{2}\mu\omega_w^2(\beta - \beta_w)^2 \quad w = 2, N_w \end{aligned} \quad (4.126)$$

where  $N_h$  is the number of humps and  $N_w$  is the number of wells ( $w$  runs from 2 to  $N_w$  the first well, corresponding to equilibrium deformation, being not included in parameterization). The energies  $E_{fh(w)}$  represent maxima and minima of the potential,  $\beta_{h(w)}$  are the corresponding abscissae, the harmonic oscillator frequencies  $\omega_{h(w)}$  define the curvature of each parabola and  $\mu$  is the inertial mass parameter, assumed independent of  $\beta$  and approximated by the semi-empirical expression  $\mu \approx 0.054A^{5/3} \text{ MeV}^{-1}$ , where  $A$  is the mass number.

The discrete transition states are rotational levels built on vibrational or non-collective band-heads, characterized by a given set of quantum numbers (angular momentum  $J$ , parity  $\pi$  and angular momentum projection on the nuclear symmetry axis  $K$ ) with the excitation energies:

$$\begin{aligned} E_{h(w)}(KJ\pi) &= E_{fh(w)} + \epsilon_{h(w)}(K, \pi) + \\ &+ \frac{\hbar^2}{2\mathfrak{I}_{h(w)}}[J(J+1) - K(K+1)] \quad h = 1, N_h; w = 2, N_w \end{aligned} \quad (4.127)$$

where:  $\epsilon_{h(w)}(K, \pi)$  are the energies of the lowest rotational level belonging to band  $K\pi$  and  $\hbar^2/2\mathfrak{I}_{h(w)}$  are the inertial parameters (the decoupling parameter for  $K = 1/2$  bands was neglected). A parabolic barrier with height(depth)  $E_{h(w)}(J, K, \pi)$  and curvature  $\hbar\omega_{h(w)}$  is associated to each transition state. Usually, these are free parameters and their values are extracted from systematics or are obtained from the fit of the experimental fission cross section. The values of the perpendicular moments of inertia taken from RIPL are equal to  $100\hbar^2/\text{MeV}$  for the inner saddle,  $200\hbar^2/\text{MeV}$  for the outer saddle and approximately  $75\hbar^2/\text{MeV}$  for the ground state [118].

It should be noted that for axial asymmetric shapes at the inner saddle, additional  $2J+1$  rotational levels for each  $J$  should be assumed. On the other hand the positive parity bands  $K^\pi = 1/2^+, 3/2^+, 5/2^+, \dots$  at the outer saddle are assumed to be double degenerated due to mass asymmetry. This degeneracy lift is taken into account at level of transmission coefficients as described later.

The transition state spectrum has a discrete component up to a certain energy  $E_{ch}$ , above which it is continuous and described by the level density functions,  $\rho_{fh}(EJ\pi)$ , accounting for collective enhancements specific to the nuclear shape asymmetry at each saddle point (see next Section).

In the optical model for fission, the damping of the vibrational states within wells is simulated by introducing negative imaginary potentials,  $iW_w$ , in the corresponding deformation ranges (Figure 4.1). This causes absorption of the incoming flux in this wells

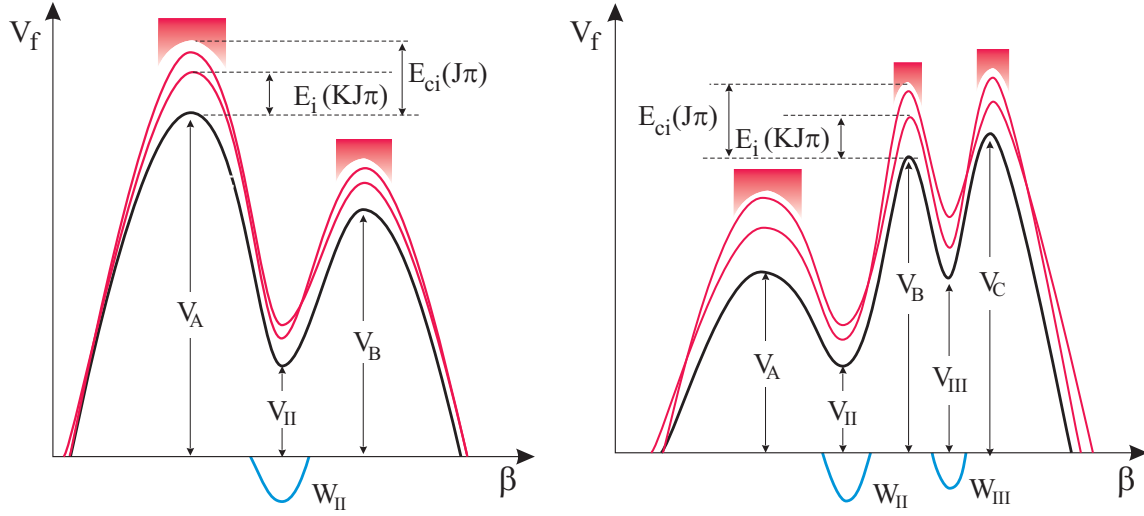


Figure 4.1: Fission barrier's parameterization in the optical model for fission.

[119, 120, 121]. The strengths  $W_w$  are assumed to be quadratic functions of deformation,  $\beta$ , like the real part, and to be energy dependent:

$$W_w(\beta) = -\alpha_w(E_x)[E_x - V_w(\beta)] \quad w = 2, N_w. \quad (4.128)$$

The  $\alpha_w(E_x)$  energy dependence, which controls the strength of the imaginary parts of the fission potential, is chosen to allow the fit of the resonances in sub-barrier fission cross section and to be consistent with physical values for the transmission coefficients at higher energies

$$\alpha_w(E_x) = W_{1w} + W_{2w}[E_x - E_w(K, J\pi)] + W_{3w} \exp[E_x - E_h(K, J\pi)] \quad (4.129)$$

where  $W_i$  are coefficients given in the fission input and  $E_h(K, J\pi)$  is the heighst of the humps delimiting the well  $w$ .

The multi-modal approach assumes Brosa's channel concept and the hypothesis that the bifurcation points appear in the deformation region corresponding to the second minimum [122]. Consequently, different discrete and continuous spectra for the transition states at the outer saddle are considered for each mode. This is illustrated in Figure 4.2 for two modes known as super-long symmetric (SL) and standard asymmetric (S1).

The parameters of the fission barriers can be retrieved from 3 files selected by the directive input FISBAR.

- FISBAR=1 (default value) selects the file */RIPL/fission/empirical-barriers.dat* which contains the fission barrier parameters for the most important preactinide and actinide nuclei. For pre-actinides the file provides the heights for the single-humped barriers while EMPIRE adds the default value for the width  $\hbar\omega_{w2} = 0.3$  MeV. For actinides are given both the heights and the widths for the humps of double-humped

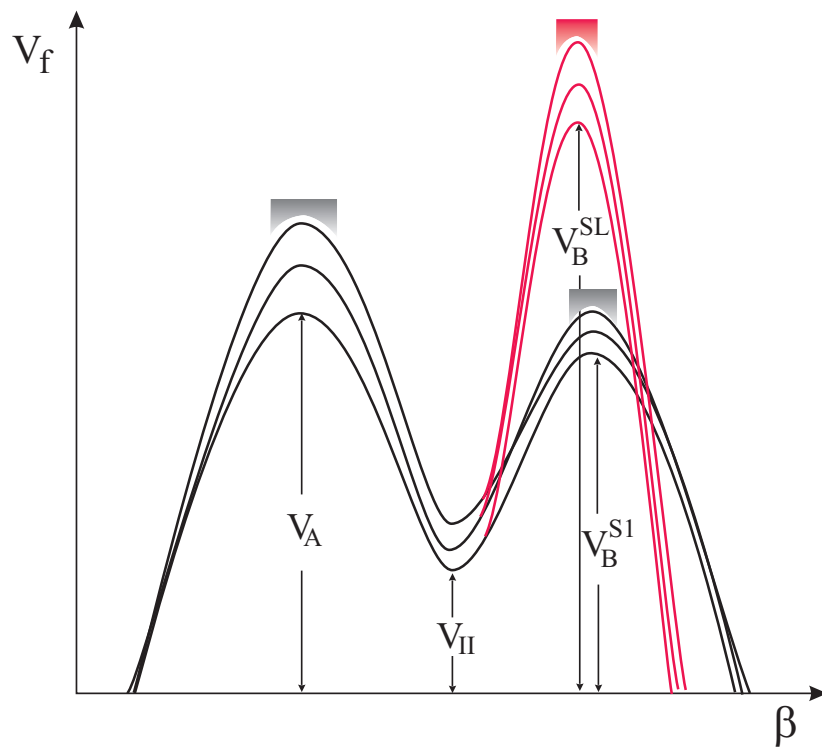


Figure 4.2: Double-humped fission barriers used in multi-modal calculations.

barriers The code provides for the parameters of the isomeric well the default values  $V_{w2} = 2$  MeV and  $\hbar\omega_{w2} = 1$  MeV.

- FISBAR=0 selects the file */data/fisbar.dat* where the user can store heights (depths) and widths for humps and wells of single-, double- or triple-humped fission barriers.
- FISBAR=2 selects the file */data/HFB-parab-fisbar.dat* which contains heights (depths) and widths for humps and wells of single-, double- or triple-humped barriers resulted from the parabolic parametrization of HFB numerical barriers (see next paragraph) for 59 actinides.

**(ii) Numerical barriers** The fission paths have been estimated within the HFB model with BSk14 Skyrme force [100] for all nuclei with  $90 \leq Z \leq 102$  lying between the valley of  $\beta$ -stability and the neutron drip lines, i.e about 1000 nuclei. Generally, for most of the neutron-rich nuclei, three barriers are found.

The fission barriers, obtained by projecting the 3-D energy surfaces along the quadrupole deformation parameter are provided in tabular form in */RIPL/fission/HFB2007* directory. Generally, for most of the neutron-rich nuclei, three barriers are found. In Figure 4.3 are presented the HFB fission barriers of several actinides. For an accurate description of the fission cross section the barrier can be renormalized. The global scaling of the width of the entire barrier is reached by multiplying the quadrupole deformation with a factor  $n_\beta$  read from the fission input

$$\beta_i = n_\beta \beta_i \quad i = 1, N_p \quad (4.130)$$

where  $N_p$  is the number of points for which the numerical barrier is defined.

The global scaling of the height of the entire barrier is reached by multiplying the fission potential with a factor  $n_h$  read from the fission input (see the fission Input/Output description for details)

$$V(\beta_i) = n_h V(\beta_i) \quad i = 1, N_p. \quad (4.131)$$

An independent normalization of each hump is realized by keeping the bottom of the well(s) unchanged

$$V_h(\beta_i) = V_h(\beta_i) + n_{b,h} V_h(\beta_i - (V(\beta))_{min}) \quad (4.132)$$

with  $i$  running in the appropriate deformation regions.

Specialized subroutines for smoothing, finding extrema points, interpolation and integration have been implemented in order to use numerically defined barriers. This capability qualifies Empire as a valuable tool for testing global microscopic fission parameters and for using them in applications requiring a blind description of fission for nuclei far from stability.



Figure 4.3: HFB fission barriers [123]. The horizontal line indicates the neutron separation energy.

#### Level densities at fission saddles

There are two types of level densities at saddles implemented in EMPIRE: one based on Enhanced Generalized Superfluid Model (EGSM) and the second based on Hartree-Fock-Bogoliubov + combinatorial method (HFB). They can be selected by the directive input FIDEN. It is recommended to use the same density model for equilibrium and saddles deformations.

**EGSM** (FIDEN=0 default option). When using EGSM to describe the normal states corresponding to the equilibrium deformation it is natural to use the same model to describe the level densities for the deformations specific to the saddle points, also referred to as the level densities of the transition states. Considering that there are no experimental data available for normalization, the starting values of the parameters entering the transition state density are obtained by using physical arguments to adjust the parameters of the normal states at equilibrium deformation for the saddle point deformation. The final values are deduced from the fit of the experimental data for neutron-induced fission cross sections. The main differences between the density of the normal states and the density of the transition states are outlined below.

The calculation of the level density parameter  $a_{fh}$  for the transition states at the hump  $h$  requires knowledge of its asymptotic value  $\tilde{a}_{fh}$  of the damping of the shell effects  $\gamma_{fh}$  and of the shell correction  $\delta W_{fi}$ . All these quantities are interrelated and depend on their corresponding values for the equilibrium deformation; therefore, it is difficult to provide a general prescription for their calculation. The default values of these parameters follow the recommendations in RIPL or are deduced from previous fits of the experimental data:

- for the ratio of the asymptotic values of the level density parameter at the saddle points and equilibrium deformation  $\tilde{a}_f/\tilde{a}$  was adopted the value 1;
- pairing at saddles is parameterized following RIPL as  $\Delta_f = 14A^{-1/2}$ ,
- the values, in MeV, for the inner and the outer barrier of the shell corrections recommended are calculated according to:

$$\begin{aligned} \delta W_{f1} &= \begin{cases} 2.6 & Z \leq 97 \\ 2.6 - 0.1(Z - 97) & Z \geq 97 \end{cases} \\ \delta W_{f2} &= \begin{cases} 0.6 + 0.1(Z - 97) + 0.04(N - 143) & Z < 97 \\ 0.6 + 0.04(N - 143) & Z \geq 97 \end{cases} \end{aligned} \quad (4.133)$$

In case of a third hump, by default  $\delta W_{f3} = \delta W_{f2}$ .

- for the the damping of the shell effects was adopted the value  $\gamma_f = 0.6 \text{ MeV}^{-1}$ ;
- the vibrational enhancement at saddles is higher than that for equilibrium deformation roughly with a factor of 4;

All the remaining parameters, including the moments of inertia, have been calculated according to the formulae presented in section 4.2.4 by replacing the equilibrium deformation with the deformations corresponding to the saddle points.

The order of symmetry of the nuclear shape at saddles has an important impact on the transition state spectrum. This is taken into account by multiplying the level density by an enhancement factor  $f_{sym}$  associated with the nuclear shape symmetry at each saddle and determined in Ref. [124]:

$$f_{sym} = \begin{cases} 1 & \text{axial, mirror symmetry} \\ \sqrt{\frac{\pi}{2} \mathfrak{S}_{||} \cdot T} & \text{axial asymmetry, mirror symmetry} \\ 2 & \text{axial symmetry, mirror asymmetry} \end{cases} \quad (4.134)$$

By default, the nuclear shape at the inner saddle is considered axial and mirror symmetric if the number of neutrons is less than 144 and axial asymmetric and mirror symmetric for the rest of nuclei while for the outer saddle(s) the shape is considered to be axial symmetric and mirror asymmetric.

To overcome the shortcomings in modeling the densities of the transition states and to provide flexibility for nuclear data evaluation there are two possibilities to adjust the level density at each saddle: a shift in the effective excitation energy  $U_h = E_x - E_{ch} + \Delta_f$

$$U_h^* = U_h + \delta_h \quad (4.135)$$

and a global scaling factor  $N_h$ . In the end, the level density at the saddle point  $h$  reads:

$$\rho_{fh}^{EGSM}(U_h, J\pi) = \rho^{EGSM}(U_h^*, J\pi) f_{sym} N_h \quad (4.136)$$

with the parameters entering  $\rho^{EGSM}$  specific to the saddle point deformation.

It should be noted that the uncertainty of above estimates is significant [119], therefore they can be modified to reproduce the experimental data in different energy ranges.



**HFB** (FISDEN=3) The HFB combinatorial method developed to estimate the level densities at ground-state deformation [125] (see section 4.2.5) has been used to calculate coherently the level densities at the saddle points, making use of the corresponding HFB predictions for the single-particle level scheme and pairing strength at the corresponding deformation.

The HFB combinatorial model level density [125] at each of the 2 (or 3) highest saddle point barriers and of the 1 (or 2) shape isomers are given in a table format (in an energy, spin and parity grid identical to that for the ground-state level densities given in section 4.2.5) in the directory */RIPL/fission/leveldensities/*. Each isotopic chain is included in a *zXXX.dat* file (where XXX corresponds to the atomic number  $Z$ ) in the subdirectories *Max1/*, *Max2/*, *Max3/*, *Min1/*, *Min2/* corresponding to the first, second and third saddle points (sorted by increasing quadrupole deformations) and first and second minima, respectively (if there are only 2 barriers, the data for the third saddle and second minimum are missing in the respective files). The second and third saddles as well as the second minimum are found to be left-right asymmetric within the HFB framework. For these reasons, tabulated level densities have already been multiplied by a factor of 2 (see Eq. 4.134). In contrast, the inner barrier and first isomer may or may not be triaxial (note that in the HFB approach, it has been estimated using the approximation of axial symmetry), and therefore the corresponding level density in the tables has not been enhanced by the  $f_{sym}$  (Eq. (4.134)) factor. The appropriate enhancement is applied by EMPIRE.

For many nuclear physics applications a renormalization procedure of the level densities based on experimental data is required, in particular for nuclear data evaluation or for an accurate estimate of reaction cross sections. Though the HFB combinatorial level densities at the saddle deformations are provided in a table format, it is possible to renormalize them using a relation similar to Eq. (4.97) applied for the ground-state level densities

$$\rho_{fh}^{HFB_{norm}}(U_h, J\pi) = \exp\left(\alpha_h \sqrt{U_h - \delta_h}\right) \rho_{fh}^{HFB}(U_h - \delta_h, J\pi) N_h. \quad (4.137)$$

The energy shift  $\delta$  and the scaling factor  $\alpha$  are free parameters which can be adjusted at each saddle deformation to optimize the fit to the fission cross section. These parameters can be expected to reach values similar to those derived for the ground-state level densities [125], i.e., typically  $\pm 1$  MeV for  $\delta$  and  $\pm 0.5$  MeV $^{-1/2}$  for  $\alpha$ . In addition a global scaling factor  $N_h$  can be applied. These values reflect the remaining uncertainties in the level density predictions on the basis of the mean-field combinatorial approach.

### Transmission mechanisms

The single-hump transmission coefficient,  $T_h$  is expressed in first-order WKB approximation in term of the momentum integral for the hump [126, 127]:

$$T_h = \frac{1}{1 + \exp(2K_h)} \quad (4.138)$$

with

$$K_h = \pm \left| \int_{a_h}^{b_h} [2\mu(E_x - V_h(\beta))/\hbar^2]^{1/2} d\beta \right| \quad (4.139)$$

where the + sign is taken when the excitation energy is lower than the hump under consideration and the – when it is higher. In the latter case, the intercepts are complex conjugate ( $b_h = a_h^*$ ) and the WKB approximation is valid when their imaginary parts are small, *i.e.*, for energies slightly higher than the hump.

As it is known, in the case of a single parabolic barrier, formula (4.138) yields the well-known Hill-Wheeler transmission coefficient [119]

$$T_{HW} = \frac{1}{1 + \exp[(2\pi/\hbar\omega_h)(V_h - E_x)]}, \quad (4.140)$$

which is an exact result.

For a double-humped barrier the transmission coefficient calculated in WKB approximation reads

$$T_{d(0)} = \frac{T_1 T_2}{1 + 2A^{1/2} \cos(2\nu_2) + A} \quad (4.141)$$

where  $A = (1 - T_1)(1 - T_2)$  and  $\nu_2$  represents the momentum integral for the well. In the intermediate wells, where the intercepts,  $a_j$  and  $b_j$ , are real, the momentum integrals depending on the real parts of the potential are approximated as:

$$\nu_w = \int_{a_w}^{b_w} [2\mu(E_x - V_w(\beta))/\hbar^2]^{1/2} d\beta. \quad (4.142)$$

For barriers with more than two humps, the transmission coefficients can be calculated iteratively, using as reference the above equations.

In case of fission, the transmission through a multi-humped barrier depends on the degree of damping of the vibrational states in the potential minima. The extreme assumptions possible for a real fission potential are:

- zero damping valid at very low excitation energies with respect to the barrier minima where  $T_f = T_{d0}$  and
- complete damping valid for excitation energies close or above the barrier maxima where the humps can be considered decoupled and the fission coefficient becomes:

$$\frac{1}{T_f} = \sum_h^{N_h} \frac{1}{T_h} \quad (4.143)$$

Using the directive input FISOPT, one can choose between the simplified calculation corresponding to the complete damping (FISOPT=0) and the full optical model formalism which describes partial damping (FISOPT=1,2,3). It should be noted that FISOPT=0 option, used in almost all reaction codes, leads to an overestimation of the fission cross section if is used for subbarrier excitation energies.

In the optical model for fission by using a complex fission potential to describe the partial damping of the vibrational states in the wells a smooth transition between the extreme situations described above becomes possible. Within this model fission occurs either by direct transmission through the barrier, or by reemission into the fission channel after absorption into the isomeric well(s) (see Figure 4.4). The fission transmission coefficients associated with these two mechanisms are the direct transmission coefficient ( $T_d$ ) and the indirect ( $T_i$ ) one, respectively, the sum of their contributions representing the total fission coefficient ( $T_f$ ).

In [117] is presented a recursive method to calculate the transmission coefficients through a barrier with  $N_h$  humps and  $N_w$  wells. Using the notation appropriate for recursive derivation the general expression for the fission coefficient is

$$T_f = T_d(1, N_h) + R \sum_{w=2}^{N_w} T_i(w). \quad (4.144)$$

where  $T_d(1, N_h)$  represents the direct transmission coefficient through all humps (starting with hump 1 and ending with hump  $N_h$ ),  $T_i(w)$  stands for the indirect transmission coefficient associated to the well  $w$  and  $R$  is a normalization factor described later.

Because the general formulae are difficult to be followed and considering that for practical applications only the double- and triple-humped barriers are of interest, here are presented the fission coefficients for these particular cases.

**Double-humped barrier.** The incoming flux can be transmitted directly through the barrier or can be absorbed in the isomeric well. The fraction absorbed in the isomeric well can: (i) be re-emitted in the fission channel (indirect prompt fission), (ii) return back to a class I state or (iii) undergo  $\gamma$ -transition to the isomeric state. The isomeric state, in turn, can decay by delayed (isomeric) fission or by shape transition to class I states. In the present version of EMPIRE the  $\gamma$ -transition to the isomeric state and hence the delayed fission are not considered. They are going to be implemented soon because they might make a difference in those cases where the compound nucleus is populated in states with small excitation energies with respect to the bottom of the isomeric well, as could happen in photofission.

In the case of a double-humped barrier, the general expression of the fission coefficient given in Eq. 4.144 becomes

$$T_f = T_d(1, 2) + RT_i(2) = T_d(1, 2) + T_a \frac{T_d(2, 2)}{\sum T(2)}, \quad R = 1 \quad (4.145)$$

The expression of the direct transmission coefficient through a double-humped barrier in the presence of absorption is a generalization of Eq. 4.141. It is obtained by adding to the real momentum integrals  $\nu_w$  the imaginary contributions  $\delta_w$  corresponding to the imaginary potential [120]

$$\delta_w = - \left( \frac{\mu}{2\hbar^2} \right)^{1/2} \int_{a_w}^{b_w} \frac{W_w(\beta)}{[E - V_w(\beta)]^{1/2}} d\beta \quad w = 2, \quad (4.146)$$

$$T_d(1, 2) = \frac{T_d(1, 1)T_d(2, 2)}{e^{2\delta_2} + 2A^{1/2} \cos(2\nu_2) + Ae^{-2\delta_2}} \quad (4.147)$$

where  $A = [1 - T_d(1, 1)][1 - T_d(2, 2)]$  and  $T_d(h, h)$  represents the transmission coefficient through the hump  $h$  given by the Hill-Wheeler formula (Eq.4.140).

The absorption coefficient for a double humped barrier is

$$T_a(1, 2) = T_d(1, 2) \left[ e^{2\delta(2)} - \frac{[1 - T_d(2, 2)]e^{-2\delta(2)}}{T_d(2, 2)} \right]. \quad (4.148)$$

where the notation  $T_a(1, 2)$  stands for the absorption coefficient describing the shape transition from minimum 1 to minimum 2. The denominator of the second term in Eq.4.145 stands for the sum of the transmission coefficients for the competing channels specific to the second well

$$\sum T(2) = T_d(1, 1) + T_d(2, 2). \quad (4.149)$$

AS mentioned before, the gamma-decay in the isomeric well was neglected.

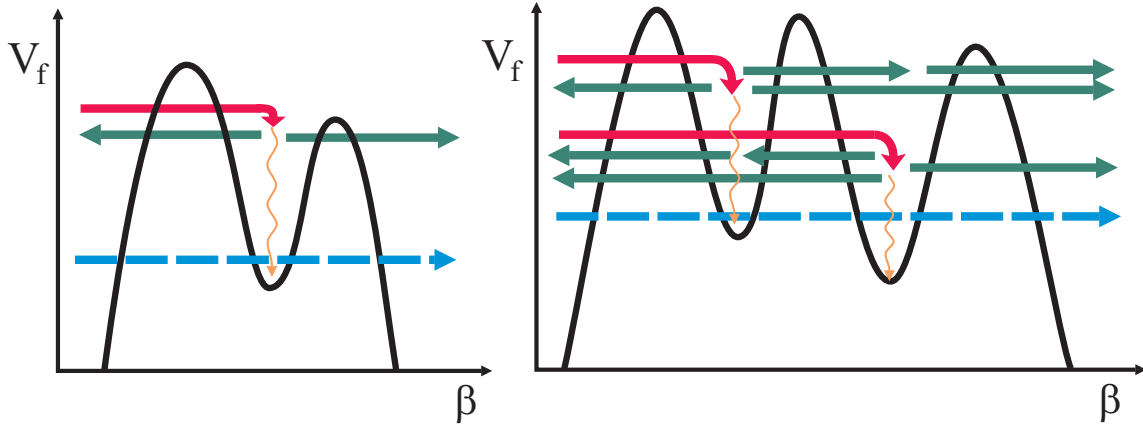


Figure 4.4: Transmission mechanisms through double- and triple-humped fission barriers.

**Triple-humped barrier.** The general expression of the fission coefficient given in Eq.4.144 becomes in the case of a triple-humped barrier

$$T_f = T_d(1, 3) + R[T_i(2) + T_i(3)], \quad (4.150)$$

The direct transmission coefficient through all the humps is calculated using Eq.4.147 in which the transmission through the outer hump  $T_d(2, 2)$  is replaced with the direct transmission through the outer humps  $T_d(2, 3)$

$$T_d(1, 3) = \frac{T_d(1, 1)T_d(2, 3)}{e^{2\delta_2} + 2A^{1/2} \cos(2\nu_2) + Ae^{-2\delta_2}} \quad (4.151)$$

where  $A = [1 - T_d(1, 1)][1 - T_d(2, 3)]$  and

$$T_d(2, 3) = \frac{T_d(2, 2)T_d(3, 3)}{e^{2\delta_3} + 2A^{1/2} \cos(2\nu_3) + Ae^{-2\delta_3}} \quad (4.152)$$

where  $A = [1 - T_d(2, 2)][1 - T_d(3, 3)]$ .

$$T_i(2) = T_a(1, 2) \left[ \frac{T_d(2, 3)}{\sum T(2)} + \frac{T_a(2, 3)}{\sum T(2)} \cdot \frac{T_d(3, 3)}{\sum T(3)} \right] R \quad (4.153)$$

$$T_i(3) = T_a(1, 3) \left[ \frac{T_d(3, 3)}{\sum T(3)} + \frac{T_a(3, 2)}{\sum T(3)} \cdot \frac{T_d(2, 3)}{\sum T(2)} \right] R. \quad (4.154)$$

The forward absorption coefficients are calculated in terms of direct transmission coefficients across the humps on the right sides of the corresponding wells:

$$T_a(1, 2) = T_d(1, 3) \left[ e^{2\delta(2)} - \frac{[1 - T_d(2, 3)]e^{-2\delta(2)}}{T_d(2, 3)} \right]. \quad (4.155)$$

$$T_a(1, 3) = T_d(1, 3) \left[ e^{2\delta(3)} - \frac{[1 - T_d(3, 3)]e^{-2\delta(3)}}{T_d(3, 3)} \right]. \quad (4.156)$$

$$T_a(2, 3) = T_d(2, 3) \left[ e^{2\delta(3)} - \frac{[1 - T_d(3, 3)]e^{-2\delta(3)}}{T_d(3, 3)} \right]. \quad (4.157)$$

The backward absorption coefficient from the well 3 into the well 2 is calculated in terms of the direct transmission coefficients across the humps on the left sides of the two wells:

$$T_a(3, 2) = T_d(2, 1) \left[ e^{2\delta(2)} - \frac{[1 - T_d(1, 1)]e^{-2\delta(2)}}{T_d(1, 1)} \right]. \quad (4.158)$$

The sum of the transmission coefficients for the competing channels specific to the wells 2 and 3 are

$$\sum T(2) = T_d(1, 1) + T_d(2, 3) + T_a(2, 3) \quad (4.159)$$

$$\sum T(3) = T_d(2, 1) + T_d(3, 3) + T_a(3, 2) \quad (4.160)$$

$$R = \left[ 1 - \frac{T_a(2, 3)}{\sum T(2)} \frac{T_a(3, 2)}{\sum T(3)} \right]^{-1}. \quad (4.161)$$

### Effective fission coefficients

The fission coefficients presented up to now correspond to transmission through a single barrier ( $K, J\pi$ ). In Eq. 4.125 enters the fission coefficient corresponding to the transmission through all barriers characterized by the quantum numbers  $J\pi$ . The calculation of this effective fission coefficient is described below.

The structure of the saddle transition states is complex and still difficult to be predicted accurately. It depends on the odd-even- $A$  type and on the asymmetries of the nuclear shape at saddle deformation. In the present formalism we attempt to keep the spirit of the optical model for fission and also the fission input manageable by the users but to consider in the same time the partial lift of degeneracy associated to the nuclear shape asymmetry. The idea was to apply to the discrete transition states the same enhancement factors as for the density functions which describe the transition states in continuum. Obviously, due to the spin-parity selection rules, this method is not equivalent to taking into account properly the double degeneracy of the  $K^\pi$  bands at the outer saddle(s) for instance, but our tests indicated that the impact on the fission cross section is similar. Because the transmission coefficients calculation in the optical model for fission requires a full fission path along the quadrupole deformation, the enhancements were applied on the transmission coefficients and not on the discrete levels.

The total transmission coefficient through one hump is sum of two contributions corresponding to the discrete and continuous part of the transition state spectrum

$$T_h(EJ\pi) = \sum_{K \leq J} d_{sym}(h) T_h(EKJ\pi) + \int_{E_{ch}}^{\infty} \frac{\rho_h(\varepsilon J\pi) d\varepsilon}{1 + \exp \left[ -\frac{2\pi}{\hbar\omega_h} (E - V_h - \varepsilon) \right]} \quad h = 1, N_h \quad (4.162)$$

where

$$T_h(EKJ\pi) = T_d(h, h) \quad (4.163)$$

and the enhancement  $d_{sym}(h)$  reads

$$d_{sym} = \begin{cases} 1 & \text{axial, mirror symmetry} \\ 2J+1 & \text{axial asymmetry, mirror symmetry} \\ 2 & \text{axial symmetry, mirror asymmetry} \end{cases} \quad (4.164)$$

Increasing the excitation energy, the strength of the imaginary potential increases and the entire flux transmitted through the inner hump is absorbed in the second (isomeric) well ( $T_{abs} \rightarrow T_A$ ), and the direct transmission through the entire barrier disappears ( $T_{dir} \rightarrow 0$ ). Therefore, the direct fission occurs only for sub-barrier excitation energies and occurs only through discrete channels

$$T_{dir}^{(h,h')}(EJ\pi) = \sum_{K \leq J} \min(d_{sym}(h), d_{sym}(h')) T_{dir}^{(h,h')}(EKJ\pi) \quad (4.165)$$

where

$$T_{dir}^{(h,h')}(EKJ\pi) = T_d(h, h') \quad h \neq h'; \quad h, h' = 1, N_h \quad (4.166)$$

For the indirect fission coefficient, the way the sum rule applies depends on the assumptions concerning the preservation of the quantum number  $K$  in the isomeric well(s). In the description of fission cross sections, one can consider two extreme limits: the first limit assumes that fission mainly proceeds through discrete transition states characterized by well-defined values of  $K$  and is known as “no K-mixing” approximation; the second limit considers that the excitation of internal degrees of freedom in the second well makes it possible for the nucleus to change its  $K$  value during the time the energy is bound in internal motions and this effect is referred to as “full K-mixing”. The effect of these approximations on the fission probability is very small, but they can affect significantly the angular correlations of the fission fragments [121]. The appropriate choice for the purpose of nuclear data evaluation is the “full K-mixing” approximation, not only for physical reasons, but also because it can be applied for any excitation energy. Formally, “full K-mixing” is described by adding the absorption from different transition states irrespective of the associated  $K$  value into a quantity preserving the spin and parity. The continuum fission channels contribute at higher energies, where the class II states are completely damped and the entire flux transmitted through the inner barrier is absorbed in the isomeric well. The main consequence is that the absorption coefficient for a certain  $J\Pi$  is:

$$T_{abs}^{(w,w')}(EJ\pi) = \sum_{K \leq J} d_{sym}(h) T_{abs}(EKJ\pi) + \int_{E_{ch}}^{\infty} \frac{\rho_h(\varepsilon J\pi) d\varepsilon}{1 + \exp \left[ -\frac{2\pi}{\hbar\omega_h} (E - V_h - \varepsilon) \right]} \quad h = w \quad (4.167)$$

with

$$T_{abs}^{(w,w')}(EKJ\pi) = T_a(w, w') \quad w \neq w' \quad (4.168)$$

The optical model for fission provides a realistic description of the fission cross section, including the resonance structure at subbarrier excitation energies due to the coupling among discrete vibrational states in different wells. Therefore, the model is recommended to be used when high accuracy in description of the experimental data is required. As mentioned before, in such cases, the parameters of the fission barriers associated to the transition states are considered free parameters and their values are extracted from systematics or from the fit of the experimental data. Even if the predictive power of the model is not very good, the descriptive power could be impressive.

**Surrogate optical model for fission.** In most of the cases, there are no available information about the barriers' parameters associated to the discrete transition states, therefore the transition state spectra are considered exclusively continuous and described by density functions. Analyzing the expressions of the fission coefficients in the previous paragraph, it can be easily noticed that the coupling among the vibrational states in the wells, determined by the degree of their damping, is contained only in the discrete terms. By cutting them, the general expression of the fission coefficient reduces to Eq.4.143 which corresponds to full damping, or in other words, to decoupled transmissions through independent humps (Figure 4.5.a). Using this expression would overestimate fission cross section of fertile nuclei at low energies. To overcome this disadvantage, in EMPIRE was

implemented an alternative way to consider partial damping, which does not involve imaginary potential or discrete transition states. In this surrogate of the optical model for fission, the degree of damping is taken into account by defining the total fission coefficient as a weighted sum of the direct coefficient corresponding to zero-damping and the indirect coefficient corresponding to full damping

$$T_f(E_x J \pi) = (1 - p(E_x)) T_{dir(0)}^{cont}(E_x J \pi) + p(E_x) T_{ind(f)}^{cont}(E_x J \pi). \quad (4.169)$$

The term  $T_{dir(0)}^{cont}$  describes the direct transmission without absorption through barriers associated to transition states in continuum. In order to calculate it, a level density describing the entire fission barrier would be needed (Figure 4.5.b). Making the assumption that the direct transmission is controlled by the minimum level density at saddles the direct fission coefficient is calculated as

$$T_{dir}^{cont}(E_x J \pi) = \int_0^\infty T_{dir(0)}(\varepsilon J \pi) \rho_{min}(\varepsilon J \pi) d\varepsilon \quad (4.170)$$

where  $T_{dir(0)}$  is given by Eq.4.141. The indirect coefficient  $T_{ind(f)}^{cont}$  is calculated with Eq.4.143, where  $T_A$  and  $T_B$  are given by the second term in Eq.4.162. The weight  $p(E_x)$  ranges from 0 for excitation energies close to the bottom of the well(s) to 1 for excitation energies close to the height of the lowest hump [128]. Compared to the optical model for fission, this

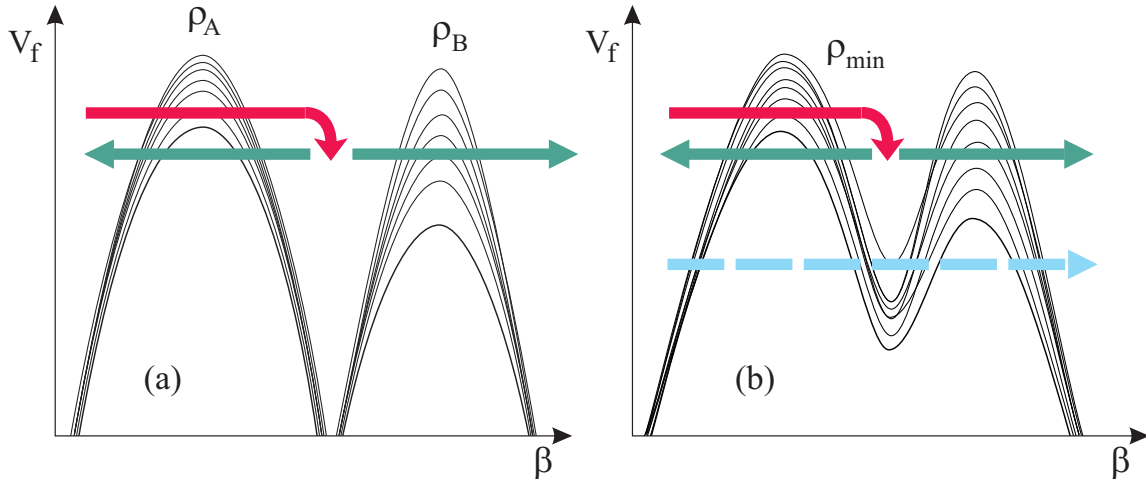


Figure 4.5: Illustration of the transmission mechanisms through fission barriers: (a) decoupled transmissions through independent humps, (b) direct transmission at low energies (dashed arrow) and decoupled transmissions at energies comparable or higher than the barrier height (full arrows).

alternative approach has the advantage that describes the direct and indirect fission mechanisms without involving many parameters. It can be used also when discrete transition states are considered, but the resonant structure is not equally well reproduced. In the



optical model for fission, with increasing energy the imaginary potential strength increases and the resonances get damped (become wider and flatter until they disappear). In the surrogate approach the resonances, coming from the direct term, remain undamped, only their contribution diminishes together with the increase of the weight  $p$ .

It is recommended to use this model when only information about the fundamental barrier and the level densities at saddles are available. The model was used to test microscopic barriers defined numerically [128], a relevant example being presented in Figure 4.6.

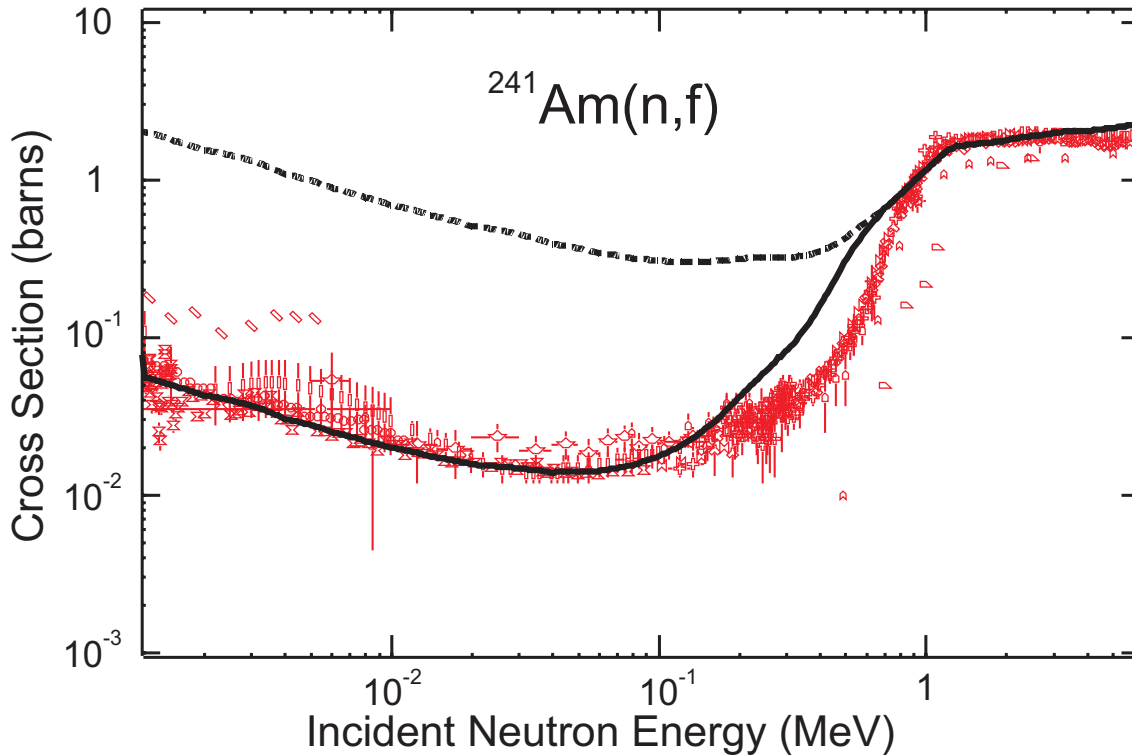


Figure 4.6: Neutron induced fission cross section of  $^{241}\text{Am}$  calculated with microscopic fission barrier [123] and level densities at saddles [129]. The full curve was obtained using Eq.4.169 and dashed curve was obtained using Eq.4.143.

### Multi-modal fission

In multi-modal fission different discrete and continuous spectra for the transition states at the outer saddle are considered for each mode. In Empire code are considered 3 modes: the super-long symmetric (SL) to which is associated a high and narrow barrier where the nuclear shape is supposed to be mass symmetric and 2 standard mass asymmetric (S1) and (S2).

In the multi-modal fission the total fission probability is the sum of each mode contribution

$$P_f = \sum_m P_{f,m} \quad (4.171)$$

with

$$P_{f,m} = M_m \cdot \frac{T_f}{T_f + \sum_d T_d} \quad (4.172)$$

where  $M_m$  is the mode weight ( $M_m = T_{h2,m} / \sum_m T_{h2,m}$ ) and  $T_f$  is the total fission coefficient

$$T_f = \frac{T_{h1} \sum_m T_{h2,m}}{T_{h1} + \sum_m T_{h2,m}}. \quad (4.173)$$

The multi-modal fission is selected by the key input FISM0D> 0: FISM0D=1 stands for (SL) + (S1) (illustrated in Figure 4.2) and FISM0D=2 for (SL) + (S1)+ (S2). It is implemented only for two humped barrier, for EGSM saddle-densities and in the limit of full damping (FISOPT=0).

#### 4.4.2 Sierk model for fission (FISSHI=1)

##### Fission barriers

The liquid-drop spin dependent fission barriers for  $19 < Z < 102$  are calculated using the BARFIT subroutine [14], which also provides ground state energies and the compound nucleus stability limit with respect to fission (i.e., spin value at which liquid-drop fission barrier disappears). BARFIT consists of a fit to the barriers calculated by Sierk within the rotating droplet model, using Yukawa-plus-exponential double folded nuclear energy, exact Coulomb diffuseness corrections, and diffuse-matter moments of inertia. The calculated barriers for  $l = 0$  are accurate to a little less than 0.1 MeV. The output from the BARFIT subroutine is a little less accurate. Errors may be as large as 0.5 MeV but the characteristic uncertainty is in the range of 0.1-0.2 MeV. The values of ground state energy are generally approximated to within about 0.1-0.2 MeV. The approximate value of the stability limit is nearly always within  $0.5\hbar$  of the calculated one.

For nuclei with  $Z \geq 102$  the recent parametrization of the Thomas-Fermi fission barriers at zero spin is used [130] .

$$B_f(J = 0) = S(N, Z)F(X), \quad (4.174)$$

where  $S$  is proportional to the nominal surface energy of the nucleus, and is given by

$$S = A^{2/3}(1 - kI^2), \quad (4.175)$$

with  $I = (N - Z)/A$  and  $k = 1.9 + (Z - 80)/75$ . The fissility is proportional to the ratio of the nominal Coulomb and surface energies of a sphere:

$$X = Z^2/A(1 - kI^2). \quad (4.176)$$

The function  $F$  is

$$\begin{aligned} F(X) &= 0.000199749(X - X_0)^3 & \text{for } X_1 \leq X \leq X_0 \\ F(X) &= 0.595553 - 0.124136(X - X_1) & \text{for } 30 \leq X \leq X_1 \end{aligned} \quad (4.177)$$

with  $X_0 = 48.5428$  and  $X_1 = 34.15$ . These formulae predict vanishing barriers for nuclei with  $Z \geq 110$ . Spin dependence is not provided by Eqs. 4.174-4.177. The EMPIRE code assumes that angular momentum dependence calculated with BARFIT for  $Z=102$  and  $A=256$  is also valid for the heavier nuclei.

The full fission barrier is a sum of the liquid-drop part and the shell correction  $\delta_W$  taken with the opposite sign. The latter is assumed to gradually disappear with spin  $J$  and temperature  $T$  so that the fission barrier becomes

$$B_f(T, J) = B_{ld}(J) - f(T) g(J) \delta_W. \quad (4.178)$$

The temperature fade-out function was found [95] to be

$$\begin{aligned} f(T) &= 1 & \text{for } T < 1.65 \text{ MeV} \\ f(T) &= e^{1.066(1.65-T)} & \text{for } T \geq 1.65 \text{ MeV}. \end{aligned} \quad (4.179)$$

For the angular momentum fade-out the following formula is used [95]

$$g(J) = \frac{1}{1 + \exp[(J - J_{1/2})/\Delta J]} + d \cdot \exp[(J - J_G)^2/\Delta J_G^2], \quad (4.180)$$

where the first term accounts for the overall decrease of the shell correction due to the increasing nuclear deformation, while the second one (of Gaussian type) permits the inclusion of fluctuations characteristic of the particular nucleus. The parameters  $J_{1/2}$  and  $\Delta J$  vary slowly with the mass number. Typical values for heavy nuclei are about 20-25 for  $J_{1/2}$  and 2-3 for  $\Delta J$ . The Gaussian correction can be used only if the relevant parameters can be determined from the experimental data.

The saddle-point moments of inertia are calculated using Sierk's routine MOMFIT [14], which provides a fit to the advanced liquid-drop model calculations as mentioned in subsection 4.2.4.

### Dissipation effects

The fission process is delayed by the dissipation effects. They are treated in an approximate, time-independent approach [131, 132, 133], which takes into account: (i) the stationary limit of Kramers [133] and (ii) the exponential factor [132] applied to the Kramers' fission width to account for the transient time after which the statistical regime is reached. The classical Hill-Wheeler fission width  $\Gamma_f^{HW}$  is modified to obtain Kramers limit

$$\Gamma_f^K = \Gamma_f^{HW} (\sqrt{1.0 + (\beta_v/2\hbar\omega)^2} - \beta_v/2\hbar\omega) \quad (4.181)$$

where  $\beta_v$  is the reduced dissipation coefficient and  $\omega$  describes the potential curvature at the fission saddle point. In addition, the fission width is reduced to account for the transient time needed to form a saddle point [132]

$$\Gamma_f = \Gamma_f^K \exp\left(-1.51768\tau \sum_x \Gamma_x\right), \quad (4.182)$$

where  $x$  runs over all particle channels and  $\tau$  is given by

$$\begin{aligned} \tau &= \beta_v^{-1} \ln(10 \frac{B_f}{T}) & \text{for } \beta_v < 3.2 \cdot 10^{-21} \text{ s}^{-1} \\ \tau &= 0.19531 \beta_v \ln(10 \frac{B_f}{T}) & \text{for } \beta_v \geq 3.2 \cdot 10^{-21} \text{ s}^{-1} \end{aligned} \quad (4.183)$$

$T$  is a nuclear temperature, and  $\beta_v = 3.2 \cdot 10^{-21} \text{ s}^{-1}$  is assumed to separate under-damped and over-damped motion.

### 4.4.3 Prompt Fission Neutrons

The prompt fission neutrons play an important role in neutronics calculations for nuclear applications. It has been shown that estimated uncertainties in the prompt fission neutron spectrum can significantly impact the results of transport simulations for critical assemblies as well as reactor sensitivity calculations [134]. The main difficulty with the modeling of prompt fission neutron spectra (PFNS) is that their shape is not well defined experimentally. In addition, it is also important to know the PFNS as a function of both the fissioning nucleus and its excitation energy. Due to this sensitivity, PFNS has to be included in the adjustment to avoid unphysical modification of other quantities, e.g., fission cross sections, that might result from compensating deficiencies in the PFNS. In the current version of the EMPIRE code we have implemented PFNS calculations using Los Alamos and Kornilov models. We have decided to include both formulations to have some model variations and flexibility; since there is a controversy regarding the lower energy part of the spectra - the Los Alamos model tends to predict lower values versus the Kornilov model. Other shape differences are also significant.

#### Los Alamos model for prompt fission neutron spectra

The Madland-Nix or Los Alamos model [135] constitutes the basis for the evaluation of prompt fission neutrons spectra in most current evaluated nuclear data libraries. According to the Los Alamos model [135], both the Watt and Maxwellian spectra neglect two important physical effects: 1) the distribution of fission-fragment residual nuclear temperature that results from the initial distribution of fission-fragment excitation energy and the subsequent cooling of the fragments as neutrons are emitted and 2) the energy dependence of the cross section for the inverse process of compound nucleus formation. Furthermore, the Maxwellian spectrum also neglects the center-of-mass motion of the fission fragments from which the neutrons are emitted; therefore, the agreement between spectra and data is achieved by adjusting parameters to values that are somewhat unphysical. The Los Alamos

model addresses these inconsistencies by taking the distribution of fission-fragment residual nuclear temperature to be triangular in shape, extending linearly from zero to a maximum value  $T_m$ , and calculating the energy-dependent compound nucleus cross section for representative average fission fragments by use of an optical model. This permits  $N(E)$  to be calculated easily for any fissioning nucleus at any excitation energy. Weisskopf statistical evaporation theory [136] is used to explain the emission of neutrons from an excited compound nucleus (CN) at a given temperature  $T$ , and a triangular distribution of initial fission fragments residual temperatures is assumed.

This model is the basis for evaluation of prompt fission neutrons spectra in most currently evaluated nuclear data libraries. This relatively simple and compact formalism, with only a handful of adjustable parameters, has been very successful in predicting the prompt fission neutrons spectra for neutron-induced as well as spontaneous fission reactions for a wide range of actinides and incident neutron energies. More refined and/or elaborate versions of the Los Alamos model have been developed in recent years for evaluation purposes, but they all rely on the implementation of this model in the first place. The Los Alamos (LA) model is described at length in Ref. [135]. We will only summarize its main features here.

**Center-of-mass neutron energy spectrum.** The neutron energy spectrum in the center-of-mass of a fission fragment is given by

$$\phi(\epsilon) = \frac{2\sigma_c(\epsilon)\epsilon}{T_m^2} \int_0^{T_m} k(T) T \exp(-\epsilon/T) dT \quad (4.184)$$

with the temperature-dependent normalization constant  $k(T)$

$$k(T)^{-1} = \int_0^\infty \sigma_c(\epsilon) \epsilon \exp(-\epsilon/T) d\epsilon. \quad (4.185)$$

$\sigma_c(\epsilon)$  is the energy-dependent cross section for the inverse process of CN formation. Equation (4.184) was obtained by integrating over a triangular distribution of temperatures with a maximum temperature  $T_m$ .

**Laboratory neutron energy spectrum.** In the laboratory system, the neutron energy spectrum  $N(E)$  for a fission fragment moving with a kinetic energy per nucleon  $E_f$  is

$$N(E) = \frac{1}{4\sqrt{E_f}} \int_{(\sqrt{E}-\sqrt{E_f})^2}^{(\sqrt{E}+\sqrt{E_f})^2} \frac{\phi(\epsilon)}{\sqrt{\epsilon}} d\epsilon, \quad (4.186)$$

where  $E$  is the laboratory neutron energy.

Inserting (4.184) into (4.186), the laboratory neutron energy spectrum  $N(E)$  becomes

$$N(E) = \frac{1}{2\sqrt{E_f}T_m^2} \int_{(\sqrt{E}-\sqrt{E_f})^2}^{(\sqrt{E}+\sqrt{E_f})^2} \sigma_c(\epsilon) \sqrt{\epsilon} d\epsilon \times \int_0^{T_m} k(T) T \exp(-\epsilon/T) dT, \quad (4.187)$$

with  $k(T)$  given by Eq. (4.185).

Considering the most probable fragmentation only, the average center-of-mass neutron energy spectrum  $\phi(\epsilon)$  is therefore given by an average over the spectra for the light and heavy fragments as

$$\phi(\epsilon) = \frac{1}{2} (\phi_L(\epsilon) + \phi_H(\epsilon)), \quad (4.188)$$

and similarly for the laboratory neutron energy spectrum  $N(E)$

$$N(E) = \frac{1}{2} (N_L(E) + N_H(E)). \quad (4.189)$$

In the last two equations, it is implicitly assumed that half of the emitted neutrons come from the light fragment and the other half from the heavy fragment.

**Average prompt neutrons multiplicity.** The average prompt fission neutrons multiplicity  $\bar{\nu}_p$  is simply obtained from energy conservation:

$$\bar{\nu}_p = \frac{\langle E^* \rangle - \langle E_\gamma^{tot} \rangle}{\langle S_n \rangle + \langle \epsilon \rangle}, \quad (4.190)$$

where  $\langle E^* \rangle$  is the average total excitation energy and is equal to

$$\langle E^* \rangle = \langle E_r \rangle + B_n + E_n - \langle E_f^{tot} \rangle. \quad (4.191)$$

$\langle E_r \rangle$  is the average fission energy release,  $B_n$  is the neutron binding energy of the target nucleus,  $E_n$  is the neutron incident energy,  $\langle E_f^{tot} \rangle$  is the average total fission-fragment kinetic energy,  $\langle E_\gamma^{tot} \rangle$  is the average total energy carried away through gamma-ray emission,  $\langle S_n \rangle$  is the average neutron separation energy of the fission fragments, and  $\langle \epsilon \rangle$  is the average energy of the outgoing neutron in the center-of-mass reference frame.

**Multiple-chance fission.** At higher incident neutron energies, above the neutron binding energy, the excited compound system may emit one or several neutrons before undergoing fission. Although the neutrons emitted prior to fission are not directly related to the ones emitted from the fission fragments, in the LA model they are treated in a similar way. In the case of multiple-chance fission, the prompt fission neutron spectrum in the laboratory system can be written as

$$N(E) = \frac{\sum_i P_f^i \left( \sum_{j=1}^{i-1} \phi_j(E) + \bar{\nu}_i N_i(E) \right)}{\sum_i P_f^i (i - 1 + \bar{\nu}_i)} \quad (4.192)$$

where  $\phi_j(E)$  is the pre-fission evaporation spectrum for the  $(j+1)^{th}$ -chance fission channel, and  $P_f^i$  is the  $i^{th}$ -chance fission probability.

The average prompt neutron multiplicity can be obtained similarly

$$\bar{\nu} = \frac{\sum_i P_f^i (i - 1 + \bar{\nu}_i)}{\sum_i P_f^i} \quad (4.193)$$

The  $i^{th}$  prompt neutron multiplicity  $\bar{\nu}_i$  is given by

$$\bar{\nu}_i = \frac{\langle E_i^* \rangle - \langle E_{\gamma_i}^{tot} \rangle}{\langle S_n^i \rangle + \langle \epsilon_i \rangle}, \quad (4.194)$$

where the average total excitation energy for the  $i^{th}$ -chance fission is

$$\begin{aligned} \langle E_i^* \rangle &= \langle E_r^i \rangle + B_n(A) + E_n - \langle E_f^i \rangle \\ &\quad - \sum_{j=1}^{i-1} (B_n(A - j + 1) + \langle \epsilon_j \rangle) \end{aligned} \quad (4.195)$$

Here,  $\langle \epsilon_j \rangle$  is the mean kinetic energy of the neutron evaporated from the  $(Z, A - j + 1)$  nucleus.

### Kornilov model for prompt fission neutron spectra

The Kornilov model [137] is actually a phenomenological systematics that allows to reproduce measured PFNS. The essential argument for including the Kornilov model in the EMPIRE code in addition to the Los Alamos model is the fact the both models differ in predicted shape of the PFNS. The Kornilov model tends to provide results that are higher at low emission energies than the Los Alamos model. This difference has been shown to influence integral testing. Therefore, it has been considered important to use both models in the assimilation procedure, which eventually might help to decide which model performs better.

The Kornilov model makes use of two Watt spectra to describe emission of neutrons with energy  $E$  from a fragment  $i$  (low mass ( $i = l$ ) and high mass ( $i = h$ )) created in the fission event induced by a neutron with energy  $E_o$

$$\begin{aligned} W_i(E, E_{\nu i}, T_i(E_o)) &= M(E, T_i(E_o)) \exp\left(-\frac{E_{\nu i}}{T_i(E_o)}\right) \frac{\sinh(\sqrt{bE})}{\sqrt{bE}} \\ b &= \frac{4E_{\nu i}}{T_i^2(E_o)}, \end{aligned} \quad (4.196)$$

where Maxwellian  $M(E, T_i(E_o))$  is given by

$$M(E, T_i(E_o)) = \frac{2\sqrt{E}}{T_i(E_o)\sqrt{\pi T_i(E_o)}} \exp\left(-\frac{E}{T_i(E_o)}\right). \quad (4.197)$$

This formula is obtained by assuming that neutron spectra are described by a Maxwellian  $M(E, T_i(E_o))$  in the center of mass system (CM) and transforming this spectra to the laboratory frame of reference (Lab). The temperature  $T_i(E_o)$  of each fission fragment is made dependent on the incident neutron energy  $E_o$ . As in the Los Alamos model, it is assumed that neutron energy spectrum is an average over the spectra emitted from the both fragments.

$$F(E) = 0.5(W_l(E, E_{\nu l}, T_l(E_o)) + W_h(E, E_{\nu h}, T_h(E_o))) \quad (4.198)$$

The  $E_{\nu i}$  are calculated as

$$E_{\nu l} = \frac{A_h}{A_l A} \alpha T_{KE} \quad (4.199)$$

$$E_{\nu h} = \frac{A_l}{A_h A} \alpha T_{KE},$$

where  $A_l$ ,  $A_h$ , and  $A$  are masses of the two fission fragments and of the fissioning nucleus,  $\alpha$  is the adjustable parameter reducing available total kinetic energy  $T_{KE}$ , which in turn is calculated following Malinovskii *et. al.* [138], where a heavy fragment with mass  $A_h$  has atomic number  $Z_h$  given by

$$Z_h = \frac{Z}{A} A_h - 0.5 \quad (4.200)$$

and accordingly for the low mass fragment we have

$$Z_l = Z - Z_h \quad (4.201)$$

$$A_l = A - A_h. \quad (4.202)$$

The default value of the  $\alpha$  parameter in Eq. 4.199 is set according to Tab. 4.1 (1.0 is used for the nuclei not contained in Tab. 4.1). In addition,  $\alpha$  can be controlled through the input in order to scale the total kinetic energy  $T_{KE}$  entering the calculations. Values for  $T_l$  and  $T_h$  are calculated by

$$T_{l,h}^x = T_{l,h}^{Cf} \sqrt{\frac{U^x A^{Cf}}{U^{Cf} A^x}} \quad (4.203)$$

with  $T_l^{Cf} = 0.902$  MeV and  $T_h^{Cf} = 0.7675$  MeV, while  $U = E_r + B_n + E_0 + T_{KE} = U_0 + E_0$ , where  $E_r$  is the energy release,  $B_n$  is the neutron binding energy,  $E_0$  the projectile energy, and  $T_{KE}$  the total kinetic energy of the fragments. We used  $U_0^{Cf} = 32.9$  MeV.

### Implementation of the PFNS in EMPIRE code

Both Los Alamos and Kornilov models were coded as EMPIRE subroutines and linked to the code resources so that all necessary input data are made automatically available to the subroutines. The PFNS specific input data are read in through the standard EMPIRE input subroutine and can be adjusted individually. The standard EMPIRE approach allowing to adjust model parameters in function of incident energy is also used for the PFNS parameters that can thus be made energy dependent. Four parameters are defined in Empire for fitting PFNS as follows.



Table 4.1: Value of the parameter  $\alpha$  from Eq. 4.199 used to adjust the total kinetic energy for various materials.

Material	$\alpha$
$^{232}\text{Th}$	0.947
$^{233}\text{U}$	0.920
$^{235}\text{U}$	0.936
$^{238}\text{U}$	0.880
$^{237}\text{Np}$	0.873
$^{252}\text{Cf}$	0.809

- PFNTKE: This parameter is used to scale the total kinetic energy of the fission fragments,  $T_{\text{KE}}$ .
- PFNALP: This parameter is used to scale the value of  $\alpha$  as defined in Eq. 4.199, which scales the energy of both the light and heavy fragments  $E_{\nu l}$  and  $E_{\nu h}$ .
- PFNRAT: This parameter is used to adjust the ratio of the kinetic energy of the light to heavy fragments,  $E_{\nu l}/E_{\nu h}$ .
- PFNERE: Used to scale the total fission energy release  $E_r$  as defined in section 4.4.3.

All four of these parameters take a default value of 1.0; if unspecified the default values in the Empire code are used.

The current implementation does not include neutrons emitted from the compound nucleus before the fission thus it is formally restricted to the first chance fission. This restriction makes the current implementation to be applicable at incident energies up to 4-5 MeV, the typical threshold for the (n,nf) reaction, which is generally sufficient for most reactor applications. The addition of pre-fission neutrons is foreseen.

EMPIRE has been extended to automatically retrieve experimental PFNS data from the EXFOR library and translate them into a form useful for plotting. Comparison plots showing results of calculations along with the experimental data can be generated from the EMPIRE GUI. An option is provided to plot calculated and experimental data normalized to the Maxwellian distribution at an arbitrary temperature. When choosing this option each experimental data set is divided by the Maxwellian value and normalized so that the integral of the spectrum is unity. The same procedure is applied also to the calculated results. Therefore, only shapes of the PFNS are compared while the absolute value is defined by the product of a fission cross section and multiplicity of fission neutrons at a given incident energy. An example plot obtained using this system is shown in Fig. 4.7. The same figure illustrates also sensitivity of the PFNS calculations to the perturbation of the total kinetic energy of the fission fragments  $T_{\text{KE}}$  by 5%.

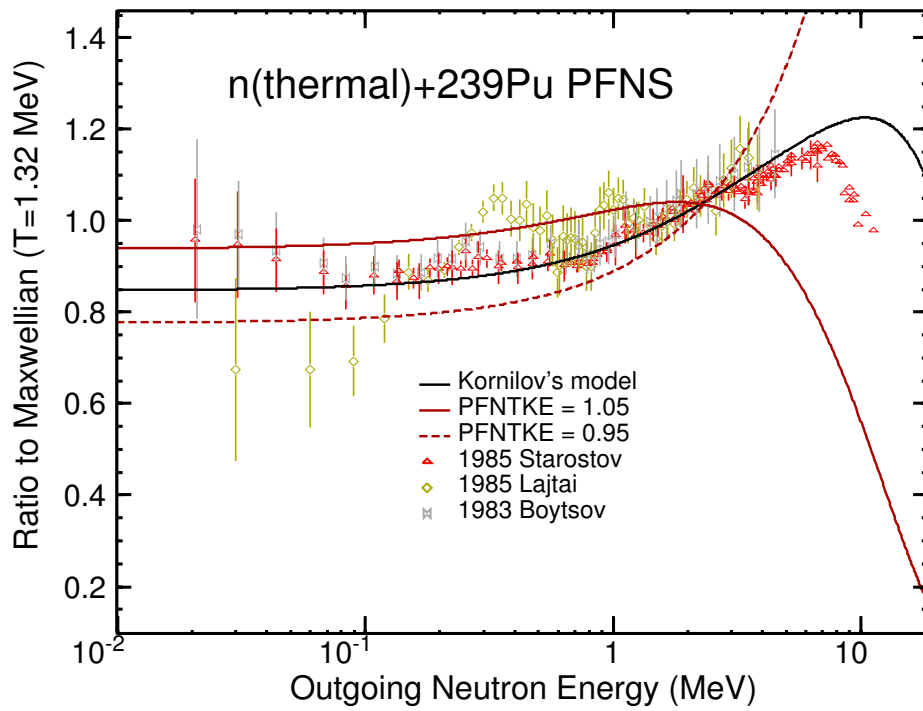


Figure 4.7: Calculated prompt fission neutron spectrum for thermal neutron induced fission on  $^{239}\text{Pu}$  compared with the experimental data. The effect of changing total kinetic energy of the fragments by 5% in both direction is shown in red. The results are normalized to the Maxwellian distribution with  $T = 1.32$  MeV.

## 4.5 Nuclear astrophysics S-factor

Although EMPIRE is a model code used primarily for nuclear data evaluation, it has the inherent capabilities to be used as a nuclear reaction model code for nuclear astrophysics applications. In that vein, the S-factor has been implemented into the EMPIRE code. The formalism that follows is valid for nonresonant reactions only. The S-factor removes the barrier penetrability (s-wave) and the  $1/E$  dependence of the cross section. It is generally expressed as

$$S(E) = \sigma(E)E \exp[2\pi\eta] \quad (4.204)$$

where  $\sigma(E)$  is the cross section and  $E$  is the center of mass energy,

$$2\pi\eta = 0.9895106848 Z_p Z_t \sqrt{\frac{\mu}{E}} \quad (4.205)$$

$$\mu = M_p M_t / (M_p + M_t), \quad (4.206)$$

where  $Z_p$  and  $Z_t$  are the charge of the projectile and target respectively,  $M_p$  and  $M_t$  stand for projectile and target masses and universal constants entering the numerical factor are taken from NIST CODATA 2010. The assumption is that within the Gamow window ( $E = E_0 \pm \frac{\Delta}{2}$  which is the narrow burning regime where reactions take place at a given stellar temperature), the S-factor is constant. The current calculation of the S-factor in EMPIRE can treat  $\gamma$ 's, neutrons and protons in the exit channel with either an  $\alpha$  or proton (only p, $\gamma$  and p,n for this case) in the incident channel.

The S-factor can be plotted via the EMPIRE GUI. An S-FACTOR.zvd file is produced for the selected reaction and can be merged with the separate S-factor c4 data file. To allow the comparison a neutron in the outgoing channel is assigned MT=1004, a proton MT=1103 and a  $\gamma$  MT of 1102.



**Part II**

**NUCLEAR DATA EVALUATION**



Evaluation of nuclear data has been a major driving force in evolution of the EMPIRE code. EMPIRE-2.19 was extensively used in the development of the ENDF/B-VII.0 library for which it produced 78 full evaluations (nearly 20% of the whole neutron sublibrary). This major exercise was also a most thorough test and validation of the system. The EMPIRE based evaluations in ENDF/B-VII.0 can be divided into (i) fission products evaluated mostly at BNL in cooperation with KAERI, LANL, ORNL and LLNL, (ii) iridium isotopes evaluated by the BNL-LANL collaboration and (iii) actinides ( $^{232}\text{Th}$  and  $^{231,233}\text{Pa}$  evaluated in the frame of the IAEA coordinated research project. The list of fission products includes 19 priority materials:  $^{95}\text{Mo}$ ,  $^{99}\text{Tc}$ ,  $^{101}\text{Ru}$ ,  $^{103}\text{Rh}$ ,  $^{105}\text{Pd}$ ,  $^{109}\text{Ag}$ ,  $^{131}\text{Xe}$ ,  $^{133}\text{Cs}$ ,  $^{141}\text{Pr}$ ,  $^{153}\text{Eu}$ ,  $^{143,145}\text{Nd}$ ,  $^{147,149,150,151,152}\text{Sm}$ , and  $^{155,157}\text{Gd}$ . Nearly all evaluations cover the standard energy range from  $10^{-5}$  eV up to 20 MeV. However, the actinide evaluations extend up to 60 MeV proving that EMPIRE is not limited to the classical ENDF energy range.

Recent developments focused on the covariances and resonance region. Need to produce a large number of covariances for the ENDF/B-VII.1 library was the major task that shaped development of the code over last 6 years. In parallel, there has been a necessity that a wealth of information contained in the Atlas of Neutron Resonances makes its way to the new version of the evaluated library. This motivated development of the resonance module of EMPIRE, which also includes covariance capabilities. These two aspects are leading subjects of this chapter, followed by the detailed description of the method used in EMPIRE for generating exclusive spectra, recoils, details of nuclear data formatting and fitting of the optical model potential.





# Chapter 5

## Resonance module

**WARNING:** The module requires that electronic version of the Atlas be installed in the *empire/Atlas*. The copy rights for Atlas belong to the publisher (Elsevier), and until restrictions on its distribution are lifted most users will not be able to install Atlas and therefore to use the resonance module of EMPIRE.

Since the 3.1 version of the EMPIRE code is equipped with the module that makes use the information contained in the Atlas of Neutron Resonances [139] to produce resonance files and related covariances for the ENDF-6 formatted files. This module facilitates practical application of the extensive compilation of the measurements in the resonance region performed since the discovery of the neutron.

The resonance module[140, 141] automates most of the procedures involved in evaluation of the resonance region. It is designed so that it can be executed within EMPIRE or as a stand-alone program. The module reads data from the electronic version of Atlas of Neutron Resonances, performs analysis of the available resonances, provides statistical distributions, and computes cross sections and covariances in the resonance region. The module also generates various plots allowing for verification of the procedure. The resonance parameters, their uncertainties and covariances are stored in ENDF-6 format. The formatted file can be later integrated into an ENDF-6 file generated by the EMPIRE code.

### 5.1 Architecture of the module

The module consists of the GUI script (`resonance.tcl`), I/O and analysis tools (`READRP` and `SCANR`), the processing code (`THERMX`), and the physics computation codes (`PTANAL` and `WRIURR`[142]):

**resonance.tcl** graphic user interface that accepts user-supplied input, controls the codes, plots results of statistical analysis of resonances, and compares graphically calculated cross sections with experimental data and other evaluated nuclear data libraries such as ENDF/B-VII.0, JEFF-3.1 and JENDL-3.3.

**READRP** reads basic physical parameters from the Atlas and RIPL.

<b>SCANR</b>	performs and plots the least square fit of the resonances to determine the upper boundary of the resolved resonance region.
<b>THERMX</b>	computes cross sections for sensitivity calculations (modified version of RECENT).
<b>PTANAL and WRIURR</b>	calculate Porter-Thomas distribution and write resonance parameters in the resolved and unresolved resonance regions. (these codes are modified with respect to the original versions to accommodate new formulae and features, retrieve the Atlas file, and fix some bugs).

The module also requires experimental data in the computational format (installed in *empire/EXFOR* directory), c4zvd and gnuplot for plotting, RECENT[15] and SIGMA1[15] codes for cross section generation, and KALMAN, empty and some additional scripts including addKalman.py and kalmanResonance for production of covariance matrix. To make it functional, 'xterm' also needs to be installed.

## 5.2 GUI control panel

At a start-up, the module reads all the necessary data for the target nucleus including individual, as well as average, resonance parameters from the Atlas of Neutron Resonances and RIPL and displays them on the screen. The evaluator has the possibility to modify the nuclear parameters before starting the calculations. Fig. 5.1 shows an example screen shot for Mn-55.

The left part of the screen is the editable input area. The evaluator has a possibility to start the new evaluation for another nuclide by entering the new ZA and MAT and then pressing the 'Reload' button. SF, Gg, D represent the strength function, average gamma width and average level spacing, respectively. Emax of the resolved and unresolved resonance regions is automatically calculated by retrieving the resonance parameters from Atlas and by reading the first excited level from RIPL respectively. In the case the  $E_{max}$  of the resolved resonance region is larger than that of the unresolved region, as shown in Fig. 5.1, the module will generate a warning.

The right part of the screen provides the buttons for displaying various plots useful for the analysis of resonances. These can be edited by clicking on the button labelled 'Edit resonance parameters'. The modified parameter table is stored on the local directory and can be reverted to the original one if necessary. The program for viewing the parameter tables and the one for visualizing plots can be both customized as in the EMPIRE GUI. For a verification purpose, the data from Atlas of Neutron Resonances can be displayed by clicking the button labelled 'Atlas of Neutron Resonances'.

Fig. 5.2 shows the "Execute" tab of the GUI. The upper part provide access to various codes that should be run to create ENDF-6 formatted file and point-wise cross sections. It contains also buttons to display comparison plots of the calculated, measured and evaluated cross sections. The resonance parameter covariances (MF=32) can be generated using

File   Input   Outputs   Help

---

**Input**   **Execute**     

---

ZA:    MAT:      

**s-wave**   **p-wave**   **d-wave**  

SF:         

Gg:         

D :    spin cut-off :   

**Resolved region**

E<sub>max</sub> :    R' :

G<sub>n0\_cut</sub>:    G<sub>n1\_cut</sub>:

**Unresolved region**

a l.d.p. :    gPower :

E<sub>max</sub> :    energies:

☐ Energy dependent D and neutron width for s-wave

☐ Energy dependent D and gamma width for p-wave

☐ Energy dependent D and gamma width for d-wave

Figure 5.1: The screen shot of GUI main control panel (“Input” area)

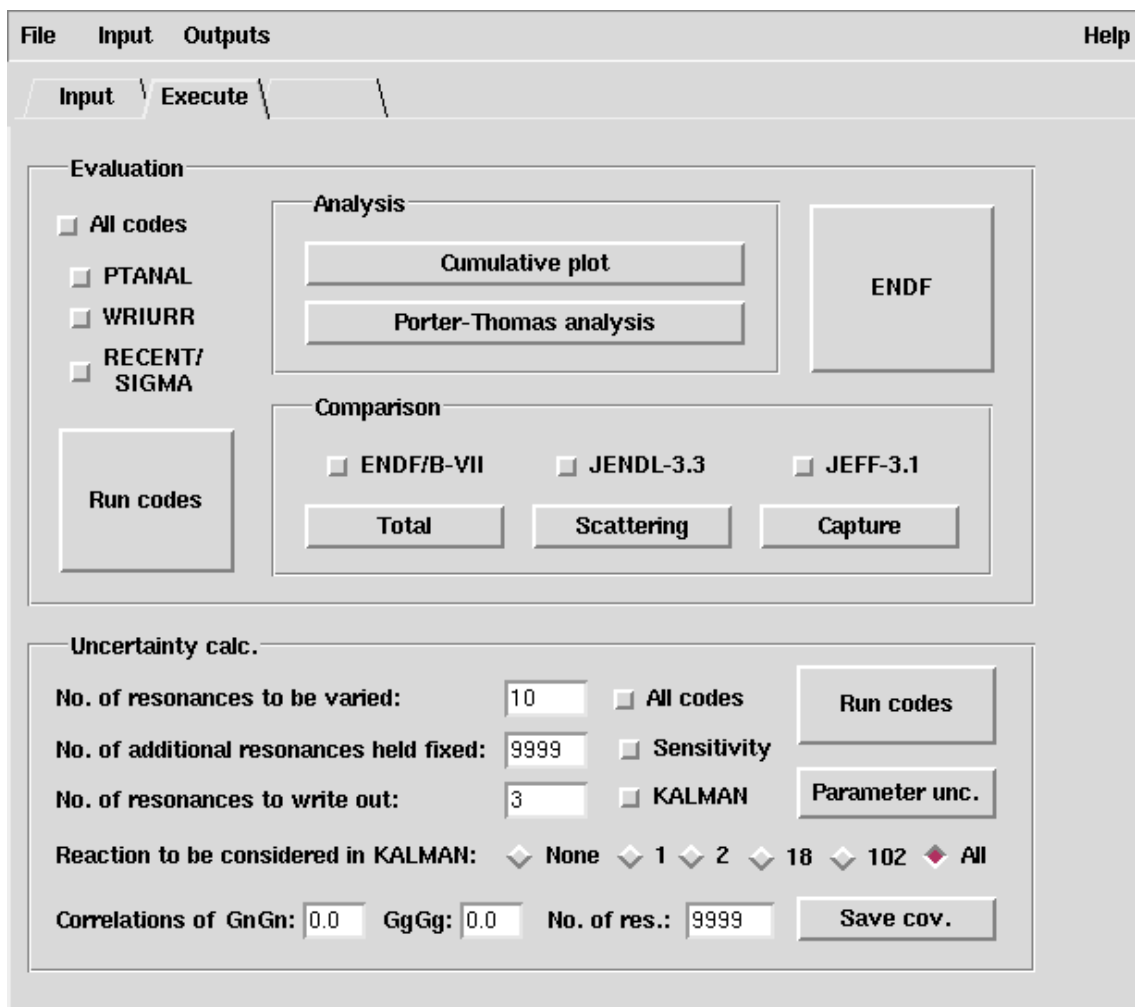


Figure 5.2: Screen shot of GUI main control panel ("Execute" tab)

KALMAN filter and previously calculated sensitivity matrices. When doing this correlations among neutron widths and among gamma widths can be supplied by the evaluator. Resulting ENDF file including the resonance parameters and covariance matrix can be stored as a file named  $[Z*1000+A]\text{-res.endf}$  by clicking on the “Save cov.” button on the bottom of the screen. Most tasks are performed in the background and their respective output files can be accessed through the “Outputs” menu on the top.



# Chapter 6

## Determination of covariances

In recent years there has been an increasing demand from nuclear research, industry, safety and regulatory bodies for best estimate predictions of system performance, such as the design and operational parameters of nuclear reactors, to be provided with their confidence bounds. Estimates of the accuracy of predictions of such integral quantities can be obtained through the propagation of uncertainties in evaluated microscopic neutron cross section data.

A methodology for evaluating cross section covariance data has therefore been developed within the EMPIRE code system. The methodology covers the thermal energy, resolved resonance, unresolved resonance and fast neutron regions and builds on the following major components:

- Nuclear reaction model code EMPIRE,
- Atlas of Neutron Resonances [139],
- Kalman filter code [143] and Monte Carlo sampling [144].

EMPIRE provides a natural environment for implementing the covariance evaluation capabilities. It is built around a physics core designed for modeling low- to-intermediate-energy nuclear reactions. It incorporates an extensive set of nuclear reaction models able to describe all relevant reaction mechanisms, each of them conveniently coupled to the up-to-date library of input model parameters [145]. The code is also suitable for massive calculations, is easy to use, has readily available default input values for all parameters, and is applicable to a wide range of target nuclei and incident neutron energies from about 1 keV to 150 MeV. Results may be stored in ENDF-6 format and subsequently plotted against experimental data for verification.

The resonance module extends EMPIRE's covariance capability to the thermal and resonance ranges. The module utilizes the recently published Atlas of Neutron Resonances [139], a monumental work by S.F. Mughabghab represents the 5<sup>th</sup> edition of what was previously well known as the BNL-325 Reports. The resonance module contains an electronic version of these resonance parameters along with modernized versions of the

legacy codes used to develop and maintain the Atlas. In addition, the Atlas contains parameter uncertainties and the resonance module was extended to utilize this information for producing covariances in the thermal and epithermal regions.

The generation of covariances at the NNDC is based on the deterministic Kalman filter technique, which is used in the thermal and resonance range as well as in the fast neutron range. The IAEA developers opted for the stochastic Monte Carlo (MC) procedure to generate the model-prior, coupled to the generalized least-squares code GANDR [146] to include the experimental data. There are several fundamental and operational differences between the two methods. MC propagates uncertainties of model parameters by means of random sampling while deterministic propagation of uncertainties, using the first-order Taylor expansion, is used in the Kalman approach. Accordingly, higher-order effects are included in MC but not in Kalman. The two approaches currently also differ regarding treatment of experimental data; it is naturally included in Kalman whereas a generalized least squares code GANDR must be run with the MC generated model-based prior as input.

It is evident that both methods have their advantages and disadvantages. Availability of both approaches within a single code system offers the user the choice of the appropriate method for a given application.

## 6.1 EMPIRE-KALMAN approach

In order to assess the direction of the gradient in the multi-parameter space that minimizes  $\chi^2$ , the fitting code has to evaluate how much the cross sections change when a certain parameter is varied in a given direction, i.e. the sensitivity of the cross section in respect to each parameter variation. This information is contained in the *sensitivity matrix* file.

The Kalman filter technique is used both in the resonance and in the fast neutron region. It is based on minimum variance estimation and naturally combines covariances of model parameters, of experimental data and of cross sections. This universality is a major advantage of the method. KALMAN uses measurements along with their uncertainties to constrain covariances of the model parameters via the sensitivity matrix. Then, the final cross section covariances are calculated from the updated covariances for model parameters. This procedure consistently accounts for the experimental uncertainties and the uncertainties of the model parameters ensuring that the final cross section uncertainties are at least as good as the smaller of the two. We emphasize that under the term “reaction model” we mean also the resonance region described by models such as the Multi-Level Breit-Wigner formalism.

### 6.1.1 Sensitivity calculation

The key ingredient of the method is the sensitivity matrix, which represents complex nuclear reaction calculations. If we denote the combination of nuclear reaction models as an operator  $\hat{\mathbf{M}}$  that transforms the vector of model parameters  $\mathbf{p}$  into a vector of



cross sections  $\sigma(\mathbf{p})$  for a specific reaction channel, then the sensitivity matrix  $\mathbf{S}$  can be interpreted as the linear term in the expansion of the operator  $\hat{\mathbf{M}}$ ,

$$\begin{aligned}\hat{\mathbf{M}}\mathbf{p} &= \sigma(\mathbf{p}) \\ \hat{\mathbf{M}}(\mathbf{p} + \delta\mathbf{p}) &= \sigma(\mathbf{p}) + \mathbf{S}\delta\mathbf{p} + \dots\end{aligned}\quad (6.1)$$

We use ‘hat’ to stress that  $\hat{\mathbf{M}}$  is the operator rather than a matrix. In practice, the elements  $s_{i,j}$  of the sensitivity matrix are calculated numerically as partial derivatives of the cross sections  $\sigma$  at the energy  $E_i$  with respect to the parameter  $p_j$ ,

$$s_{i,j} = \frac{\partial\sigma(E_i, \mathbf{p})}{\partial p_j}. \quad (6.2)$$

In case of covariance determination, the initial values of the parameters,  $\mathbf{p}_0$ , are already optimized, *i.e.*, when used in the model calculations they provide the evaluated cross sections. Their covariance matrix  $\mathbf{P}_0$  is assumed to be diagonal while the uncertainties of the parameters are estimated using systematics, independent measurements or educated guesses. The model-based covariance matrix (prior) for the cross sections,  $\mathbf{C}_0$ , can be obtained through a simple error propagation formula,

$$\mathbf{C}_0 = \mathbf{S}\mathbf{P}_0\mathbf{S}^T, \quad (6.3)$$

where superscript T indicates a transposed matrix.

The experimental data, if available, are included through a sequential update of the parameter vector  $\mathbf{p}$  and the related covariance matrix  $\mathbf{P}$  as

$$\begin{aligned}\mathbf{p}_{n+1} &= \mathbf{p}_n + \mathbf{P}_n\mathbf{S}^T\mathbf{Q}_{n+1}(\sigma_{n+1}^{\text{exp}} - \sigma(\mathbf{p}_n)) \\ \mathbf{P}_{n+1} &= \mathbf{P}_n - \mathbf{P}_n\mathbf{S}^T\mathbf{Q}_{n+1}\mathbf{S}\mathbf{P}_n.\end{aligned}\quad (6.4)$$

Here,

$$\mathbf{Q}_{n+1} = (\mathbf{C}_n + \mathbf{C}_{n+1}^{\text{exp}})^{-1}, \quad (6.5)$$

where  $n = 0, 1, 2, \dots$  and  $n + 1$  denotes update related to the sequential inclusion of the  $(n + 1)^{\text{th}}$  experimental data set. In particular, the subscript 1  $\equiv 0 + 1$  denotes updating model prior ( $n = 0$ ) with the first experiment. Vector  $\mathbf{p}_{n+1}$  contains the improved values of the parameters starting from the vector  $\mathbf{p}_n$ , and  $\mathbf{P}_{n+1}$  is the updated covariance matrix of the parameters  $\mathbf{p}_{n+1}$ . The  $\mathbf{C}_{n+1}^{\text{exp}}$  is the cross section covariance matrix for the  $(n + 1)^{\text{th}}$  experiment. The updated (posterior) covariance matrix for the cross sections is obtained by replacing  $\mathbf{P}_0$  with  $\mathbf{P}_{n+1}$  in Eq. (6.3),

$$\mathbf{C}_{n+1} = \mathbf{S}\mathbf{P}_{n+1}\mathbf{S}^T. \quad (6.6)$$

The updating procedure described above is often called Bayesian, although Eqs. (4-6.6) can be derived without any reference to the Bayes theorem.

The experimental covariance matrix,  $\mathbf{C}_n^{\text{exp}}$ , is usually non-diagonal, due to the correlations among various energy points  $E_i$ . Assuming that systematic experimental uncertainties are fully correlated, the matrix elements are expressed through the statistical,  $\Delta^{\text{sta}}\sigma_n^{\text{exp}}$ , and systematic,  $\Delta^{\text{sys}}\sigma_n^{\text{exp}}$ , experimental uncertainties. This yields

$${}_nC_{i,i}^{\text{exp}} = (\Delta^{\text{sta}}\sigma_n^{\text{exp}}(E_i))^2 + (\Delta^{\text{sta}}\sigma_n^{\text{exp}}(E_i))^2 \quad (6.7)$$

and, for  $i \neq k$ ,

$${}_nC_{i,k}^{\text{exp}} = \Delta^{\text{sys}}\sigma_n^{\text{exp}}(E_i) \times \Delta^{\text{sys}}\sigma_n^{\text{exp}}(E_k). \quad (6.8)$$

An important technical issue, which has to be addressed in most of the covariance methods, is ensuring that the energy grid,  $E_i$ , for the model calculations and experimental data is the same to enable matrix operations in Eqs. (4-6.6). In the KALMAN code this is achieved by bi-spline interpolation of model cross sections and sensitivity matrices.

The above description can easily be generalized to account for correlations among different experiments. To this end one should construct a single vector containing all experimental points and the related covariance matrix, which now may contain blocks correlating different experiments. Only one update is needed in such a case but the covariance matrices are much bigger (in the current implementation of the Kalman filter the model-based covariance matrix is expanded to match the experimental one).

The quality and consistency of the evaluated cross sections can be assessed by scalar quantity

$$\chi^2 = \sum_{n=1}^N (\boldsymbol{\sigma}_n^{\text{exp}} - \boldsymbol{\sigma}(\mathbf{p}_N))^T (\mathbf{C}_n^{\text{exp}})^{-1} (\boldsymbol{\sigma}_n^{\text{exp}} - \boldsymbol{\sigma}(\mathbf{p}_N)), \quad (6.9)$$

where  $\mathbf{p}_N$  is the final set of model parameters corresponding to the inclusion of  $N$  experiments. A value of  $\chi^2$  per degree of freedom exceeding unity indicates underestimation of the evaluated uncertainties. It is a fairly common practice to multiply such uncertainties by a square root of  $\chi^2$  per degree of freedom to address this issue.

## 6.2 EMPIRE-MC approach

The Monte-Carlo (MC) method is used in EMPIRE only in the fast neutron region. Its application to determination of covariances for the nuclear reaction observables is very transparent [144]. First, model input parameters that play a significant role in defining reaction observables of interest are identified. Then, the EMPIRE code is run a number of times with relevant input parameters being drawn randomly within the assumed limits around the central (optimal) values of the parameters. Typically, a flat distribution is used for drawing but there is also a provision for the Gaussian one. Each such calculation covers the desired incident energy range and produces a full set of cross sections, spectra, angular distributions and other observables. Standard statistical methods are used to obtain covariances for the calculated quantities automatically including cross-reactions correlations. The same approach can also be used for estimating cross-correlations between any two quantities.

The MC calculations are conceptually straightforward and free of certain simplifying assumptions, *e.g.*, the assumption of a linear response of the observables to the variation of parameters, which is inherent in the KALMAN method. There is no need for a preliminary sensitivity calculation and the computing time is independent of the employed number of model parameters. These advantages come at a price - the number of required calculations is in the range of hundreds and the convergence of the results has to be demonstrated.

The standard implementation of the MC method has no provision for incorporating experimental data. The final uncertainties and correlations depend only on the assumed uncertainties of the model parameters. These can be verified and adjusted ‘a posteriori’ by comparing calculated results with the spread and uncertainties of the experimental data. However, such verification and adjustment is subjective and lacks strict statistical justification. Nevertheless, the model-based covariances obtained with the MC method constitute a reliable benchmark for validating faster but more approximate KALMAN calculations. The standard implementation of the MC method has no provision for incorporating experimental data; the uncertainties and correlations depend only on the assumed uncertainties of the model parameters. However, the so-obtained covariance matrix can be used as a prior in a full analysis by the generalized least-squares method, taking experimental data and their uncertainties rigorously into account, *e.g.*, the GANDR system had been used in recent IAEA evaluations. Furthermore, the model-based covariances obtained with the MC method constitute a reliable benchmark for validating the faster but linear-model calculations with the KALMAN code.

## 6.3 EMPIRE resonance covariance module

Generation of MF32 covariances is achieved in several steps:

- Uncertainties for resonance parameters and thermal values are retrieved from the electronic version of the Atlas. The missing information is supplied by making use of systematics or estimates. These uncertainties are put into an MF=32 file of resonance parameter covariances in the compact representation. This initial matrix is diagonal since no correlations are provided in the Atlas.
- The correlations between various parameters are estimated.
- The resonance parameter uncertainties are adjusted so that the uncertainties of thermal values are reproduced, as discussed below.

The resonance module has been designed to ensure consistency among thermal cross section uncertainties and uncertainties of the resonance parameters, a feature that was not addressed during the development of the Atlas database. Thermal cross sections are usually measured with higher accuracy than resonance parameters. In order to take advantage of their superior precision while still ensuring internal consistency of the estimated covariances, we have coupled the resonance module with the Kalman filter code, which allows for an objective adjustment of the original uncertainties.

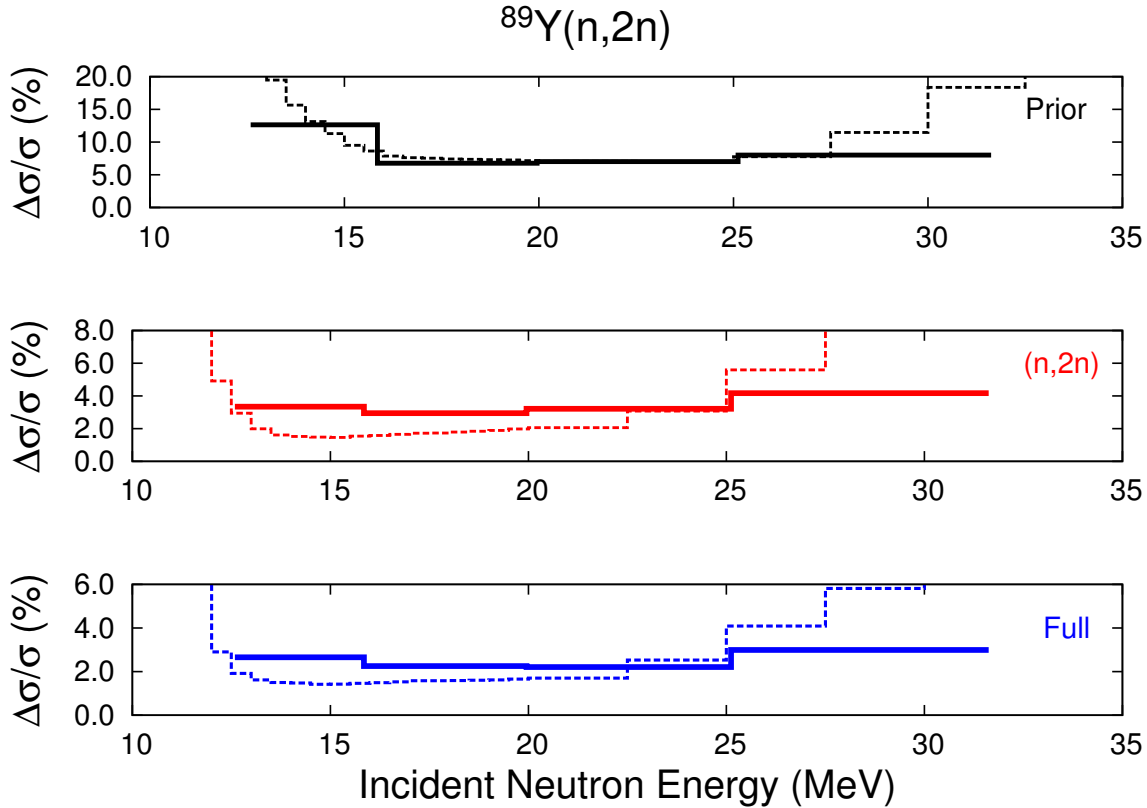


Figure 6.1: Comparison of the  $^{89}\text{Y}(n,2n)$  cross section uncertainties obtained with GANDR (solid lines) and KALMAN (dashed lines) illustrating inclusion of experimental data. The top panel shows the model-based uncertainties (prior), the middle panel includes (n,2n) data only, and the bottom panel includes experimental data for all reaction channels.

## 6.4 Inclusion of experimental data

Inclusion of experimental data into the covariance determination still appears to be a major issue. The KALMAN method accounts for them naturally but suffers from the general deficiency of all least squares type approaches - uncertainties tend to reach values that are considered far too small if very many experimental data are included in the analysis. One practical remedy to this problem is to prevent uncertainties of the model parameters to fall below some sensible limit (e.g., a systematic uncertainty of an experiment). While this procedure, often referred as marginalization, is simple and effective, it introduces certain arbitrariness into the estimation of uncertainties.

The classical formulation of the MC approach does not account for the experimental data. Thus, in the current practice, the prior (model-based cross section covariance), obtained with the EMPIRE-MC calculations, was fed into the Generalized Least Squares code ZOTT incorporated in a more general GANDR system by D.W. Muir [146].

## 6.5 Conclusions

The cross section covariance capabilities of the EMPIRE code cover the full energy range relevant to applications, including thermal, resonance and fast neutron regions. This puts EMPIRE in a unique position to provide complete sets of covariance data for most of the nuclei, such as the fission products and structural materials. The code is also well capable of treating actinides. The modules for estimating covariances for neutron multiplicities and for fission spectra are integrated into the EMPIRE code but need adequate parametrization.

In the fast neutron region there are two complementary methods implemented in EMPIRE for determining covariances. The Kalman filter approach is based on variance minimization while the stochastic one is based on the Monte Carlo sampling followed by the GANDR least-squares fitting of experimental data. The model-based covariances obtained with the two methods are practically equivalent. There is also a possibility of using KALMAN generated model-based prior with the GANDR code. The Kalman filter technique is used by the resonance module of EMPIRE to impose consistency among resonance parameter uncertainties and cross section uncertainties at the thermal energy. In general, the KALMAN code turns out to be a very powerful and useful tool for adjusting model parameters throughout the whole evaluation procedure.

Serious concerns were raised regarding extremely low uncertainties resulting from the least-squares analysis using model-generated priors. These low uncertainties arise, in part, from the rigidity of the model predictions, *i.e.*, intrinsic model uncertainties which are not accounted for in the procedure. Numerical experiments indicate that adding new degrees of freedom to the model has a desired effect on the output uncertainties and might be used to eliminate this deficiency.



# Chapter 7

## ENDF formatting

One of the primary design goals of the EMPIRE code is to perform theoretical calculations in support of nuclear data evaluation. To this end the code must meet certain requirements that go beyond usual features of similar codes used in pure science, e.g., calculation of nuclear recoils needed for energy balance and exclusive spectra, and ENDF-6 formatting of all calculated physical quantities, such as cross sections, spectra, angular distributions, energy-angle correlated distributions, etc.

### 7.1 Spectra of recoils

Energy spectra of recoils are calculated taking into account correlations between the excitation energy of the nucleus and the emission energy of the particle. In order to do so, the recoil energies are followed throughout the deexcitation cascade. A recoil spectrum is ascribed to each excitation energy bin for each nucleus involved in the decay chain. Emission of a particle depletes the spectrum bin of the parent and accumulate in the recoil spectrum bin of the daughter nucleus.  $\gamma$  emissions are assumed to produce no recoil but shift respective portions of the recoil spectrum to the lower excitation energy bin in the same nucleus. Transitions to discrete levels are summed directly to the ground state recoil spectrum, since particle emission from discrete levels is not considered and  $\gamma$ -emission does not change the recoil spectrum. At the end of the decay cascade all the recoil spectra for energy bins embedded in the continuum are null, and the final result is given by the ground state recoil spectra.

The following assumptions are made in the course of these calculations:

- Particle emission from a nucleus at a certain excitation energy is independent of the actual recoil energy of the nucleus. The center of mass motion of a nucleus (recoil) is assumed to have no effect on the emission of particles, as the latter involves internal degrees of freedom. Statistically, any emission depletes the recoil spectrum of the parent uniformly, so that for each emission the whole recoil spectrum corresponding to the parent energy bin is reduced by a constant factor.

- Compound Nucleus emissions are isotropic and uncorrelated between each other. However, forward peaked angular distributions of nucleons emitted through the pre-equilibrium or direct mechanisms and the center of mass motion of the first Compound Nucleus are retained and taken into account in constructing recoil spectra. We note that recoils are given in the laboratory system.

Ejectile emission energy is denoted by  $\varepsilon$ , excitation energy by  $E$ , nucleus recoil energy by  $e$ , and  $r$  and  $p$  subscripts are used to mark residuals and parent nuclei respectively. The  $d\sigma(e, E)/de$  stands for the recoil spectrum at the excitation energy  $E$  summed over spin and parity. Consider a single emission of an ejectile with energy  $\varepsilon$ ; the contribution of this emission to the recoil spectrum of the residual can be quantified. We apply momentum conservation in binary reactions to calculate the “recoil kick” energy ( $\Delta e$ ) for this single emission event

$$\Delta e = \frac{m_{ejc}}{m_r} \varepsilon, \quad (7.1)$$

in which  $m_{ejc}$  and  $m_r$  are the ejectile and recoil mass respectively. Similarly, the contribution to the residue recoil spectrum is obtained from the emission spectrum by applying the reverse factor

$$\frac{d\sigma(\Delta e, E_r)}{d(\Delta e)} = \frac{m_r}{m_{ejc}} \frac{d\sigma(\varepsilon, E_r)}{d\varepsilon}. \quad (7.2)$$

The recoil energy of the residue is obtained by adding the ejectile momentum and the momentum of the parent nucleus vectorially. We can express the residue recoil energy  $e_r$  through the “recoil kick” (Eq. 7.1) and the recoil energy of the parent  $e_p$  before emission

$$e_r(e_p, \theta) = \Delta e + e_p + 2\sqrt{\Delta e \cdot e_p} \cos(\theta), \quad (7.3)$$

where  $\theta$  is the angle between the momentum of the parent and the “recoil kick”. Thus the contribution to the recoil spectrum in the residue can be defined as

$$\frac{d\sigma(e_r, E_r)}{de_r} = \int_0^\infty \int_0^\pi \delta(e_r - e_r(e_p, \theta)) \left[ \frac{d\sigma(e_p, E_p)}{de_p} \right]_n \frac{d\sigma(\Delta e, E_r, \theta)}{d(\Delta e)} \sin(\theta) d\theta de_p. \quad (7.4)$$

where the  $\delta$  function ensures selection of the correct recoil energy and the square brackets  $\square_n$  around the parent recoil spectrum indicate that the integral was normalized to unity:

$$\int_0^\infty \frac{d\sigma(e_p, E_p)}{de_p} de_p = 1. \quad (7.5)$$

Integration in Eq. 7.4 is limited by the range of possible recoil energies. We note that Eq. 7.4 distributes the recoil cross section related to a single emission event over various recoil energies. The reason for this spread is two-fold: (i) vectorial coupling of momenta and (ii) recoil spectrum of the parent nucleus. Even in the case of a delta-function parent spectrum (the first CN), the residual spectrum covers the range from  $\Delta e + e_p - 2\sqrt{\Delta e \cdot e_p}$  to  $\Delta e + e_p + 2\sqrt{\Delta e \cdot e_p}$ , as results from Eq. 7.3. The  $d\sigma(\Delta e, E_r, \theta)/d(\Delta e)$  is assumed to be isotropic ( $\theta$  independent) except for the MSD and direct inelastic contributions, for which



angular distributions are preserved in Eq. 7.4. The recoil spectrum of the Compound Nucleus is single valued and differs from zero only at the energy of the Center of Mass motion. This is also the first-parent spectrum to which Eq. 7.4 is sequentially applied. We note that Eq. 7.4 refers to the emissions of a single type ejectile with a given emission energy. Eq. 7.4 is applied to all possible emissions including summation over different ejectile types and parent/residue excitation energies.

## 7.2 Exclusive spectra

EMPIRE may rearrange emission spectra to conform to the ENDF representation, which require that for a given reaction all pertinent subsequent emissions are summed up to produce effective spectra (for each ejectile) associated with the reaction. For example, neutron spectrum from the (n,2n) reaction should contain a sequence of two neutron emissions, which is followed by the  $\gamma$ -cascade only. Thus the contribution of the first neutron should be subtracted from the (n,n) and added to the (n,2n) spectrum.

A new algorithm for calculation of the exclusive spectra has been developed and implemented in EMPIRE-3.1. It is based on the concept of the 'population spectra', also used for the recoils, and avoids approximations inherent in the previous method. The new algorithm is more precise, never produces negative cross sections, and can treat an arbitrary number of emissions.

We want to calculate the populations and exclusive cross sections obtained from the statistical decay of nuclei remaining after a series of direct/pre-equilibrium reactions. We represent the properties of a nuclear state as  $\alpha = (E_\alpha^*, I_\alpha, \pi_\alpha, Z_\alpha, A_\alpha)$  and that of an ejectile as  $\beta = (e_\beta, j_\beta, l_\beta, z_\beta, a_\beta)$ . That is, we assume a complete description of a nuclear state, in terms of excitation energy, angular momentum, parity and charge and mass numbers, and of the emitted particle, in terms of emission energy, total and orbital angular momenta and charge and mass numbers. We do not take gamma emission into account. We write the differential occupation spectrum, that is, the differential (in energy) cross section/occupation of the state  $\alpha$ , as  $POP(\alpha)$ , with the initial spectrum obtained from the absorption/direct reaction as  $POP_0(\alpha)$ . We can determine the differential occupation of a given state by following the decay chain. In terms of the predecessors  $\alpha'$  of the nucleus in question, we can write

$$POP(\alpha) = \sum_{\alpha', \beta} \Pi(\alpha, \alpha'; \beta) POP(\alpha') + POP_0(\alpha),$$

where  $\Pi(\alpha, \alpha'; \beta)$  is the usual Hauser-Feshbach transition element,

$$\Pi(\alpha, \alpha'; \beta) = \frac{\rho(E_\alpha^*, I_\alpha, \pi_\alpha) \tau_c(I_\alpha, \pi_\alpha, I_{\alpha'}, \pi_{\alpha'}, e_\beta, j_\beta, l_\beta)}{\sum_{\tilde{\beta}, I_{\tilde{\alpha}}, \pi_{\tilde{\alpha}}} \int de_{\tilde{\beta}} \rho(E_{\tilde{\alpha}}^*, I_{\tilde{\alpha}}, \pi_{\tilde{\alpha}}) \tau_{\tilde{\beta}}(I_{\tilde{\alpha}}, \pi_{\tilde{\alpha}}, I_{\alpha'}, \pi_{\alpha'}, e_{\tilde{\beta}}, j_{\tilde{\beta}}, l_{\tilde{\beta}})}$$

where  $\rho(E_\alpha^*, I_\alpha, \pi_\alpha)$  is the density of states of the residual nucleus of spin  $I_\alpha$ , parity  $\pi_\alpha$  and excitation energy  $E_\alpha^* = E_{\alpha'}^* - B_\beta - e_\beta$ , with  $E_{\alpha'}^*$  the excitation energy of the initial

compound nucleus and  $B_\beta$  the separation energy of the emitted particle  $\beta$ . We assume that the transmission factor  $\tau_\beta(I_\alpha, \pi_\alpha, I_{\alpha'}, \pi_{\alpha'}, e_\beta, j_\beta, l_\beta)$  can be written in terms of the spherical optical model transmission coefficients in channel  $\beta$ ,  $T_\beta^{j_\beta l_\beta}(e_\beta)$ . It takes the form

$$\tau_\beta(I_\alpha, \pi_\alpha, I_{\alpha'}, \pi_{\alpha'}, e_\beta, j_\beta, l_\beta) = \frac{(1 + (-1)^{l_\beta} \pi_\alpha \pi_{\alpha'})}{2} T_\beta^{j_\beta l_\beta}(\varepsilon_\beta),$$

where the factor in parentheses ensures that parity is conserved.

We can simplify these expressions slightly by including the sums over the angular momentum of the emitted particle in the transmission factor. We write

$$POP(\alpha) = \sum_{\alpha', \beta} \Pi(\alpha, \alpha'; \bar{\beta}) POP(\alpha') + POP_0(\alpha),$$

with

$$\Pi(\alpha, \alpha'; \bar{\beta}) = \frac{\rho(E_\alpha^*, I_\alpha, \pi_\alpha) \tau_c(I_\alpha, \pi_\alpha, I_{\alpha'}, \pi_{\alpha'}, e_\beta)}{\sum_{\bar{\beta}, I_{\bar{\alpha}}, \pi_{\bar{\alpha}}} \int d\bar{\beta} \rho(E_{\bar{\alpha}}^*, I_{\bar{\alpha}}, \pi_{\bar{\alpha}}) \tau_{\bar{\beta}}(I_{\bar{\alpha}}, \pi_{\bar{\alpha}}, I_{\alpha'}, \pi_{\alpha'}, e_{\bar{\beta}})},$$

and  $\bar{\beta} = (e_\beta, z_\beta, a_\beta)$ , where we now have

$$\tau_\beta(I_\alpha, \pi_\alpha, I_{\alpha'}, \pi_{\alpha'}, e_\beta) = \sum_{j=|I_\alpha - I_{\alpha'}|}^{I_\alpha + I_{\alpha'}} \sum_{l=|j - s_\beta|}^{j + s_\beta} \frac{(1 + (-1)^l \pi_\alpha \pi_{\alpha'})}{2} T_\beta^{jl}(\varepsilon_\beta),$$

after taking into account angular momentum conservation when defining the sums.

We also wish to calculate exclusive cross sections, which we define as the double differential cross section/occupation for obtaining a nucleus in the state  $\alpha$  after emitting a particle  $\beta$ . This cross section, which we write as  $POPcse(\alpha, \beta)$ , takes into account all emissions of a particle  $\beta$  that lead to the final state  $\alpha$ . By following the decay chain, the exclusive cross section  $POPcse(\alpha, \beta)$  can be obtained as,

$$\begin{aligned} POPcse(\alpha, \beta) &= \sum_{\alpha'} \Pi(\alpha, \alpha'; \beta) POP(\alpha') + POPcse_0(\alpha, \beta) \\ &\quad + \sum_{\alpha' \beta'} \Pi(\alpha, \alpha'; \beta') POPcse(\alpha', \beta), \end{aligned}$$

where  $POPcse_0(\alpha, \beta)$  is the contribution of the absorption/direct reaction. The expression for the exclusive cross section has two additional terms. The first is just that of a transition to  $\alpha$  through emission of the particle  $\beta$ , which is proportional to the transition element  $\Pi(\alpha, \alpha'; \beta)$ . The second is the contribution from all anterior emissions of a particle  $\beta$  that, in the last transition, lead to the state  $\alpha$ . This can be written in terms of the exclusive cross sections of the predecessors,  $POPcse(\alpha', \beta)$ .

We can immediately sum over the emitted particle angular momenta,  $j_\beta$  and  $l_\beta$ , to write the equation defining the exclusive cross section as

$$\begin{aligned} POPcse(\alpha, \bar{\beta}) &= \sum_{\alpha'} \Pi(\alpha, \alpha'; \bar{\beta}) POP(\alpha') + POPcse_0(\alpha, \bar{\beta}) \\ &\quad + \sum_{\alpha' \bar{\beta}'} \Pi(\alpha, \alpha'; \bar{\beta}') POPcse(\alpha', \bar{\beta}). \end{aligned}$$

Ideally, we would also like to obtain expressions summed over  $I_\alpha$  and  $\pi_\alpha$  for both  $POP(\alpha)$  and  $POP_{cse}(\alpha, \bar{\beta})$ . However, for this to be possible, the summed transition element

$$\Pi(\bar{\alpha}, \alpha'; \bar{\beta}) = \frac{\sum_{I_\alpha, \pi_\alpha} \rho(E_\alpha^*, I_\alpha, \pi_\alpha) \tau_c(I_\alpha, \pi_\alpha, I_{\alpha'}, \pi_{\alpha'}, e_\beta)}{\sum_{\bar{\beta}, I_{\bar{\alpha}}, \pi_{\bar{\alpha}}} \int d\epsilon_{\bar{\beta}} \rho(E_{\bar{\alpha}}^*, I_{\bar{\alpha}}, \pi_{\bar{\alpha}}) \tau_{\bar{\beta}}(I_{\bar{\alpha}}, \pi_{\bar{\alpha}}, I_{\alpha'}, \pi_{\alpha'}, e_{\bar{\beta}})}$$

would have to be independent of  $I_{\alpha'}$  and  $\pi_{\alpha'}$ . In general, this is not the case, so that the general equations should be used. In EMPIRE, the general equation is used to determine  $POP(\alpha)$  but not  $POP_{cse}(\alpha, \bar{\beta})$ . In particular, the angular momentum dependence of the  $POP_{cse}(\alpha', \bar{\beta})$  contributions to  $POP_{cse}(\alpha, \bar{\beta})$  are neglected. We could easily avoid this approximation but calculation time would grow by orders of magnitude - the increase that would not be justified by more precise splitting of inclusive spectra into its exclusive components.

When the angular momentum dependence can be neglected, the expressions reduce to Weisskopf-Ewing ones. This is possible when we can approximate the density of states as

$$\rho(E_\alpha^*, I_\alpha, \pi_\alpha) \approx \frac{1}{2} \rho(E_\alpha^*, I_\alpha) \approx \frac{1}{2} (2I_\alpha + 1) \rho(E_\alpha^*, 0)$$

for the states occupied in the reaction. It is then possible to reduce the summed transition element to

$$\Pi(\bar{\alpha}, \alpha'; \bar{\beta}) = \frac{(2s_\beta + 1) \mu_\beta \epsilon_\beta \sigma_\beta(\epsilon_\beta) \rho(E_\alpha^*, 0)}{\sum_{\bar{\alpha}, \bar{\beta}} \int d\epsilon_{\bar{\beta}} (2s_{\bar{\beta}} + 1) \mu_{\bar{\beta}} \epsilon_{\bar{\beta}} \sigma_{\bar{\beta}}(\epsilon_{\bar{\beta}}) \rho(E_{\bar{\alpha}}^*, 0)}$$

and write the summed equations as

$$POP(\bar{\alpha}) = \sum_{\alpha', \beta} \Pi(\bar{\alpha}, \alpha'; \bar{\beta}) POP(\bar{\alpha}') + POP_0(\bar{\alpha})$$

and

$$\begin{aligned} POP_{cse}(\bar{\alpha}, \bar{\beta}) &= \sum_{\alpha'} \Pi(\bar{\alpha}, \alpha'; \bar{\beta}) POP(\bar{\alpha}') + POP_{cse0}(\bar{\alpha}, \bar{\beta}) \\ &\quad + \sum_{\alpha' \bar{\beta}'} \Pi(\bar{\alpha}, \alpha'; \bar{\beta}') POP_{cse}(\bar{\alpha}', \bar{\beta}) . \end{aligned}$$

In EMPIRE, the general equation maintaining the full angular momentum dependence is used to determine  $POP(\alpha)$  but not  $POP_{cse}(\alpha, \bar{\beta})$ . The angular momentum summed forms of the exclusive cross sections,  $POP_{cse}(\bar{\alpha}, \bar{\beta})$ , are approximated as

$$\begin{aligned} POP_{cse}(\bar{\alpha}, \bar{\beta}) &= \sum_{\alpha'} \Pi(\bar{\alpha}, \alpha'; \bar{\beta}) POP(\bar{\alpha}') + POP_{cse0}(\bar{\alpha}, \bar{\beta}) \\ &\quad + \sum_{\bar{\alpha}' \bar{\beta}'} \hat{\Pi}(\bar{\alpha}, \bar{\alpha}'; \bar{\beta}') POP_{cse}(\bar{\alpha}', \bar{\beta}) \\ &= \sum_{\bar{\alpha}'} \hat{\Pi}(\bar{\alpha}, \bar{\alpha}'; \bar{\beta}) POP(\bar{\alpha}') + POP_{cse0}(\bar{\alpha}, \bar{\beta}) \\ &\quad + \sum_{\bar{\alpha}' \bar{\beta}'} \hat{\Pi}(\bar{\alpha}, \bar{\alpha}'; \bar{\beta}') POP_{cse}(\bar{\alpha}', \bar{\beta}) , \end{aligned} \tag{7.6}$$

where the effective transition matrix element is approximated using the angular momentum dependence of the decaying population,

$$\hat{\Pi}(\bar{\alpha}, \bar{\alpha}'; \bar{\beta}') = \frac{1}{POP(\bar{\alpha}')} \sum_{I_{\alpha'} \pi_{\alpha'}} \Pi(\bar{\alpha}, \alpha'; \bar{\beta}) POP(\alpha'). \quad (7.7)$$

Note that this reduces to the Weisskopf-Ewing transition matrix element when  $\Pi(\bar{\alpha}, \alpha'; \bar{\beta})$  is independent of the spin and parity,  $I_{\alpha'}$  and  $\pi_{\alpha'}$ , of the decaying nucleus.

The same approximation is used to calculate the exclusive angular distributions, with the additional assumption that the angular dependence arises from the direct / absorption contributions to the reaction,  $POPcse_0(\bar{\alpha}, \bar{\beta})$ . An exclusive angular distribution involving the emission of  $n$  particles will thus have contributions from one direct emission followed by  $n - 1$  statistical emissions, from either of two direct emissions followed by  $n - 2$  statistical emissions, etc., up to any of  $n - 1$  direct emissions followed by one statistical emission and, finally, a contribution from any of  $n$  direct emissions.

Let us denote the exclusive angular distribution of particle  $\bar{\beta}$  at angle  $\theta$  to form the residue  $\bar{\alpha}$  as  $POPcse(\bar{\alpha}, \bar{\beta}, \theta)$  with the initial direct contribution written analogously as  $POPcse_0(\bar{\alpha}, \bar{\beta}, \theta)$ . Taking into account the considerations above, we can write an approximate equation for the angular distribution as

$$\begin{aligned} POPcse(\bar{\alpha}, \bar{\beta}, \theta) &= \frac{1}{4\pi} \sum_{\bar{\alpha}'} \hat{\Pi}(\bar{\alpha}, \bar{\alpha}'; \bar{\beta}) POP(\bar{\alpha}') + POPcse_0(\bar{\alpha}, \bar{\beta}, \theta) \\ &\quad + \sum_{\bar{\alpha}' \bar{\beta}'} \hat{\Pi}(\bar{\alpha}, \bar{\alpha}'; \bar{\beta}') POPcse(\bar{\alpha}', \bar{\beta}', \theta). \end{aligned} \quad (7.8)$$

The total direct reaction contribution can be isolated as  $POPcse_d(\bar{\alpha}, \bar{\beta}, \theta)$  with

$$POPcse_d(\bar{\alpha}, \bar{\beta}, \theta) = \sum_{\bar{\alpha}' \bar{\beta}'} \hat{\Pi}(\bar{\alpha}, \bar{\alpha}'; \bar{\beta}') POPcse_d(\bar{\alpha}', \bar{\beta}', \theta) + POPcse_0(\bar{\alpha}, \bar{\beta}, \theta). \quad (7.9)$$

For a single emission, EMPIRE calculates this as

$$POPcse_d(\bar{\alpha}, \bar{\beta}, \theta) = \sum_{\bar{\alpha}'} POPcseaf(\bar{\alpha}, \bar{\alpha}', \bar{\beta}) POPcse_0(\bar{\alpha}', \bar{\beta}, \theta), \quad (7.10)$$

where

$$POPcseaf(\bar{\alpha}, \bar{\alpha}', \bar{\beta}) = 1. \quad (7.11)$$

However, in this case the representation of  $POPcseaf(\bar{\alpha}, \bar{\alpha}', \bar{\beta})$  is greatly simplified as the energy of the first residual CN is completely correlated with that of the emitted particle, so that only two energy indices are needed to represent  $POPcseaf(\bar{\alpha}, \bar{\alpha}', \bar{\beta})$ , those of  $\bar{\alpha}$  and  $\bar{\beta}$ . For second and higher emissions this is no longer the case. When all three energy indices are needed, it is more convenient to calculate  $POPcse_d(\bar{\alpha}, \bar{\beta}, \theta)$  directly.

## 7.3 EMPEND code

The ENDF formatted file is created by the user selecting the ENDF option in the input file (\*.inp). This instructs EMPIRE to write all necessary information to the output file \*.out, which may actually become very long, depending to some extent on the choice of input options in the EMPIRE calculations. This file is processed by the utility code EMPEND written by Trkov, which creates the ENDF-6 formatted file.

EMPIRE provides inclusive cross sections for production of the residues, i.e., all paths to the final nucleus are summed together (e.g., (n,np)+(n,pn)+(n,d)). Only for the reactions involving emission of a single type of particle the reaction cross sections are exclusive (e.g., (n,n), (n,2n), (n,3n), ... or (n,p), (2p),...). As described in the previous section, user may request inclusive or exclusive particle and gamma emission spectra. Employing a rather involved bookkeeping, EMPIRE can keep track of the sequential decays to produce spectra associated with the particular residue. User may choose how many emissions are treated in the exclusive approach. The remaining emissions are inclusive, i.e., rather than providing exclusive cross sections and associated spectra for each of the reactions separately, EMPIRE can output inclusive cross sections, spectra and double-differential cross sections. This means that the total emission spectra of neutrons, protons,  $\alpha$ -particles and  $\gamma$ s are printed, instead of individual contributions from the reactions, with the exception of some distinct reactions that are always treated exclusively (e.g. inelastic, (n,2n), (n,p), etc.) This is the preferred mode of EMPIRE execution when ENDF formatting is required. EMPEND automatically recognizes the calculation options from the contents and acts accordingly.

EMPIRE also calculates cross sections for the production of metastable isomers. EMPEND recognizes these and stores them in ENDF File 10. Cross sections for radionuclide production, which can not be uniquely associated with any specific reaction (i.e. an ENDF MT number) are lumped into File 3 MT 5, but to preserve the complete information, the radionuclide production is stored in File 10, MT 5. This can be done because according to ENDF-6 rules the cross sections in File 10 by definition are not required for the reconstruction of redundant reactions.

The ENDF file has to obey the rules of sorting the data in increasing order by data type (MF number) and reaction type (MT number), so several sweeps of the EMPIRE output file must be made, which may slow down the formatting process considerably. In general, the required operations are described as follows:

- In the first sweep the cross sections and the corresponding reaction Q-values are extracted. All reading is done with the REAMF3 routine.
- In the next sweep all reactions for which particle spectra are given are identified. All reading is done with the SCNMF6 routine.
- Another sweep is made for each reaction having angular distributions. This applies to the elastic and all discrete level reactions (inelastic neutron, alpha and proton emission).

- Next follows a sweep for each reaction having energy-angle correlated outgoing particle distributions.
- Finally, a sweep is made for the remaining reactions, particularly the  $(n,\gamma)$  reaction, for which the particle distributions are coded in ENDF File-6.

In the first sweep radionuclide production cross sections are located and the MT numbers are assigned, when possible. Cross sections, which can not be identified uniquely by an MT number are assigned  $MT=10(Z*1000+A)+LFS$  where LFS is the final isomeric state of the nuclide. The spin of the target nucleus, the  $S_0$ -strength function, the average gamma width, the average level spacing and the energy-dependent scattering radius are also extracted to enable the assembly of the dummy resonance parameter file.

In the second sweep, all reactions that do not have explicitly given spectra are identified. When many exclusive spectra are requested in the EMPIRE calculation, there may be cases where particle spectra are given but no MT number is assigned. The spectra are ignored, the cross sections are added to  $MT=5$  and particle production cross sections for this MT are incremented. This preserves particle multiplicities, but spectral shapes may become distorted. After the second sweep, all necessary information is available to write the comments-section (MF=1) and the prompt nu-bar (if the nuclide is fissile). For incident neutrons a dummy resonance file (File 2) is constructed. The cross section data found on the file are fitted by a cubic spline and entered into the output ENDF file on a user-defined dense energy grid, thinned to the specified tolerance and taking reaction thresholds into account. If desired, the spline interpolation may be suppressed and the energy points found on the file are entered directly into the ENDF formatted file.

The angular distributions for discrete level reactions that appear in the ENDF File 4 sections are extracted from the spectra on the EMPIRE output file, interpolated to the appropriate energy, if necessary. Legendre polynomial coefficients in the centre-of-mass are fitted to the distributions. For elastic scattering the Legendre coefficients are copied directly from the EMPIRE output; If more than 64 Legendre coefficients are required, formatting switches automatically to pointwise representation.

The correlated energy-angle distributions for continuum reactions that appear in ENDF File-6 sections are entered in Legendre polynomial representation in the centre-of-mass coordinate system. The maximum Legendre order is limited to 64. For reactions with relatively smooth angular distributions, the number of coefficients is reduced accordingly.

Photon production information for discrete levels can be stored in ENDF Files 12 and 14. The spectra for the continuum are included in File-6 (rather than File 15). File 12 contains photon transition probabilities and photon emission probabilities for discrete level reactions, while File 14 contains the corresponding angular distributions, which are assumed isotropic. The gamma spectra of the  $(n,\gamma)$  reaction are presently stored in File-6. Primary gammas, which are optionally printed in the Empire output explicitly are not formatted. This option should not be used when ENDF formatting is required. By default, primary gammas are included in the photon spectrum in tabular form.

## 7.4 EMPEND Input instructions

The program can be executed interactively from a terminal screen. The required input is entered in response to the prompts, which are the following:

- The name of the EMPIRE output file to be processed.
- The name of the ENDF formatted file to be written.
- Number of subintervals per incident neutron energy interval on the EMPIRE output file. The subintervals define the fine energy mesh for the cross sections on the ENDF formatted file. The following are applicable:
  - 0 Only the points on the EMPIRE output are entered to the ENDF formatted file.
  - 1 The points at reaction thresholds are added. The energy points above threshold are as found in the EMPIRE output file.
  - n Threshold points are entered, but in addition, each interval on the EMPIRE output is subdivided into “n” subintervals. Cross section values at intermediate points are defined by a cubic spline fit.
- Thinning tolerance limit [%] to reduce the number of cross section points. Data points, which can be reproduced from the neighboring points by linear interpolation to within the specified tolerance, are removed. Entering a negative value for the thinning tolerance limit causes thinning to be suppressed.
- ENDF material number identifier.
- NLIB number assigned to the evaluation (see ENDF-6 manual). The parameter is optional.
- ALAB, EDATE, AUTHOR string, where each of the listed parameters occupies 11 columns (see ENDF-6 manual for details). The parameters are optional.

### NOTES:

- Extensive exclusive spectra calculations in EMPIRE should be avoided when ENDF formatting is needed, since for complex reactions when a residual nuclide can be produced from more than one reaction, the assignment of spectra can not be done uniquely. It is recommended to allow up to 4 emitted neutrons and only a single charged particle.
- All text preceding the printout for first energy is transferred to the comments section in the ENDF file (FM=1, MT=451). The easiest way to insert customized comments into the ENDF file is to modify (manually) the EMPIRE output.

- The resonance file (MF=2) that is generated for files with incident neutrons is by no means a realistic cross section representation. It is given for completeness, when no information on the resonances (other than from the systematics is available). The code places resonances spaced uniformly around the thermal value according to the given average level spacing. The neutron width is defined from the S0 strength function and the gamma-widths are the average gamma widths. The assigned resonance formalism is the Multi-level Breit-Wigner formalism with energy-dependent scattering radius.

To monitor the formatting process for quality assurance purposes, the EMPEND.LOG file is written in which the details of the formatting process are recorded. A limited amount of checking is done. An entry to the log file is added in the following cases:

- The cross section obtained by integrating the spectrum should agree with the value given directly in the EMPIRE output file. If the difference exceeds 2%, a warning message is written, giving the reaction MT number, the incident particle energy, the expected cross section (i.e. the value given directly in the EMPIRE output file) and the percent difference.
- The angular distributions are fitted to determine the Legendre polynomial expansion coefficients. If the distribution reconstructed from the Legendre polynomial coefficients differs from the pointwise values on the EMPIRE output file by more than 5%, a warning message is written, giving the reaction MT number, the outgoing particle ZA identifier, the incident and the outgoing particle energies and the percent difference in the fitted distribution from the pointwise value on the file.

Additional messages monitor the progress of the data formatting process.



## **Part III**

# **STRUCTURE OF EMPIRE CODE**



# Chapter 8

## Code

The full EMPIRE system resides in a user defined directory (e.g., *empire/*) which name is specified in an environment variable EMPIREDIR. We remind that the operation of the code depends on the file naming scheme which has to be strictly preserved. The work is organized by projects; each project has a user assigned name (e.g., [Fe56-project](#)), which forms a root of all the project files (e.g., [Fe56-project.inp](#), [Fe56-project-lev.col](#), [Fe56-project.lst](#), ...). All project files are located in the same working directory selected by the user.

### 8.1 Directory structure

The full EMPIRE system has the following directory structure (subdirectories preceded by '/'):

- **user defined directory** (e.g., *empire/*) includes the following files and subdirectories:
  - **Makefile** - Makefile used to compile the whole EMPIRE package (physics core in */source* and all utility codes in the */util* directory)
  - **/source** - source of the EMPIRE physics code divided into modules and Makefile
  - **/data** - EMPIRE library of input parameters
  - **/RIPL** - RIPL library of input parameters following the original structure of RIPL-3 [145])
    - \* **/levels** - discrete levels
    - \* **/densities** - level density parameters for various models and tables of microscopic HFB level densities
    - \* **/optical** optical model parameters and other data relevant to optical model calculations

- \* **/gamma** - data relevant to  $\gamma$ -strength functions
- \* **/fission** - data relevant to fission
- \* **/masses** - nuclear masses, g.s. deformations and abundances
- **/work** - directory in which input and output files of the calculations are stored; there can be any number of these directories with arbitrary names; starting with EMPIRE-3.1 working directories can also be placed anywhere in the system if environment variable EMPIREDIR is set (see section 8.8.6).
- **/scripts** - bash, python and Tcl/Tk scripts designed to streamline the use of EMPIRE. Scripts are described in more detail in section 8.8
- **/EXFOR** - Full EXFOR library of experimental data translated into C4 format
  - \* **/neutrons** - neutron experiments organized by isotope
  - \* **/protons** - neutron experiments organized by isotope
  - \* **/gammas** - neutron experiments organized by isotope
  - \* **/other** - neutron experiments organized by isotope
  - \* **parseC4.py** - Python script to split the master C4 file into incident particles and isotope oriented files; the master C4 file is released twice a year by the IAEA
  - \* **EXFOR14A.DAT** - dictionary linking EXFOR reaction strings to the ENDF-6 MF/MT denomination
- **/util** - utility codes
  - \* **/empend** - converts EMPIRE results into the ENDF format
  - \* **/c4sort** - sorts experimental data in the computational format file
  - \* **/fixup** - reconstructs redundant MT sections
  - \* **/legend** - calculates linearly interpolable angular distributions
  - \* **/lsttab** - tabulates ENDF and EXFOR data in PLOTTAB format
  - \* **/sixtab** - converts ENDF File 6 into Law 7 representation
  - \* **/x4toc4** - converts retrieved EXFOR data into the computational format
  - \* **/plotc4** - plots the comparison between calculated and experimental data
  - \* **/c4zvd** - ZVView plotting package
  - \* **/checkr** - ENDF-6 format checking
  - \* **/endres** - merges resonance parameters from file \*-res.endf into the new ENDF-6 formatted file containing EMPIRE results to produce full evaluation
  - \* **/fizcon** - more ENDF-6 format checking
  - \* **/psyche** - ENDF-6 file physics checking
  - \* **/linear** - makes all cross section in File 3 linearly interpolable
  - \* **/pltlst** - prepares a list of experimental data for the selected nuclide that can be compared to the data reconstructed from an ENDF file (the list file has identical format as the report file from PLOT4)

- \* **/recent** - reconstructs cross sections from the resonance parameters
- \* **/sigma1** - Doppler broadens cross sections in the resonance range
- \* **/stanef** - standardizes ENDF-6 formatted file
- \* **/zvvddx** - plots angular distributions, energy spectra and double-differential cross sections using package
- \* **/endres** - merges existing resonance parameters into ENDF-6 formatted file produced by EMPEND.
- \* **/Calc-Cov** - Codes and scripts for calculating cross section covariances using Monte Carlo (parameter uncertainties must be specified in the input file).
- \* **/cs2zvd** - Produces zvd plots of cross sections directly from EMPIRE output without ENDF-6 formatting.
- \* **/endf33zvd** - Produces three-dimensional zvd plots of covariances.
- \* **/IO** - Set of f90 modules for reading and writing ENDF-6 files .
- \* **/kalman** - KALMAN code for generating covariances and fitting experimental data.
- \* **/kercen** - C++ code for generating covariances in the resonance region using kernel approximation method to be executed as a standalone code.
- \* **/mrgmat** - Code for merging ENDF-6 files for different materials into a single file.
- \* **/pltzenmat** - Produces zed plot of cross section sensitivity to model parameters.
- \* **/resonance** - Resonance module for extracting data from the Atlas of Neutron Resonances and producing ENDF-6 formatted resonance file with covariances.
- \* **/stan** - Modern f90 replacement for STANEF.
- **/empy** - supplemental python modules for EMPIRE. See section 8.7 for more detail
- **/doc** - documentation (includes this manual)
- **/test-cases** - collection of test cases to validate installation of the EMPIRE package
- **/benchmarks** - collection of benchmarks to be used by developers
- **/Atlas** - electronic version of Atlas of Neutron Resonances (**not provided in the EMPIRE distribution!**)

The *empire* directory can be placed anywhere within the file system. For the correct functioning of the system scripts the internal structure of the *empire* directory must be preserved. The user may choose to create additional *work* directories, e.g., for each separate project or reaction studied. The additional directories may have any name and can be

placed anywhere in the system where a user has writing permission but only if the environment variable EMPIREDIR is set to point to the *empire* directory. If the EMPIREDIR is not set all working directories must be on the same level as the *work* directory (i.e., they must be sub-directories of *empire*).

## 8.2 Installation

The distribution of EMPIRE consists of five *.tgz* files and the installation script *setup-emp*. The *.tgz* files contain

- *empire-3.2.tgz* - contains EMPIRE source, parameter library, *work* sub-directory, PREPRO2000 and ENDVER packages, and format checking codes (mandatory).
- *x4cd.tgz* - EXFOR library of experimental data (... appropriate text is needed) format.
- *HFB-lev-dens.tgz* - contains files with tabulated level densities calculated in the frame of the HFB approach. Size of this file after decompression is about 145 Mb. Users who do not intend to use this option for level densities may choose not to install them.
- *fis-lev-den.tgz* - contains files with tabulated level densities at inner and outer fission barrier calculated in the frame of the HFB approach. Users who do not intend to use this option for level densities may choose not to install them.
- *X4-2-17.tgz* - obsolete Fit is (... appropriate text is needed)

Out of these files only *empire-3.2.tgz* is required to run calculations, *x4cd.tgz*, *HFB-lev-dens.tgz*, and *fis-lev-den.tgz* are optional and *X4-2-17.tgz* is redundant if *x4cd.tgz* can be used.

The easiest recommended way of installing EMPIRE is using the *setup-emp* script, which guides the user through the installation procedure. The script can be used to install sources downloaded from the Web sites as well as those provided on the CD-ROM. The script can be placed anywhere in the file system and can be invoked by typing:

*setup-emp*

at the shell prompt. The three *.tgz* files are assumed to be located in the same directory. The installation script allows the target directory to be selected and files to be installed. It also compiles all of the package using the default gfortran compiler or any other compiler specified by the user (the compiler itself must already be installed on the system).

EMPIRE can also be installed manually. To this end the *empire-3.2.tgz* file has to be uncompressed and untarred with the following commands (on UNIX systems):

```
gunzip empire-3.2.tgz
tar xvf empire-3.2.tar
```

or with a single command

```
tar xvf empire-3.2.tgz
```

on the systems which allow such an action (e.g., Linux). The same should be done with the *X4-2-xx.tgz* and *HFB-lev-dens.tgz* files if the user chooses to install them. The three *.tgz* files must be located in the same directory. The decompressed files will be placed according to the directory structure described in the previous section, with *empire* directory on the level of the *.tgz* files. The whole package can be compiled by invoking *make* command in the *empire* directory. This will execute the *make* command in the following sub-directories:

- *empire/source/*
- *empire/util/(all sub-directories)*

Users have to ensure that FORTRAN compiler is called properly. To this end, one should edit *Makefile* files in the above mentioned directories and fix calls to FORTRAN compiler. By default *gfortran* is used on Linux, MacOS X and Windows. Several other typical options are included in the *Makefile* files. These are commented with the *#* character in the first column. Users should remove this character on the line corresponding to the desired compiler and comment a line with *gfortran* instead. Systems that do not allow for the *make* utility will have to compile all *.f* and *.c* files manually using something like

```
fort *.f *.c -o empire
```

in the *empire/source/* directory. The utility executables should be named after their respective directories, i.e., *plotc4*, *x4toc4*, etc.. In most cases this is achieved with the *-o* option as in the example above. This syntax may differ for various compilers.

For full functionality EMPIRE requires the following software:

- FORTRAN (GNU *gfortran* 4.4 or later is recommended as a freely available compiler for all platforms, including Linux, Mac OS X and Windows; in case of Windows *gfortran* 4.4 contains basic bash shell, *awk*, and *gcc* that are sufficient to run EMPIRE scripts)
- C-compiler
- C<sup>++</sup>-compiler (for the *kercen* module only)
- *gnuplot* (for plotting only)
- bash shell (default on Linux and Mac, for Windows freely available with *gfortran* 4.4)

- Tcl/Tk, itcl (provided in the EMPIRE distribution)
- python (default on Linux and Mac, for Windows provided with the EMPIRE distribution)

However, only the generic FORTRAN compiler is needed to perform basic calculations. We stress that all the remaining components are freely available on the Internet for practically any operating system (including UNIX and MS Windows).

### 8.3 Array dimensions

All the dimensions are set in the *dimension.h* file and some of them can be changed if necessary. Those parameters which may require modifications in everyday use of the code are listed below.

<b>NDNUC</b>	maximum number of nuclei involved in the calculation (default 200, typically 250 for reactions up to 100MeV)
<b>NDEXCLUS</b>	maximum number of nuclei for which exclusive emission spectra are calculated (default 50, sufficient for ENDF=2)
<b>NDEX</b>	maximum number of energy bins in the continuum discretization (default 121, it is recommended that NDEX is about twice the number of energy bins NEX requested in the input )
<b>NDLW</b>	maximum number of partial waves to be considered in calculations (default 50, for light and heavy ion projectiles this limit should be increased to about 100 due to higher angular momenta involved in the HI reactions)
<b>LEVCC</b>	maximum number of coupled channels in CC optical model calculations (default 20, all collective levels in the *-coll.lev file with their sequential number larger than NDLEVCC are only considered in the DWBA approximation; if coupling of such levels is needed the LEVCC parameter has to be increased accordingly)
<b>NDLV</b>	maximum number of discrete levels in any nucleus (default 40 imposed by the ENDF-6 format; if no ENDF-6 formatting is performed this number might be increased however the excitation energy of the level should be below neutron binding)
<b>NDBR</b>	maximum number of branching ratios for each level (default 40)
<b>NDMSCS</b>	number of steps in Multi-step Compound (default 4)



## 8.4 Parameter libraries

Input parameters are stored in two distinct areas reflecting their origin - original EMPIRE input library can be found in the *empire/data* directory, while the result of the IAEA coordinated project RIPL [35, 145] are stored in the *empire/RIPL* folder. The latter directory follows structure and content of the RIPL-3 library, although files not used by EMPIRE are omitted. Accordingly, RIPL-3 documentation can be consulted for more details. The advent of the more complete and more up to date RIPL database has reduced the original *empire/data* library to a few EMPIRE-specific files and neutron resonance parameters from ENDF/B-VII.1. As a matter of principle, to maintain traceability of the parameters used in the calculations, these libraries MUST NOT be modified by a user. In the first run EMPIRE creates local copies of the relevant data and only these files should be adjusted to improve calculations.

Below we list RIPL files being used in EMPIRE. We refer to the original references [35, 145] for details regarding the format, origin and discussion of the data. Each file is also accompanied by the *readme* file that explains its contents and format.

- RIPL library
  - Discrete levels (*empire/RIPL/levels/xxxx.dat*)
  - Masses (*empire/RIPL/masses/mass-frdm95.dat*)
  - Natural abundances (*empire/RIPL/masses/abundance.dat*)
  - Experimental deformation parameters  $\beta_2$   
(*empire/RIPL/masses/gs-deformations-exp.dat*)
  - Myers-Swiatecki shell corrections  
(*empire/RIPL/densities/shellcor-ms.dat*)
  - Level density parameters for the Enhanced Generalized Superfluid Model and normalization factors that can be applied improve precision of the global systematics  
(*empire/RIPL/densities/total/level-densities-egsm.dat* )  
(*empire/RIPL/densities/total/level-densities-egsm-norm.dat*)
  - HFB plus combinatorial nuclear level densities at ground state deformations, actual data are given in *xxxx.tab* files while *xxxx.cor* files contain corrections needed to reproduce experimental  $D_0$ .  
(*empire/RIPL/densities/total/level-densities-hfb/xxxx.tab* ) and  
(*empire/RIPL/densities/total/level-densities-hfb/xxxx.cor* )
  - HFB predictions of the fission paths  
(*empire/RIPL/fission/HFB2007/xxxx.tab* )
  - HFB plus combinatorial nuclear level densities at saddle and isomer deformations  
(*empire/RIPL/fission/leveldensities* )

- Fission barrier parameters recommended for the trans-thorium nuclei by V.M.Maslov and for the pre-actinides by G.N.Smirenkin  
(*empire/RIPL/fission/empirical-barriers.dat* )
- Experimental Giant Dipole Resonance parameters  
(*empire/RIPL/gamma/gdr-parameters-exp.dat*)
- Theoretical predictions of the Giant Dipole Resonance (GDR) energies and widths  
(*empire/RIPL/gamma/gdr-parameters-theor.dat* )
- Compilation of the optical model potential parameters  
(*empire/RIPL/optical/om-data/om-parameter-u.dat* )
- Index to the optical model parameters ordered by RIPL number  
(*empire/RIPL/optical/om-data/om-index.txt* )
- Index to the optical model parameters ordered by Z  
(*empire/RIPL/optical/om-data/om-index-by-Z.txt* )
- References to the optical model parameters  
(*empire/RIPL/optical/om-data/om-references.txt* )
- Recommended deformation parameters (beta-2 and beta-3) for collective levels  
(*empire/RIPL/optical/om-data/om-deformations.dat*)
- Average parameters of s- wave neutron resonances  
(*empire/RIPL/resonances/resonances0.dat* )
- Average parameters of p- wave neutron resonances  
(*empire/RIPL/resonances/resonances1.dat* )
- Internal EMPIRE library
  - Neutron reaction cross sections for CN to be used in PFNS calculations based on Los Alamos model  
(*empire/data/CNxs.dat* )
  - Neutron reaction cross sections on heavy fission fragment to be used in PFNS calculations based on Los Alamos model  
(*empire/data/HFxs.dat*)
  - Neutron reaction cross sections on light fission fragment to be used in PFNS calculations based on Los Alamos model  
(*empire/data/LFxs.dat* )
  - Deformation parameters by Moeller-Nix  
(*empire/data/deflib.dat* )
  - EMPIRE internal library of fission barriers  
(*empire/data/EMPIRE-fisbar.dat* )

- $\Gamma_\gamma$  - spline fit to experimental data at thermal energy by J. Kopecky  
(*empire/data/Ggamma.dat* )
- Parabolic fit to HFB barriers  
(*empire/data/HFB-parab-fisbar.dat*)
- Level density parameters for EGSM, Gilbert-Cameron (EMPIRE) and GSM (RIPL) models (this file is used rather than *empire/RIPL/densities/total/level-densities-egsm.dat* )  
(*empire/data/level-densities-par.dat*)
- Full set of resonance parameters from ENDF/B-VII.1  
(*empire/data/resonances.endf*)

## 8.5 List of EMPIRE modules

The EMPIRE source is divided into modules which generally correspond to nuclear reaction mechanism or certain physical quantity. Communication among the modules is assured by a set of COMMONS located in the *global.h* file that is included whenever necessary. Each of the modules is described shortly below.

### **empire\_ctl.f**

*empire\_ctl.f* prepares files and input for optical model fitting or sensitivity calculations and controls these calculations. It calls the module *main.f* , which controls the nuclear model calculations, as many times as needed to perform the desired operation.

### **main.f**

*main.f* calls the module *input.f* for reading the input data and parameters, controls flow of calculations and prints final results. Also contains the RECOIL subroutine, which constructs recoil spectra when the ENDF=2 option is selected.

### **input.f**

Sets default values of input parameters, reads mandatory input and calls READIN for optional reading. Accesses data bases to retrieve discrete levels, binding energies, deformations and shell-corrections as well as experimental data from the EXFOR library. Defines the collective levels to be used by CCFUS and TRISTAN. Retrieves optical model parameters from the RIPL library and reads level density parameters. Finally, prints out input parameters to the output file (*\*.lst*).

**ccfus.f**

Calculates fusion cross section for heavy ions in terms of a simplified Coupled-Channels approach. Collective states in target and projectile are identified in *input.f* and used in the CC calculations. As a first guess ground state deformation is assumed for all the collective states, and these can be modified by the user in subsequent runs. CCFUS also provides the fusion barrier used by other routines (e.g., distributed barrier model)

**tl.f**

This module determines the optical model transmission coefficients. Optical model parameters are retrieved from the RIPL-2 library and subroutine ECIS06 is called. The transmission coefficients are calculated inside the *tl.f* for heavy ions only. For light particles this task is delegated to ECIS06, and *tl.f* module ensures the proper transfer of calculated transmission coefficients to the rest of the system.

**subecis06m.f**

This module contains the ECIS06 Coupled Channel code by J. Raynal, which calculates total, elastic and absorption cross sections, elastic angular distribution, inelastic cross sections to collective levels and their respective angular distributions, as well as transmission coefficients. ECIS06 also provides analyzing powers but these are not used by the current version of EMPIRE. ECIS06 implements Coupled-Channels and DWBA models into EMPIRE. We note that ECIS06 has been converted into a subroutine in EMPIRE.

**fusion.f**

Calculates initial Compound Nucleus population after projectile absorption using transmission coefficients obtained either from the optical model or the distributed barrier model (for heavy ions). Also handles additional possibilities (reading absorption cross section for each partial wave from the external file, reading total absorption cross section from input, and reading critical value of angular momentum  $l_{cr}$ ) that are available for heavy ion induced reactions (see Section 1.1).

**MSD-orion.f**

Calculates two step Multi-step Direct amplitudes in the frame of the TUL theory. The results are later used by TRISTAN to produce Multi-step Direct cross sections. ORION is called from *main.f* and all input parameters are transferred through formal parameters rather than global common (too many conflicts in variable names). Communications with *MSD-tristan.f* occur through TAPE15.

**MSD-tristan.f**

Calculates two step Multi-step Direct cross sections from the results of ORION stored on TAPE15 folding them with the QRPA response functions (vibrational collectivity).

The module distributes the MSD spectrum over the residual nucleus continuum assuming that the spin distribution is proportional to the spin distribution of the 2-exciton states. MSD contribution is also distributed over discrete levels although in a very approximate and arbitrary way, feeding mostly 2+ and 3- levels (4+ to lesser extent) that are possibly close to the collective states of these multipolarities.

**MSC-NVWY.f**

Calculates Multi-step Compound decay in terms of the NVWY theory. Neutrons, protons, and  $\gamma$ s are taken into account. Number of considered steps is fixed in the *dimension.h* file as a value of the NDMSCS parameter. If this number of steps is high enough, whole decay of the first CN is calculated within the MSC model, and Hauser-Feshbach calculations (*HF-comp.f*) are not invoked.

**ph-lev-dens.f**

Contains a number of routines for the calculation of particle-hole state densities to be used by the MSC model. These routines also include accessible level densities for different type of transitions and take into account the binding condition.

**ddhms.f**

Computes preequilibrium spectra with Hybrid Monte Carlo (HMS) simulation formalism developed by Blann and implemented by Chadwick. Treatment of the angular momentum transfer has been developed by Chadwick and Oblozinsky. The original code has been converted into a subroutine. Transfer of input data and results is undertaken by the EMPTRANS subroutine.

**pcross.f**

The exciton model module, developed especially for EMPIRE, which takes into account emission of nucleons, primary gammas and clusters. The latter are treated within the Iwamoto-Harada formalism. PCROSS adopts the never come-back approximation, allows for incident clusters and gammas but ignores spin coupling and does not provide angular distributions.

**HRTW-comp.f**

Calculates decay of the Compound Nucleus in terms of the HRTW theory (width fluctuation correction). Uses modified routines of standard Hauser-Feshbach (DECAY, DE-

CAYG, FISSION) and HRTW\_MARENG to decompose capture cross sections into partial wave components. In addition, contains a number of subroutines which are specific to the HRTW theory, and used to calculate the elastic enhancement factor, effective transmission coefficients, and bookkeeping of reaction channels.

## HF-comp.f

This Hauser-Feshbach module performs the bulk of Compound Nucleus calculations. Follows decay of states in the continuum in the parent nucleus to the continuum and to discrete levels in the residual nucleus through emission of light particles (neutrons, protons,  $\alpha$ s, and eventually a single type light ions). Also calculates full  $\gamma$ -cascade to the continuum and to discrete levels as well as discrete transitions between low lying levels, along with fission widths in which two viscosity effects are taken into account.

Intermediate results are stored on scratch arrays SCRT (continuum) and SCRTL (discrete levels) and are normalized with the initial CN population and divided by the Hauser-Feshbach denominator. The results are accumulated in the population array POP. Note, that particle emission from discrete levels is not considered.

If ENDF=1 option is specified *HF-comp.f* module decomposes particle and  $\gamma$ -spectra into components related to individual reactions. For example, a piece of the first-emission double-differential spectrum corresponding to the subsequent neutron emission is moved to the second-emission spectrum. Under these circumstances, it is assumed that no  $\gamma$ s are emitted between the two subsequent neutron emissions. At present, only two emissions are considered with ENDF=1 option, i.e., (n,3n) reaction spectra can not be processed into the ENDF format. One should invoke ENDF=2 option, which makes use of the cumulative representation (MT=5), to overcome this limitation.

## bar\_mom.f

Contains subroutines BARFIT and MOMFIT that were written by Sierk. The first one provides fission barrier height, ground-state energy, and angular momentum at which fission barrier disappears. The second subroutine calculates the three principal-axis moments of inertia.

The results arise from fits of fission barriers and moments of inertia calculated by Sierk in 1983-1985 using Yukawa plus exponential double folded nuclear energy, exact Coulomb diffuseness corrections and diffuse-matter moments of inertia. The calculated barriers are accurate to a little less than 0.1 MeV but the fit is a little less accurate. Worst errors might be as large as 0.5 MeV.

## lev-dens.f

Contains all subroutines used to calculate the level densities for all approaches used in EMPIRE. Includes retrieval of level density parameters and HFB level densities and functions

for damping the collective effects. Cumulative plots of discrete levels and their comparison with the level density predictions are also performed within this module.

### **gamma-strgth.f**

Prepares deformation-dependent Giant Multipole Resonance parameters (for GDR, GQR and GMR) using built-in systematics and calculates  $\gamma$ -ray strength functions. Allows for a combination of the GMR and Weisskopf estimates. In the case of E1, uses generalized Lorentzian including energy-dependent GDR width and the non-zero limit at  $E_\gamma=0$ .

### **gamma-strength-analytic.f**

Calculates dipole radiative strength functions for  $\gamma$ -decay and photo-absorption using one of the following approaches MLO1, MLO2, MLO3, EGLO, GFL, SLO (adapted from the code provided by V. Plujko to RIPL).

### **print.f**

A small module, which prints histograms of spectra emitted from subsequent nuclei, and provides energy integrated cross section for these emissions.

### **pipe.f**

A small subroutine to execute UNIX command line from a FORTRAN code.

### **auxiliary.f**

Set of auxiliary subroutines that contain general algorithms or perform numerical operations not related to any particular physical model. The module includes subroutines for fitting Legendre polynomials, integration, matrix inversion, interpolation, finding nucleus and ejectile index and setting to zero variables in EMPIRE.

### **dtrans.f**

A subroutine for deuteron induced direct stripping (d,p) and pick-up (d,t) following C. Kalbach's code PRECOC-1997 introduced to EMPIRE by A. Ignatyuk.

### **fis\_io.f**

Subroutine that creates FISSION.INP (to become *\*-inp.fis*) which contains all fission parameters that are independent of energy and fission output file (FISS.OUT) that contains fission results for the last incident energy.

**fitbarrier.f**

Routines involved in fission calculations, including fitting numerical barriers with parabolas, WKB of fission transmission coefficients.

**optman.f**

This module replaces ECIS when soft-rotator CC calculations are requested for selected RIPL potentials.

## 8.6 Flow of calculations

Listed below are the essential steps in the calculation of the nucleon induced reaction involving preequilibrium and Hauser-Feshbach decay:

1. read EMPIRE input file (*.inp*)
2. construct table of nuclei involved
3. read from the input parameter library (or stored local input files if they exist)
  - (a) optical model parameters
  - (b) discrete levels
  - (c) collective levels
  - (d) masses and binding energies
  - (e) level density parameters or pre-calculated tables of level densities
  - (f) fission barrier parameters (for fissionable nuclei)
  - (g) shell corrections
  - (h) ground state deformations
  - (i) low energy observables (resonance spacings,  $\gamma$ -strength functions,  $\Gamma_\gamma$ )
4. calculate
  - (a) optical model including direct excitation of discrete levels if requested
  - (b) pre equilibrium emission of  $\gamma$ 's, nucleons and clusters
  - (c) compound nucleus decay including full  $\gamma$ -cascade and fission
  - (d) prompt fission spectra
5. retrieve experimental data from the EXFOR library.
6. write local input files



7. Determine optical model cross sections including direct excitation of collective levels if requested: fusion cross section and direct inelastic scattering are calculated (codes ECIS or OPTMAN).
8. calculate preequilibrium emission (usually not all of the below listed PE models are used; in case of competing PE models internal selection rules are applied to select specific contribution from a single model and suppress those from the other models)
  - (a) calculate double-differential cross sections for inelastic scattering in terms of the MSD mechanism, populate residual nucleus continuum and discrete levels, store recoil spectra (first CN only).
  - (b) calculate neutron, proton,  $\alpha$ , deuteron, triton,  $^3\text{H}$ , and  $\gamma$  emission spectra in terms of the exciton model (code PCROSS), populate residual nuclei continuum and discrete levels (first CN only).
  - (c) calculate neutron, proton, and  $\gamma$  emission spectra in terms of the HMS model (code DDHMS), populate residual nuclei continuum and discrete levels, store recoil spectra (first CN only).
  - (d) calculate neutron, proton, and  $\gamma$  emission spectra in terms of the MSC mechanism, populate residual nuclei continuum and discrete levels (first CN only).
9. calculate neutron, proton,  $\alpha$ , deuteron, triton,  $^3\text{H}$ ,  $\gamma$ , and eventually light ion emission widths in the frame of the Hauser-Feshbach model.
10. calculate fission according to the selected fission model.
11. normalize emission and fission widths with the Hauser-Feshbach denominator and fusion cross section to obtain compound nucleus spectra and population of continuum and discrete levels in residual nuclei.
12. print results for the decay of the nucleus considered.
13. select new nucleus and repeat steps 15 through 19 until all requested nuclei have been processed. The selection scheme is the following: starting from the compound nucleus, neutrons are subtracted until the number of neutron emissions specified in the input is reached. Then one proton is subtracted from the compound nucleus, and all nuclei with decreasing neutron number are considered again. In the Z-N plane the calculations are performed row-wise from the top-right corner (compound nucleus) to the left. When a row is completed the one below is considered.
14. select the compound nucleus for consideration.
15. write input/output files
16. print inclusive spectra, read new incident energy from the input file (*.inp*) and repeat steps 4 and 7 through 20.

## 8.7 empy: python modules for EMPIRE

EMPIRE has recently been extended with several python modules designed mainly for easier interaction with ENDF-formatted files and with processed files (following processing by the NJOY and PUFF codes). Contents of the empy module include:

- covEndf.py, MF31.py, MF32.py, MF33.py and MF35.py: modules for reading and writing ENDF-formatted covariances.
- readNJOY.py, readPUFF.py, and boxr.py: interact with output of the processing codes NJOY and PUFF.
- sg33.py: output covariances in the exchange format designed for the WPEC subgroup 33

To use empy, the user must set the PYTHONPATH environment variable in order to locate the module inside python:

```
export PYTHONPATH=/path/to/empire
```

For more information about empy, see the file ‘empire/empy/info.py’, or use python’s online, interactive help system:

```
>python
>import empy
>help( empy )
or:
>from empy import readNJOY
>help( readNJOY )
```

## 8.8 Executing EMPIRE

EMPIRE can be executed either with the included Graphical User Interface (GUI), or from the command-line using scripts. The Graphic User Interface mode is the most convenient, and is recommended if a Tcl/Tk interpreter is available. Where the Tcl/Tk interpreter is not available, the user is advised to use the script mode. For the sake of clarity, we start by describing the ‘script-driven’ mode of EMPIRE:

EMPIRE execution most commonly involves the following four operation sequences, which are described in more detail below:

- “runE” sequence prepares data, runs the main calculation and prepares ZVView plots of pre-defined cross sections.
- “format” sequence generates the ENDF formatted file.

- “verify” sequence checks the ENDF file for formal correctness and internal consistency.
- “process” sequence performs post-processing to prepare a derived ENDF file, from which more advanced plotting is done.

This complete sequence is intended for the production of evaluated files in ENDF-6 format, but for theoretical modeling, the “runE” script is likely sufficient. However, in this case automatic plotting is limited to the cross sections. A more detailed description of the task sequences is described below.

### 8.8.1 “runE” sequence (Run EMPIRE)

The runE script sets up the environment for a new EMPIRE calculation and cleans-up the directories before launching a new EMPIRE calculation. More specifically, the following tasks are performed:

- The EMPIREDIR environment variable is set, if necessary (see section 8.8.6 for more information)
- Unnecessary files from a previous run are deleted.
- Locally modified files containing input parameters are retrieved.
- EMPIRE is executed; case-related files are renamed as appropriate.
- If the experimental data in computational C4 format are not available, they are generated from the EXFOR file, if present.

The “project name” is defined at this step. Usually this identifies the nuclide that is being processed (e.g. mn55, w182, u235, etc.). The project name is used in the filenames and is implied in the sections below whenever the “\*” appears in the filename.

### 8.8.2 “format” sequence

The following tasks are performed:

- EMPEND is executed to produce an ENDF file from the “short” EMPIRE output (with extension \*.OUT). The input file for EMPEND is generated within the script. The output file \*-e.endf is produced.
- ENDRES is executed (conditionally, if the new resonance file file \*-res.endf is present on the local directory). The dummy resonance file in the ENDF file generated by EMPEND is replaced with the resonance data on the \*-res.endf file. The comments from the specified file are appended after the original comments. All resonance data

in ENDF File 2 are replaced. The background cross sections in the total, elastic, fission (if present) and radiative capture are set to zero from  $10^{-5}$  eV to the upper energy covered by the resonance parameters in the selected file. The lower energy of the elastic angular distribution is extrapolated to  $10^{-5}$  eV, if needed. The resonance covariance data in MF=32 are also copied, if available. The ENDRES input file is taken from the standardised input file ENDRES.INP, which can be modified by the user, if needed. The main parameters that can be changed are the filename from which the resonances are taken and the value of the LSSF flag, which defines how the unresolved resonance parameters are used (LSSF=0 to use URR to calculate cross sections; LSSF=1 to use URR for selfshielding only). The output ENDF file is \*-endres.endf and the log file is \*-log.endres.

- STANEF is executed to update the dictionary section in the new ENDF file. The STANEF input file is generated within the script.

The final output ENDF file from this sequence of operations is \*.endf.

### 8.8.3 “verify” sequence

The ENDF Utility codes CHECKR, FIZCON and PSYCHE are executed to verify formal correctness and internal consistency of the final ENDF file. The input files are generated within the script. The output files are \*-log.checkr, \*-log.fizcon and \*.log.psyche for the corresponding checking code.

### 8.8.4 “process” sequence

The Pre-Pro codes and some of the codes from the ENDVER package are executed to prepare the ENDF-formatted data for plotting. The output file \*-s.endf is produced. The following codes and scripts are executed on the ENDF file:

- LINEAR is used to linearise any cross sections, which are not defined with log interpolation in energy or cross section.
- RECENT is used to reconstruct the resonance parameters into tabular cross section values.
- SIGMA1 numerically Doppler-broadens the cross sections to 300 K.
- LEGEND converts angular distributions in ENDF File 4, given by Legendre polynomial representation, into tabular form.
- SIXTAB converts double-differential data into angle-energy sets in tabular form (ENDF option LAW=7).
- “plotlst” script prepares the experimental data for plotting. It checks for the presence of the C4 file of experimental data and links auxilliary dictionary files for local use.

- PLTLST code generates a table of available types of nuclear data that can be reconstructed and compared with the information in the evaluated nuclear data files.

### 8.8.5 “run” sequence

All the main processing sequences (‘runE’, ‘format’, ‘process’ and ‘verify’) are executed one after another.

### 8.8.6 Script mode

The EMPIRE distribution contains several scripts located in the *empire/scripts* directory. These scripts use UNIX bash-shell and in some cases python, both of which must be installed on the system. Each script performs one or more steps, including those described in the previous section, taking care of moving, renaming and deleting the files and invoking the execution of appropriate codes. Scripts assume certain naming convention for the files, in particular, all input files must end with *.inp* extension. Unless specified differently, each script is invoked with a single parameter; the name of the input file without *.inp* extension (file root-name). For example, calculations with the input file *Mo100.inp* can be performed using the *runE* script and typing

```
../scripts/runE Mo100
```

in the *empire/work* directory (or any other directory at the same level as *work*). General philosophy is that the root-name of the input file (*Mo100* in the example above) defines a project name. Scripts modify generic file names produced by the codes, renaming them by the project name plus the specific extension. These extensions must not be modified as they define the contents of the file (see Tables 8.1 and 8.2) and are used as identifiers by the system. The project is set up by creating the EMPIRE input file with arbitrary root-name and *.inp* extension. In the following, we replace root-name with the asterisk ‘\*’ and refer to the files through their extensions.

### EMPIREDIR environment variable

In the above example, EMPIRE was executed in the ‘empire/work’ directory. In this case EMPIRE automatically finds the path to all required scripts. If the user wishes to work in other directories outside of ‘empire’, an environment variable should be set so that the system knows where to find the required scripts and executables.

In bash, for example, the variable may be set in any of the bash setup files (*.bashrc*, etc) with the line:

```
export EMPIREDIR=/path/to/empire
```

On Windows, the variable should be added to the registry.

Again, setting the EMPIREDIR variable is only required in order to run a project some place other than in a direct sub-directory of the empire installation directory.

### List of available scripts

The following scripts are provided:

<b>runE</b>	executes the “runE” sequence described in the previous section.
<b>format</b>	executes the “format” sequence described in the previous section.
<b>process</b>	executes the “process” sequence described in the previous section.
<b>verify</b>	executes the “verify” sequence described in the previous section.
<b>run</b>	executes all of the above sequences one after the other.
<b>staneF</b>	runs ENDF-6 format standardization code STANEF
<b>c4</b>	converts EXFOR data in the <i>*.exf</i> file into the computational format (file <i>*.c4</i> ) (included in <b>runE</b> )
<b>sortc4</b>	sorts experimental data in the computational format ( <i>*.c4</i> file) (included in <b>runE</b> )
<b>plot</b>	runs PLOT4 to create comparison plots of experimental and calculated cross sections; the log-file from PLOT4 is an index of experimental data that can be compared to quantities derived from evaluated nuclear data files (obsolete)
<b>plotlst</b>	produces the index of experimental data without doing the lengthy PLOT4 run
<b>storemul</b>	moves all files matching pattern <i>za*\$2*</i> to the directory <i>../\$1</i> (creates <i>../\$1</i> if it does not exists). <i>\$1</i> and <i>\$2</i> are the parameter of the script, e.g., to move files obtained related to isotopes of iron (using input files of the type <i>za260xx.inp</i> ) to the directory <i>../default_om</i> one should issue a command <b>../scripts/storemul default_com 260</b>
<b>clean</b>	removes all files related to a given project (except the input file <i>*.inp</i> ) and any <i>core</i> file. This script must be run each time a project is changed by adding new channels or by modifying projectile or target in the input file <i>.inp</i> .
<b>cleansel</b>	removes selected files related to the given project

Table 8.1: The most important files generated by EMPIRE for a given project (usually not all are used). User created files are marked with ♣.

extension	generic name	contents of the file
*.inp ♣	INPUT.DAT	EMPIRE input
*.fus ♣	FUSION	set of $l$ -dependent transmission coefficients (one per each line) used for determination of the fusion cross section (optional)
*.lst	LIST.DAT	standard EMPIRE output
*.out	OUTPUT.DAT	'short' EMPIRE output (for ENDF-6 formatting )
*.lev	LEVELS	discrete levels for all nuclei involved in the run
*-lev.col	TARGET_COLL.DAT	collective levels used in ECIS06 calculations
*-lev.col	TARGET_COLL_RIPL.DAT	collective levels read from RIPL database
*.-omp.ripl	OMPAR.RIPL	optical model parameters read from the RIPL database
*.-omp.dir	OMPAR.DIR	optical model parameters used for DWBA or CC calculations with ECIS06
*-aOMP.lst	OMP_A.DAT	$\alpha$ -potential by Kumar and Kailas (RIPL)
*-inp.fis	FISSION.INP FISSION.OUT	input parameters related to fission channel detailed output of fission calculations including intermediate results for purpose of checking
*-e.endf		results in ENDF-6 format produced by EMPEND
*-res.endf	ENDRES.DAT	ENDF file - source of resonance parameters
*-lin.endf	ENDFB.OUT	ENDF file linearized
*-rec.endf	ENDFB.OUT	ENDF file with reconstructed resonances
*-sig.endf	ENDFB.OUT	ENDF file Doppler-broadened with SIGMA
*-l.endf	LEGEND.OUT	ENDF file with reconstructed index
*-s.endf		ENDF file after processing with PREPRO codes (for plotting but not legal ENDF file!)
*.endf		ENDF-6 formatted file, including neutron resonances, processed with FIXUP and STANEF (the final ENDF file for distribution)
*.exf	EXFOR.DAT	experimental data from EXFOR (if installed)
*.c4	C4.DAT	EXFOR data in computational format
*.war		warnings extracted from the EMPIRE output *.lst
*-fiss.xsc	FISS_XS.OUT	cross sections for different fission chances
*-prev.endf		ENDF formatted file from the previous run
*-prev.lst		listing from the previous run

Table 8.2: The most important files for a given project (continuation).

extension	generic name	contents of the file
*.ps		plots comparing calculated and experimental data
*-cum.ps	CUMULPLOT.PS	cumulative plots of discrete levels
*-cum.ps	FITLEV.PS	cumulative plots of discrete levels
*.x42c4.lst		output of X4TOC4 code
*.x42c4.errs		EXFOR entries not translated by X4TOC4
*-MT.zvd		ZVView file for plotting MT (MT=2, 4, 16,...)
*- <i>xxx</i> .zvd		ZVView plot of <i>xxx</i> cross sections plotted directly by EMPIRE
*.rng	R250SEED.DAT	random number generator seed
*.sys	SYSTEMATICS.TXT	short file with the results of systematics
*.xsc	XSECTIONS.OUT	full set of calculated cross sections
*-tl	TL	results of OM, CC, and ORION calculations
*-inp.sen	SENSITIVITY.INP	input for calculating sensitivity matrix
*-mat.sen	SENSITIVITY.MATRIX	sensitivity matrix
*-c4.kal		exp. data used in KALMAN; usually *.c4 subset
*-expxsc.kal		experimental cross sections for KALMAN
*-expcorr.kal		experimental covariance matrix for KALMAN
*-out.kal		KALMAN code output
*-xsc.kal		KALMAN adjusted cross sections
*-cov.kal		KALMAN generated covariance matrix
*-\$k-err.kal		KALMAN produced uncertainties
*-par.kal		model parameter correlations from KALMAN
*-MC-cov.out	MC_covar.out	covariance matrix with the Monte Carlo sampling
*-nubar.endf	NUBAR-EVAL.ENDF	nu-bar taken over from the ENDF/B-VII
*-pfnm.out	PFNM.OUT	prompt fission neutron multiplicities
*-pfns.out	PFNS.OUT	prompt fission neutron spectra
*-ecis-vib.in	ecVIB.inp	ECIS input for the vibrational model
*-ecis-rot.in	ecROT.inp	ECIS input for the rotational model
*-ecis-vibrot.in	ecVIBROT.inp	ECIS input for the vib-rot model
*-ecis-rot.out	ECIS_ROT.out	ECIS output for rotational model (single energy)
*-ecis-vib.out	ECIS_VIB.out	ECIS output for vibrational model (single energy)
*-ecis-vibrot.out	ECIS_VIBROT.out	ECIS output for vib-rot model (single energy)
*-optman.in	OPTMAN.INP	input for the OPTMAN code
*-optman.out	OPTMAN.OUT	output of the OPTMAN code
*-ompfit.lst	FIT.OUT	results of the optical model potential fit



Table 8.3: List of log-files

extension	contents of the file
*-log.endres	produced by ENDRES when merging EMPIRE results with the resonance region
*-log.checkr	results of format checking with code CHECKR
*-log.fizcon	results of physics checking with the code FIZCON
*-log.psyche	results of format checking with code PSYCHE
*-log.legend	produced by the PREPRO code LEGEND
*-log.linear	produced by the PREPRO code LINEAR
*-log.recent	produced by the PREPRO code RECENT (resonance reconstruction)
*-log.sigma1	produced by the PREPRO code SIGMA1 (Doppler broadening)
*-log.plotc4	produced by the code PLOT4 (cross section plotting)

**cleanall** removes **all** output files for all projects in a current directory; only input files (*\*.inp*) are retained

**store** moves *.inp*, *.lst*, *.out*, *.ps*, *.endf*, and *.res* files for all projects (*.inp* files are copied rather than moved) to a subdirectory specified as a parameter to *store*. If the subdirectory does not exist, one will be created, which avoids old files being overwritten by new ones (e.g., when calculations are repeated with modified parameters). For example, the results of calculations with the Moldauer's optical-model parameters can be saved in the subdirectory *OM-Moldauer* by issuing the command:

```
../scripts/store OM-Moldauer
```

**grepawk** handy tool for extracting specific excitation function from the EMPIRE output *.lst* and arranging into two columns (incident energy, cross section). Such a representation allows any standard package to be used (e.g., gnuplot or xmgr) to plot excitation functions for any calculated cross section (e.g., population of a certain discrete level). The user must create a file with the project root-name and extension *.pat* containing two line pattern as in the example below:

```
incident energy
.3350 MeV      7.0 level
```

The first line must be left intact. The second should be changed according to the needs, and has to be the exact string that uniquely identifies a line of the output from which the cross section is to be extracted. A convenient method is to cut and paste between *.lst* and *.pat* files. As usual, script is invoked with the project name as a parameter. UNIX package

Table 8.4: Most frequently used MT numbers and corresponding reactions

Reaction	MT
tot	1
elastic	2
inelastic	4
(n,2n)	16
(n,3n)	17
(n,f)	18
(n,n $\alpha$ )	22
(n,np)	28
(n,np $\alpha$ )	45
(n, $\gamma$ )	102
(n,p)	103
(n, $\alpha$ )	107
(n,p $\alpha$ )	112

“awk” is used to scan the *.lst* output. Each time a line is encountered that matches “incident energy”’, the projectile energy is extracted. When a match occurs to the second line of *.pat* file, the requested cross section is identified as the word immediately before the “mb” string and extracted. The resulting excitation function is written to the file *.res*. Note that each use of *grepawk* will overwrite the *.res* file. Starting with version 2.16, similar functionality can be achieved with the *zvpl* script which produces *\*.zvd* and calls ZVView to display this file.

**zvd** plots comparisons of calculated and experimental data using ZVView graphic package. Script is called with MT number and project name as parameters. For example, to plot (n, $\gamma$ ) reaction for the *100mo* project one should type:

```
../scripts/zvd 102 100mo
```

in which *zvd* script uses *\*-s.endf* file for plotting. If this does not exist, script invokes the **process** script to reconstruct (n,inl), (n,p) and (n, $\alpha$ ) reactions and produce File 6 in a form suitable for plotting. This file is processed along with *\*.c4* that contains experimental data to produce *\*-MT.zvd* file (*MT* is any legal ENDF-6 format MT number). List of typical MT numbers is given in the Table 8.4

**zvcomb** allows an arbitrary number of existing *zvd* plots to be combined into one. If *zvcomb* is called without any parameter, a list of available *\*.zvd* files is displayed on the terminal, so that the names can be pasted onto the

command line.

**zvpl** similar to `grepaw` but produces `*.zvd` file and displays by calling ZVView. Can be operated from the Graphic User Interface *Xrun.tcl*.

**zvv** combines and displays various ZVView plots as a single plot, e.g.,  
`../scripts/zvv nb93*.zvd`

**zvvddx** create a ZVView plot of excitation functions, angular distributions, spectra, or double-differential cross sections (intended for use within the Graphic User Interface *Xrun.tcl*)

**mtacomp** produces ZVView plots that compare experimental data with the results of up to three sets of calculations (or evaluations) in the ENDF format for a given MT number and target. The syntax is:

```
../scripts/mtacomp MT comp root dir1 name1 file2 name2 file3 name3
```

where: MT stands for the ENDF reaction code (see Table 8.4), *comp* is an arbitrary string added to names of plot files, *dir1* points to the directory containing the first ENDF file, *file1* and *file2* indicate the remaining two ENDF files and *namei* are labels of the respective curves. Note, that *dir1* must contain the ENDF file named *root-s.endf* and optionally EXFOR data in the computational format in the file named *root.c4*. The naming convention is automatically ensured if the files were created by EMPIRE. There are no restrictions on the names of the remaining two ENDF files. The script is intended for use within the GUI but can also be run manually.

**acomp** same as *mtacomp* but does the job for the whole list of MTs in Table 8.4; therefore, MT is omitted from the list of parameters. The script is intended for use within the Graphic User Interface but can also be run manually.

**showzvd** calls ZVView package for each `.zvd` file from the argument list.

**accept-omp-fit** script to copy files resulting from the omp fit onto those used in the calculations. These can also be used as an intermediate step in fitting.

**add-Kalman.py** Run PTANAL and WRIURR to create basic MF2 and MF32. Run Kalman update. May want to add experimental uncertainties, and definitely want to lock down R' parameter (*za\*\*\*.c4* and *za\*\*\*-parcorr.kal* files respectively) before running Kalman then use this code to push new values back into MF2/MF32.

**cs2zvd** produces ZVView plots from the `*.xsc` files.

<b>empire3</b>	calls Xrun.tcl setting DISPLAY variable.
<b>fis-sion-chances.plt</b>	
<b>kalman</b>	the major script controlling the whole sequence of calls involved in the determination of covariance matrix (genkal, c4tokal, kalman3, kalend2, corr.gp). The syntax is:  <pre>../scripts/kalman root MT MAT EXPDAT</pre> where EXPDAT controls use of experimental data: 0 no experimental data, 1 experimental data for the selected reaction, 2 experimental data for all reactions. MT and MAT have their usual ENDF-6 meaning. MT is only used to select the reaction for which covariance matrix is ENDF-6 formatted (one at a time). MT does not(!) affect KALMAN calculations that are always performed on the full set of observables included in the sensitivity matrix so that full covariance matrix including reaction cross correlations is calculated. The calculations are, however, affected by the choice of experimental data through EXPDAT. User has an option to neglect them altogether, use those for a selected reaction only or use the full set of experimental data. The kalman script requires that files with cross sections (*.xsc), sensitivity input (*-inp.sen) and sensitivity matrix (*-mat.sen) for a given project exist in the working directory.
<b>kalmanResonance</b>	clone of the kalman script but adjusted to neutron resonance region. The syntax and the codes controlled by the script are the same.
<b>mergeMF33</b>	inserts ENDF-6 formatted file with covariances (usually obtained with multiple use of the kalman script) with the existing evaluation.
<b>mergecov</b>	merges covariances for individual reactions into a single MT33 file MF32 is added at the beginning if exists
<b>rec-ch-part</b>	reconstruct inelastic, (n,p) and (n, $\alpha$ ) reactions by summing partial cross sections (e.g., MT=51, 52, 53, ... for inelastic) with FIXUP
<b>rec-elastic</b>	reconstruct elastic by subtracting MT=3 from MT=1 with FIXUP
<b>rec-total</b>	reconstruct total by summing MT=3 and MT=2 with FIXUP
<b>resonance.tcl</b>	GUI for the resonance module of EMPIRE. It allows to extract data from the Atals of Neutron Resonances, perform analysis of the resonates, format them in the MF=2 file, and produce covariances of resonance parameters in the MF=32 representation.
<b>runjoy</b>	runs standard NJOY run to produce ACE file from the ENDF-6 formatted EMPIRE calculations.

- sampling.sh** runs requested number (default 100) of random EMPIRE calculations and calls `$EMPIREDIR/util/Calc_Cov/Calc_Cov.exe` to calculate full covariance matrix based on Monte Carlo sampling. This matrix contains full set of cross-correlations and can be used as a prior in least-squares fitting of experimental data.
- zvvsenmat** plots sensitivity matrix (must be present) to allow visual analysis of sensitivities in support of manual fitting of experimental data.

Note that C4 library must be installed, or the appropriate C4 file has to be downloaded from the IAEA-NDS or BNL-NNDC Web sites, in order to compare calculations with experiment. In most cases plots are created from the ENDF formatted file but starting with the 3.1 version the set of ZVView plots is generated directly by EMPIRE for most important cross sections (these files are denoted as `*-zxxx.zvd`, where `xxx` takes values such as 'tot', 'el', 'non', 'f', or 'g' ).

### 8.8.7 GUI mode

The Graphic User Interface (GUI) mode is the most convenient way of running EMPIRE, and requires Tcl/Tk to be installed on the computer. Actually, the Tcl scripting language and the related graphic Tool kit (Tk) are available freely for practically any operating system [147]. On most Linux distributions Tcl/Tk is installed by default. For convenience of the user EMPIRE-3.1 comes with the ActiveTcl package, which is easy to install and seems to run on various flavors of Linux (version for Windows is also available from <http://www.activestate.com/Products/ActiveTcl/>).

Standard GUI of EMPIRE-3.2 is a Tcl script `Xrun.tcl` that can be started in any 'working' directory by typing

```
$EMPIREDIR/scripts/Xrun.tcl &
```

We start discussion of the GUI with a few features that apply across the entire interface:

- Action of many buttons is simply calling an appropriate script with a project name as an argument.
- Double-click on the file in the list will generally open it with the default application (i.e., text files will be open with the selected editor, PostScript files with the selected viewer, and `*.zvd` files will be displayed using ZVView). Within lists typical mouse selection modes are usually available (although the first file only will be open for editing):
  - a single-click selects the file,
  - continuous selection by dragging mouse with the left button pressed,
  - continuous selection by clicking left mouse button while holding shift key pressed at the end of the region,

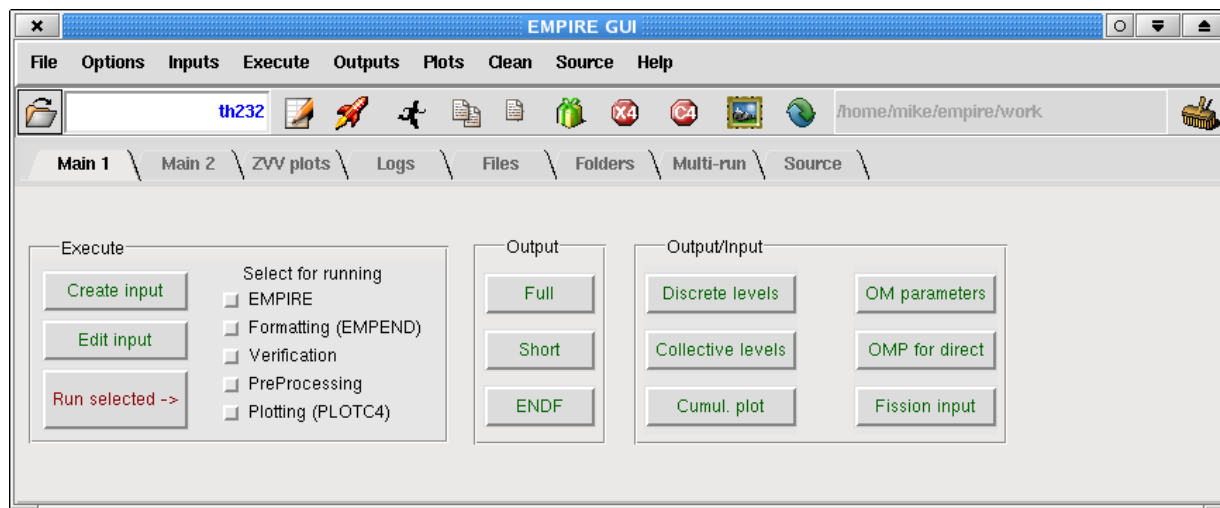


Figure 8.1: EMPIRE GUI - Main1 panel

- arbitrary multiple selection by clicking left mouse button while holding 'Ctrl' key pressed.
- Whenever Tcl/Tk allows a 'balloon-help' is showed when cursor remains above the button or icon for a short period of time. This help is hoped to be sufficient to operate the interface without additional instructions. Note that if cursor is moved fast across the interface the 'balloon-help' which appears on the screen might refer to a button different from the one to which the cursor actually points. To be sure that the help is correct keep in mind that help string always starts exactly below the middle of a button or icon.
- Colours on the GUI buttons follow 'traffic light scheme' - green means that pressing button at any time will not make any damage, red warns that some data or files that have been obtained before or manually edited might be lost (overwritten). Generally, all buttons involving editor calls are green while button involving execution of codes or deleting files are red. Similar distinction is introduced between the files - red is used for those which are likely to have been manually edited and green or orange for those which are easy to recreate by rerunning the code .

Due to a large number of operations and extended lists the new GUI is organized in a form of a notebook with several panels. Generally, there are several equivalent ways of performing the same operation and the user may choose the one which suits him best. All basic functions, such as running the code and viewing the results can be achieved from the pull-down menus and icon-denoted buttons below the menu bar. On the other hand, more advanced features such as plotting and file management can only be accessed from the various panels.

All operations (except multiple run) begin with the selection of the project name that will be used as a root of the input file name (say 56Fe). Existing project can be selected

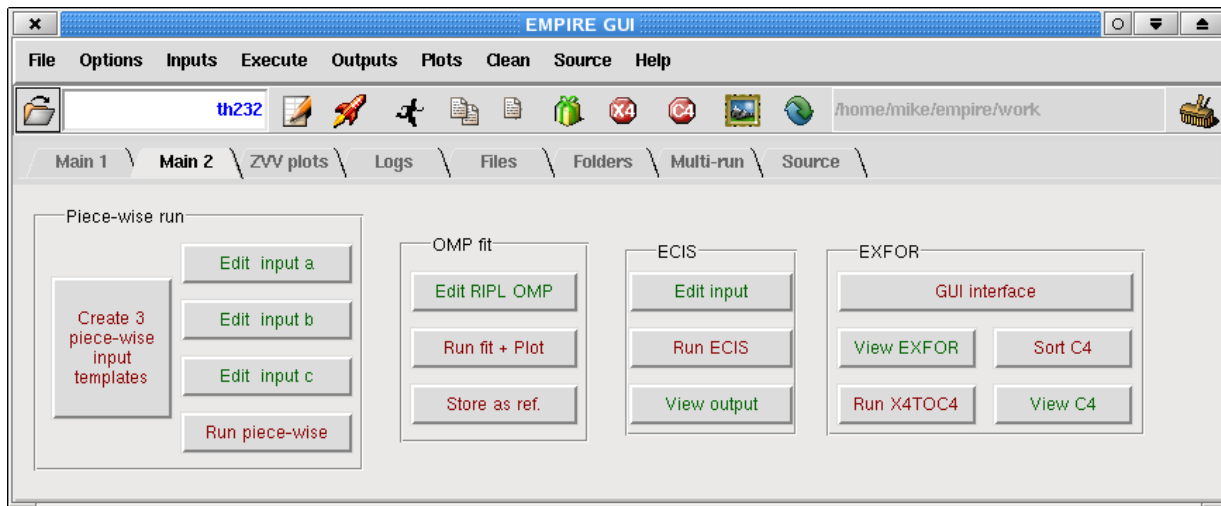


Figure 8.2: EMPIRE GUI - Main2 panel

by clicking on the 'open folder' icon to the left of the GUI. The following icons (from left to right) allow to (i) edit input, (ii) launch full chain of calculations, (iii) run EMPIRE only, (iv) view long EMPIRE output, (v) view short EMPIRE output, (vi) view ENDF-6 formatted file, (vii) view EXFOR data, (viii) view EXFOR data in computational format, (ix) view PLTC4 plots, (x) refresh list of files, (xi) change working directory, and (xii) remove all files related to the project except input. More operations are possible from individual GUI panels.

**Main1 panel** - (Fig. 8.1) provides for essential control of calculations. It allows to create a new input file (clicking on the "Create" button copies the standard input file *skel.inp* to *56Fe.inp* and opens it for editing), executing selected parts of the system (physics calculations, formatting, verification, preprocessing and plotting). One should keep in mind, that format verification and preprocessing can only be performed if EMPIRE calculations and ENDF-6 formatting were carried out before, and plotting is only possible starting from the preprocessed file. Main1 panel gives also access to output and output/input files produced by EMPIRE in the first run.

**Main2 panel** - (Fig. 8.2) provides additional four features for which there was not enough room on the Main1 panel.

- 'OMP fit' provides for manual fitting of the optical potential parameters. The three buttons in the frame allow to: (i) open the incident channel optical potential and edit it's content, (ii) run calculations and produce comparison plots of newly calculated cross sections with the reference ones (by default, the first calculation become the first reference), (iii) establish currently modified potential as the new reference potential if it is better than those tried before.
- EXFOR section will provide access to the Web based EXFOR retrieval that is avail-

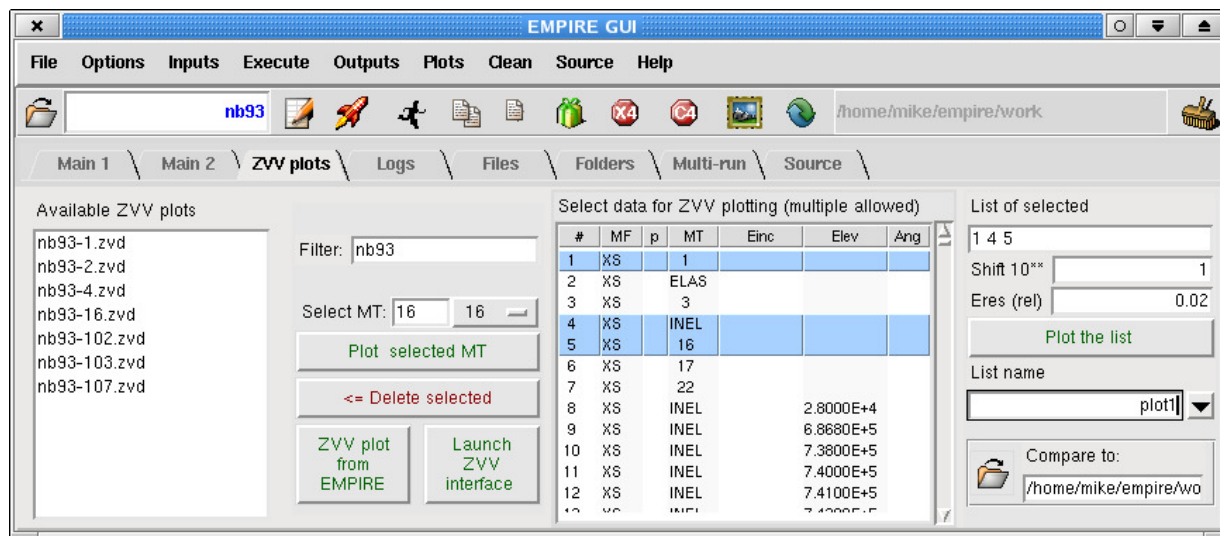


Figure 8.3: EMPIRE GUI - ZVView plots panel

able from the IAEA and NNDC web sites. Under normal circumstances this retrieval is not necessary as experimental data in the C4 format are extracted internally by EMPIRE during the first run. However, user may choose to use Web retrieval interface in order to exercise direct control on the retrieved data and take advantage of very powerful features available through the on-line retrieval. These include, automate application of corrections and generation of covariances for the experimental data if very basic information on the uncertainties is available in the EXFOR file. Last but not least, Web retrieval guarantees access to the most up to date version of EXFOR. When the EXFOR interface is closed the resulting file with experimental data is automatically renamed to conform to the current project. It is up to the user to ensure that the data retrieved are actually relevant to the calculations. If data are retrieved in the original EXFOR format they have to be converted into the computational format ('Run X4TOC4' button) and sorted ('Sort C4' button). The same sequence of buttons should also be used if users decides to modify the existing *\*.exf* file (e.g., by removing or adding certain entries). The recommended option is to download from the Web site the C4 version of the data. This option offers the advantage of using the most up to date and most complete dictionary when translating with the X4TOC4 code, which guarantees the highest conversion rate and reliability of the conversion of the EXFOR reaction string to the ENDF-6 format specification (MF/MT).

- ECIS section allows to view the most recent input and output of ECIS06 code (note that these files are overwritten in each calculation for each incident energy)

**ZVV plots panel** (Fig. 8.3) provides for a powerful interface to the ZVView plot-



ting package. The window to the left lists all ZVView plots (\*.zvd files) that have been previously created. User can display them by double-clicking on any of them. Selecting several plots and double-clicking on the last one will combine all the selected curves into a single plot. Note that 'Filter' field allows to restrict displayed files to those containing filter string in the name (by default Filter is set to the project name). There are 4 possibilities of creating ZVView files:

- Selecting MT number and hitting 'Plot selected MT' (note that any valid ENDF-6 MT number can be typed into the field in addition to those which can be selected from the predefined list). The MT number is included in the plot filename for identification (e.g., *56Fe-102.zvd* for capture). This method allows to plot only excitation functions (cross sections) for the current calculations (ENDF-6 formatted file must exist).
- Hitting 'Launch ZVV Interface' will start more powerful GUI that allows to create the same type of plots as before but including up to 3 additional ENDF-6 formatted files for comparison.
- 'ZVV plots from EMPIRE' is a bit cumbersome way of creating a cross section ZVView plot by selecting unique string identifying output line containing the cross section of interest, pasting it into the other window and filling additional information (next line, title, etc.) as requested. The advantage of this method is that the ENDF-6 formatted file is not required and any cross section (number followed by 'mb') in the long output (\*.lst) can be plotted. This includes quantities that can not be plotted with the previous methods since not stored in the ENDF-6 formatted file (such as cross sections for the population of discrete levels in any nucleus or intensities of  $\gamma$ -rays).
- Selecting plots from the window to the right of the GUI (list created by PLOTCH4 or *pltlst* script). This is the only possibility of plotting angular distributions, and energy spectra with the ZVView package. For the relevant line being included in the list there must be a match between experimental data and calculations (i.e., plots are only possible if adequate experimental data are available). Multiple selection can be plotted and each of such selections can be stored by specifying its name in the 'List name' field. When multiple selection is plotted the individual curves are offset from each other by a number of decades specified in the 'Shift 10\*\*' field. It implies that the  $y$ -scale be logarithmic unless shift is set to 0. 'Eres (rel)' is the experimental relative energy resolution used to spread discrete lines (e.g., elastic) and to smooth continuum in the plotted energy spectra. The 'Compare to' field allows to select another ENDF-6 formatted file to be included in the plots. Note that in order to obtain correct plots the additional file should be preprocessed in a way analogous to the original EMPIRE file (resonances will not be plotted unless the cross sections are reconstructed from the resonance parameters and double-differential data will not be plotted unless converted into the right format).

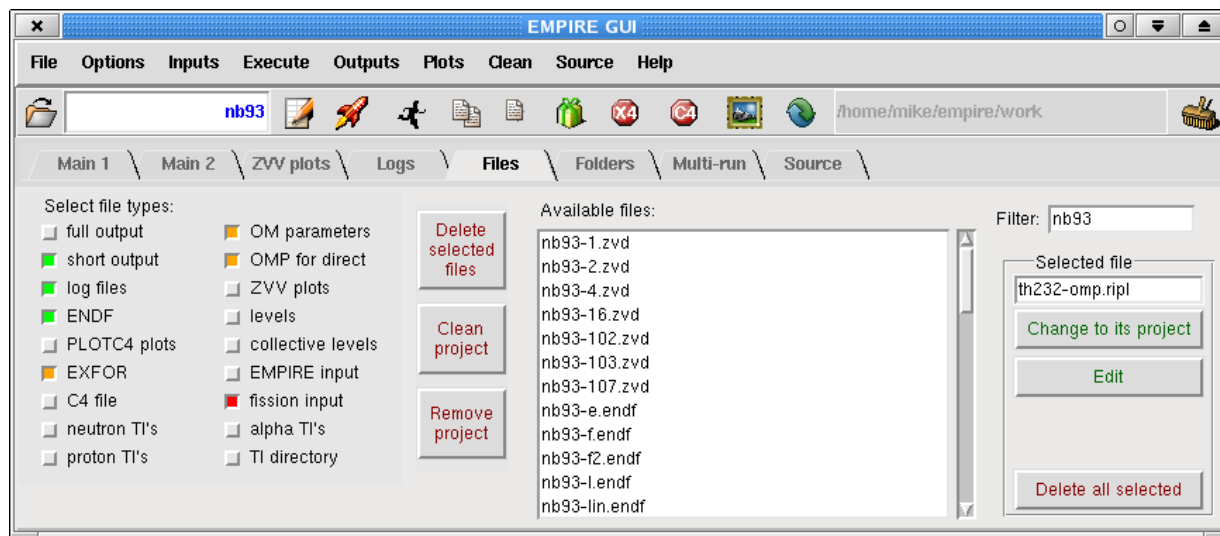


Figure 8.4: EMPIRE GUI - Files panel

**Files panel** (Fig. 8.4) offers file management functions tailored to facilitate operation of the EMPIRE code. Large number of files produced in a single EMPIRE run might result in a very crowded working directory if the latter contains several projects. Files panel is designed to facilitate access to files belonging to a current project by setting default value of the filter to the root-name of the project. User can modify filter value to restrict further list of the files (e.g., filter set to *56Fe\*.endf* will show only files with extension *\*.endf* belonging to the *56Fe* project) or relax it to display more files (e.g., filter set to *inp* will show input files for all projects). We note that, selecting a file with a name consisting only of the root-name and extension (e.g., *56Fe.exf* but not *56Fe-log.psyche*) and hitting 'Change to its project' button is a convenient way of redirecting GUI toward another project. The left part of the panel provides for a convenient removal of the selected types of files belonging to the current project. In addition, individual files can be removed by clicking on the 'Delete all selected' button. A double-click on any of the listed files will open it with an appropriate application.

**Archive panel** - (Fig. ) This panel is intended for storing milestone results of the project in the local or remote Svn repository for the archival purpose that allows to track development of the project over time and restore certain calculations if needed. In particular, one can easily produce comparison plots between any two stored versions or between the current and any of the stored versions.

**Folders panel** - (Fig. ) The folders panel is a sort of simple file manger that allows edit and delete files in the subdirectories of empire/. EMPIRE specific feature of which differs Folders panel from other and arguably more versatile file mangers is the capability of creating the new folder and moving there all the files related to a given EMPIRE project

(creating an archival copy) leaving in the original directory only those files that are need to continue calculations. Similarly to the File panel the Folders panel contains Filter that is very useful to narrow down displayed files, e.g., only *\*-\*.zvd* files of the given project.

**Multi-run panel** - (Fig. ) 'Multi-run' panel allows to perform massive calculations for many nuclei with a few mouse clicks. The left hand side window allow to load the full set of stable isotopes ('Load all' button is not yet functional). Then one can select an arbitrary number of the isotopes to create a list of targets (the list can be given a name and stored for future use). Unstable isotopes can be added to the list from the input field under the second window from the left. The output files to be kept after calculations must be selected using 'Keep only' radio-buttons. At least one 'green light' is needed to run calculations. This is enforced to protect user against running hours of calculations only to find out that all the files were deleted right after each calculation was completed. All calculations are performed in the same directory, selected in the input field in the upper-right corner of the GUI. If the input files do not exist they are created form the default *skel.inp* file by replacing 'xxx' in the second line of the input by actual mass and atomic numbers. User has a full control of the input by adjusting *skel.inp* accordingly. Once the actual input files are created they are being reused in the subsequent run. In between the runs, user may introduce arbitrary modifications to the input files. EMPIRE automatically generates 'root' names combining 'za' prefix with a typical ENDF  $Z*1000+A$ .

**Source panel** - (Fig. ) Source panel allow easy access to the FORTRAN modules in the *empire/source* directory. Each module can be edited, dimensions can be changed and *empire* executable can be recompiled. There is also a button for building the whole EMPIRE package.

## 8.9 Input/Output files

### 8.9.1 \*.inp (INPUT.DAT; main input)

EMPIRE is set up to read as much data as possible from the RIPL input directory *empire/RIPL/* [20] and the local input parameter library (*empire/data*). The user has to supply only those input parameters that the code can not know. These are the incident energy, the projectile, the target and the number of emitted particles to be followed. The current version can treat multiple emissions of the following ejectiles: neutrons, protons,  $\alpha$ , deuterons, tritons, helions ( $^3\text{He}$ ) and light ions.

With the default library of input parameters it is possible to execute a 'first-shot' calculation with minimal effort. In the second step, the user may wish to regain control over the input in order to make appropriate adjustments to the parameters. This can be done in a selective way in the optional part of the EMPIRE input, or directly in local project files produced by EMPIRE during its first run.

It should be noted that there is a difference in the way EMPIRE accesses general input library in the first and subsequent runs of a given project. In the first run the code

extracts relevant data from the input parameter library and creates local project files with discrete levels (*\*.lev*), collective levels (*\*-lev.col*), optical model parameters (*\*-omp.ripl*, and *\*-omp.dir*), fission parameters *\*-inp.fis* and relevant EXFOR data (*\*.exf* and *\*.c4*) files. Once these files exist the code uses them instead of the files contained in the general input library. This has two advantages: (i) time is spared because the case specific files are smaller and can be read fast, (ii) the user may edit case specific files *\*.lev*, *\*-omp.\**, *\*-inp.fis*, and *\*.c4* files and modify them without affecting files in the general input library. Editing the *\*-omp.\** files is a convenient method of adjusting some of the optical model parameters without the necessity of typing the whole set from scratch. Editing the fission parameter *\*-inp.fis* file is a convenient method of adjusting fission parameters; editing the collective level file allows for a selection of additional coupled levels, discrete levels embedded in the continuum, etc.

Input data are taken from different sources in the following decreasing priority (i.e. those listed above overwrite those listed below):

1. case specific files (*\*.lev*, *\*-lev.col*, *\*-omp.\**, *\*-inp.fis*)
2. input file (*\*.inp*)
3. general input parameter library including both the local and RIPL libraries

Note, that all the case specific files, except (*\*.inp*), are created by the code during the first run, and therefore the user has to create only the (*\*.inp*) file described below.

### Mandatory input

Input to EMPIRE consists of two parts. The first is mandatory and contains basic data necessary to specify the case, and the structure is illustrated by the following example:

```

14.8                               ;INCIDENT ENERGY (IN LAB)
56      26                         ;TARGET A , Z
1      0                           ;PROJECTILE A, Z
3                               ;NUMBER OF NEUTRONS TO BE EMITTED
1                               ;NUMBER OF PROTONS TO BE EMITTED
1                               ;NUMBER OF ALPHAS TO BE EMITTED
1                               ;NUMBER OF DEUTERONS TO BE EMITTED
1                               ;NUMBER OF TRITONS TO BE EMITTED
1                               ;NUMBER OF HELIONS (3He=h) TO BE EMITTED
0      0.      0.                 ;NUMBER OF L.I. TO BE EMITTED, AND ITS A AND Z

```

The first line specifies the incident energy in the laboratory system (in MeV). The second and third are used to specify the mass and atomic numbers of a target and a projectile respectively. The next seven lines define the number of emissions to be followed for each ejectile. In the above example, all reactions up to (n,3npdth) will be calculated. The code automatically sums over all possible decay sequences to reach the given residual

nucleus. Accordingly, each reaction includes all possible permutations of ejectiles (e.g.  $\sigma_{(n,npd)} = \sigma_{(n,2n2p)} + \sigma_{(n,dd)} + \sigma_{(n,nh)} + \sigma_{(n,\alpha)} + \sigma_{(n,pt)}$ ). The last line of the mandatory input provides for the inclusion of the emission of one type of heavy or light ion. This option is provided for backward compatibility (and future development). The current EMPIRE version does not allow emission of ions heavier than the  $\alpha$ -particle (all lighter ions are accounted for explicitly). If such need arises, please contact the authors.

The mandatory part of the input is in a free format, while the comments following the semicolon only serve to facilitate input preparation and are ignored by the code.

### Optional input

The mandatory input is followed by optional input, which allows modifications to the default model parameters. Optional input consists of an arbitrary number of records, entered in any order and closed with the GO record, which indicates the end of the input. In the simplest case (all defaults), only the GO record must be entered. Each optional record starts with an alphanumeric keyword **NAME**. If the first character of the line (i.e. **NAME(1:1)**) is \*, # or !, then this line contains comments and is ignored by the code. If the first character of the line **NAME(1:1)** is @, then this line contains a title, which will be printed in EMPIRE outputs; obviously the title is not used in any calculations. Multiple titles are allowed. Users are strongly encouraged to use titles and comments in EMPIRE inputs; that will be a significant step toward a better documentation of our theoretical calculations and evaluations.

The optional-input keyword **NAME** is followed by the value VAL and four positional parameters I1, I2, I3, I4. The keyword indicates a physical quantity, such as the binding energy or level density parameter, or a scaling parameter (e.g. TOTRED). VAL takes numerical value of the quantity or scaling parameter).

The positional parameters are typically used to specify to which nucleus the quantity should be applied (generally if these are omitted the value is applied to all nuclei in the given calculation). Positional parameters may be also used to indicate the estimated uncertainty of the quantity defined by the input keyword (except optical model parameters for which the uncertainty is defined by VAL). Each record must be in the FORTRAN fixed-length format:

```
FORMAT (A6,G10.5,4I5) NAME,VAL,I1,I2,I3,I4
```

Fixed format allows to avoid typing zeros if no input is needed for some positional parameters, but attention should be paid by user to keep numbers in the right position.

The GO record indicates end of the optional input and starts calculations. It may be followed by an unlimited list of incident energies (one per record) terminated with a record containing a negative value. Anything below this line will be ignored by the code.

A complete list of model parameters and options that can be controlled through the optional input entries is given in the Appendix [A](#).

### 8.9.2 \*-inp.fis (FISSION.INP)

This file is created and used only if FISSHI=0. It collects all incident energy independent input parameters related to fission of the nuclei involved in reaction for which the fissility condition is fulfilled. It follows general EMPIRE philosophy of input/output files: it is created by the code if missing and it is read by the code if it exists. All numerical values in this file representing default fission parameters may be changed except those for which it is said explicitly otherwise.

The *\*-inp.fis* file must be deleted manually if one of the following changes has been done in main input:

$$\text{FISBAR} = 3 \leftrightarrow \text{FISBAR} < 3$$

$$\text{FISMOD} = 0 \leftrightarrow \text{FISMOD} > 0$$

If  $\text{FISOPT} = 0 \rightarrow \text{FISOPT} > 0$  one has to make sure that the number of transition states at each extremum is the same.

The *\*-inp.fis* file is divided into sections corresponding to each fissioning nucleus. Each section starts with the key-word “Isotope”. Therefore in the following examples we will have as reference the line containing “Isotope” denoted L=1.

**Example 1** Fission input created if FISSHI=0; FISOPT=0,1,2,3; FISBAR<3, FISDEN=0,2; FISDIS=0,1; FISMOD=0

- L=6 - number of parabolas  $N_{\text{parab}}$  (used to describe the entire barrier) and number of wells  $N_w$  (the number of minima excluding the one corresponding to equilibrium deformation); they cannot be changed.
- L=9 - parameters of the fundamental barrier in the following order: pairs of height-width ( $E_{f_h(w)}, \hbar\omega_h(w)$ ) for each hump (maximum) followed by similar pairs for the wells, all expressed in MeV; these parameters entering Eq. 4.126 have initial values depending on FISBAR.
- L=12 - inertial parameters  $\hbar^2/2\mathfrak{I}_{h(w)}$  used in Eq. 4.128 to build rotational levels in MeV.
- L=15 - quadrupole deformations corresponding to the extrema of the fission barrier. The values printed correspond to the initial barrier parameters. If barrier parameters have been modified, EMPIRE calculates and uses the new deformations which are printed in *\*-fiss.out* but not in *\*-inp.fis*. Therefore their change would have no impact.
- L=20+w; ( $w = 1, N_w$ ) - parameters used in the energy dependence of the strength of the imaginary potential corresponding to each well (Eq. 4.129). There are two differences compared to the older version of the code: (i) the energy dependence was

changed, therefore the values of  $W_i (i = 1, 3)$  are changed accordingly, and (ii) there is a set of parameters for each well (instead a single set as it was before), meaning that to make them compatible with the present version of the code, the old files containing triple-humped barrier have to be changed by copying L=21 in L=22 also.

- L=25+ $N_w$  - number of discrete states for the first hump  $N_{dis}(h_1)$ . It is written and read as 'I2' format starting after "=" sign and has the maximum value equal to 30. For FISOPT>0 The number of discrete states and their order ( $K\pi$ ) must be the same. For FISOPT=0, the discrete states number might differ from one hump to another. However their values have to be equal to the number of lines below, associated to each discrete state.
- L=26+ $N_w + k$ ; ( $k = 1, N_{dis,h}$ ) - spin projection on the symmetry axes, parity and excitation energy with respect to the top of the hump  $K, \pi, \epsilon_h$  (entering Eq. 4.128) plus the width  $\hbar\omega_h$  for all discrete transition states (rotational band-heads) at hump  $h$ . This sequence of lines plus the one above are repeated for each extremum: first for the humps and next for the wells. All the numbers on these lines can be changed but keeping in mind that for FISOPT>0 the number of discrete states and the order of  $K\pi$  must be the same for all extrema.
- L=29+ $N_w + [N_{dis,h} + 2] * N_{parab} + h$ ; ( $h = 1, N_h$ ) - data used for FISDEN=0: hump index, degree of asymmetry of the nuclear shape at saddle  $B_{sym,h}$ , shell-correction  $\delta W_{f_h}$ , energy shift  $\delta_h$  in the effective excitation energy,  $\gamma_{f,h}$ , the ratio  $\tilde{a}_{f,h}/\tilde{a}$  of the asymptotic values for saddle and equilibrium deformations, the lower limit of transition state continuum spectrum  $E_{c,h}$ , parameters defining vibrational damping  $T_{1/2,h}, DT_h$  and the global scaling factor  $N_h$ .

The degree of asymmetry has the following significance

$$B_{sym,h} = \begin{cases} 1 & \text{axial, mirror symmetry} & h = 1, \quad N < 144 \\ 2 & \text{axial asymmetry, mirror symmetry} & h = 1, \quad N \geq 144 \\ 3 & \text{axial symmetry, mirror asymmetry} & h = 2, (3) \end{cases} \quad (8.1)$$

and selects the values of  $f_{sym}$  (Eq. 4.134) and  $d_{sym}$  (Eq. 4.164).

- L=34+ $N_{parab} + [N_{dis,h} + 2] * N_{parab} + h$ ; ( $h = 1, N_h$ ) - data used for FISDEN=2: the degree of asymmetry of the nuclear shape at saddle  $B_{sym,h}$  and the normalization parameters  $\delta_h, \alpha_h$  and  $N_h$  from Eq. 4.137.
- L=38+ $N_{parab} + [N_{dis,h} + 2] * N_{parab} + N_h + w$ ; ( $w = 1, N_w$ ) - weights  $p_w$  entering Eq. 4.169; if nonzero, direct transmission in continuum is added to the direct transmission coefficient.

Below is a real example of the fission input file corresponding to the cases discussed above.

Isotope:

-----  
 Z= 92 A=238  
 -----

Nr.parabolas =3      Nr.wells=1

Va	ha	Vb	hb	Vi	hi (in Mev)
6.300	0.800	5.700	0.500	1.400	1.000

h2/2J(A)	h2/2J(B)	h2/2J(I)	(in MeV)
0.0050	0.0025	0.0035	

Beta2(A)	Beta2(B)	Beta2(I)
0.4099	0.9337	0.6285

=====  
 Parameters of the imaginary potential used only if FISOPT>0  
 =====

W0	W1	W2
1.0000	0.1000	0.1000

=====  
 Discrete transitional states  
 =====

Number of discrete states at barrier 1 = 2

Jdis	Pidis	Edis	homega
0.0	-1	0.700	0.800
1.0	-1	0.400	0.800

Number of discrete states at barrier 2 = 2

Jdis	Pidis	Edis	homega
0.0	-1	0.100	0.500
1.0	-1	0.500	0.500

Number of discrete states at barrier 3 = 2

Jdis	Pidis	Edis	homega
0.0	-1	0.000	1.000
1.0	-1	0.000	1.000

=====  
 Quantities used only if FISDEN=0 to calculate LD at saddles  
 =====

	Asym	shell-corr	delta	gamma	atilf/ati	Ecf	VIB1/2	VIBdt	Norm
Barrier 1	2	2.600	0.307	0.600	1.000	0.000	1.000	0.100	1.000
Barrier 2	3	0.220	0.307	0.600	1.000	0.000	1.000	0.100	1.000

=====  
 Coefficients used only if FISDEN=3 to adjust HFB LD at saddles  
 =====

	Asym	Delta	alpha	Norm
Barrier 1	2	0.000	0.000	1.000
Barrier 2	3	0.000	0.000	1.000



```
=====
Coefficient(s) used to calculate the direct continuum weight(s)
=====
Well 1      0.000

*****
*****
```

**Example 2** Fission input created if FISSHI=0; FISOPT=0,1,2,3; FISBAR=3, FISDEN=0,2; FISDIS=0; FISMOD=0

- L=9 - number of points  $N_p$  for which the numerical path is defined; cannot be changed.
- L=9+n; ( $n = 1, N_p$  - index  $n$ , fission potential  $V(\beta)_n$ , quadrupole deformation  $\beta_n$ ).
- L=11+ $N_p$  - number of parabolas  $N_{parab}$  (used to describe the entire barrier) and number of wells  $N_w$  (the number of minima excluding the one corresponding to equilibrium deformation); they cannot be changed.
- L=14+ $N_p$  - indexes of extrema; they cannot be changed.
- L=16+ $N_p$  - normalization factors for the numerical barrier:  $n_{b,h}$ ; ( $h = 1, N_h$ ),  $n_\beta$ . The width scaling  $n_\beta$  enters Eq. 4.130, and the independent height normalization factors  $n_{b,h}$  enter Eq. 4.132. If  $n_{b,1}=10$ , then  $n_{b,2}$  represents the global normalization factor entering Eq. 4.131. It should be mentioned that the effect of normalization can be seen in \*fis.out, but not in \*inp.fis.
- Subsequent lines contain the same information as presented in Example 1.

Below we show an example of the fission input file with numerical fission barriers.

Isotope:

```
-----
Z= 92  A=239
-----
```

```
=====
RIPL-3 HFB numerical fission barrier
=====
96
 1      0.000      0.307
 2      0.648      0.336
 3      1.565      0.364
 4      2.597      0.388
 5      3.468      0.413
...
94      0.475      2.888
```

```

95      0.462      2.889
96      0.000      2.890

```

```

Nr.parabolas =5      Nr.wells=2

```

```

Index of extrema

```

```

      10      20      36      55      58

```

```

Normalization factors for humps

```

```

      0.000      0.000      0.000      1.000

```

```

=====
      Va      ha      Vb      hb      Vc      hc      Vi      hi      Vo      ho (in Mev)
      5.990      0.652      6.542      0.403      3.675      0.086      1.798      0.505      3.317      0.163

```

```

h2/2J(A) h2/2J(B) h2/2J(C) h2/2J(I) h2/2J(0) (in MeV)

```

```

      0.0050      0.0025      0.0017      0.0035      0.0020

```

```

Beta2(A) Beta2(B) Beta2(C) Beta2(I) Beta2(0)

```

```

      0.5480      1.2610      1.8600      0.8810      1.7610

```

```

=====
Parameters of the imaginary potential used only if FISOPT>0
=====

```

```

      W0      W1      W2
      1.0000      0.1000      0.1000
      1.0000      0.1000      0.1000

```

```

=====
Discrete transitional states
=====

```

```

      Number of discrete states at hump 1 = 4

```

```

Kdis Pidis Edis homega
0.5   1     0.000 0.652
2.5   1     0.080 0.652
0.5  -1     0.050 0.652
1.5  -1     0.010 0.652

```

```

      Number of discrete states at hump 2 = 4

```

```

Kdis Pidis Edis homega
0.5   1     0.000 0.403
2.5   1     0.010 0.403
0.5  -1     0.010 0.403
1.5  -1     0.080 0.403

```

```

      Number of discrete states at hump 3 = 4

```

```

Kdis Pidis Edis homega
0.5   1     0.000 0.086
2.5   1     0.000 0.086
0.5  -1     0.000 0.086
1.5  -1     0.000 0.086

```

```

      Number of discrete states in well 4 = 4

```

```

Kdis Pidis Edis homega
0.5   1     0.000 0.505
2.5   1     0.000 0.505

```

```
0.5  -1    0.000  0.505
1.5  -1    0.000  0.505
```

Number of discrete states in well 5 = 4

```
Kdis  Pdis  Edis  homega
0.5    1    0.000  0.163
2.5    1    0.000  0.163
0.5   -1    0.000  0.163
1.5   -1    0.000  0.163
```

```
=====
Quantities used only if FISDEN=0 to calculate LD at saddles
=====
```

		Asym	shellcorr	Ushif	gamm	atilf/atil	Ecf	VIB1/2	VIBdt	Norm
Barrier 1	2	2.600	0.300	0.600	1.000	0.000	1.000	0.100	1.000	
Barrier 2	3	0.260	0.300	0.600	1.000	0.000	1.000	0.100	1.000	
Barrier 3	3	0.260	0.300	0.600	1.000	0.000	1.000	0.100	1.000	

```
=====
Coefficients used only if FISDEN=3 to adjust HFB LD at saddles
=====
```

		Asym	Delta	alpha	Norm
Barrier 1	2	0.000	0.000	1.000	
Barrier 2	3	0.000	0.000	1.000	
Barrier 3	3	0.000	0.000	1.000	

```
=====
Coefficient(s) used to calculate the direct continuum weight(s)
=====
```

```
Well 1    0.000
Well 2    0.000
```

```
*****
*****
```

**Example 3** Fission input created if FISSHI=0; FISOPT=0; FISBAR<3, FISDEN=0; FISDIS=0,1; FISM0D=2

The file structure is the one described in Example 1, therefore will be mentioned only the differences specific to multimodal fission. In general the parameters for the outer barrier are doubled, if FISM0D=1, describing (SL) and (S1) or tripled, if FISM0D=2, describing (SL),(S1) and (S2).

- L=9 - parameters of the fundamental barrier in the following order: pairs of height-width  $(E_{f,1}, \hbar\omega_1), (E_{f,SL}, \hbar\omega_{SL}), (E_{f,S1}, \hbar\omega_{S1}), (E_{f,S2}, \hbar\omega_{S2})$  followed by similar pairs for the wells, all expressed in MeV;
- L=28+ $N_w$  +  $N_{dis}$  +  $k$ ; ( $k = 1, N_{dis,2}$ ) - spin projection on the symmetry axes, parity and excitation energy with respect to the top of the outer humps (SL),(S1) and (S2):  $K, \pi$ , and pairs height-width  $(\epsilon_2 - \hbar\omega_2)$  for (SL),(S1) and (S2) and for all discrete transition states.

- $L=30+N_w + [N_{dis,h} + 2] * N_{parab} + h2$ ; ( $h2=FISMOD+1$  - data used for FISDEN=0: hump index, mod index, degree of asymmetry of the nuclear shape at saddle  $B_{sym,h}$ , shell-correction  $\delta W_{fh}$ , energy shift  $\delta_h$  in the effective excitation energy,  $\gamma_{f,h}$ , the ratio  $\tilde{a}_{f,h}/\tilde{a}$  of the asymptotic values for saddle and equilibrium deformations, the lower limit of transition state continuum spectrum  $E_{c,h}$ , parameters defining vibrational damping  $T_{1/2,h}$ ,  $DT_h$  and the global scaling factor  $N_h$  for (SL),(S1) and (S2).

Below we report example of the fission input for the multimodal fission.

Isotope:

```
-----
Z= 94  A=243
-----
```

Nr.parabolas =3      Nr.wells=1

Va	ha	Vb(SL)	hb(SL)	Vb(ST1)	hb(ST1)	Vb(ST2)	hb(ST2)	Vi	hi (in Mev)
6.050	0.700	7.450	1.200	5.450	0.700	5.550	0.700	2.000	1.000

h2/2J(A)	h2/2J(B)	h2/2J(I)	(in MeV)
0.0050	0.0025	0.0035	

Beta2(A)	Beta2(B)	Beta2(I)
0.4438	0.9232	0.6634

```
=====
Parameters of the imaginary potential used only if FISOPT>0
=====
```

W0	W1	W2
1.0000	0.1000	0.1000

```
=====
Discrete transitional states
=====
```

Number of discrete states at hump 1 = 4

Kdis	Pidis	Edis	homega
0.5	1	0.000	0.700
2.5	1	0.080	0.700
0.5	-1	0.050	0.700
1.5	-1	0.010	0.700

Number of discrete states at hump 2 = 4

Kdis	Pidis	Edis	homega				
0.5	1	0.000	1.200	0.000	0.700	0.000	0.700
2.5	1	0.010	1.200	0.010	0.700	0.010	0.700
0.5	-1	0.010	1.200	0.010	0.700	0.010	0.700
1.5	-1	0.080	1.200	0.080	0.700	0.080	0.700

Number of discrete states in well 3 = 4

Kdis	Pidis	Edis	homega
0.5	1	0.000	1.000
2.5	1	0.000	1.000

```
0.5  -1    0.000  1.000
1.5  -1    0.000  1.000
```

```
=====
Quantities used only if FISDEN=0 to calculate LD at saddles
=====
      Asym shellcorr Ushif   gamm  atilf/atil   Ecf   VIB1/2   VIBdt   Norm
Barrier 1    2    2.600   0.300   0.600   1.000   0.000   1.000   0.100   1.000
Barrier 2    1 0    0.540   0.300   0.600   1.000   0.000   1.000   0.100   1.000
Barrier 2    2 0    0.540   0.300   0.600   1.000   0.000   1.000   0.100   1.000
Barrier 2    3 0    0.540   0.300   0.600   1.000   0.000   1.000   0.100   1.000
```

```
=====
Coefficients used only if FISDEN=3 to adjust HFB LD at saddles
=====
      Asym   Delta   alpha   Norm
Barrier 1    2    0.000   0.000   1.000
Barrier 2    3    0.000   0.000   1.000
```

```
=====
Coefficient(s) used to calculate the direct continuum weight(s)
=====
Well 1    0.000
```

```
*****
*****
```

### \*-inp.sen (SENSITIVITY.INP)

The sensitivity input instructs EMPIRE which parameters should be considered in the sensitivity matrix and how much are they going to be varied. Contrary to other input files in EMPIRE, the sensitivity input is not directly linked to the particular case since the reference is made to the compound nucleus and the nuclei involved in the decay chain are identified by the number of neutrons and protons which were removed from the compound nucleus rather than specifying their actual number (as in the main input file *\*.inp*). Therefore, the default input can be used for any nucleus but care should be taken to use only those parameters that are relevant to the models and mechanisms used in the actual calculations and, on the other side, to include all the parameters that are relevant to the calculations. For example, it makes no sense to vary fission parameters in the case of neutron reaction on iron, or modifying MSD parameters if MSD is not being used but it's even worse not to vary fission parameters for the case of uranium.

The sensitivity input is created automatically in the first run by copying the default file *skel-inp.sen*. As usual in EMPIRE, user is supposed to adjust this file by taking into account reaction mechanisms and models used in the main input, available experimental data and scope of the research.

The structure of the file follows the optional input in *\*.inp* - the same keywords are used except that

- the first parameter (val) specifies the perturbation, e.g., 0.05 means perturbation of the parameter specified by the keyword by 5%.
- the second positional parameter indicates how many protons were removed from the compound nucleus
- the third positional parameter indicates how many neutrons were removed from the compound nucleus
- the fourth positional parameters retains its original meaning (usually it indicates an ejectile)

For example, the following line of input

```
UOMPVV      0.03      00  01   1      ! omp real vol. depth for Z-0 N-1 nucl.
```

indicates that the real depth of the optical model for the neutron (4<sup>th</sup> parameter equal 1) on the residue nucleus after emitting one neutron from the compound nucleus (3<sup>rd</sup> parameter equal 01) will be perturbed by 3%.

### 8.9.3 \*.lst (LIST.DAT; lengthy output)

As the main output of EMPIRE, the size of the file depends on the controls IOUT and NOUT specified in input (\*.inp). In the extreme case, no output except warnings is produced (note that all essential results are written to the file \*.out, which is not affected by IOUT and NOUT).

The file begins with the code banner and printout of the parameters specified in the optional input. Lack of a message regarding any given parameter means that the default value has been used in the calculations. The next segment of the output specifies the incoming channel and model parameters such as binding energies, fission barriers, shell corrections, ground state deformations and list of optical model systematics used in the calculations. The message is printed to notify the user on eventual re-normalization of the internal level density systematics to the experimental results. Re-normalization is performed only if experimental values of the *a*-parameter for at least 3 nuclei involved in the calculations are found in *empire/data/ldp.dat*. The introductory part of the output is followed by the results of calculations for each decaying nucleus.

In the case of Compound Nucleus all calls to the ORION code are listed and the outputs of TRISTAN and ORION codes (the latter only if *IOUT* > 3) are printed. Next, the fusion cross section and associated spin/parity distributions are given. For each decaying nucleus (including Compound Nucleus) the production cross section, population of discrete levels, intensities of discrete  $\gamma$ -lines and emitted spectra of  $\gamma$ s, neutrons, protons,  $\alpha$ s and eventually light ions are printed. Output for a given incident energy is completed by inclusive spectra of all  $\gamma$ s and particles emitted along the de-excitation chain. This scheme is repeated for each incident energy apart from the code banner and optional input printout. The general

structure of the output can be summarized as follows (depending on input options some items might be missing in an output):

- code banner
- optional input
- matrix of models usage
- 1<sup>st</sup> incident energy
  - Compound Nucleus
    - \* input parameters
    - \* elastic, reaction and total cross sections
    - \* inelastic scattering to collective levels
    - \* pre-equilibrium models' results
    - \* fusion cross section
    - \* population and decay of discrete levels
    - \* residue production cross section
    - \* fission cross section
    - \* emission spectra
  - 1<sup>st</sup> residue
    - \* model parameters
    - \* discrete level population before their  $\gamma$ -de-excitation
    - \* population and decay of discrete levels in
    - \* residue production cross section
    - \* fission cross section
    - \* emission spectra
  - 2<sup>nd</sup> residue
    - \* ...
  - last residue
    - \* ...
    - \* inclusive emission spectra
  - 2<sup>nd</sup> incident energy
    - \* ...
  - last incident energy
    - \* ...

### 8.9.4 \*.out (OUTPUT.DAT)

This EMPIRE output is used by EMPEND for creating the ENDF-6 formatted file.

### 8.9.5 \*.fus (FUSION)

This file is used to input arbitrary fusion cross sections, overriding any other options regarding fusion determination that might be contained in the input. The file is a simple column of fusion cross sections for subsequent partial waves starting with  $l = 0$  (one cross section per line in a free format). Cross sections for any number of partial waves can be introduced but the code will consider only those below the actual value of NDLW (see Section 8.3). Other limitations on the number of partial waves can be set in the input or internally by the code (e.g., stability of a liquid drop against rotation or disappearance of the fission barrier, see Section A).

### 8.9.6 \*.lev (LEVELS)

File \*.lev contains discrete levels for all nuclei involved in a given calculation. This file is produced by EMPIRE during the first run by extracting relevant information from the RIPL library (files empire/RIPL/levels//z\*.dat) retaining the original format.

File \*.lev most probably requires modification. For certain applications, missing branching ratios, uncertain spins, parities and levels may have to be supplied or modified. However, most likely some levels may need to be cut-off in order to make the scheme consistent with the level density parameterization. The user has to set  $N_{max}$  (6<sup>th</sup> item in the first line of the isotope section) to the required value. Contrary to 2.17 and earlier versions of EMPIRE, excess levels **must not** be removed.

### 8.9.7 \*-lev.col (TARGET\_COLL.DAT)

The first run with the DIRECT option different from zero results in EMPIRE creating a file that contains collective levels to be used in the Coupled-Channels or DWBA calculations. Whenever possible coupled-channel data (i.e. coupled levels and coupling model) are taken from the optical segment of the RIPL library (note that CC potentials in RIPL contain the necessary information on the levels to be coupled and the coupling model), while data for additional collective levels are retrieved from the \*.lev file. If the necessary information is not available in RIPL (spherical optical potential is being used), the code tries to identify collective levels internally among those available in \*.lev file. In such circumstances, the g.s. deformation is assigned to the g.s. rotational band, and default dynamic deformations are ascribed to each collective level (note that band deformation is used in the rotational model and dynamic deformations are used in the vibrational model). The format of the \*-lev.col file is analogous to the one used in the optical segment of the RIPL library (see Refs. [35, 145]). Additional uncoupled collective levels may be also retrieved from the \*.lev file, depending on input keyword ECDWBA. The default cut-off energy is  $3x30/A^{2/3}$ , and



the default maximum spin 4 (e.g. with these defaults all levels with excitation energy less than 2.4 MeV for  $^{238}\text{U}$ , and less than 6.2 MeV for  $^{56}\text{Fe}$  are considered). Default selection rules for energy and spin could be modified in the input.

A first sample, containing 16 collective levels in  $^{238}\text{U}$  including 5 coupled levels defined in the coupled-channel rigid-rotor potential RIPL 2408 is reproduced below. Please note the keyword “deformed” in the third line that defines the rigid-rotor coupling model. In this sample file those collective levels are divided in three groups:

- The first group contains five levels used in the Coupled Channels calculations (read from RIPL). These are the collective levels in the target, which happen to be consecutive in the EMPIRE file with discrete levels (*\*.lev*) hence their numbering is 1 through 5. In general, coupled collective levels are mixed with the uncoupled ones, thus their  $N$  numbers in the *\*.lev.col* file are NOT necessarily consecutive nor sequential. However, their numbers have to correspond to the desired discrete level number (from level file *\*.lev*), otherwise calculated collective cross section will be misassigned. Dynamical deformations are dummy entries for levels of the ground-state rotational band, as the GS-band deformation is determined from the nucleus deformation given in the sixth line of the file.
- The second group are uncoupled collective levels, with  $N$  from 26 through 36, which are considered in the additional DWBA calculations. In order to distinguish them from the coupled-levels 20 is added to their serial number in the *\*.lev* file (it implies that only first 20 levels can be used in the CC calculations. The number 20 is also printed in the second line of the file, and corresponds to the parameter LEVCC defined in *dimension.h*). CC calculations can couple as many as LEVCC - 1 levels, if a larger number is needed, then the LEVCC parameter should be modified and EMPIRE code recompiled.
- The third group, marked as “cont”, consists of dummy collective levels embedded in the continuum that may not be included in *\*.lev*. Their numbering follows the second group but actual numbers of these “dummy” levels have no importance. They might, but do not have to, coincide with some of the discrete levels in the original RIPL file. The levels in this group are used in the DWBA calculations to the continuum, and their scattering cross sections are spread among neighboring continuum energy bins using a gaussian function with the energy resolution defined by parameter RESOLF.

How these three groups of levels are actually used in the calculations depends on the value of the DIRECT keyword:

- Direct excitation of all collective levels is only considered if DIRECT > 0.
- If DIRECT = 1 or 2, coupled channels are calculated within the CC method, remaining levels by DWBA.

- If DIRECT = 3, then scattering on all collective levels is calculated within the DWBA approach, using the dynamical deformation listed in the file. One-phonon states are assumed.

Collective levels selected automatically from available target levels

N < 20 for coupled levels in CC calculation

92 238 nucleus is treated as deformed

```

Ncoll  Lmax  IDef  Kgs  (Def(1,j),j=2,IDef,2)
  16     8    6    .0   .228E+00  .620E-01  -.556E-02

```

N	E[MeV]	J	pi	Nph	L	K	Dyn.Def.
1	.0000	.0	1.	1	0	0	.100E-01
2	.0449	2.0	1.	0	0	0	.200E-01
3	.1484	4.0	1.	0	0	0	.200E-01
4	.3072	6.0	1.	0	0	0	.200E-01
5	.5181	8.0	1.	0	0	0	.200E-01
26	.6801	1.0	-1.	0	0	0	.843E-01
27	.7319	3.0	-1.	0	0	0	.843E-01
30	.9272	.0	1.	0	0	0	.200E-01
33	.9661	2.0	1.	0	0	0	.200E-01
35	.9972	.0	1.	0	0	0	.200E-01
36	.9976	3.0	-1.	0	0	0	.200E-01
38	1.0373	2.0	1.	0	0	0	.200E-01 cont
40	1.0577	3.0	1.	0	0	0	.200E-01 cont
41	1.0597	3.0	1.	0	0	0	.200E-01 cont
42	1.0603	2.0	1.	0	0	0	.200E-01 cont
44	1.1057	3.0	1.	0	0	0	.200E-01 cont

The symbols are :

<b>Ncoll</b>	number of collective states in the coupled-channel rotational model for a particular <i>iz</i> , <i>ia</i>
<b>Lmax</b>	maximum <i>l</i> value for multipole expansion
<b>IDef</b>	largest order of deformation
<b>Kgs</b>	<i>k</i> for the rotational band
<b>Def</b>	deformation parameters, <i>l</i> =2,4,6,...through Lmax
<b>E</b>	level excitation energy (MeV)
<b>J</b>	level spin

<b>pi</b>	level parity
<b>Nph</b>	1 for pure 1-phonon state 2 for pure 2-phonon state
<b>L</b>	level orbital momentum
<b>K</b>	level spin projection
<b>Dyn.Def.</b>	vibrational model deformation parameter. Not used for coupled levels.

A second sample, containing 33 collective levels in  $^{238}\text{U}$  obtained for a rigid-soft rotor coupled-channel potential RIPL 2412 is reproduced below. Please note the keyword “dynamically deformed” in the third line that defines the rigid-soft rotor coupling model. All levels belong to the discrete region (continuum was defined to start above 1.3 MeV). Coupled channels correspond to level number  $j \leq 30$ ; there are 14 coupled channels in this case.

```
Collective levels: RIPL 2412 CC OMP, rigid+soft rotor model
N < 30 for coupled levels in CC calculation
92 238 nucleus is treated as dynamically deformed
```

```
Ncoll Lmax IDef Kgs (Def(1,j),j=2,IDef,2)
33 8 6 0.0 0.230E+00 0.600E-01 -0.640E-02
```

N	E[MeV]	J	pi	2*K	Nc	Nb	Dyn.Def.
1	0.0000	0.0	1.	0	0	0	0.230E+00
2	0.0449	2.0	1.	0	0	0	0.100E-01
3	0.1484	4.0	1.	0	0	0	0.100E-01
4	0.3072	6.0	1.	0	0	0	0.100E-01
5	0.5181	8.0	1.	0	0	0	0.100E-01
6	0.6801	1.0	-1.	0	0	1	0.550E-01
7	0.7319	3.0	-1.	0	0	1	0.550E-01
9	0.8266	5.0	-1.	0	0	1	0.550E-01
10	0.9272	0.0	1.	0	0	3	0.800E-02
13	0.9661	2.0	1.	0	0	3	0.800E-02
15	0.9972	0.0	1.	0	0	2	0.100E-01
18	1.0373	2.0	1.	0	0	2	0.100E-01
22	1.0603	2.0	1.	4	0	4	0.200E-01
24	1.1057	3.0	1.	4	0	4	0.200E-01
38	0.7759	10.0	1.	0	0	0	0.100E-01
41	0.9305	1.0	-1.	0	0	0	0.500E-02
42	0.9501	2.0	-1.	0	0	0	0.500E-02
46	0.9976	3.0	-1.	0	0	0	0.500E-02
47	1.0280	4.0	-1.	0	0	0	0.500E-02

49	1.0564	4.0	1.	0	0	0	0.500E-02
50	1.0577	3.0	1.	0	0	0	0.500E-02
51	1.0597	3.0	1.	0	0	0	0.500E-02
55	1.1288	2.0	-1.	0	0	0	0.500E-02
56	1.1307	4.0	1.	0	0	0	0.500E-02
57	1.1357	1.0	1.	0	0	0	0.500E-02
60	1.1630	4.0	1.	0	0	0	0.500E-02
61	1.1680	4.0	1.	0	0	0	0.500E-02
62	1.1689	3.0	-1.	0	0	0	0.500E-02
63	1.2238	2.0	1.	0	0	0	0.500E-02
65	1.2393	3.0	1.	0	0	0	0.500E-02
67	1.2609	4.0	1.	0	0	0	0.500E-02
68	1.2692	6.0	1.	0	0	0	0.500E-02
69	1.2785	2.0	1.	0	0	0	0.500E-02

The symbols are :

<b>Ncoll</b>	number of collective states in the coupled-channel rotational model for a particular <i>iz</i> , <i>ia</i>
<b>Lmax</b>	maximum <i>l</i> value for multipole expansion
<b>IDef</b>	largest order of deformation
<b>Kgs</b>	<i>k</i> for the rotational band
<b>Def</b>	deformation parameters, <i>l</i> =2,4,6,...through Lmax
<b>E</b>	level excitation energy (MeV)
<b>J</b>	level spin
<b>pi</b>	level parity
<b>2*K</b>	twice the level spin projection quantum number <i>K</i>
<b>Nc</b>	Flag indicating isobar-analogue states (> 0) or normal states (=0)
<b>Nb</b>	Band number. The ground-state band always has Nb=0.
<b>Dyn.Def.</b>	vibrational model deformation parameter. Not used for the ground state band.

A third sample, containing 10 collective levels in <sup>56</sup>Fe obtained for a soft-rotor coupled-channel potential RIPL 2602 is reproduced below. Please note the keyword “soft” in the third line that defines the soft-rotor coupling model. All levels belong to the discrete region (continuum was defined to start above 3.5 MeV). Coupled channels correspond to level number j 30; there are seven coupled channels in this case.

Collective levels: RIPL CC OMP + default, soft rotor  
 N < 30 for coupled levels in CC calculation  
 26 56 nucleus is treated as soft

Soft rotator hamiltonian parameters for OPTMAN  
 .25666E+01 .48922E+00 .12600E+00 .32552E+00 .23200E+00 -.46000E+00  
 .53202E-07 .93896E-01 .69718E+00 .64617E+00 .14557E+00 .29933E+00  
 .35000E+00 .48730E-02 .00000E+00 .73536E+01 .00000E+00

Ncoll  
 10

N	E[MeV]	J	pi	Ntu	Nb	Ng	-----	No
1	.0000	.0	1.	1	0	0	.500E-02	0
2	.8468	2.0	1.	1	0	0	.500E-02	0
3	2.0851	4.0	1.	1	0	0	.500E-02	0
4	2.6576	2.0	1.	2	0	0	.500E-02	0
5	2.9415	.0	1.	1	1	0	.500E-02	0
7	3.0762	3.0	-1.	1	0	0	.500E-02	0
36	2.9599	2.0	1.	1	0	0	.500E-02	0
38	3.1201	1.0	1.	1	0	0	.500E-02	0
39	3.1229	4.0	1.	1	0	0	.500E-02	0
40	3.3698	2.0	1.	1	0	0	.500E-02	0

The symbols are :

<b>Ncoll</b>	number of collective states in the coupled-channel rotational model for a particular <i>iz</i> , <i>ia</i>
<b>Lmax</b>	maximum <i>l</i> value for multipole expansion
<b>IDef</b>	largest order of deformation
<b>Kgs</b>	<i>k</i> for the rotational band
<b>Def</b>	deformation parameters, <i>l</i> =2,4,6,...through Lmax
<b>E</b>	level excitation energy (MeV)
<b>J</b>	level spin
<b>pi</b>	level parity
<b>Ntu</b>	Number of solution for spin J (close to the approximate spin projection K)

**Nb**  $\beta$ -vibration quantum number.

**Ng**  $\gamma$ -vibration quantum number.

**No** Octupole vibration quantum number.

**Dyn.Def.** vibrational model deformation parameter. Not used in this case.

A fourth and last sample, containing 10 collective levels in  $^{56}\text{Fe}$  obtained for a vibrational coupled-channel potential RIPL 425 is reproduced below. Please note the keyword “spherical” in the third line that defines the vibrational coupling model. All levels belong to the discrete region (continuum was defined to start above 3.5 MeV). Coupled channels correspond to level number  $j \leq 30$ ; there are seven coupled channels in this case.

```
Collective levels: RIPL CC OMP + default, vibr. model
N < 30 for coupled levels in CC calculation
26 56 nucleus is treated as spherical
```

```
Ncoll
10
```

N	E[MeV]	J	pi	Nph	L	K	Dyn.Def.
1	.0000	.0	1.	0	0	0	.500E-02
2	.8468	2.0	1.	1	0	0	.240E+00
7	3.0762	3.0	-1.	1	0	0	.197E+00
4	2.6576	2.0	1.	2	0	0	.500E-02
5	2.9415	.0	1.	2	0	0	.500E-02
3	2.0851	4.0	1.	2	0	0	.500E-02
36	2.9599	2.0	1.	1	0	0	.500E-02
38	3.1201	1.0	1.	1	0	0	.500E-02
39	3.1229	4.0	1.	1	0	0	.500E-02
40	3.3698	2.0	1.	1	0	0	.500E-02

The symbols are :

**Ncoll** number of collective states in the coupled-channel rotational model for a particular  $iz$ ,  $ia$

**Lmax** maximum  $l$  value for multipole expansion

**IDef** largest order of deformation

**Kgs**  $k$  for the rotational band

**Def** deformation parameters,  $l=2,4,6,\dots$ through Lmax

**E** level excitation energy (MeV)

<b>J</b>	level spin
<b>pi</b>	level parity
<b>Nph</b>	1 for pure 1-phonon state 2 for pure 2-phonon state
<b>L</b>	level orbital momentum
<b>K</b>	level spin projection
<b>Dyn.Def.</b>	vibrational model deformation parameter

Users may choose to modify the *\*-lev.col* file to fit experimental data. In fact, such modifications are expected to be necessary if the file was created internally rather than copied from the RIPL optical model library. In particular, deformation parameters (both static and dynamic) should be given appropriate attention since cross sections are very sensitive to their values. Static deformation parameters can be modified automatically using the FITOMP option.

### 8.9.8 **\*-fiss.out (FISSION.OUT)**

Contains details of the fission calculations such quantities as level densities at saddles, fission transmission coefficients and fission probabilities, that are usually beyond interest of the typical user of the code. Therefore, the file exists only under generic name and is overwritten each time the code is run. The format of the file is self-explanatory.

### 8.9.9 **\*.xcs (XS.OUT)**

Concise table of total, elastic, reactions (absorption), fission, and all residue production cross sections (the latter can usually be identified with the cross sections for particular reactions) in the column format convenient for plotting.

### 8.9.10 **\*-preq.xcs (PREQ\_XS.OUT)**

Contains table of direct and preequilibrium contributions to the first emissions.

### 8.9.11 **\*-fiss.xcs (FISS\_XS.OUT)**

Contains table of fission cross sections for different fission chances in the column format convenient for plotting.

### 8.9.12 \*-omp.ripl (OMPAR.RIPL)

Set of optical model parameters for all nucleus-ejectile combinations involved in the calculations extracted from the RIPL library. This file is created by EMPIRE if RIPL potential is requested in the input and the *\*-omp.ripl* file does not already exist (typically during the first run). The format is identical to the RIPL optical segment (see Refs. [35, 145]). Optical model parameters contained in the *\*-omp.ripl* file can be modified manually if desired.

### 8.9.13 \*-omp.dir (OMPAR.DIR)

Used to store optical model parameters that are input to ECIS06 for Coupled-Channels or DWBA calculations. The format is the same as that of the *\*-omp.ripl* file described above, and coincides with the RIPL format (see Refs. [35, 145]) used to represent optical model parameters. The reason for creating *\*-omp.dir* file, in addition to the *\*-omp.ripl*, is in order to use the Coupled-Channels optical model potential for the incident channel, in which CC or DWBA calculations are performed, and the spherical potential for the calculation of transmission coefficients when DIRECT=1 or 2 options are used. Depending on the combination of input options, *\*-omp.dir* can be empty. Optical model parameters contained in the *\*-omp.dir* file can be modified manually if desired or automatically using the FITOMP option.

### 8.9.14 \*.endf (OUTPUT.ENDF)

EMPIRE results (in ENDF format) from processing with the EMPEND, FIXUP, ENDRES and STANEF codes. This is the final properly formatted ENDF-6 file.

### 8.9.15 \*-s.endf

\*.endf file processed with a chain of codes: FIXUP, LINEAR, RECENT, SIGMA1, LEG-END and SIXTAB. Intermediate files are removed by the *process* script. Note, that this file is intended only for plotting and does not respect certain limits imposed by the ENDF-6 format.

### 8.9.16 \*-mat.sen (SENSITIVITY.MATRIX)

Sensitivity matrix calculated with EMPIRE when KALMAN option in the main input is set to 1 and sensitivity input *\*-inp.sen* is present in the working directory. The matrix contains a block for each model parameter that has been included in the sensitivity input. These blocks contain a line for each incident energy and a column for each reaction calculated by EMPIRE. The sensitivities printed in the matrix represent relative change of the cross section to the perturbation of the parameter but they are not divided by the perturbation (this is done later when the matrix is prepared to be used by the KALMAN code). We choose



this representation since it makes analyses of the sensitivities immediate - if the individual perturbations are reasonable the sensitivities can be compared directly without referring to the perturbation themselves.

### 8.9.17 \*.exf (EXFOR.DAT)

Starting with the 3.1 version EMPIRE accesses experimental through the C4 file. The IAEA NDS generates this file twice a year by processing the latest version of the EXFOR master file through the X4TOC4 code using the most current version of the dictionary, which ensures highest possible rate of translation. Retrieval from the C4 is much simpler than from the original EXFOR library and is not subject to the dependency problems, which were frequent in the previous releases. Since knowledge of the EXFOR file might be of interest we preserve in the current EMPIRE version processing capabilities available previously. User may decide to download the EXFOR file from the IAEA or NNDC Web servers, store it in the working directory with the extension *.exf* and process it into C4 file. The EXFOR format is 'human readable', and provides the user with sufficient information about the experiment. A typical excerpt is given below

```

SUBENT      10827001      861124
BIB          13          46
INSTITUTE   (1USALRL)
REFERENCE   (J,PR/C,19,2127,7906)
            (C,80BNL,1,245,8007) UPDATED VALUES.
AUTHOR      (S.M.GRIMES,R.C.HAIGHT,K.R.ALVAR,H.H.BARSCHALL,
            R.R.BORCHERS)
TITLE       CHARGED PARTICLE EMISSION IN REACTIONS OF 15-MEV
            NEUTRONS WITH ISOTOPES OF CHROMIUM, IRON, NICKEL, AND
            COPPER.
INC-SOURCE (D-T) 400-KEV DEUTERONS ON ROTATING TITANIUM TRITIDE
            TARGET
SAMPLE      2.5-CM DIAMETER FOIL WITH DIAPHRAGM TO AVOID CONTAMIN-
            ANTS FROM FOIL HOLDERS.
DETECTOR     (SOLST) PAIR OF SILICON SURFACE BARRIER DETECTORS, 15
            AND 1500 MICRO-METERS THICK, SPACED 19-MM APART.
METHOD      TRIPLE LENS MAGNETIC QUADRAPOLE SPECTROMETER USED.
            DIFFERENT REACTION ANGLES OBTAINED BY MOVING TRANSPORT
            SYSTEM ALONG ITS AXIS. NINE DIFFERENT CURRENT SETTINGS
            USED FOR MAGNETS TO COVER ENERGY RANGE OF EMITTED
            PARTICLES
MONITOR      (1-H-1(N,EL)1-H-1,,SIG)
            (1-H-2(N,EL)1-H-2,,SIG)
CORRECTION   ENERGY SPECTRA CORRECTED FOR ENERGY LOSS IN TARGET
ERR-ANALYS   ERRORS IN PRODUCT OF SPECTROMETER SOLID ANGLE AND
            ABSOLUTE NEUTRON FLUX DUE TO-
            -ERRORS IN POLYETHYLENE STOPPING POWER, LESS THAN
            3-PERCENT
            -ERRORS IN ELASTIC CROSS SECTIONS FROM HYDROGEN, LESS
            THAN 1-PERCENT
            -ERRORS IN ELASTIC CROSS SECTIONS FROM DEUTERIUM, LESS
            THAN 10-PERCENT
            -ERROR IN SOLID ANGLE OF TARGET TO NEUTRON SOURCE
            RATIO FOR CH(2) OR CD(2) COMPARED TO THAT OF SAMPLE
            FOILS, 8-PERCENT
            OTHER ERRORS DUE TO-
            -TARGET FOIL THICKNESS ERRORS, 2.5-PERCENT
            -EFFECT OF STATISTICS AND THE LEGENDRE POLYNOMIAL FIT,

```

```

              7-PERCENT (FOR PROTONS, ALPHAS) TO 15-PERCENT (DEUT-
              ERONS)
STATUS      (APRVD) APPROVED BY S.M.GRIMES, 86/11/21.
              PARTIAL CROSS SECTIONS TAKEN FROM PRIVATE COMM.,
              GRIMES, 79/5.
HISTORY     (790605C)
              (820819A) REFERENCE UPDATE, BIB CORRECTIONS.
              (830830A) BIB CORRECTIONS.
              (860422A) BIB UPDATES.
              (860709A) BIB UPDATED, SUBENTS 71-103 ADDED.
ENDBIB      46
COMMON      1          3
EN
MEV
  14.8
ENDCOMMON   3
SUBENT      10827012    790716
BIB         4          6
REACTION    (24-CR-52(N,D)23-V-51,PAR,SIG)
SAMPLE      SAMPLE IS 2.1 MILLI-GMS/SQ-CM THICK, ENRICHED TO
              99.9-PERCENT CR-52
MONITOR     (1-H-2(N,EL)1-H-2,,SIG) NEUTRONS ON THICK CD(2) RAD-
              IATOR
ERR-ANALYS  COMBINED ERROR IS 20-30 PERCENT
ENDBIB      6
NOCOMMON    usually
DATA        4          11
E-MIN      E-MAX      DATA      DATA-ERR
MEV         MEV        MB         MB
  1.5       2.0       0.2       0.15
  2.0       2.5       0.5       0.2
  2.5       3.0       0.7       0.25
  3.0       3.5       0.6       0.2
  3.5       4.0       1.0       0.3
  4.0       4.5       0.3       0.15
  4.5       5.0       0.9       0.3

```

### 8.9.18 \*.c4 (empire/util/x4toc4/c4.dat)

The C4 file is the preferential way of accessing experimental data. This file contains relevant EXFOR data translated into computational format by the X4TOC4 code. An excerpt from the .c4 file of experimental data for the (n,2n) reaction on  $^{124}\text{Sn}$  is shown below.

```

1 24052  3 16  1.2722+7 8000.000 0.038800 1.5000-3
1 24052  3 16  1.2744+7 8000.000 0.041200 1.6000-3
1 24052  3 16  1.3251+7 10000.00 0.121900 5.0000-3
1 24052  3 16  1.3271+7 10000.00 0.123700 5.1000-3
1 24052  3 16  1.3888+7 9000.000 0.240600 9.7000-3
1 24052  3 16  1.3902+7 9000.000 0.250600 0.010100
1 24052  3 16  1.4251+7 8000.000 0.322000 0.012500

```

The original file also contains information on the EXFOR sub-entry number, the first author and the year of publication. These data are placed far to the right and are not displayed here. The user may wish to modify this file by deleting or adding some lines. A detailed description of the format is given in the source of the X4TOC4 code, while we list only the most important columns (fields).

Field #	Contents
2	Z*1000+A
3	ENDF File (3-cross sections)
4	ENDF MT number (here MT=16 stands for (n,2n))
5	incident energy (in eV)
6	incident energy resolution (in eV)
7	cross section (in b)
8	cross section error (in b)

### 8.9.19 \*.ps (empire//util/plotc4/plot.ps)

PostScript plots comparing calculations with experimental data. These static plots, produced by the PLOT4 code, have been superseded by the interactive ZVView plots and are rarely used.

### 8.9.20 \*-cum.ps

PostScript plots compare cumulative number of discrete levels and level densities fitted to reproduce the last level. Plots are only produced for Gilbert-Cameron or EMPIRE-specific level densities when FITLEV > 0 is specified in the input. All nuclei involved in a calculation and with at least 3 known discrete levels are included.

### 8.9.21 \*-ompfit.lst (FIT.OUT)

Information about variations in optical model or deformation fit parameters and the minimization of  $\chi^2$  is written here. This file is written only when FITOPT > 0 is specified in the input.

### 8.9.22 \*.x42c4.lst (empire/util/x4toc4/x4toc4.lst)

Output of the X4TOC4 code for the last run. Provides a log of the translation from EXFOR to computational format if such translation has been performed.

### 8.9.23 \*.x42c4\_errs (empire/util/x4toc4/errors)

List of EXFOR entries not translated by the X4TOC4 code to the computational format, for example, when X4TOC4 is not able to resolve the reaction string.

### 8.9.24 Log files

Full EMPIRE run will, in general, produce a number of *\*-log* files, which report summary of results and eventual problem encountered during formatting, format checking

preprocessing, and plotting. These files, named after codes that generated them, include: *\*-log.checkr* *\*-log.empend* *\*-log.endres* *\*-log.fixup* *\*-log.fixup2* *\*-log.fizcon* *\*-log.legend* *\*-log.linear* *\*-log.plotc4* *\*-log.psychc* *\*-log.recent* *\*-log.sigma1* and should be inspected as a part of the Quality Assurance.

## 8.10 Plotting capabilities

All pertinent experimental data in EXFOR are retrieved during the first run of the code and plotted against the ENDF-formatted file using a chain of ENDF Pre-Processing codes (PREPRO [15]) and X4TOC4 [16] and PLOT4 [16]. These codes are called by EMPIRE in a transparent way by bash scripts. Fig. 8.5 shows typical example of such a plot. High quality plots can be produced interactively using the ZVView package of Zerkin [17].

### 8.10.1 ZVView

The plotting capabilities of EMPIRE rely on the graphic package ZVView by Zerkin [17]. This software is operated from the EMPIRE GUI and produces publication quality plots. The scale can be changed, selected data sets can be excluded from the plot, and data points values displayed; changes can also be made to the plot title, subtitle, symbols and colors, data fitting, smoothing and others. Plots can be exported to the PostScript or encapsulated PostScript format for inclusion in the L<sup>A</sup>T<sub>E</sub>X document.

Contrary to PLOT4, ZVV plots are not generated automatically. The user has to select a desired reaction from the EMPIRE GUI () button or type MT number in the entry box at the bottom of the GUI) and click on the  button. Internal scripts and components of the ZVView package process the ENDF and *\*.c4* files to produce the *\*-MT.zvd* file, which is then displayed with the ZVView.

ZVV plots can also be combined to include different reactions on the same graph. Clicking on the  button will open the terminal with a list of all ZVV plots available in the *work* directory. The user may select any number of them to be included in a single plot. Usually, the plot title has to be set within the ZVView environment before saving.

Additional functionality is offered by the ZVView GUI (see Fig. 8.6), which permits comparison of up to three calculations (or ENDF files), and experimental data (see Fig. 12.1, 12.2 and 12.3). It is primarily intended as a tool for checking the effect of different options used in the calculations or comparing the results with other evaluations. Usually, one would undertake a set of calculations and use the script *store* to move (or copy) all the relevant files to a specified directory. For example, to store the project with root-name “fe56” in a *case1* directory, one should type:

```
../scripts/store ../case1 fe56
```

inside the *work* directory (note that *case1* will be on the same level as *work*). Thus, the working directory is free to run new calculations with the modified input. These results can

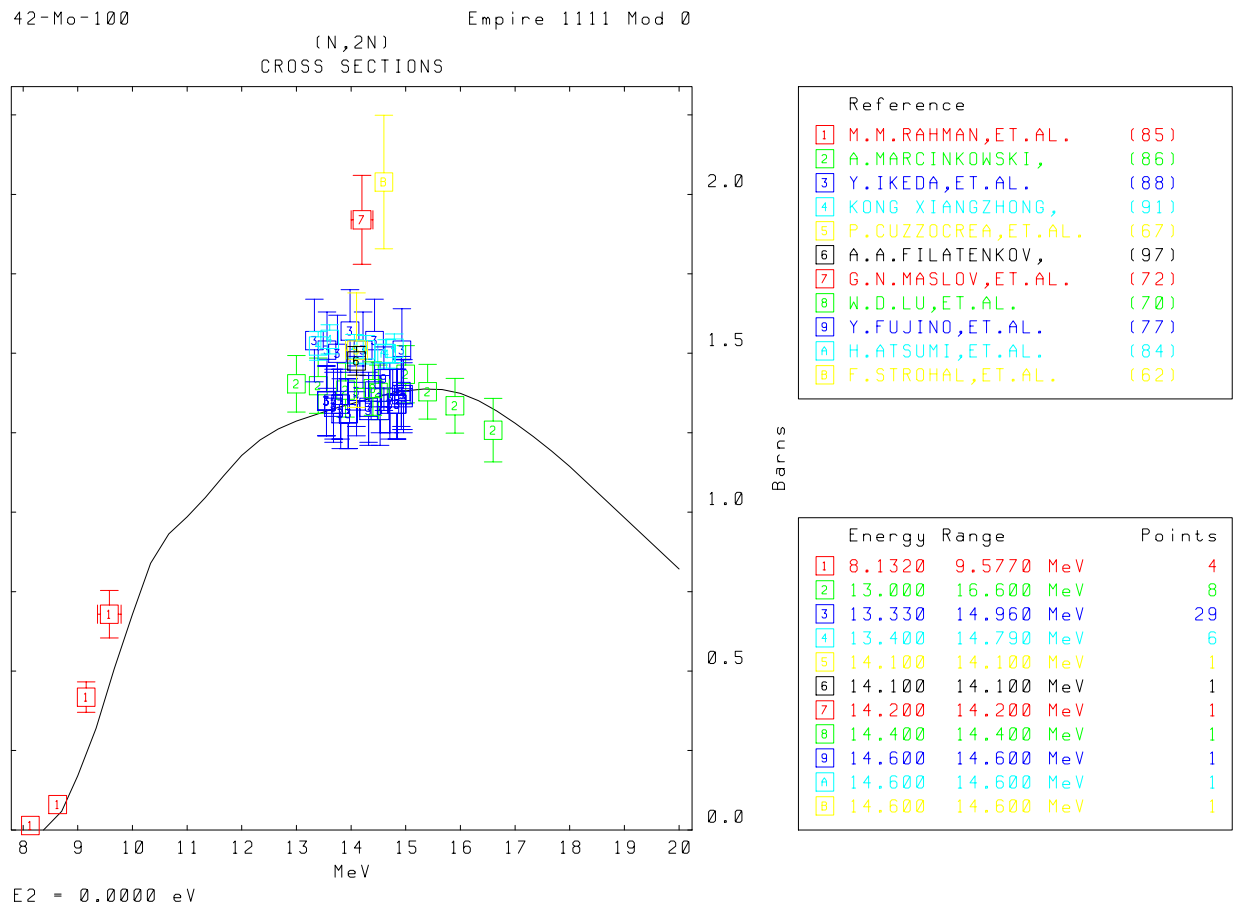


Figure 8.5: Comparison of the experimental data extracted from the EXFOR library with the results of EMPIRE calculations using default parameters. This plot is produced automatically when running EMPIRE with the *run* script or clicking the Run+Format+Plot button in GUI mode.

again be stored in another directory (e.g., *case2*) and the third set of calculations executed in the *work* directory. If experimental data are to be plotted, the *\*.c4* file with the same root-name should be present in the first directory, which is ensured if EXFOR data were extracted by EMPIRE. Clicking the Compare ENDF file button of the EMPIRE GUI launches ZVV GUI, as shown in Fig. 8.6. Note that the root-name of the project and *work* directory are by default transferred to ZVV GUI. Comparisons can be made by pointing the “File 2:” and “File 3:” fields to other files containing ENDF formatted data (e.g., stored in *case1* and *case2* directories). We stress that while the first set is referenced through its directory and default names *\*-s.endf* and *\*.c4* the other two are identified by respective arbitrary file names. An arbitrary suffix identifying the comparison plots and labels for each curve should be entered in the respective fields. At this stage the system is ready to create the requested plots (Create selected button). One can also choose to create all plots at once (Create all button), although they can be viewed one by one or merged together. ZVV GUI can also be used to create simple ZVV plots by replacing the EMPIRE GUI function. Leaving labels related to “File 2:” and “File 3” fields and suffix blank, simple ZVV plots can be created for all the reactions with just one mouse click. Setting the project field to “\*” (without “”) creates plots for all reactions and targets for which *\*-s.endf* files exist in the *work* directory. This comparison capability is not limited to the EMPIRE results; any evaluated file in the ENDF format can be compared with another ENDF file or with EMPIRE calculations, providing that the first file is named (or linked) as *\*-s.endf* and placed in the *work* directory.

As a rule, only the ENDF-formatted files can be plotted with PLOT4 or ZVView. This choice is not only a matter of convenience but was deliberately selected to validate the final (ENDF-formatted) product. The only exception to this rule is provided by the Create ZVV GUI button, which allows the user to construct and plot any excitation function directly from the EMPIRE output. Hence, the user has to supply a string which unambiguously identifies the cross section. The *gawk* script scans EMPIRE output (*\*.lst*) for the lines containing the specified string and extracts a number (cross section) followed by the “mb” string along with the respective incident energy value. The results are sent to ZVView for plotting.

## 8.11 Plans for further development

Following extensions are foreseen in the future releases of the EMPIRE code:

1. Inclusion of isospin,
2. Improved parametrization of the elastic enhancement factor,
3. ENDF-formatting of primary gammas.
4. Improved description of direct reactions (e.g. breakup, pickup, etc.) for reactions with incident complex particles (e.g. deuteron, triton and  $^3\text{He}$ ),

**Show ZVV plots**

### Create/Show ZVV Plots

Project root name:

Suffix for plots:

Project directory and other ENDF files:

Directory:

Label for curve 1:

File 2:

Label for curve 2:

File 3:

Label for curve 3:

Select MT:

- ☐ 1 total
- ☐ 2 elastic
- ☐ 4 inelastic
- ☐ 16 (x,2n)
- ☐ 17 (x,3n)
- ☐ 22 (x,na)
- ☐ 28 (x,np)
- ☐ 45 (x,npa)
- ☐ 102 (x,g)
- ☐ 103 (x,p)
- ☐ 107 (x,a)
- ☐ 112 (x,pa)

Create selected

Create all

Show selected plots

Show all

Merge selected plots

Exit

Figure 8.6: Graphic User Interface to ZVView to compare up to three calculations (or ENDF files) and merge different reactions on a single ZVV plot.

5. Implement particle decay of discrete levels that is relevant for the treatment of direct reactions (e.g.  $^{12}\text{C}(n,n+3\alpha)$ ) in the outgoing channels.
6. Inclusion of heavy-ion optical potential (Sao Paulo potential).



**Part IV**

**WORKING NOTES**



# Chapter 9

## Avoiding problems

Consideration and observation of the following remarks will help to avoid problems when running the EMPIRE code:

- Each modification of the EMPIRE input file (\*.inp) that involves a change of projectile, target, or the number of emitted particles must be followed by the execution of the *clean* script in order to remove input/output files that do not match the new case. One should keep in mind that *clean* will also remove all the files that might have been modified manually (such as \*.lev, \*-omp.dir, etc.). If these files are compatible with the new input and are to be preserved they have to be renamed by adding a prefix before executing the *clean* script.
- Any serious calculations should be preceded by a test run using FITLEV set to a positive value in order to check the completeness of the discrete level schemes and their consistency with the level densities. Such calculations should be repeated after each change of the input file (\*.inp) that requires running the *clean* script (see above). Calculation times for such runs are very short.
- If the ENDF option is selected, the incident energies should be in increasing order.
- Log files \*.war, \*.x42c4\_errs and empend.log should be checked for possible warnings and error messages.
- Irregularities in the excitation functions such as (n,2n) or (n,p) are usually due to improper level density parametrization (check cumulative plots of discrete levels) or to the overestimated MSD contribution (check response functions and ensure that the levels to which they are adjusted are actually the collective ones).
- Irregularities in the increasing part of the excitation function for inelastic scattering are usually due to insufficiently dense mesh of incident energies.



# Chapter 10

## Fitting discrete levels

Running EMPIRE with the FITLEV option is strongly recommended before any cross section calculations are attempted. This allows a check of whether the discrete level schemes for the involved nuclei are complete and consistent with the level density parametrization. If the whole package is properly installed, plots of cumulative number of levels will be stored in the *\*-cum.ps* file and can be inspected in the PostScript viewer (ghostview) by clicking on the Levels button in the “Plots:” section of the GUI. Two somewhat extreme examples of such plots are shown in Fig. 10.1 and 10.2. Fig. 10.1 demonstrates 10 levels in  $^{96}\text{Pd}$ , which could not be matched with the level densities, which usually happens when the levels are over extend. Then, levels that were not detected experimentally are missing in the spectrum, and the resulting high energy end of the cumulative plot is too low. Missing levels are more likely in the high-energy region of the spectrum and reducing the number of levels considered may restore agreement; neglecting the highest 4 levels in  $^{96}\text{Pd}$  leads to a reasonable fit, as shown in the Fig. 10.2. Graphical representation helps to identify the level at which cumulative plot starts to bend, and levels lying above this point should be excluded from consideration. One should edit *.lev* file and decrease  $N_{max}$  parameters (6<sup>th</sup> entry in the first line of a given isotope section) to remove levels in excess. The next step after the modified *\*.lev* file is saved is to rerun the code and check whether the applied cuts are sufficient. If this is not the case, the whole procedure should be repeated and further levels removed. Note, levels are only removed from the local file of the specific case being calculated, and that *Zxxx.dat* files in the parameter library are not affected.

There are no restrictions on the contents of the input file (*\*.inp*) used for displaying the cumulative plots except that the FITLEV record must be included with VAL different from 0. Dispositions that do not consider level densities are ignored as the code exits after the plots are completed without performing any cross section calculations.

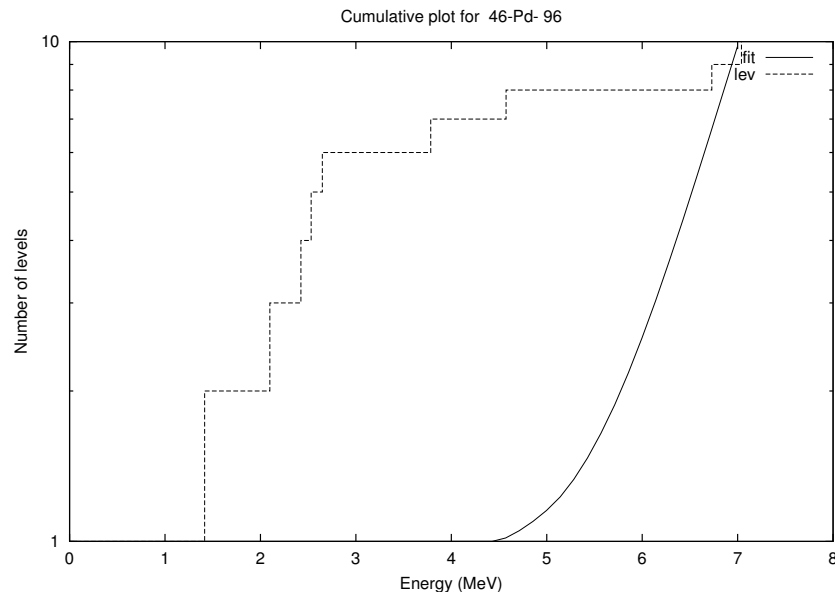


Figure 10.1: Cumulative plot of 10 discrete levels in  $^{96}\text{Pd}$  which could not be reproduced by the level density calculations (EMPIRE-specific level densities with default parametrization were used).

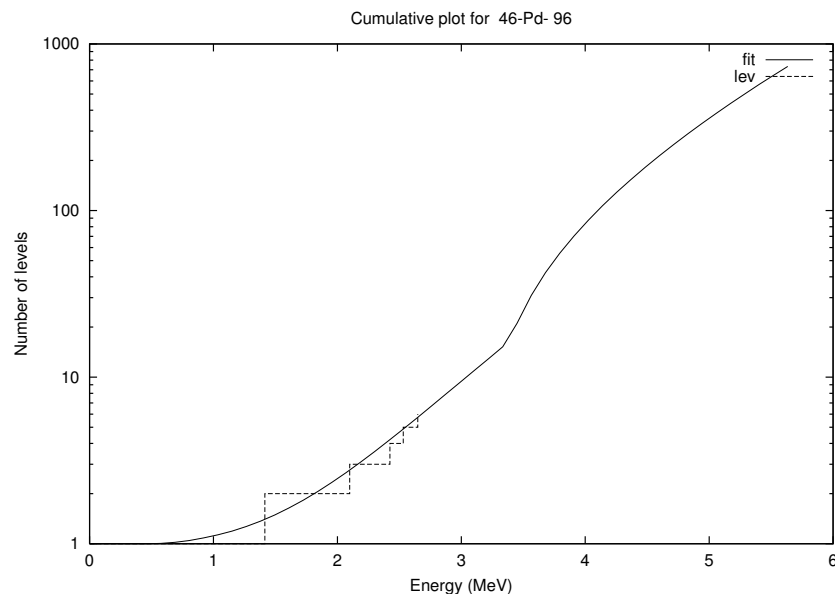


Figure 10.2: Same as Fig. 10.1 but after restricting the fit to the first 6 levels only. Note the difference of two orders of magnitude in the level densities around 6 MeV.

# Chapter 11

## Handling OM potentials

Interface to the RIPL optical model segment has been developed by Capote. This interface allows the use of any type of Optical Model Potential (OMP) contained in the library (including dispersive ones) by specifying the OMP catalog number in the optional input (list of available OMPs can be accessed from the EMPIRE GUI through the menu `Help`  $\Rightarrow$  `RIPL-omp`). The OMPOT record contains two numerical values in addition to the usual keyword. The first value is the OMP catalog number entered with a **negative** sign, which indicates that the potential is going to be taken from RIPL rather than from the internal sets coded in EMPIRE. The second value defines the type of particle. For example,

**OMPOT -401. 1** selects RIPL Wilmore-Hodgson global potential (RIPL number 401) for neutrons,

**OMPOT -4004. 2** selects RIPL CC potential for protons (to be used for  $^{197}\text{Au}$  only).

The code will create *\*-omp.ripl* file containing parameters for the selected potentials for all nuclei and particles involved in the calculations. This file can be edited in order to adjust OMP parameters extracted from RIPL. RIPL Coupled-Channels Optical Model Potentials (CC-OMP) include collective discrete levels and related deformations, and thus the *\*-omp.ripl* contains all information needed to run Coupled-Channel (CC) calculations.

The ECIS06 module, along with the RIPL interface, bring into EMPIRE an easy access to a large number of optical model potentials. However, the related input keywords (DIRECT, DIRPOT and OMPOT) must be used with considerable care. In the following, we will explain different combinations of these keywords, focusing on the use of optical model parameters within EMPIRE. To this end we will discuss several examples of neutron induced reactions on a spherical nucleus ( $^{54}\text{Fe}$ ) with dynamic deformation (vibrational case), and on a deformed one ( $^{153}\text{Eu}$ ) with static deformation (rotational case). The general input file may contain the following lines:

DIRECT	x.	call ECIS for CC, CC full or DWBA
DIRPOT	-xx.	RIPL OMP for direct (inelastic) channel
OMPOT	-xx.      z	RIPL OMP for particle z

In the following examples we use case-specific file names as created when script or GUI modes are used to run the code. We recall that the correspondence between the case specific names and those generated by the code is the following:

***\*-omp.dir***       $\Longleftrightarrow$  *OMPAR.DIR*

***\*-omp.ripl***       $\Longleftrightarrow$  *OMPAR.RIPL*

***\*-lev.col***       $\Longleftrightarrow$  *TARGET\_COLL.DAT*

with “\*” standing for the actual root-name of the file.

## 11.1 DWBA with RIPL OMP

Apply the DWBA model to the spherical vibrational nucleus  $^{54}\text{Fe}$ . Our goal is to perform calculations using default spherical RIPL potentials for all channels, but including inelastic scattering calculated by ECIS06 with the DWBA option using RIPL spherical OMP catalog number 10. The input file must contain two lines:

**DIRECT**      3.

**DIRPOT**      -10.

Resulting OMP files:

***\*-omp.ripl***      default RIPL OMP used for all the channels in the HF calculations.

***\*-omp.dir***      spherical OMP employed in the DWBA calculations of the inelastic scattering to collective discrete levels, in this case RIPL OMP potential catalog number 10.

We can adjust the inelastic scattering cross sections in subsequent runs by changing OMP inside the *-omp.dir* file and/or by changing dynamic deformations inside the *\*-lev.col* file (initial deformation values are 0.15 for quadrupole and 0.05 for octupole vibrations).



## 11.2 Coupled-Channels with RIPL spherical OMP

Our goal is to perform calculations for  $^{54}\text{Fe}$  using default RIPL potentials for all the channels, but including inelastic scattering calculated by the ECIS06 CC option using RIPL spherical OMP potential catalog number 10. The input file must contain 2 lines:

```
DIRECT      1.
DIRPOT      - 10.
```

Resulting OMP files:

***\*-omp.ripl***     RIPL OMP used for all the channels in the HF calculations.

***\*-omp.dir***     spherical OMP employed for the CC calculations of the inelastic scattering to collective discrete levels, in this case RIPL OMP catalog number 10.

We can adjust the inelastic scattering cross sections in subsequent runs by changing OMP inside the *\*-omp.dir* file or by changing dynamic deformations inside the *\*-lev.col* file.

## 11.3 Coupled-Channels with RIPL CC OMP for inelastic scattering

We intend to perform calculations for  $^{153}\text{Eu}$  using RIPL spherical potential catalog number 221 for all neutron channels (local potential for  $^{153}\text{Eu}$ ) except the inelastic channel, for which we are going to calculate cross sections with the CC method using the RIPL CC-OMP potential catalog number 2004. The input file must contain 3 lines:

```
DIRECT      1.
DIRPOT      -2004.
OMPOT       -221.      1
```

Resulting OMP files:

***\*-omp.dir***     deformed (CC) OMP employed for the CC calculations of the inelastic channel, (RIPL potential catalog number 2004 in this case (contains collective levels and respective deformations)).

***\*-omp.ripl***     RIPL spherical OMP catalog number 221 used in the HF calculations of neutron channels.

The inelastic scattering cross sections can be adjusted in subsequent runs by changing OMP inside the *\*-omp.dir* file or by changing the static deformation of the ground state band inside the same file. We are using a true CC-OMP from RIPL and collective levels are stored together with the potential parameters inside the *\*-omp.dir* file.

## 11.4 Complete Coupled-Channels with RIPL CC OMP for inelastic scattering

Our aim is to perform exact calculations for  $^{153}\text{Eu}$  using default EMPIRE potentials for all charged particle channels and the RIPL spherical OMP catalog number 221 (local potential for  $^{153}\text{Eu}$ ) for all neutron channels except inelastic, for which we are going to calculate cross sections and transmission coefficients consistently using the CC method and the RIPL CC-OMP catalog number 2004. The input file must contain three lines:

```
DIRECT      2.
DIRPOT      -2004.
OMPOT       -221.      1
```

Resulting OMP files are:

- \*-omp.ripl***      CC-OMP employed for the CC calculations of the fusion and inelastic channels (RIPL CC-OMP number 2004 (contains collective levels and respective deformations)). In addition, the file contains RIPL S-OMP number 221 employed for all other neutron channels except inelastic.
- \*-omp.dir***      is not created since a true CC-OMP is used consistently and all relevant parameters are contained in the *\*-omp.ripl* file.

The inelastic scattering cross sections can be adjusted in subsequent runs by changing either S-OMP inside the *\*-omp.ripl* file or the static deformation of the ground state band inside the *\*-lev.col* file (initial value is the experimental g.s. quadrupole deformation). Note that the CC-OMP and the CC method are also used for the calculation of the fusion cross section.

# Chapter 12

## Effects of parameter modifications

The parameter libraries and internal systematics contained in the EMPIRE code perform reasonably well in reproducing cross sections for major neutron induced reactions up to 20 MeV. However, one can not expect that global parametrization will provide perfect fits to all channels and at all incident energies. Weak reaction channels may differ substantially from the experimental data. In view of the uncertainties associated with the model parameters, certain adjustments were made in order to fit measured cross sections. Guidance is given below on parameter tuning, indicating the most sensitive methods and, if possible, describing the effect of their modification.

It is strongly recommended that various available options in the code are exploited before any attempt is made to change the parameters. This guarantees that physically meaningful parameters are used. For example, the user may try different optical model potentials, various formulations and/or parameterizations of level densities and eventually different preequilibrium models. These attempts should, at least, provide the user with the best starting point for parameter adjustment. We note that various options may provide very different results as illustrated by the following three sets of calculations:

<b>standard</b>	Wilmore-Hodgson S-OMP for neutrons and Becchetti-Greenlees for protons, EMPIRE-specific level densities with internal systematics, and discrete levels up to $N_{max} = 10$ (note that in EMPIRE-3.2 Koning-DeLaroche potential is a standard),
<b>Ko-Be</b>	Koning-DeLaroche S-OMP for neutrons and protons, discrete levels up to the $N_{max}$ recommended by RIPL (limited to 40 by the ENDF-6 format), and EMPIRE-specific level densities,
<b>Ko-Be-Go</b>	as above but using HFB microscopic level densities <a href="#">[148]</a> instead of the Empire-specific ones.

Figs. [12.1](#), [12.2](#) and [12.3](#) show comparison of the results obtained using the above sets of parameters in three sample cases. Differences of a factor of 2 are observed, and therefore

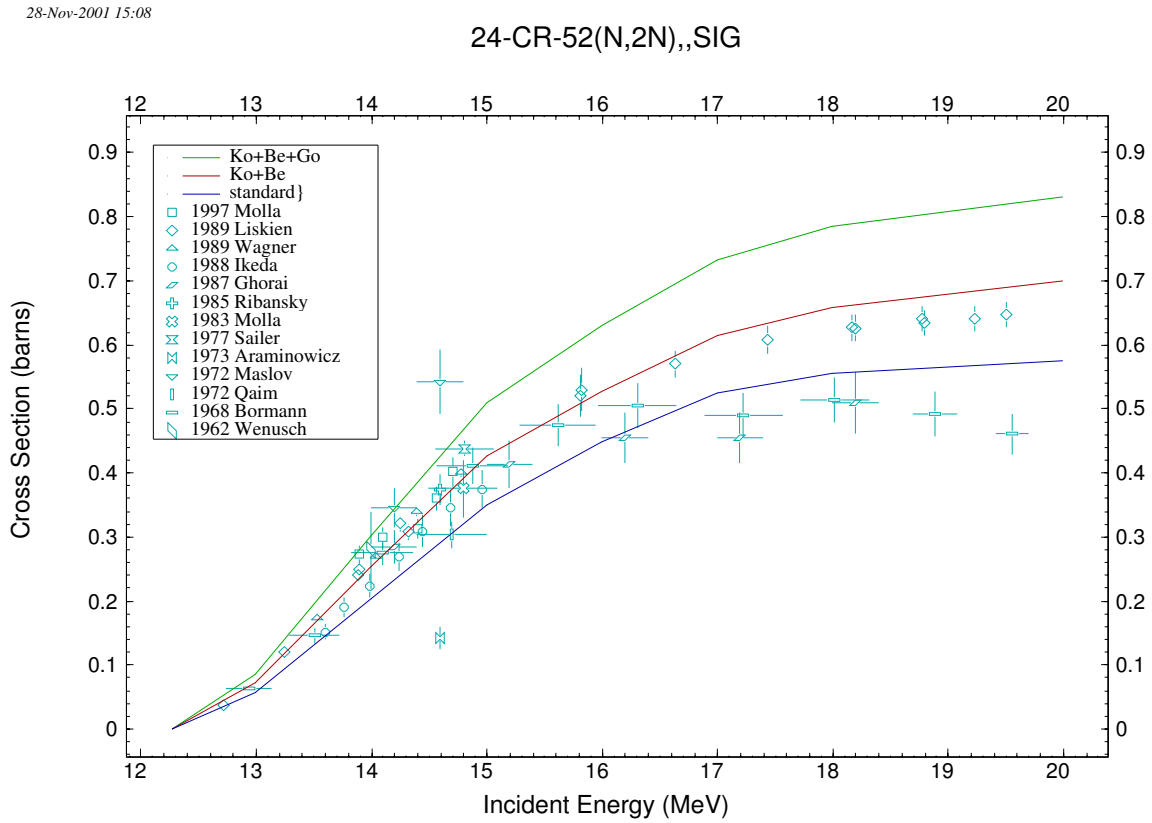


Figure 12.1: Comparison of experimental data with results calculated using three sets of parameters for the  $^{52}\text{Cr}(n,2n)$  reaction (see text).

28-Nov-2001 15:49

## 24-CR-52(N,P),,SIG

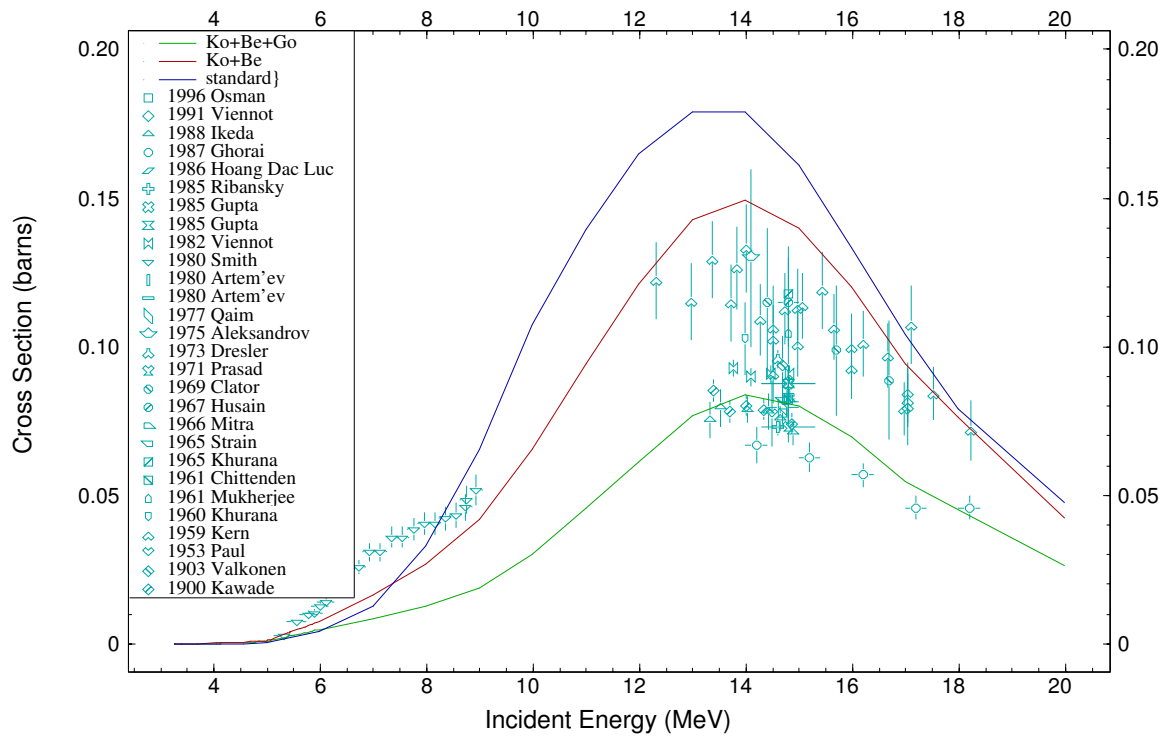


Figure 12.2: Comparison of experimental data with results calculated using three sets of parameters for the  $^{52}\text{Cr}(n,p)$  reaction (see text).

28-Nov-2001 15:53

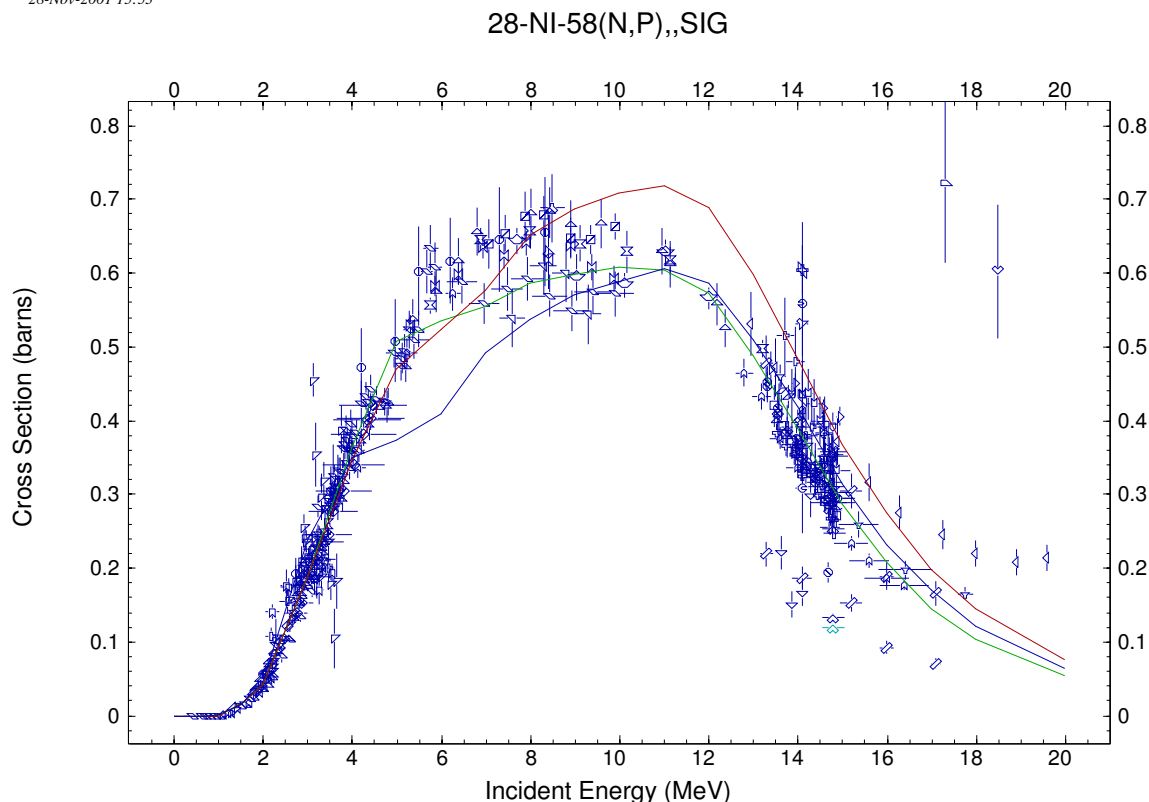


Figure 12.3: Comparison of experimental data with results calculated using three sets of parameters for the  $^{58}\text{Ni}(n,p)$  reaction (see text).

changing the default options may considerably improve the comparison with experimental data. However, this approach may still not be sufficient in some cases, and the next step would be to determine which reaction mechanism is most likely to be responsible for the disagreement, remembering that neutron capture below 10 MeV and the low energy part of the particle spectra are essentially due to Compound Nucleus decay. The high energy part of particle spectra is dominated by the preequilibrium emission, and population of the collective discrete levels in inelastic scattering arises mainly from the direct reactions. We also note that at incident energies below 50 MeV the multiple-chance preequilibrium emission is rather small and multiple particle emission is governed by the statistical decay. The list below should help pinpoint the mechanism that might be causing a problem:

- **Nucleon spectra at high ejectile energies underestimated (overestimated)** - these are usually related to the underestimated (overestimated) preequilibrium emission.
- **Tails of the inelastic scattering cross sections underestimated (overestimated)** - again caused by too low (too high) preequilibrium contribution.

- **Inelastic cross sections to discrete levels underestimated (overestimated)** - lack of or too low (too high) contribution from the direct reactions is the most likely reason. In case of under-estimation, user should ensure that Coupled-Channel or DWBA option is turned on (DIRECT=1, 2, or 3). Generally, the Coupled-Channel option will provide higher cross sections than DWBA.
- **Capture cross sections below 10 MeV underestimated (overestimated)** - as mentioned before, the Compound Nucleus is responsible. The discrepancy might be traced to  $\gamma$ -ray strength function being too low (too high) or to the ratio of level densities in the daughter nuclei and the Compound Nucleus being too low (too high) ( $\rho_n/\rho_{CN}$  - note that the neutron channel is usually the main competitor).
- **Capture cross sections above 10 MeV underestimated** - be sure that the exciton model PCROSS is turned on. The preequilibrium emission of  $\gamma$ s (or the Direct-Semidirect mechanism) is responsible for more than 90% of the capture cross section in this energy range.
- **Cross sections underestimated (overestimated) in all channels** - can be traced to an inadequate optical potential that provides too low (too high) absorption cross section.
- **Wrong total cross section** - obviously an inadequate optical potential.
- **Wrong angular distributions for elastic scattering** - again would assume an inadequate optical potential to be the main reason. At low energies where few inelastic channels are open, there might be a non-negligible contribution from the symmetric compound elastic, which could be affected by the wrong  $\rho_n/\rho_{CN}$  ratio.
- **Cross sections for the  $\alpha$ -channel underestimated** - for nuclei with masses larger than about 100, the discrepancy is not due to wrong parameters but to the lack of a preequilibrium emission of clusters in the present version of EMPIRE. One may compensate for this deficiency by increasing level densities in the residue after  $\alpha$  emission or by increasing the diffuseness of the optical model potential for  $\alpha$ -particles. However, the resulting parameters will be unphysical. Such an intervention may only be justified for lighter nuclei, for which preequilibrium emission of  $\alpha$ -particles is relatively unimportant.
- **Fission cross sections underestimated (overestimated)** - for neutron induced fission, the current fission model coded in EMPIRE is too crude. One may try to cure the problem by decreasing (increasing) the fission barrier or increasing (decreasing) level densities at the saddle point, but this should be considered as an arbitrary fitting exercise without much physical meaning. Tuning fission cross sections in the HI induced reactions will be discussed later on.

- **Excitation functions shifted in energy** - for nuclei far from the stability line (typical for HI induced reactions), this effect can be traced to incorrect binding energies (masses). A modest change of binding energies (of the order of 0.5 MeV) can be justified as being within the uncertainty of the theoretical masses. However, this argument does not hold for nuclei close to the stability valley since experimental nuclear masses are known with a rather high accuracy.
- **Structure in the continuum part of the inelastic scattering spectrum “out of phase”** - this structure originates from the MSD contribution. When the spectrum does not match experiment, the user may attempt to tune calculations by changing the positions of collective levels to which the response functions are fitted.
- **Double-differential spectra for inelastic scattering to continuum at small angles ( $< 40^\circ$ ) underestimated** - MSD mechanism is responsible for the major part of the cross section in this range. Choosing the compressional form factor for the  $l = 0$  transfer (default is the surface form factor) should bring substantial improvement. In fact, from the physical standpoint this *is* the factor that should be used for the  $l = 0$  transfer. The different default is being used due to the numerical instabilities that happen occasionally when this physically-correct option is selected.
- **Wrong ratio between two competing channels (e.g.,  $\sigma(n,n) / \sigma(n,p)$ )** - at low incident energies this ratio is governed by the Compound Nucleus decay and may be distorted by an inappropriate ratio of level densities in the two competing channels. Actually, the cross section ratio is approximately proportional to the level density ratio in the respective residual nuclei. Also, the optical model potential may have a significant effect. At higher incident energies, the preequilibrium contribution starts to play a role, and a reference for one of the preequilibrium channels may provide a solution.
- **Wrong slope of the increasing part of the excitation function** - a crucial role is played by the discrete levels in the residual nucleus and the optical model potential (transmission coefficients), of which the discrete levels are easier to control. Changing the number of accepted levels may effectively increase or decrease the available phase space for the particular decay mode.
- **Production of residues in HI induced reaction underestimated (overestimated)** - for lighter nuclei in which the fission channel is not dominant, the fusion cross section might be too small (or too big). Competition between fission and particle emission may constitute an additional source of error for the highly fissile (heavy) nuclei. In such a case, decreasing (increasing) strength of the fission channel is usually an effective way of increasing (decreasing) residue production.

The mechanisms and parameters that are expected to be the most important and effective in solving a particular problem have been noted in the above discussion. However, we are always dealing with a complicate interplay of different factors and in some cases the



major sources of error may differ from those indicated. However, the user should be able to identify the most critical reaction mechanism or a key input quantity in most cases, and be able to avoid a random search for optimal parameters.

So far we have discussed the symptoms and possible reasons for operational problems. Knowing the disease, we should now look for the most appropriate treatment. We will indicate those input parameters to which particular models or input quantities (such as fusion, level densities and,  $\gamma$ -ray strength functions) are most sensitive. However, parameters not mentioned below may also influence the results. Generally, their effect should be less pronounced but they might become one of the key players in particular situations. In addition, these assessments are complicated and most of the parameters are correlated; for example, deficiencies in one parameter can be compensated by a change in another leading to unrealistic values. Therefore, it is important to understand the physical reason for a discrepancy and proceed accordingly, and to fit all available observables rather than a single cross section. Such an approach increases the user's confidence in the final results. Finally, fitting a single experimental point that differs dramatically from the calculated value can be dangerous, especially when the exercise involves a strong channel. The experimental point might simply be wrong. Such cases are known in the EXFOR library, either because of an erroneous experiment or a compilation error. In particular, if the experimental data fall well below the calculated cross section, the user should check whether the measurement concerned the total cross section for the reaction channel or the cross section to the isomeric or ground state.

In the discussion that follows, we group parameters according to the reaction mechanism or input quantity to which they are relevant, and refer to them by keywords defined in the input description (see Section 8.9.1).

## 12.1 Fusion

We have to distinguish between Heavy Ion (HI) and Light Ion ( $A < 5$ ) or nucleon induced reactions. For HI induced reactions one may use following parameters to control fusion cross section:

- |               |   |
|---------------|---|
| <b>FUSRED</b> | scales calculated fusion cross section with an arbitrary factor to set the parameter directly to the desired value, but lacks any physical significance and predictive power. Should be used as the last resource unless the fusion cross section is known from a more microscopic model or experiment.   |
| <b>BFUS</b>   | Fusion barrier height in the distributed barrier model $B_{fus}$ (Eq. 1.2) is by default calculated by the CCFUS and used for the HI induced reactions only. Even a slight decrease of the barrier height can produce a considerable increase of the fusion cross section (and vice versa) when the incident energy (in CM) is close to the barrier height. This effect tends to disappear at higher incident energies. |

<b>SIG</b>	SIGMA in the distributed barrier model (Eq. 1.2) is by default set to $0.05B_{fus}$ . Increase of SIGMA will also increase the fusion cross section. Similarly to BFUS, the effect is most pronounced at low energies and tends to disappear at higher values.
<b>EXPUSH</b>	Extra-push energy (default value is 0) is very effective at decreasing the HI fusion cross section when increased. Physically justified for a fusion of massive systems.
<b>CRL</b>	Critical $l$ -value for the HI fusion (Eq. 1.5) sets fusion cross section to the required value - much like FUSRED.
<b>DFUS</b>	Diffuseness in the transmission coefficients of HI fusion (Eq. 1.5) does not change the fusion cross section, but defines the spin distribution. Larger DFUS, the higher the spins populated, and this effect may contribute to an increase of the fission cross section and resulting reduction in the evaporation residues.

There are fewer possibilities for nucleon or LI induced reactions as the cross section for fusion (also referred as absorption or reaction) is calculated using the optical model. Users may try different parameterizations available in the RIPL library or internal OMP systematics. If this fails, increasing the imaginary part of the OMP will increase the absorption cross section. However, users are advised that blind modification of the OMP can easily produce physically unrealistic results.

## 12.2 Coupled-Channels (ECIS)

CC calculations are most sensitive to the deformations of collective levels, which can be adjusted by editing the *\*lev.coll* file (see Section 8.9.7). Actually, if the collective levels are selected internally rather than taken from the RIPL library along with the CC optical model potential, these deformations *should* be adjusted. The code sets them by default to the g.s. deformation for the rotational model and to the arbitrarily fixed values for the vibrational model. These values can only be considered as a first guess. Increasing the band deformation for the rotational model or dynamic deformations for the vibrational model results in an increase of the calculated direct cross sections (opposite is true if the deformations are decreased).

Adding more collective levels to the *\*lev.coll* file will generally increase the total direct cross section, and may result in a substantial increase of the cross section to the introduced levels. Generally, the overall effect is not very significant as high energy levels are usually only weakly coupled. Substantial increase of the direct cross section, especially for the highly deformed nuclei, can be achieved by using the CC approach instead of DWBA. As a rule, CC model *should* be the preferred choice in such cases.

Obviously, the cross sections calculated with the CC model are sensitive to the OMP. The effect might be considerable but is difficult to predict due to the large number of parameters involved. Generally, deeper imaginary part of the OMP (especially the imaginary surface component) will result in the higher cross sections.

## 12.3 Multi-step Direct

The microscopic character of the MSD model limits the possibilities of influencing the results compared with the classical models (such as the exciton model). A certain degree of flexibility is provided by the pairing gap parameters (GAPP for protons and GAPN for neutrons). The dependence is non-linear, and it is difficult to predict the impact of any change. MSD results are slightly more sensitive to the EFIT parameters, which define the energies of the collective levels to which response functions for different multipolarities are fitted. Again, due to the non-linearity, the results of the change are hard to predict, the effect has an oscillating character. However, on average, decreasing the EFIT value for a given multi-polarity results in an increase in strength for the  $l$ -transfer under consideration and a higher MSD cross section. We stress again that EMPIRE sets EFIT values internally to the energy of the lowest discrete level which can be coupled to the ground state with a given  $l$  transfer (except  $l = 0$  transfer for which the self-consistent value is taken by default). This assignment might be erroneous if there happens to be a non-collective and low energy level with a suitable spin. In such a case, the EFIT value should be corrected manually by entering the EFIT keyword with the proper energy of the true collective level. Modifications in the EFIT values will generally affect the structure observed in the MSD spectra by shifting maxima to different energies, and the user is advised to try first the self-consistent values for EFIT before attempting any arbitrary modifications.

Substantial increases in the MSD contribution at *forward angles* can be obtained by switching to the compressional form factor for the  $l = 0$  transfer (COMPFF=1). As already mentioned before, this option is physically sound and strongly recommended.

The last resource involves multiplying the response function by an arbitrary factor through the RESNOR entry. Factors larger than 1 will increase MSD cross sections, and values smaller than 1 will reduce it. This procedure has no physical meaning and may eventually lead to the MSD emission being larger than the absorption cross section.

## 12.4 Multi-step Compound

The most significant MSC contribution to the nucleon spectra is located between the Compound Nucleus (low energies) and the MSD contributions (middle-high energies). MSC mechanism accounts for about 20-30% of the total emission at incident energies close to 10 MeV and decreases with the increasing incident energy. Therefore, one should not expect too much from tuning this mechanism. Similarly to MSD, the user's freedom to modify MSC is rather limited. The parameters that have the largest effect are as follows:

- GDIV** Single particle level densities defining particle-hole level densities in MSC set to  $A/13$  by default. Increasing (decreasing) GDIV will result in a higher (lower) MSC cross section. Note that increasing GDIV is justified for nuclei close to the magic numbers, as their level densities are significantly lower.
- TORY** Ratio of the cross sections for unlike and like nucleon-nucleon interaction (e.g.,  $\sigma_{np}/\sigma_{nn}$ ). Can be used for adjusting the relative share between neutron and proton emission. The default value of 4, as derived from the free nucleon scattering, is generally accepted, although some doubts have been expressed as to whether the free scattering value should be applied to the scattering inside nuclear matter. Increasing (decreasing) this parameters will favor (suppress) the charge exchange channel.
- D1FRA** Ratio of the GDR spreading width to the total GDR width (default: 0.8) is relevant to  $\gamma$ -emission only. While there is not much room for increase, decreasing the ratio will also reduce the already low  $\gamma$ -emission through the MSC mechanism.

## 12.5 Level densities

The variety of nuclear level densities available in EMPIRE calls for additional guidance on their use. Only three options are recommended: Empire-specific, Gilbert-Cameron (GC) and HFB; all remaining options (such as Rocol with level density parameter  $a=A/8$ ) are included for comparison but their accuracy is much lower than the three recommendations. The GC level densities, especially when adjusted to known experimental data, may be the most accurate at excitation energies up to the neutron binding and slightly above. However, GC level densities do not lend themselves to extrapolation to higher excitation energies and to nuclei far from the stability line. Energy extrapolation in GC might be dangerous because of the collective effects which are implicitly contained in the level density parameter  $a$ . While this can be an acceptable approximation at low excitation energies for which level densities are fixed by fitting experimental data (discrete levels and neutron resonance spacings), there is no physical justification for extending such a treatment to higher energies. In fact, collective effects, as implicitly accounted for in the GC approach, increase exponentially with excitation energy instead of decreasing and eventually disappearing. In this respect, EMPIRE-specific and microscopic HFB densities behave properly and should be preferred at excitation energies well above neutron binding.

EMPIRE-specific level densities, in addition to explicit treatment of the collective effects and their damping, also include the effects of dynamic deformation, which is induced by the rotation of a nucleus at high spin. This deformation affects level densities through the modification of nuclear moments of inertia. The yrast line is taken into account by setting level densities to zero whenever the thermal energy available for single particle motion is negative. Thermal energy is calculated as the difference between the total excitation energy and the energy needed for rotation. Spin and energy ranges are also formally unlimited

in the EMPIRE-specific level densities. These features make the approach particularly suited for the heavy ion and high-energy nucleon-induced reactions. On the other hand, EMPIRE-specific level densities are fitted to the experimental data in a manner similar to the GC, suggesting that their predictions at low energies should be comparable to those of GC or even better due to the use of the BCS model below critical energy. Therefore, EMPIRE-specific level densities are generally recommended, and are used as a default in the EMPIRE.

However, EMPIRE-specific level densities suffer the same uncertainty as GC when extrapolating from the stability line, because both rely on experimental parameterization of the level density parameter  $a$ , which is only possible for stable or close to stable nuclei. For nuclei far from the stability line, the HFB densities based on realistic schemes of single particle levels offer higher reliability. The physics involved in this approach is clearly superior to the treatment used in the two models discussed above, which makes HFB densities more suitable for extrapolation. In addition, the tabulated values provided by Goriely for RIPL-3 and available in EMPIRE were adjusted to the same experimental data as the other two phenomenological approaches. Therefore, results of the HFB model at low energies should not differ significantly from those provided by the GC or EMPIRE-specific models. Comparisons of cross section calculations for about 300 reactions on targets from  $^{40}\text{Ca}$  to  $^{208}\text{Pb}$  show that microscopic level densities can compete with the phenomenological ones to the extent that makes them the preferred choice far from the stability line. On the other hand, one should keep in mind that tables of level densities are limited to excitation energies below 150 MeV and spins up to  $30\hbar$ , which prevents their use for the Heavy Ion induced reactions well above the Coulomb barrier.

The Hauser-Feshbach results are very sensitive to the level densities, and more precisely to their ratio in the neighboring nuclei. Generally, changing level densities is the most effective way of adjusting cross sections. As mentioned at the beginning of this Section, various formulations of the level densities provided in EMPIRE should be considered with their default parameterization first. Only if this exercise does not produce sensible results should the user attempt to vary the model parameters. The three recommended and most accurate models are (i) EMPIRE-specific, (ii) Gilbert-Cameron, and (iii) HFB. All of them are fitted to match the discrete levels. While the pre-calculated HFB level densities can not be modified, EMPIRE and Gilbert-Cameron offer more significant flexibility. First of all, they are affected by the number of discrete levels in the calculations (it is assumed that cumulative plots had already been checked for consistency using the FITLEV option). Generally, adopting fewer levels increases the level densities between the last discrete level and neutron binding energy, and considering more levels tends to decrease level densities in the same region (see Fig. 10.1 and 10.2). However, this general statement may not hold in cases with strong irregularities in the cumulative plots. Extending the discrete level scheme too far involves a risk of including the region with missing levels which would lead to an unphysical reduction of level densities. The new RIPL library of discrete levels contains estimates of the completeness of the scheme ( $N_{max}$ ), which is used by EMPIRE as a default. These values have been compared with the EMPIRE level densities (i) and (ii) and were found to be compatible in about 75% of cases. The user should decrease  $N_{max}$

in the remaining 25%. If this reduction is insufficient the discrete level region may extend too far. Another extreme involves too few levels, in which there is a risk of fitting level densities to a bunch of collective levels that are shifted toward lower energies because of their collective nature. The resulting level densities might be considerably overestimated.

Changing the level density models and the number of discrete levels may fail, and the user may be forced to adjust the level density parameters themselves. Depending on the model there are different possibilities for explicit adjustment of level density parameters. EMPIRE-specific level densities:  $a$ -parameter is energy and spin dependent, and can not be read as a single input entry. However, there is a possibility of applying a factor (ATILNO) to the asymptotic value of the  $a$ -parameter, which is equivalent to multiplying each  $a$ -parameter (larger  $a$  values correspond to larger level densities). There are no other parameters in the EMPIRE-specific level densities that can be controlled from the input. The Gilbert-Cameron level densities offer more flexibility: all of the parameters can be specified in the input file. However, it is a responsibility of the user to ensure that these parameters are internally consistent (i.e., fulfill matching conditions and fit discrete levels). A much safer approach involves the introduction of the  $a$ -parameter and one other ( $U_x$ ,  $E_o$ , and  $T$ ), and allows the code to take care of the internal consistency. As usual, level densities increase with  $a$ -parameter. The constant temperature component (low energy) of the level densities increases with decreasing  $T$  and  $E_o$ , and higher values of  $U_x$  correspond to higher level densities. Finally, within the Gilbert-Cameron approach coded in EMPIRE, there are three built in systematics for  $a$ , that can be selected with the GCROA keyword:

**GCROA**        = 0 Ignatyuk systematics,  
                   = -1 Arthur systematics,  
                   = -2 Ilijnov systematics (default).

## 12.6 Fission

Fission can be scaled quite effectively with a number of parameters, especially in the HI induced reactions. The reduced dissipation coefficient  $\beta_v$  is controlled by the keyword BETAV, and decreases the fission channel when moved further out from the 3.2 value (corresponding to  $\beta_v = 3.2 \cdot 10^{-21} \text{ s}^{-1}$ ), separating the under-damped and over-damped motion. All remaining input parameters affect directly (e.g., QFIS) or indirectly the height of the fission barrier, and can be divided into those that control shell correction damping with spin and temperature and those that modify the fission barrier by adding a Gaussian centered at a certain spin. All of them are listed below:

**QFIS**        Liquid drop fission barrier multiplier. QFIS > 1 decreases fission channel.

**SHRJ**        Shell correction to fission barrier is damped to 1/2 (Eq. 4.180) at the spin defined by SHRJ. For negative shell corrections, lowering SHRJ will increase the fission channel, at least at sufficiently high incident energies. Opposite is true for positive shell corrections.

<b>SHRD</b>	Diffuseness of the shell correction damping (Eq. 4.180). The size and sign of the effect depend on the actual spin population of the fissioning nucleus.
<b>TEMP0</b>	Temperature at which temperature-damping of the shell correction (Eq. 4.179) starts to be effective. Increasing (decreasing) this value will decrease (increase) fission above the temperature defined as $\min(\text{TEMP0}, 1.65)$ (1.65 is the default value) and will have no effect on the fission cross sections at incident energies corresponding to lower temperatures.
<b>SHRT</b>	Multiplier in the exponent of the temperature-damping of the shell correction (Eq. 4.179). Increasing this parameter will increase fission above the temperature selected with TEMP0 (no change below).
<b>DEFGA</b>	Amplitude of the Gaussian term defined by Eq. 4.180. Setting to a positive value will increase fission barrier and therefore decrease fission channel, but only if the states with spins within the range defined below by DEFGW and DEFGP are populated. On the contrary, a negative value will increase the fission cross section. The Gaussian term is used to simulate irregularities in the shell correction related to the incidental bunching or de-bunching of single particle levels due to the rotation-induced change in nuclear deformation. Generally, the effect will only be observed in the limited range of incident energies.
<b>DEFGW</b>	$\Delta J_G$ (width in spin) in the Gaussian (term of Eq. 4.180). Increasing DEFGW will magnify the effect described above and enlarge the range of incident energies being affected.
<b>DEFGP</b>	$J_G$ (spin position) of the Gaussian (term Eq. 4.180). The value of DEFGP defines the mean value of the incident energy range affected by the Gaussian term, which increases with DEFGP. Setting this parameter above the maximum spin for nucleus stability reduces or even eliminates the effect.

## 12.7 GDR parameters ( $\gamma$ -ray strength functions)

The EMPIRE input file provides the user with a full control of the GDR parameters. This possibility might be worth trying as the present version of the code makes use of the built-in systematics by default. This systematic approach is usually reasonable for nuclei with  $A > 100$ , but for lighter nuclei the experimental data show less regular behavior. GDR widths are particularly widely scattered and their deviation from systematics may reach 3 MeV. Also, peak cross sections for nuclei with  $A > 225$  can differ from the systematics by as much as 100 mb. The experimental values for the GDR parameters can be found in RIPL-2. Other multiplicities can also be modified by entering them explicitly in the input file but their effect on the cross sections is rather small.



The overall increase of the  $\gamma$ -ray strength function can be obtained by increasing the GDR peak cross sections (CSGDR1 and CSGDR2). Increase of the low energy part of the strength function (usually most important for the capture cross sections) can be attained by lowering the positions of the GDR peaks (EGDR1 and EGDR2), especially the lower one (EGDR1). Another effective method leading to a similar result involves increasing the GDR widths (again the lower one is more significant). Opposite actions will reduce the  $\gamma$ -ray strength function. If the dynamic option is selected (i.e., GDR parameters depend on angular momentum and temperature), shifts with respect to the calculated values can be introduced in place of the explicit values of the parameters. These shifts are coded in the input file under keywords: GDRWA1, GDRWA2, GDRESH, GDRSPL, GDRST1, and GDRST1.

Additionally, the mixing of Weiskopf model and Giant Resonance Model are defined by MIXGDR (E1), MIXGQR (E2) and MIXGMR (M1) parameters for multipolarities quoted in parentheses. Default values of these parameters are 1, meaning that a pure GR model is assumed (Weiskopf contribution is zero).

Drastic changes of the default GDR parameters are likely to be unphysical. Thus, the product of the peak cross section and GDR width is constrained by the sum rule, and users should ensure that the inputted values respect this limitation.

## 12.8 Avoiding unreasonably low uncertainties

Quite often, Kalman filter analysis involving a vast amount of experimental data results in uncertainties that are far lower than systematic uncertainties even of the most precise measurement. This happens in spite of the fact that proper experimental covariances, accounting for systematic uncertainties, are supplied as an input to the KALMAN code. This issue rises serious concern and puts the validity of the approach in question. Therefore, it is important to understand the origin of low uncertainties in order to judge how far they can be trusted and how they can eventually be avoided.

One of the sources of the problem is the implicit Kalman filter assumption that the model itself is perfect. Thus, any uncertainties in model calculations are only due to the uncertainties of the model parameters. Often, the shape of a calculated excitation function is constrained. , *i.e.*, even with a substantial variation of model parameters it is not possible to alter the shape or the absolute value of the function in an arbitrary fashion. We illustrate this point on the example of the  $^{93}\text{Nb}(n,\text{tot})$  reaction in Fig. 12.4. The depth and radius of the real part of the optical model potential are essentially determining the shape and magnitude of the total cross section. The two quantities are known to be strongly correlated, therefore it is sufficient to consider only one of them. In Fig. 12.4 we show the change of total cross section in response to the variation of the real potential depth by 5%. One observes that this does not provide for scaling of the absolute value of the cross section. Such scaling is actually the degree of freedom that would be needed to accommodate systematic uncertainties in the measurements that in most cases amount to scaling cross sections up and down without changing its shape. Lack of this possibility



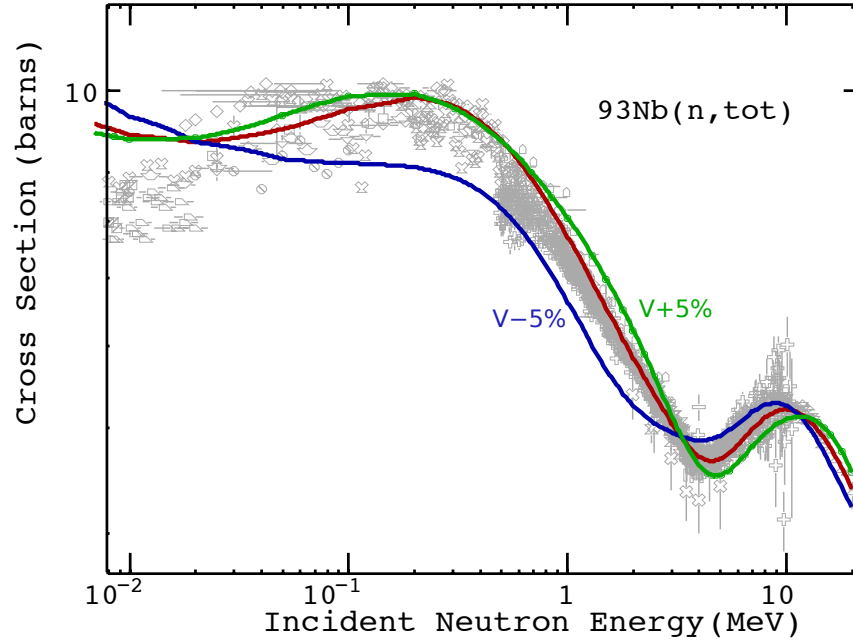


Figure 12.4: Effect of 5% variation of the depth of the real optical potential on the  $^{93}\text{Nb}(n,\text{tot})$  cross section. The baseline values are in red.

might have a dramatic effect on parameter uncertainties - any scaling of the cross section appears incompatible with the model calculations since it can not be reproduced by any sensible variation of the model parameters. If the model were perfect we would have to conclude that the systematic experimental uncertainties are overestimated. To avoid such a reduction we introduce intrinsic model uncertainty by defining a fictitious model parameter,  $p_{\text{mod}}$ , that multiplies model predicted cross sections. The prior value of this parameter is one.

Our preliminary studies indicate that the Kalman filter adjusts the uncertainty of the fictitious model parameter,  $\Delta p_{\text{mod}}$ , to reproduce the smallest systematic uncertainty. Thus, if the whole energy range is adequately covered by the experimental data the final result is well-defined. In the energy ranges without measurements the result, to some extent, depends on the initial (assumed) uncertainty of the new parameter,  $\Delta p_{\text{mod}}$ . Naturally, if no experimental data are available the discussed contribution to the uncertainty is defined by  $\Delta p_{\text{mod}}$ . In such a case, however, the cross section uncertainties are determined primarily by the propagation of uncertainties of the genuine model parameters, which are much larger than the intrinsic model uncertainties. The latter can, therefore, be neglected especially since there should be no uncertainties small enough to raise any concern. The procedure is particularly useful to simulate intrinsic uncertainties in the optical model, *i.e.*, it is meant to be applied to the total cross sections. These are often very well measured which, combined with the rigid shape of the optical model predictions, results in extremely low uncertainties. There is no need to invoke such a procedure for other nuclear reaction models, *e.g.*, compound nucleus and preequilibrium emission, since their formulations

include parameters which, to a large extent, provide for a scaling degree of freedom.

An additional source of low uncertainties has been discussed in the contribution by Leeb [149] to the present Workshop - neglecting correlations among numerous experiments implies statistical independence of the respective systematic uncertainties and leads to reducing final uncertainty below individual systematic uncertainty. We refer to the original paper by Leeb for a description of an approximate method allowing one to avoid this source of underestimation.

# Chapter 13

## Parameter fitting

### 13.1 Fitting Optical Model Parameters

When the FITOMP option is selected in the input, EMPIRE will perform automatic fitting of parameters in the direct optical model parameter file, OMPAR.DIR (*\*-omp.dir*), and of deformation parameters in the file containing the collective target levels, TARGET\_COLL.DAT (*\*-lev.col*). The fitting procedure also uses the experimental data file in C4 format, C4.dat (*\*.c4*). To ensure the existence of these files, EMPIRE should be executed at least once before fitting begins and should be executed with the DIRECT option selected and an incident channel optical potential (initially) defined using the DIRPOT option, both in the initial run and during fitting. At the moment, the FITOMP option only works for neutron or proton scattering.

All data relevant to an optical model fit - total, elastic and collective inelastic cross sections and elastic and collective inelastic angular distributions - within the requested energy range are selected from the C4.dat file and included in the  $\chi^2$  to be minimized. The data points in the  $\chi^2$  are weighted in the standard manner using the experimental uncertainties given in the C4.dat file. Natural element data can be inserted in the C4.dat file and used in the fit. In the case of neutron scattering, the file *empire/RIPL/resonances/resonances0.dat* is also searched for an s-wave strength function, which is included in the experimental data set when found.

The lower limit of the energy range for calculations used in a fit is initially taken to be 1 keV while the upper limit is taken to be 30 MeV, unless modified using the FITEMX option in the input. All relevant experimental data within this range in the C4.dat are included in the  $\chi^2$ . The incident energies given in the input file define the grid of energies used for calculations, unless the FITGRD option is used. When the input file energies are used, the data points outside of the energy interval they define are not taken into account. That is, the fitting procedure will interpolate calculations but will not extrapolate them. When the FITGRD option is used, the energy interval is extended to include all data points in the initial energy range. In both cases, the grid of incident energies is compared with those of the experimental data and superfluous values are eliminated to speed up the

calculation.

The parameters to be adjusted are specified by using the FITabc or FITDEF options, described in more detail below. The RIPL parametrization described in Refs. [35, 145] is used to identify the optical model parameters, any of which may be adjusted. The adjustable deformations are simply those of the collective level file. Quadrupole and hexadecapole deformations are permitted for nuclei identified as rotational, while quadrupole and octapole dynamical deformations are permitted for those identified as vibrational. The FITabc and FITDEF options typically identify the desired parameter and furnish a shift in its initial value and the maximum variation allowed during the fit with respect to its (shifted) initial value. If no parameter adjustment is requested or all adjustable (possibly shifted) parameters have a maximum allowed variation of zero, the  $\chi^2$  is calculated but no fitting is performed. At most 20 parameters may be shifted and/or adjusted simultaneously.

At present, the optical model fitting is performed using a simple numerical gradient search to minimize the  $\chi^2$ . The adjusted parameters are stored in the modified OM-PAR.DIR (*\*-omp.dir*) and TARGET\_COLL.DAT (*\*-lev.col*) files. Information on the fit is written in the FIT.OUT (*\*-ompfit.lst*) file. When a fit is complete, EMPIRE is run one last time with all options and energies given in the input file, excepting the fit ones.

## 13.2 Using Kalman filter for parameter fitting

The multi-parameter, linearly fitting code KALMAN has proven to be very useful in improving evaluation procedure. Starting from an initial input, KALMAN is able to determine an “optimal” set of parameters that minimizes the overall  $\chi^2$ . In order to do this, KALMAN varies the values of a given set of parameters and analyzes the effects produced in the cross sections.

Below, when describing filenames and instructions for the command line, the string ‘\*’ was adopted to correspond to the main project name, that is, the root of EMPIRE’s input filename (the filename without the extension ‘.inp’)

The Kalman utility within the Empire package was initially developed with the purpose of fitting only cross sections. However, the KALMAN code itself is completely oblivious to what quantity it is fitting since it simply receives as inputs only the experimental data sets for which the  $\chi^2$  will be minimized, the original functions before the fit, the parameters that modify each function and their sensitivities. It is thus the role of the auxiliary codes and of the *kalman* script to manipulate the information given by EMPIRE and write them in the appropriate format for the KALMAN code. Having this in mind, the Kalman utility was generalized in order to be able to also fit prompt fission neutron spectra (PFNS). Four PFNS-specific parameters were introduced into EMPIRE code: PFNTKE, PFNALP, PFNRAT, and PFNERE (see section 4.4.3). Each incident energy produces a spectrum that is a function of the neutron outgoing energy. In order to accommodate bi-dimensional fits, such as that involved with PFNS, the whole Kalman process had to be modified. In the descriptions below the differences and similarities in format, structure and processing between fitting cross sections and PFNS will be detailed.

We note that EMPIRE-KALMAN system is a general and powerful tool for evaluation of nuclear reactions. In addition to covariance calculations it may also be used to adjust model parameters to reproduce experimental cross sections and other observables within the selected reaction models and initial uncertainties of model parameters. Therefore, the Kalman filter can be used throughout the whole evaluation procedure to ensure consistency between cross sections, model parameters, and related covariance matrices.

The evaluator may choose to perform a sequential update using experimental data for several/all reactions or just for a single one. In the former case, all considered reactions are correlated and unique set of parameters along with the related covariance matrix are produced. On the other hand, poor experimental data in one reaction channel can negatively influence predictions for other channels.

### 13.2.1 Calculation of sensitivity matrices

The sensitivity matrix file ('\*-mat.sen' for cross sections, '\*-pfns-full-mat.sen') for PFNS, may be obtained through two different manners: using one of Empire's own sub-routines; or using a python script to break the calculation into smaller parts and submit them to be run in parallel. Both methods follow the same concept and they are described in the following subsections. Actually, the sensitivity contained in those files is not the true sensitivity, but rather the so-called *realistic sensitivity*, which is the true sensitivity divided by the central value and multiplied by twice the interval of variation. The reason for this is that the realistic sensitivity provides much more information regarding the relative importance of the parameters.

#### Sequential calculations

By setting input parameter KALMAN to the value of 1 in EMPIRE's input, instead of performing a regular run of EMPIRE calculations, it will read the sensitivity input file in order to calculate the sensitivity matrices. This is very useful for simple fits and when access only to a sequential machine is available. However, when fitting more than just a few parameters, the sequential approach may take a prohibitive amount of time to conclude the calculation. As additional limitations, EMPIRE's sensitivity routines have not yet been prepared to generate sensitivity matrices for PFNS and for a certain class of cross-section parameters. For these reasons, it is advised for the user to perform parallel calculations instead, in order to generate sensitivity matrix files.

#### Parallel calculations (*sensitivity.py* python script)

One may use the *sensitivity.py* script, present in the 'empire/empy/qsubEmpire' directory, to generate sensitivity-matrix file. This method splits the full calculation into single energy runs, submitting each incident energy for execution by a different processor node, shortening dramatically the total execution time. Firstly, it creates a directory, named '\*\_orig/',

to where all the original input files are copied, for the calculation of the cross sections corresponding to central values of the parameters. Afterwards, the script reads the sensitivity input file to determine which parameters are going to be varied. Then, for each parameter, it creates two directories with names of the form ‘\*\_keyword\_I1\_I2\_I3\_I4plus/’ and ‘\*\_keyword\_I1\_I2\_I3\_I4minus/’, where *keyword* is the parameter name, and *I1-I4* are the four parameter options. All input files are also copied to those directories. However, in each directory, the input file is modified by changing the value of the parameter corresponding to the directory name. If the directory has the suffix ‘plus’ then the relative increment defined in the sensitivity input is added to the original parameter value. Likewise, for the directories with the suffix ‘minus’, then the same relative increment is subtracted from the original parameter value. Inside each of those directories, the script *qsubEmpire.py*, located in ‘empy/qsubEmpire/’ directory, is called. It then splits each run into separate directories with the same input parameters but containing only one value of incoming energy, and finally submits each of those as different jobs to different CPU’s for calculation.

The *sensitivity.py* script has basically five execution options:

- **-i**: Initializes the inputs and prepare to run. Executing with this option simply creates the ‘\*\_orig/’ directory and all the parameter directories described above. However, *qsubEmpire.py* script is not called, so the jobs are not submitted.
- **-r**: Calls *qsubEmpire.py* script to submit jobs for running. This option should only be executed after previous initialization (**-i**)
- **-a** or **-analyze**: After running (option **-r**), this option may be used to gather all the cross-section information from files ‘\*.xsc’ in the different directories that were created and calculate the sensitivity matrix, creating the sensitivity matrix file ‘\*-mat.sen’.
- **-p** or **-pfns**: After running (option **-r**), this option may be used to reorganize and gather all the PFNS information from files ‘\*-pfns.out’ in the different directories that were created and calculate the PFNS sensitivity matrix, creating the PFNS sensitivity matrix file ‘\*-pfns-full-mat.sen’.
- **-c** or **-clean**: This option is used to delete all the auxiliary directories that might have been created by a previous initialization or run of *sensitivity.py*

If executing *sensitivity.py* without specifying any options, it assumes options **-i** and, sequentially, **-r**. There are some examples of the option usage below:

```
$EMPIREDIR/empy/qsubEmpire/sensitivity.py u235 -i
$EMPIREDIR/empy/qsubEmpire/sensitivity.py u235 -r
$EMPIREDIR/empy/qsubEmpire/sensitivity.py u235
(this is equivalent of executing, in order, both commands above)
$EMPIREDIR/empy/qsubEmpire/sensitivity.py u235 -a
$EMPIREDIR/empy/qsubEmpire/sensitivity.py u235 -c
```

### 13.2.2 Kalman script

For KALMAN to run properly, its inputs (sensitivities, experimental data to be fitted, list of parameters, central values for cross sections and parameters, etc.) must be found in the appropriate files and in the expected format. Preparing those files manually for each run of KALMAN may prove to be a cumbersome and prone-to-error task. For this reason, it is convenient to use the *kalman* script, from the ‘**scripts**’ directory. This script connects the different ingredients needed for the fit and organizes the results in a clear way, with the help of auxiliary codes.

The *kalman* script is called in a very simple manner by providing values for a set of variables in the command line, right after the script call. These variables are referred in the script as **file**, **MT**, **MAT**, **EXPDAT**, **PFNS**, and **EINC**, in this order. The first option corresponds to the project name, that is, EMPIRE’s regular input file name without the extension ‘.inp’. The second option is the MT number that should be fitted by KALMAN. The next string corresponds to the material number (**MAT**) of the target. The variable **EXPDAT** defines which experimental sets will be used in the fit, by assuming the values 0, 1, or 2. **EXPDAT**=0 implies that all experimental data will be ignored (no fit); **EXPDAT**=1 indicates that only experimental data for the selected MT will be considered; while **EXPDAT**=2 informs the KALMAN code that agreement to all experimental data available in the c4 file should be considered for fitting. At this point, it is relevant to state that, when **EXPDAT**=2, the data agreement of the cross section (or **PFNS**) for a given reaction (or incident energy) may not improve, or may even get worse after the fitting. This is due to the fact that the overall  $\chi^2$  is being minimized and worsening of agreement with data for a given reaction (or incident energy) is likely being compensated by improvement of the agreement for all other reactions (or incident energies). When **PFNS** has value 0 (default), KALMAN will fit only cross sections, while when **PFNS**=1 it will fit prompt fission neutron spectra (**PFNS**). When **PFNS**=1, the variable **EINC** corresponds to the incident energy for which **PFNS** will be fitted. The options **PFNS** and **EINC** may be omitted when fitting cross sections since they serve only to fit **PFNS**. For the time being, these fits are independent and there is no correlation between cross sections and **PFNS**.

Examples of valid calls of *kalman* script:

```
kalman pu239 18 9437 2
```

```
kalman u235 18 9228 2 1 2.53E-8
```

In order to run properly, KALMAN needs to find a list of files in the working directory, otherwise it will abort and print an error message. Those files are: the ENDF file (\***.endf**’), the sensitivity input file (\***-inp.sen**’), the sensitivity matrix file (\***-mat.sen**’), and the EMPIRE’s cross section file (\***.xsc**’). If fitting **PFNS** instead of cross sections, the last two files aforementioned are not necessary. However, KALMAN will then need the content of files ‘\***-pfns.out**’ and ‘\***-pfns-full-mat.sen**’.

After finishing running, the *kalman* script creates several output files containing important information regarding the fits. Such files, with a brief the description, are listed below:

- ‘\*-out.kal’: Standard output from KALMAN. Contains information about the data sets used for fitting, the  $\chi^2$  obtained, the final values for the fitted parameters and their corresponding uncertainties, and the correlation between parameters.
- ‘\*-expcorr.kal’: Provides the fraction of the experimental uncertainty that corresponds to systematical errors for each data set. This file is initially generated by the code ‘genkal’, as file ‘fort.12’, having the default value of 0.200 for all experiments.
- ‘\*-MT-err.kal’, where *MT* corresponds to the same script variable *MT* which was selected in the command line: Contains the covariances and uncertainties of the fitted curve.
- ‘\*-par.kal’: Model parameter correlations
- ‘\*-xsc.kal’: Final curves found by KALMAN for all reactions (or incident energies, in the PFNS case)
- ‘\*-cov.kal’: Contains the uncertainties (in units of %) and correlations for all incident (or outgoing in the PFNS case) energies.
- ‘\*-expxsc.kal’: Contains the experimental data used in the fit.
- ‘\*-parcorr.kal’: Contains a list of the varied parameters, with their initial values (usually set to 1.0) and ranges of variation. Additionally, it also contains, correlation matrix for the parameters, which is usually diagonal in the first default calculation. This matrix might be changed or updated if the parameter correlation matrix is known. Then, true sensitivity matrices for each reaction (or each incident energy, in the PFNS case) are printed.
- ‘\*-pfns.kal’: File containing the PFNS for the fitted incident energies.
- ‘\*-MT-cov.gpd’, where *MT* corresponds to the same script variable *MT* which was selected in the command line: File to plot a three-dimensional graph of the covariances using *gnuplot*
- ‘\*-MT-c4.gpd’, where *MT* corresponds to the same script variable *MT* which was selected in the command line: File that contains the experimental data for the reaction corresponding to the *MT* number used in the KALMAN fit. May be plotted together with ‘\*-MT-xsc.gpd’ using ‘*gnuplot*’.
- ‘\*-PFNS-INDEX-c4.gpd’: File that contains the pfns experimental data for the incident energy corresponding to the index *INDEX*, as listed in file ‘\*-pfns.kal’. May be plotted using ‘*gnuplot*’.
- ‘\*-MT-xsc.gpd’, where *MT* corresponds to the same script variable *MT* which was selected in the command line: Contains both the curves before and after the KALMAN fit. It may be plotted together with ‘\*-MT-c4.gpd’ using *gnuplot*.



Plots of the fit can be made using the information contained in files `*.gpd` with the help of the widely-available plotting tool `gnuplot`. Plots of the parameter correlations resulting from the KALMAN fits can be made with `util/kalman/corr.gp`; correlations of the PFNS parameters with `util/kalman/corr-pfns.gp`. This plotting process is described in Section 13.2.2.

## Experimental Data

For fitting either cross sections or PFNS, KALMAN needs access to the experimental data so it can calculate and compare the  $\chi^2$  at each point. The codes `c4tokal` and `pnt2kal` read experimental data in computational format (c4 files) and write in a way that is understandable by the KALMAN code. The former process cross section data while the latter PFNS data.

**Handling Cross-Section Experimental Data - `c4tokal`.** The code `c4tokal` reads the cross-section experimental data from the file `*-kal.c4`, if it exists. Otherwise, it looks for the existence of file `*.c4`. The reason for the additional `*-kal.c4` file is that it is common, during the fitting process, that one might want to exclude data points or even whole data sets from the fit. This way the user can edit the file `*-kal.c4` while keeping the original and more complete `*.c4` unaltered.

EMPIRE's cross-section file `*.xsc` is read by `c4tokal` only to determine the number of different reactions printed out by Empire and their corresponding nomenclature. In addition, the sensitivity input file `*-inp.sen` is read to obtain the number of parameters to be varied in the fit.

After gathering all this information, `c4tokal` creates a series of output files, which will be read by KALMAN. Below is a brief description of each of those files:

- **fort.75:** contains data points, their absolute errors, and the MT number
- **fort.10:** contains only the data points
- **fort.11:** contains only relative errors for each energy
- **fort.12:** contains correlations between different experiments
- **KALMAN.INP:** automatically-generated input for the main KALMAN fitting code

**Handling PFNS Experimental Data - `pnt2kal`.** When compared to cross-section fitting, preparing PFNS experimental data require additional steps due to the fact that PFNS is usually presented after normalization to Maxwellian. This normalization is often done because PFNS vary largely across the values of outgoing energy. Since the value of the temperature used in the Maxwellian normalization ( $T_{maxw}$ ) is relatively arbitrary, different  $T_{maxw}$  may be used to focus on different parts of the spectra.

Instead of calling ‘`c4tokal`’, `kalman` script calls the code `pnt2kal` when fitting PFNS. This code reads the normalized PFNS experimental data from an existing ‘`*.pnt`’ file and converts it to the input format needed by KALMAN. If this file does not exist, ‘`pnt2kal`’ runs the code LSTTAB to read the PFNS data from the ‘`*.c4`’ file and generate the corresponding normalized ‘`*.pnt`’ file. In this case, the code PLOTLST is initially called to identify the index of the PFNS data in the `c4` file (with output sent to file ‘`output.plotlst`’). Then, the Maxwellian temperature  $T_{maxw}$ , to which the data will be normalized, is read from EMPIRE’s PFNS output file, ‘`*-pfns.out`’. With that value, an input file for LSTTAB, ‘`input.lsttab`’, is written. The files ‘`*-log.plotc4`’, ‘`*.c4`’, and ‘`*-s.endf`’, together with the value of  $T_{maxw}$ , read from ‘`*-pfns.out`’ are necessary to run LSTTAB. When LSTTAB is called by ‘`pnt2kal`’, its standard output is written in the file ‘`output.lsttab`’ and the standard pnt file ‘`LSTTAB.PNT`’ is renamed to ‘`*.pnt`’.

When the ‘`*.pnt`’ is ready, the PFNS data and all its relevant information are read at once and stored in a structured variable. From this, the values of incident energies ( $E_{inc}$ ) for which there are available data are extracted. Those values are compared to the ones used for the original Empire calculation of the PFNS, to check if PFNS were calculated at all incident energies found in the experimental ‘`*.pnt`’ file. If not, ‘`pnt2kal`’ aborts since it makes no sense to fit data without the initial calculation of its central values. In this case, an error message is printed with all the values of  $E_{inc}$  and indicating which matches could be found in the PFNS output from EMPIRE.

An important difference between integrating cross-section and PFNS fitting with EMPIRE is that, in the former case, the initial central values are already in an easily-readable format in the file ‘`*.xsc`’, with the cross sections for each  $E_{inc}$  in subsequent rows, and with the different reactions distributed in columns. In the PFNS case, however, the spectra are printed as sequential blocks for the different incident energies, with each block containing the distribution as a function of the outgoing energy. For KALMAN to be able to fit PFNS properly, the spectra have to be rewritten in a format similar to that of the cross sections in the file ‘`*.xsc`’. The code ‘`pnt2kal`’ does that by reading the spectra from file ‘`*-pfns.out`’ and writing them in a reformatted file, with name ‘`*-pfns.fmt`’. In this new file the PFNS are written as function of the outgoing energy, with the different  $E_{inc}$  distributed in columns. This way, we have the correspondence expressed in Table 13.1

Table 13.1: Correspondence between cross-section and PFNS files

Quantity	cross sections	PFNS
File extension	‘ <code>.xsc</code> ’	‘ <code>-pfns.fmt</code> ’
Rows	incident energy	outgoing energy
Columns	reaction	incident energy

As mentioned, the file ‘`*-pfns.fmt`’ contains the PFNS at all incident energies calculated by EMPIRE. However, it is only necessary to provide to KALMAN those spectra at the same incident energies for which there are experimental data available in the ‘`*.pnt`’

file. For this reason, `pnt2kal` reads `*-pfns.fmt` and rewrites it in file `*-pfns.kal`, keeping only the columns corresponding to  $E_{inc}$  found in `*.pnt`. This trimming process is also done to the original PFNS sensitivity file, `*-pfns-full-mat.sen`, with the outcome being printed in the file `*-pfns-mat.sen`. For doing this, the number of parameters is retrieved from the sensitivity input file `*-inp.sen`.

Finally, `pnt2kal` creates and writes to files `fort.75`, `fort.10`, `fort.11`, `fort.12`, and `KALMAN.INP`. The contents of those files are the same as in the case of cross-section fitting (section 13.2.2), with the corresponding substitutions expressed in Table 13.1. In addition to those files, `pnt2kal` also writes to a temporary file, named `ENERGYANDINDEX.TMP`, that contains some information needed later on by the *kalman* script, such as number of incident energies, and index and value of  $E_{inc}$  to be fitted. This file is deleted at the end of *kalman* script.

### Central Values - genkal

The `genkal` code converts the cross sections and sensitivities for all reactions into the format needed by the KALMAN code. The cross sections are read from file `*.xsc` and are rewritten in file `fort.50` in such a way to present the central values for the cross sections as sequential blocks, each block corresponding to one of the reactions. The sensitivity matrices are read from `*-mat.sen` and rewritten into file `fort.52`. The initial intervals within each parameter may be varied by KALMAN are also written in the file `fort.52`.

The central values and sensitivities in the case of PFNS fitting are converted to KALMAN format by the same code `genkal` that does that for cross sections. File `fort.50` is written after reading the central spectra from file `*-pfns.kal`. It will have the PFNS rewritten as sequential blocks, with each block now corresponding to the spectrum distribution for each incident energy. The PFNS sensitivity matrix will be read from file `*-pfns-mat.sen` and stored again in the file `fort.52`. As in the cross section case, the relative intervals for parameter variation will also be written in `fort.52`.

In both cross-section and PFNS cases, `fort.52` is renamed to `*-parcorr.kal` if such file does not exist beforehand. If file `*-parcorr.kal` exists, then it is copied over `fort.52` so, following the general EMPIRE policy, the existing version is used rather than the newly-generated one. The reason for this is that, after a given run of Kalman, a user might want to edit this file in order to modify some values, such as the range of variation for a given parameter.

### KALMAN code

If `genkal` and `c4tokal` (or `pnt2kal`, in the PFNS case) have run properly, then all the files needed for KALMAN to run will be ready. However, before executing KALMAN, the *kalman* script checks if the files `*-expxsc.kal`, `*-expcorr.kal`, and `*-parcorr.kal` exist. If so, the script renames them in such a way that the fitting code will use the existing files instead of the newly-generated ones. As mentioned above, this allows the user to manually modify those files according to specific needs, between two consecutive

runs of KALMAN.

Afterwards, the *kalman* script opens the standard KALMAN input file, `KALMAN.INP`, previously created by either `'c4tokal'` or `'pnt2kal'`, using a text editor. At this point, the user may choose to edit this file to modify the default options before the actual run. Once the user is satisfied with the input file, should save it and close the editor window. This will trigger execution of the KALMAN code and start the actual fitting process.

### Post-KALMAN processing

After the KALMAN code completed fitting the experimental data sets and has found an optimal set of parameters that minimizes the  $\chi^2$ , the *kalman* script does a few more operations. Firstly, it renames the output files generated by KALMAN `'fort.13'`, `'fort.14'`, and `'fort.15'` into `'*-xsc.kal'`, `'*-cov.kal'`, and `'*-par.kal'`, respectively. Secondly, it calls the code `'kalend'` which reads the KALMAN-generated covariance and writes it in the ENDF-6 format into file `'*-MT-err.kal'`. Additionally, it also creates the files `'corrplot.d'` and `'xscplot.d'`, for plotting.

Finally, before finishing, *kalman* script uses `gnuplot` to plot the calculated covariances and pre- and post-fit curves to compare with experimental data. To do this, it uses the `gnuplot`-instruction file `'util/kalman/corr.gp'` (`'util/kalman/corr-pfns.gp'`, in the case of fitting PFNS). Both files `'corr.gp'` and `'corr-pfns.gp'` are set to plot the covariances directly from file `'corrplot.d'`. The curves before and after fitting are set to be taken from file `'xscplot.d'`, for either cross-section or PFNS calculations. Both files `'corrplot.d'` and `'xscplot.d'` are directly generated by `'kalend'`. The file containing the experimental data for plotting (`'*-MT-c4.gpd'` for cross sections, or when plotting PFNS, `'*-PFNS-INDEX-c4.gpd'`) was previously generated either by `'c4tokal'` (in the case of cross sections) or by `'pnt2kal'` (in the PFNS case). However, both `'corr.gp'` and `'corr-pfns.gp'` are set to take the experimental data from file `'expxscplot.d'`. Therefore, right before calling `'gnuplot'`, *kalman* script copies file `'*-MT-c4.gpd'` (or `'*-PFNS-INDEX-c4.gpd'`, depending to which quantity has been fitted) to file `'expxscplot.d'`.

Once the `'gnuplot'` command is executed, the three-dimensional graph of the covariance should be plotted. Figure 13.1 shows examples of such graphs for the case of fission (top panel) and capture (bottom panel) of neutrons incident on  $^{235}\text{U}$ . After the user closes the covariance-graph window and hits enter on the terminal, the graph of prior- and post-KALMAN fitting curves is plotted. Figure 13.2 shows the agreements with fission (top panel) and capture (bottom panel) experimental data of the calculated cross sections before (blue curve) and after (green curve) the fit.

It is important to mention that this post-fitting calculation does not necessarily correspond to the exact result that one should get when the new values of the parameters are put back into EMPIRE's input file for a new run of EMPIRE. This happens because the Kalman filter is a linear fitting code, which means that, the effect of perturbing a given parameter will be calculated by linearly interpolating (or extrapolating) the sensitivity matrix. Hence the importance of choosing wisely the intervals of variation, both when obtaining the sensitivity matrix and when editing `'*-parcorr.kal'` to avoid falling out of

the linearity regime. The final effect of fitting parameters through KALMAN will thus only be known after the new parameter values are put back into EMPIRE's input file and new cross sections or PFNS are calculated.

### 13.2.3 Fitting example: $^{235}\text{U}$

As an example, we present below the entire process of generating the central values, sensitivities, and KALMAN fits, with a complete set of commands, for the target material  $^{235}\text{U}$ .

Once EMPIRE's initial input files have been defined and assuming EMPIRE's main input file is named as 'u235.inp', one can run EMPIRE, generate ENDF-6 formatted file, and process it for plotting by issuing the following commands:

```
$EMPIREDIR/scripts/runE u235
$EMPIREDIR/scripts/format u235 9228
$EMPIREDIR/scripts/process u235
```

or, alternatively:

```
$EMPIREDIR/scripts/run u235 9228
```

In order to calculate sensitivities, the sensitivity input file 'u235-inp.sen' must be created, containing the list of parameters to be varied. This file may contain both cross-section and PFNS parameters. Since, at the time being, those fits are independent and uncorrelated, the cross-section sensitivity file ('u235-mat.sen') will contain zero sensitivities for the PFNS parameters and, likewise, the PFNS sensitivity file ('u235-pfns-full-mat.sen') will contain vanishing sensitivities for the cross-section parameters. To calculate the sensitivities and generate the sensitivity matrix files for both cross sections and PFNS one may use the commands:

```
$EMPIREDIR/empy/qsubEmpire/sensitivity.py u235
$EMPIREDIR/empy/qsubEmpire/sensitivity.py u235 -a
$EMPIREDIR/empy/qsubEmpire/sensitivity.py u235 -p
```

At this stage, all the files needed to start the fitting process have been generated. If the user chooses to fit cross sections taking into consideration experimental data for all reactions available in the c4 file ('u235.c4'), and wishes to see the correlation and prior/post-fit graphs for fission reaction, for example, he/she may use the command:

```
kalman u235 18 9228 2
```

The result of this KALMAN run is shown in Figures 13.1 and 13.2, top pannels. If, however, the user chooses instead to see the KALMAN predictions for capture, the following command may be used:

```
kalman u235 102
```

Figures 13.1 and 13.2, bottom panels, show the results of this run.

To fit PFNS experimental data for all incident energies contained in the c4 file ('u235.c4'), but to plot the KALMAN predictions for thermal energy, one may use the command:

```
kalman u235 18 9228 2 1 2.53E-8
```

After the final parameters, which may be found in this case in file 'u235-out.kal', are put back into EMPIRE's main input file, 'u235.inp', EMPIRE may be executed again with command:

```
$EMPIREDIR/scripts/run u235 9228
```

to obtain the final results, for cross sections and PFNS, after the KALMAN fit Figures 13.3, 13.4, and 13.5 show examples of results for cross-section and PFNS fits for  $^{235}\text{U}$  using Kalman filter integrated with EMPIRE.

### 13.3 Fitting $\bar{\mu}$ and $\bar{\nu}$ in Empire with Kalman

The fitting code KALMAN, used within the EMPIRE nuclear modeling system, is a fitting package based on the Kalman fitting technique where a set of empire model parameters are adjusted to fit a set of data [150]. The required input is only the data (observables) being fit, the predicted value for those data from the model, and the "sensitivity" of each observable to each fitted parameter, where the "sensitivity" is simply the first derviative of the observable with respect to the fitted parameter. These sensitivities are calculated numerically. They are prepared as a matrix, where one dimension is the parameter index and the other is the index of the observable. For each parameter  $x_i$ , the sensitivity of observable  $OB(j)$  is calculated by adjusting the parameter up and down by a given amount, and then calculating the observables for these adjusted parameters, which are designated with a superscript  $+$  or  $-$ . The resulting sensitivity of the  $j$ th observable to the  $i$ th parameter is then simply given by

$$\text{Sens}(j)_i = (OB(j)^+ - OB(j)^-)/(x_i^+ - x_i^-) \quad (13.1)$$

This matrix of sensitivities, along with the predicted values of the observables without adjustment (often referred to as the "central values," as the parameters are set to original values between the  $+$  and  $-$  values, hence "central") are then used to adjust the parameters using the Kalman method to minimize the difference between the fitted value and the prepared set of observables in the standard C4 data format, using the usual definition of  $\chi^2$  as the sum of differences between the model predictions  $Y_i$  and measured quantities  $y_i$  divided by the measurement uncertainty  $\sigma_i$ . The sum of the squares of these ratios forms  $\chi^2$ ,

$$\chi^2 = \sum_{i=1}^n ((Y_i - y_i)/\sigma_i)^2 \quad (13.2)$$



where the summation is over all measured observables  $n$ . For further details about the Kalman approximation used in fitting see [150].

This approach has been successfully used with the Empire package for fitting cross sections. It includes, but is not limited to, total, elastic, inelastic, (n,2n), fission, and capture. The user creates a file which lists each empire parameter to be fitted along with a displacement which limits the range of the parameter when fitted by the Kalman code and also to determine the “+” and “-” values of Eq. 13.1 when calculating the sensitivity to the parameters for each fitted cross section. As such, these values should be chosen to be as large as possible as not to restrict the fit, but also not so large as to introduce nonlinearities into the calculation of the sensitivities. This amount varies for each parameter and its functional form within the EMPIRE code.

Here we discuss an extension of this fitting that will allow one to fit in addition to the usual cross sections, the prompt neutron fission spectra (PFNS), the average cosine of the scattering angle for elastic neutron scattering ( $\bar{\mu}$ ), and the average number of neutrons produced in fission ( $\bar{\nu}$ ). For a detailed description of the PFNS fitting, see section 13.2. The addition of  $\bar{\mu}$  and  $\bar{\nu}$  fitting in empire/kalman is described here.

### 13.3.1 $\bar{\mu}$ (Mubar)

When fitting EMPIRE calculations to experimental observables with Kalman, the data are prepared for the fitting code by the kalman script which controls the processing of the C4 data and the standard EMPIRE cross sections and sensitivities into the format used by the KALMAN code. A mapping function is used to map each reaction from EMPIRE to the corresponding MT as specified for that reaction in the C4 data file. This is done for various MF3 cross sections, but not for angular distributions, etc. As a first step toward including sensitivity to the angular distributions we describe the addition of the capability of fitting the  $\bar{\mu}$  as calculated by EMPIRE to experimental values. This involves 2 steps: (i) fitting of the experimental elastic angular distributions to produce an experimental value for  $\bar{\mu}$  with uncertainties and (ii) the addition of  $\bar{\mu}$  as another “reaction” in the file of cross sections produced by EMPIRE for fitting with Kalman (the XSC file). Here we describe the preparation of both the experimental and calculated values.

The experimental differential cross sections (C4 MF4/MT2) for elastic scattering are fit with a Legendre polynomial expansion to extract the coefficient from the fit for the first Legendre coefficient, which corresponds to  $\bar{\mu}$  or the average scattering cosine (here, the 0th Legendre parameter corresponds to the elastic scattering cross section). To fit these Legendre coefficients two similar approaches have been developed.

In the first approach, ang\_mu.f code, developed by A. Trkov at BNL, scans the input C4 data file and each section of elastic scattering differential cross sections are fitted using standard least-squares with the sum of the squares of the differences between the experimental cross sections and the Legendre fit being minimized. This method will iterate the fit, automatically increasing the order of the fit until the maximum relative difference between the data and the fit are less than the maximum relative error in the diff. cross section divided by  $\sqrt{2}$ , but never less than 7%. The order of the fit is also never allowed to

exceed  $l = 22$  or  $2/3$  the number of points in the angular distribution, whichever is smaller. This will produce a value for  $\bar{\mu}$  for each elastic differential cross section encountered in the C4 file from the  $0^{th}$  and  $1^{st}$  Legendre moments as

$$\bar{\mu} = \frac{c_1}{3c_0} \quad (13.3)$$

where the factor of 3 comes from re-normalizing the angular distribution by  $2l + 1$ , with  $l = 1$ . These fitted Legendre coefficients are written to the C4 file with MF154/MT2 which are paired with the calculated values for  $\bar{\mu}$  from Empire, which are assigned to MF3/MT251. The files are processed and prepared for the Kalman fitting code by the routine c4tokal.f90.

The Legendre fitting of the angular distributions will suffer if the number of data points is small or the data do not cover enough angular range to successfully constrain the fit. In an attempt to increase the coverage, when available, a second version of the Legendre fitting was developed that will group the data by incident neutron energy, which then may fit more than one C4 data section at once, increasing the number of points and angular coverage which may result in a better fit. In this version, the uncertainty of the individual data points are used in creating the  $\chi^2$ , as in Eq. 13.2. Each data set is assigned a systematic uncertainty and a scale factor is used to bring the various data sets into agreement, which is important to achieve a good fit when fitting more than one data set at a time. A scale factor  $f$  for each data set is added to the definition of  $\chi^2$  and a penalty term added for each data set weighted set's systematic error  $\sigma_f$  as shown in Eq. 13.4 (see ref. [151]).

$$\chi^2 = \sum_{i=1}^n ((Y_i - fy_i)/f\sigma_i)^2 + ((f - 1)/\sigma_f)^2 \quad (13.4)$$

The order of the Legendre fit was also automatically increased, where the order of the fit would increase until  $\chi^2 < 2.5$  but never allowed to exceed  $2/3$  of the total number of points being fit. This method yielded uncertainties on the coefficients of the Legendre polynomials which could then be directly propagated to an uncertainty in  $\bar{\mu}$  as defined in Eq. 13.3. An example of this fitting procedure is shown in Figure 13.6. Here 2 different data sets were each assigned a 5% systematic error. The fit scaled the data set of Goswami, et. al. up by 5.5% and the data set by E.Barnard, et. al., down approximately 5%. The resulting angular distribution was fit using only a  $4^{th}$  order Legendre polynomial with a reduced  $\chi^2$  of 1.92.

These procedures for fitting  $\bar{\mu}$  are fairly automated, but care must be taken and each fit must be visually checked. A common cause for a bad fit is simply insufficient angular coverage or too few points to constrain the fit, or both. An example of this type of failure is shown in Fig. 13.7. Here, there are few data points and none at forward angles. The resulting fit has a negative cross section at forward angles. The resulting value for  $\bar{\mu}$  is meaningless should not be used.

Another case where there are often problems are at high energy ( $E_n > 10$  MeV), where the angular distribution is very forward peaked. Fitting these distributions usually



requires a very high order Legendre polynomial, which can easily become unconstrained at very forward or backward angles, resulting in a bad value for  $\bar{\mu}$ . An example of such a fit at  $E_n = 15$  MeV is shown in Fig. 13.8. At high energy, it is often preferable to not fit the angular distribution but rather calculate  $\bar{\mu}$  directly, determining the the average cosine of the differential cross section as

$$\bar{\mu} = \frac{\int_{-1}^1 \frac{d\sigma(\theta)}{d\Omega} \cos\theta d\cos\theta}{\int_{-1}^1 \frac{d\sigma(\theta)}{d\Omega} d\cos\theta}. \quad (13.5)$$

For the distribution shown in Fig. 13.8, calculating  $\bar{\mu}$  using Eq. 13.5 results in a value of  $0.82 \pm 0.03$ , an acceptable value, rather than the result from the high-order Legendre fit of  $-0.815 \pm 0.0002$ , which is clearly wrong.

Of course, to successfully use Eq. 13.5 the angular coverage of the differential cross section must be sufficient to perform the integral. If this is not the case then there is little choice but to use a Legendre fit. In any case, care must be always taken when determining the value of  $\bar{\mu}$  for a given elastic differential cross section. Each fit must be visually inspected and only those that result in a good fit without problems (e.g., unconstrained or negative cross section, etc.) should be accepted for Kalman fitting. In the end, it is up to the evaluator to decide which method provides the best value for  $\bar{\mu}$  from a given differential cross section. The accepted values with uncertainties are appended to the C4 file as MF154/MT2 data, which are then paired with the EMPIRE cross predictions for  $\bar{\mu}$  for fitting with Kalman. An example of a set of  $\bar{\mu}$  derived from  $^{238}\text{U}$  elastic differential cross sections, with an EMPIRE calculation for  $\bar{\mu}$  are shown in Fig. 13.9.

The addition of calculated  $\bar{\mu}$  to the list of cross sections output by EMPIRE required a minor addition to the EMPIRE code. The differential cross sections are stored internally in EMPIRE in the center-of-mass frame from  $0^\circ$  to  $180^\circ$ , every  $2^\circ$ . As  $\bar{\mu}$  is defined as the average cosine of the elastic scattered neutrons in the *Lab* frame, these differential cross sections are first boosted to Lab and then the distribution is integrated using Eq. 13.5 to calculate  $\bar{\mu}$ . This value is then written out to the \*.xsc cross section file along with the other cross sections used for fitting with KALMAN. It will later be mapped to MF3/MT251, which is paired with  $\bar{\mu}$  from the Legendre coefficients from fits to C4 data as MF154/MT2.

### 13.3.2 $\bar{\nu}$ (Nubar)

The number of neutrons produced per fission,  $\bar{\nu}$ , can also be fit to data with the KALMAN code. Here, the the values for  $\bar{\nu}$  to be fit are directly available in the C4 data file as MF1/MT452. These values need no further processing and are paired with the calculated  $\bar{\nu}$  from EMPIRE by the c4tokal.f90 routine. Care must be taken with fitting  $\bar{\nu}$  as EMPIRE does not calculate  $\bar{\nu}$  but uses a distribution taken from an existing evaluated file, and scales it by a single parameter. Therefore, fitting  $\bar{\nu}$  should only be done when adjusting the scale parameter in EMPIRE to fit new  $\bar{\nu}$  data not being used by empire itself for  $\bar{\nu}$ . In this case, the KALMAN code can be used. The only parameter that will be adjusted is the  $\bar{\nu}$  scaling parameter PFNNUI. This can be fit along with other cross section data or

not. The parameters for the cross sections do not affect  $\bar{\nu}$ , so there will be no correlations between the  $\bar{\nu}$  scaling parameter PFNNUI and the other EMPIRE parameters. Of course, this single scaling parameter can also be set by hand in this case, by taking the ratio of the integral of the  $\bar{\nu}$  spectrum used by EMPIRE to the integral of the  $\bar{\nu}$  data being fit.

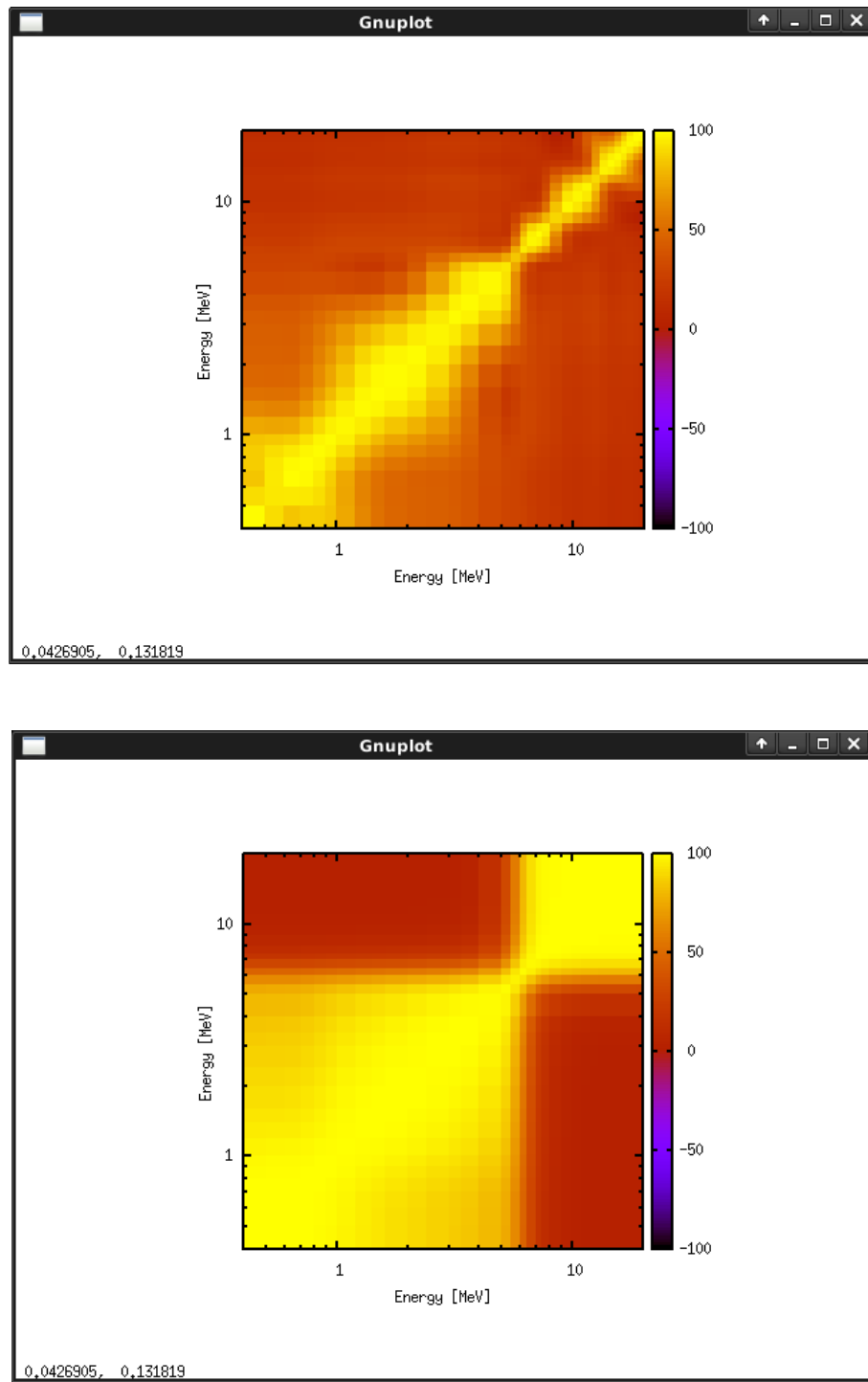


Figure 13.1: Correlation matrices for neutron-induced fission (top) and capture (bottom) reactions ( $MT = 18$  and  $102$ , respectively) for material  $^{235}\text{U}$ .

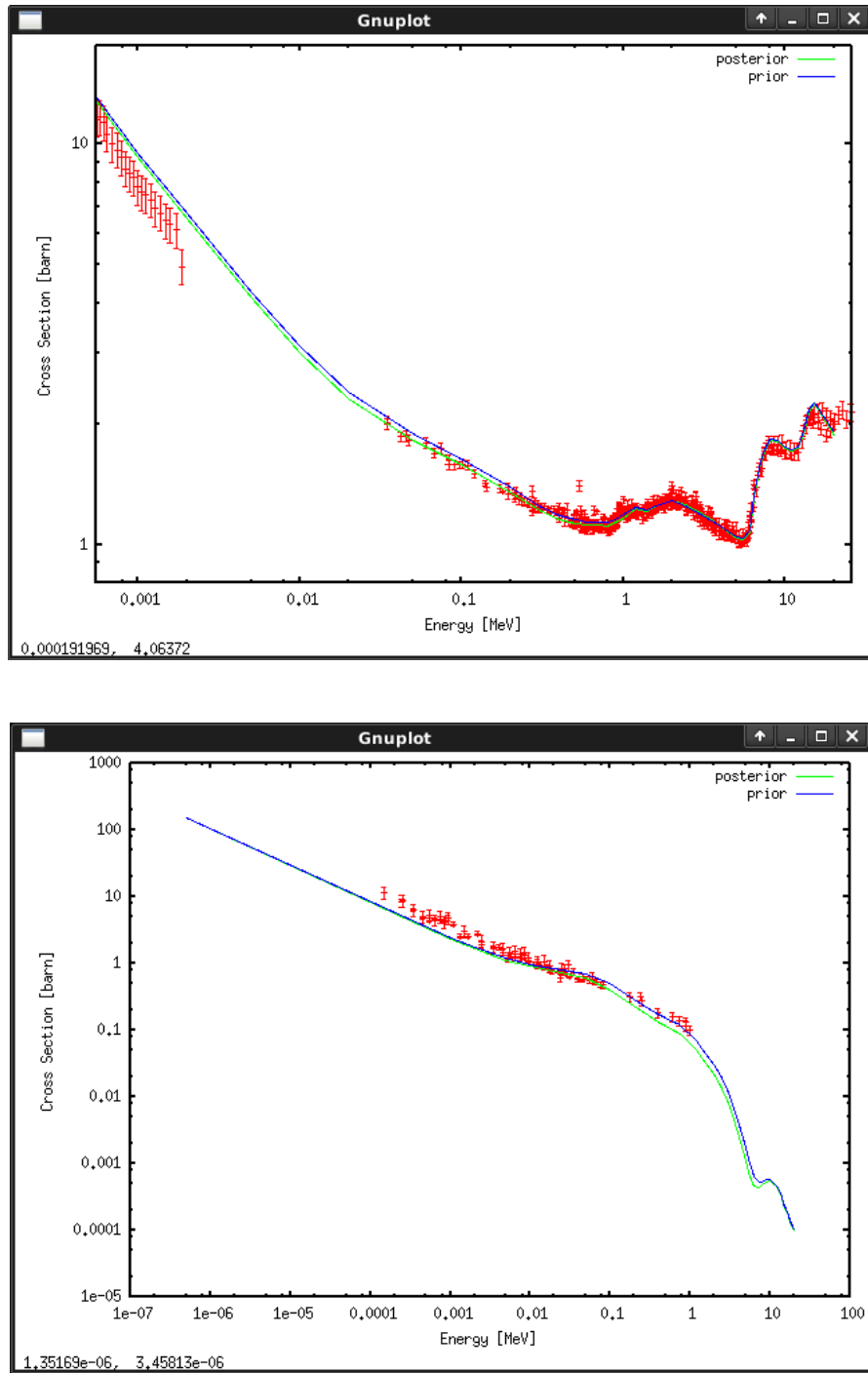


Figure 13.2: Cross section for the neutron-induced fission (top) and capture (bottom) reactions ( $MT = 18$  and  $102$ , respectively) for material  $^{235}\text{U}$ , comparing the agreement with experimental data between the curves prior and post KALMAN fitting.

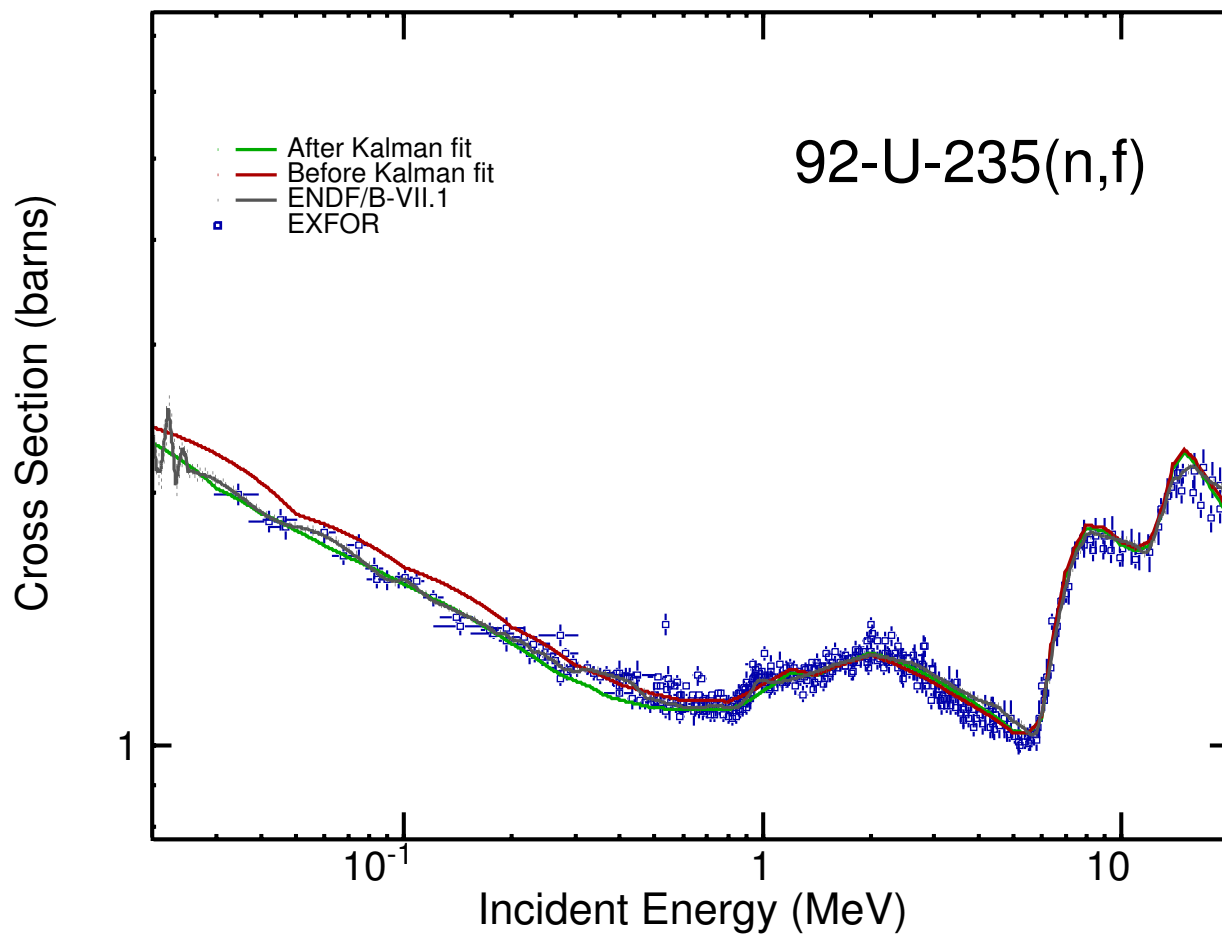


Figure 13.3: Comparison between fission cross sections calculated by EMPIRE using input parameters obtained before and after fitting using Kalman filter. Evaluation from ENDF/B-VII.1 library and experimental data from EXFOR are also plotted.

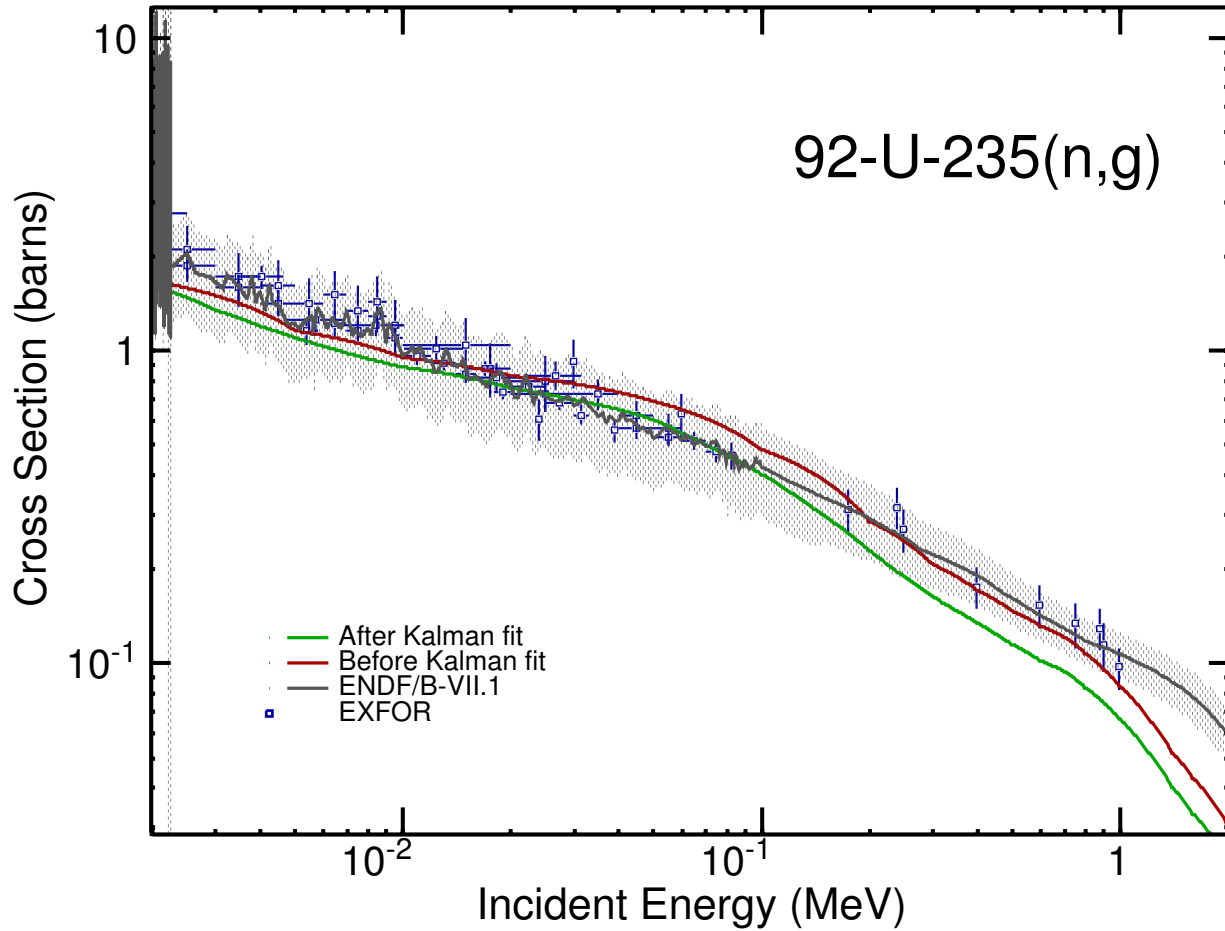


Figure 13.4: Comparison between capture cross sections calculated by EMPIRE using input parameters obtained before and after fitting using Kalman filter. Evaluation from ENDF/B-VII.1 library and experimental data from EXFOR are also plotted. Even though the agreement of the post-fit curve seems worse than that of the pre-fit one, this is compensated by improvements at other reactions, minimizing the overall  $\chi^2$ . This may happen when the option to fit data for all reactions is selected.

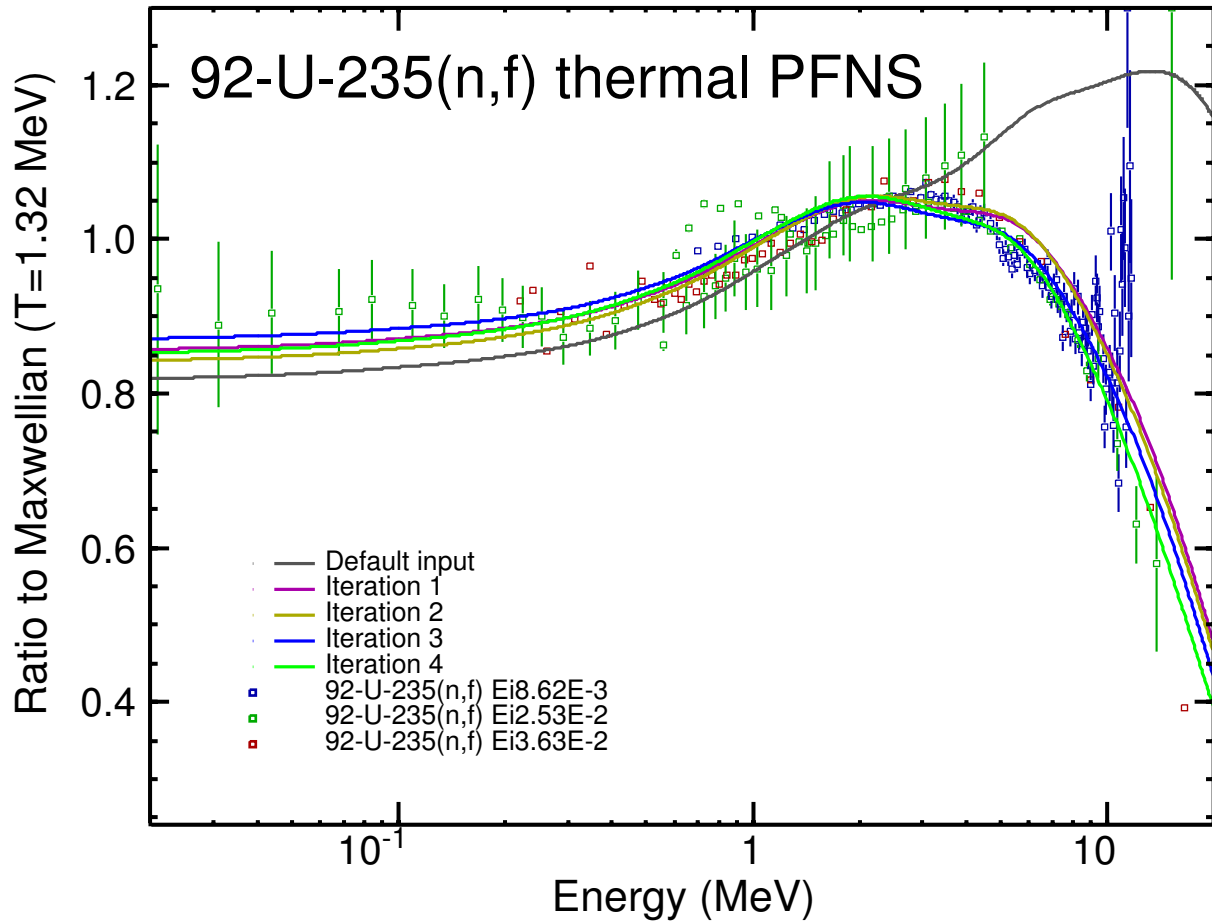


Figure 13.5: Prompt fission neutron spectra (PFNS) for thermal neutrons calculated by EMPIRE using a default input and input files containing PFNS parameters after different numbers of KALMAN-EMPIRE iterations. For iterations 3 and 4, additionally to iterating a new sequence of KALMAN and EMPIRE runs, some spurious data points were removed from the fitting process.

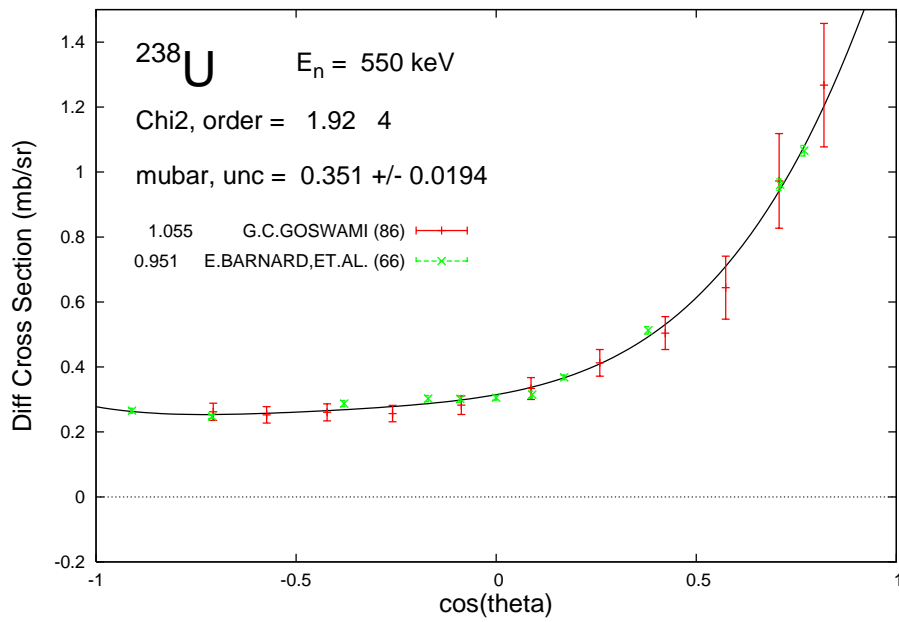


Figure 13.6: Legendre fit to differential cross section data at  $E = 550 \text{ keV}$ . There were 2 data sets available at this energy. Each data set was adjusted by a scale factor that was fitted along with the Legendre coefficients by including a penalty term in the  $\chi^2$  (see Eq. 13.4). This resulted in a good fit to the data with only a 4th order Legendre fit with a final reduced  $\chi^2$  of 1.92.



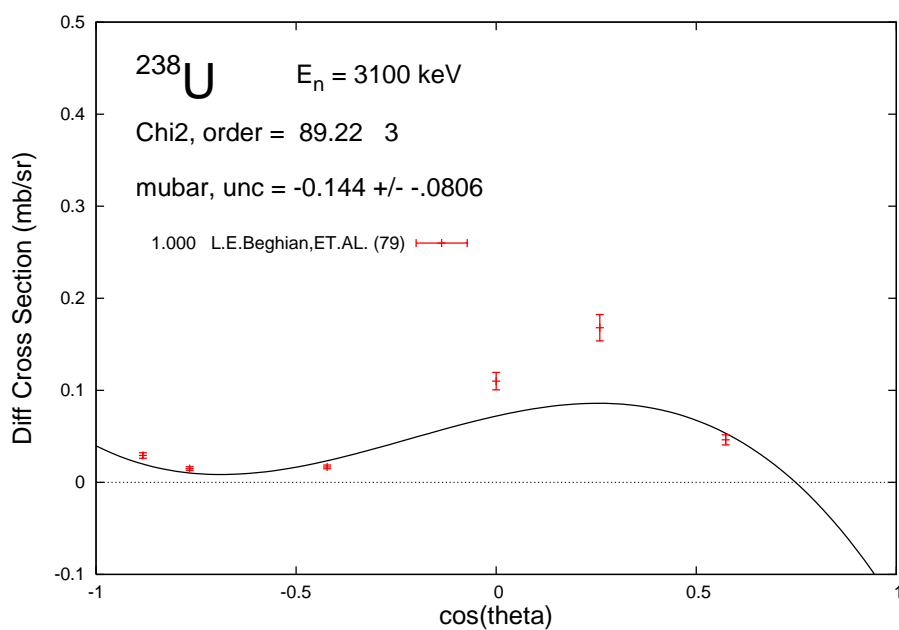


Figure 13.7: Legendre fit to differential cross section data at  $E = 3.1 \text{ MeV}$ . An example of a data set with too few points and too small angular coverage. The fit fails with negative cross sections being produced, resulting in a nonsensical value for  $\bar{\mu}$ .

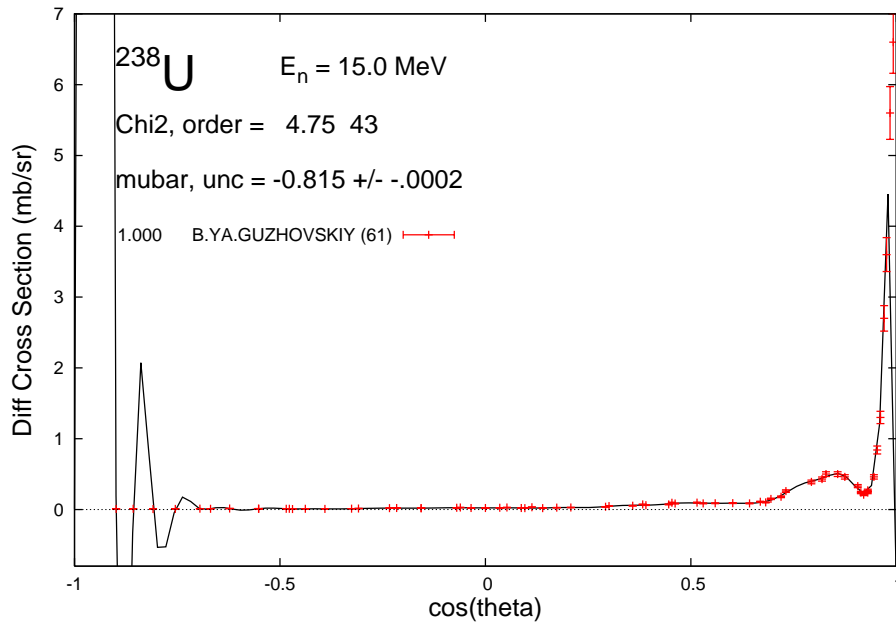


Figure 13.8: Legendre fit to differential cross section data at  $E = 15$  MeV. Here the forward angle peak of the angular distribution requires a very high order Legendre polynomial for a good fit which results in a relatively good  $\chi^2$  but the high oscillations at the rather unconstrained backward angles result in a bad value for  $\bar{\mu}$  of -0.815.

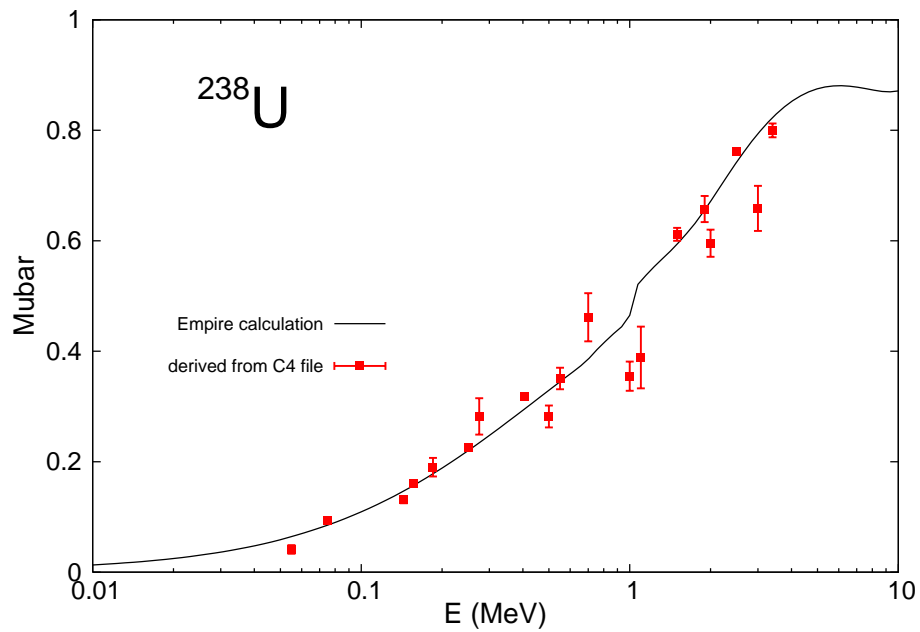


Figure 13.9: Values of  $\bar{\mu}$  from fitted elastic differential cross sections for  $^{238}\text{U}$  shown in red with uncertainties from the fit. The black curve is an EMPIRE calculation for  $\bar{\mu}$ . This curve is fit to the  $\bar{\mu}$  data with the KALMAN code, which will adjust the EMPIRE parameters based on their calculated sensitivities for  $\bar{\mu}$ .



# Acknowledgments

EMPIRE is the result of an international cooperation towards open source software, as so successfully promoted by the General Public License. A number of authors contributed to the development of the code and it would be next to impossible to list all names. We stress that the code described in this paper would not have been possible without their valuable and voluntary cooperation.

We are in debt to T. Kawano, who drew our attention to covariances and who was actively involved in the implementation of his KALMAN code in EMPIRE. We owe very special thanks to J. Raynal who has been developing his ECIS code since 1972 [6] and is still actively maintaining and extending it as evidenced by the recent release of the 2007 version. His code is the backbone of EMPIRE, TALYS and McGNASH for all optical model calculations, playing a unique role in current nuclear data evaluation efforts. Another special thanks go to the authors of GNASH (Mark Chadwick and Phil Young) as well to the principal author of TALYS (Arjan Koning) for providing a never ending source of inspiration to our continuous attempts to surpass performance and functionalities of their codes.

We also highly appreciate S. Mughabghab's help in developing the resonance module linking his Atlas of Neutron Resonances to EMPIRE, D. Brown's professional installation of EMPIRE, which brings the code closer to the users and A. Palumbo for incorporating the astrophysical S-factor calculation.

First of all, we would like to acknowledge our colleagues whose work helped to prepare this paper. H. I. Kim, G. P. A. Nobre, A. Palumbo, and M. Pigni deserve a special mention as the major users of the code. Their comments were of great value and enabled us to trace coding errors, improve stability and ease of use of the code.

We feel particularly fortunate to be able to build on two solid foundations - the comprehensive compilation of model parameters (RIPL) and the extensive compilation of experimental results (CSISRS/EXFOR). We are grateful to the recent heads of the IAEA Nuclear Data Section, Ch. Dunford, D. Muir, A.L. Nichols and R. Forrest for their continued support of the two projects. Naturally, our gratitude goes also to all participants of the three phases of the RIPL project and to all EXFOR compilers, in particular to V. McLane, S. Dunaeva and O. Schwerer, who dedicated their careers to EXFOR. Three of us (M.H., R.C. and A.T.), who had the privilege to work under the leadership of A.L. Nichols, would like to thank him for his encouragement and support for the development of EMPIRE.

We would like to thank A. Ventura who was involved in the early formulations of the fission theory used in EMPIRE, E. Běták who developed exciton model with angular momentum conservation used in earlier versions of EMPIRE, and to A. Hoering who took part in the implementation of  $\gamma$ -emission within the Multi-Step Compound mechanism.

We would like to thank A. Ignatyuk who has been a permanent source of inspiration, constructive criticism and encouragement and lately has been using EMPIRE in many different applications.

Finally, there is a group of our colleagues to whom we owe particular gratitude for their enlightenment and inspiration. It is a honour to acknowledge H.A. Weidenmüller's guidance on multi-step compound theory and the foundations of the statistical model, discussions with H. Lenske and H. Wolter on the multi-step direct model and its implementation, working with H. Hofmann on width-fluctuation corrections, and with D. Smith on the exploration of the world of covariances. EMPIRE would not have reached its current stage without illuminating discussions on pre-equilibrium emission with M. Blann, P.E. Hodgson, and E. Gadioli. We also benefited from the exchange of experience with authors of other codes. We would like to express our appreciation to S. Hilaire, P. Talou, and S. Goriely for inspiring discussions, indication of priorities, and technical suggestions.

One of us (M.H.) would like to thank A. Marcinkowski for motivating him to write the EMPIRE-1 code. He is also grateful to G. Giardina and his collaborators A. D'Arrigo, A. Lamberto, and A. Taccone who assisted the EMPIRE-2 project from the very beginning and tested preliminary versions of the code since 1993. Finally, we are indebted to R. Sturiale for LINUX support at the early stages of the development of EMPIRE development. M.S. would like to express her gratitude to G. Vladuca for inspiring her interest in fission.

Last but not least, we gratefully acknowledge the authors of the codes that are included in the physics core of EMPIRE: M.B. Chadwick (DDHMS), H. Lenske and H. Wolter (ORION and TRISTAN), J. Raynal (ECIS), E. Soukhovitskii, S. Chiba, J.M. Quesada, O. Iwamoto, K. Shibata, T. Fukahori, and G.B. Morogovskij (OPTMAN), C.H. Dasso and S. Landowne (CCFUS), and A. Sierk (BARFIT and MOMFIT). Our gratitude goes also to Ch. Dunford for his ENDF checking codes, D.E. Cullen whose suite of preprocessing codes makes an essential part of the EMPIRE system and to R. MacFarlane for his help in interfacing EMPIRE to his processing code NJOY.

The work at BNL was sponsored by the Office of Nuclear Physics, Office of Science of the U.S. Department of Energy under Contract No. DE-AC02-98CH10886 with Brookhaven Science Associates, LLC. We are pleased to acknowledge strong support by the International Atomic Energy Agency over last ten years.

# Bibliography

- [1] H. M. Hofmann, J. Richert, J. W. Tepel, and H. A. Weidenmüller, *Ann. Phys.* **90**, 403 (1975).
- [2] H. M. Hofmann, T. Mertelmeier, M. Herman, and J. W. Tepel, *Z. Physik A* **297**, 153 (1980).
- [3] H. Feshbach, A. Kerman, and S. Koonin, *Ann. of Phys.* **125**, 429 (1980).
- [4] H. Nishioka, J. J. M. Verbaarschot, H. A. Weidenmüller, and S. Yoshida, *Ann. Phys.* **172**, 67 (1986).
- [5] J. Raynal, Technical Report No. SMR-9/8, IAEA (unpublished).
- [6] J. Raynal, *Computing as a language of physics. ICTP International Seminar Course* (IAEA, ICTP, Trieste, Italy, 1972), p. 281.
- [7] E. Soukhovitskiĭ, G. Morogovski, S. Chiba, and T. Fukahori, Technical report, JAERI-Data/Code 2004-002, Japan Atomic Energy Research Institute (unpublished).
- [8] E. Soukhovitskiĭ *et al.*, Technical Report No. JAERI-Data/Code 2005-002, Japan Atomic Energy Research Institute (unpublished).
- [9] E. Soukhovitskiĭ *et al.*, Technical report, JAERI-Data/Code 2008-025, Japan Atomic Energy Research Institute (unpublished).
- [10] C. H. Dasso and S. Landowne, *Comp. Phys. Comm.* **46**, 187 (1987).
- [11] T. Tamura, T. Udagawa, and H. Lenske, *Phys. Rev.* **C26**, 379 (1982).
- [12] H. Lenske and H. H. Wolter, TRISTAN and ORION codes, private communication to M. Herman.
- [13] M. B. Chadwick, DDHMS code, private communication to M. Herman.
- [14] A. J. Sierk, *Phys. Rev.* **C33**, 2039 (1986).

- [15] D. E. Cullen, PREPRO-2000: ENDF Preprocessing Codes, Report IAEA-NDS-39, Vienna, 2000, available from <http://www-nds.iaea.org/ndspub/endf/prepro/>.
- [16] A. Trkov, ENDVER - ENDF File Verification Support Package, Available from [www-nds.iaea.org/ndspub/endf/endver/](http://www-nds.iaea.org/ndspub/endf/endver/).
- [17] V. V. Zerkin, ZVView graphics software for nuclear data analysis version 9.4, 2001, available from <http://www-nds.iaea.org/ndspub/zvview/>.
- [18] K. H. Schmidt and W. Morawek, Rep. Prog. Phys. **54**, 949 (1993).
- [19] D. L. Hill and J. A. Wheeler, Phys. Rev. **89**, 1102 (1953).
- [20] IAEA-CRP, Reference Input Parameter Library (RIPL), IAEA-TECDOC-1034, Vienna, <http://www-nds.iaea.org/ripl/>, 1998.
- [21] A. Blokhin *et al.*, Yadernye Konstanty (1991).
- [22] E. S. Soukhovitskiĭ and S. Chiba, Journal of Nuclear Science and Technology **Supplement 2**, 697 (2001).
- [23] E. S. Soukhovitskiĭ, O. Iwamoto, S. Chiba, and T. Fukahori, Journal of Nuclear Science and Technology **37**, 120 (2000).
- [24] E. S. Soukhovitskiĭ and S. Chiba, Journal of Nuclear Science and Technology **Supplement 2**, 144 (2001).
- [25] S. Chiba *et al.*, Nuclear Physics A **624**, 305 (1997).
- [26] S. Chiba *et al.*, Journal of Nuclear Science and Technology **37**, 498 (2000).
- [27] W. Sun *et al.*, Journal of Nuclear Science and Technology **40**, 635 (2003).
- [28] E. S. Soukhovitskiĭ *et al.*, Journal of Nuclear Science and Technology **40**, 69 (2003).
- [29] J.-Y. Lee *et al.*, J. Kor. Phys. Soc. **38**, 88 (2001).
- [30] E. S. Soukhovitskiĭ *et al.*, Journal of Nuclear Science and Technology **39**, 816 (2002).
- [31] E. S. Soukhovitskiĭ *et al.*, Phys. Rev. C **62**, 044605 (2000).
- [32] E. Soukhovitskiĭ, R. Capote, J. Quesada, and S. Chiba, Phys. Rev. C **72**, 024604 (2005).
- [33] R. Capote, E. S. Soukhovitskiĭ, J. M. Quesada, and S. Chiba, Phys. Rev. C **72**, 064610 (2005).
- [34] M. Chadwick *et al.*, Handbook on photonuclear data for applications: Cross sections and spectra, IAEA-TECDOC-1178, Vienna, Austria, <http://www-nds.iaea.org/photonuclear/>, 2000.



- [35] T. Belgya *et al.*, Technical Report No. IAEA-TECDOC-1506, International Atomic Energy Agency, Vienna, Austria (unpublished).
- [36] M. B. Chadwick, P. O. zinský, P. E. Hodgson, and G. Reffo, Phys. Rev. **C44**, 814 (1991).
- [37] H. Lenske *et al.*, submitted to Nucl. Phys.
- [38] H. Lenske and H. H. Wolter, Nucl. Phys. **A538**, 483 (1992).
- [39] A. Fetter and J. Walecka, *Quantum Theory of Many Body Systems* (McGraw-Hill, New York, ADDRESS, 1971).
- [40] H. Wienke, R. Capote, M. Herman, and M. Sin, Phys.Rev. C **78**, 064611 (2008).
- [41] N. V. G. K. Hagino and H.Sagawa, Nucl. Phys. **A731**, 272 (2004).
- [42] J. W. Negele, *Theory of Many-Body Systems* (Addison-Wesley, New York, 1990).
- [43] A. L. Fetter and J. D. Walecka, *Quantum Theory of Many-Particle Systems* (McGraw-Hill, New York, 1971).
- [44] A. Bohr and B. Mottelson, *Nuclear Structure* (Reading, MA. Addison-Wesley/W.A. Benjamin, Inc., USA, 1975), Vol. 2.
- [45] R. Siudak, Ph.D. thesis, Univ. Cracow (Poland), .
- [46] P. Ring and S. Schuck, *Theoretische Kernphysik* (Springer, Berlin, 1982).
- [47] V. G. Soloviev, Progr. Part. Nucl. Phys. **19**, 107 (1987).
- [48] M. Herman, G. Reffo, and H. Weidenmüller, Nucl. Phys. **A536**, 124 (1992).
- [49] K. Stankiewicz, A. Marcinkowski, and M. Herman, Nucl. Phys. **A435**, 67 (1985).
- [50] P. Obložinský, Nucl. Phys. **A453**, 127 (1986).
- [51] A. Hoering and H. A. Weidenmüller, Phys. Rev. **C46**, 2476 (1992).
- [52] M. Herman, A. Hoering, and G. Reffo, Phys. Rev. **C46**, 2493 (1992).
- [53] P. Axel, Phys. Rev. **126**, 671 (1962).
- [54] D. M. Brink, Ph.D. thesis, Oxford, 1955.
- [55] D. M. Brink, Nucl. Phys. **4**, 215 (1957).
- [56] G. F. Bertsch, private communication to A. Hoering, 1992.
- [57] J. J. Griffin, Phys. Rev. Lett. **17**, 478 (1966).

- [58] C. K. Cline and M. Blann, Nucl. Phys. **A 172**, 225 (1971).
- [59] C. K. Cline, Nucl. Phys. **A193**, 417 (1972).
- [60] I. Ribanský, P. Obložinský, and E. Bětak, Nucl. Phys. **A205**, 545 (1973).
- [61] J. M. Akkermans, H. Gruppelaar, and G. Reffo, Phys. Rev. C **22**, 73 (1980).
- [62] F. C. Williams, Nucl. Phys. **A166**, 231 (1971).
- [63] C. Kalbach, in *Proc. of the IAEA Advisory Group Meeting on Basic and Applied Problems of Nuclear Level Densities*, edited by E. M. R. Bhat (Brookhaven National Lab Report No. BNL-NSC-51694, Upton, NY, 1983), p. 113.
- [64] N. Baguer, R. Capote, and R. Pedrosa, Z. Phys. **A334**, 397 (1989).
- [65] M. Blann, Phys. Rev. Lett. **28**, 757 (1972).
- [66] E. Betak and J. Dobes, Z. Phys. **A279**, 319 (1976).
- [67] C. Kalbach, Z. Physik **A283**, 401 (1977).
- [68] M. Blann and A. Mignerey, Nuclear Physics A **186**, 245 (1972).
- [69] H. Machner, Z. Phys **A302**, 125 (1981).
- [70] S. K. Gupta, Z. Phys. **A303**, 329 (1981).
- [71] A. Iwamoto and K. Harada, Phys. Rev. C **26**, 1821 (1982).
- [72] K. Sato, A. Iwamoto, and K. Harada, Phys. Rev. C **28**, 1527 (1983).
- [73] Z. Shang *et al.*, in *Proc. IAEA Research Coordination Meeting on Methods for the calculation of neutron nuclear data for structural materials, INDC(NDS)-193/L*, edited by V. Goulo (International Atomic Energy Agency, Vienna, Austria, 1988), p. 21.
- [74] Z. Shang and Y. Jun, Technical Report INDC(CPR)-014, IAEA, Vienna, Austria (unpublished).
- [75] V. Pluyko and G. Prokopets, Phys.Lett. **76B**, 253 (1978).
- [76] E. Betak and J. Dobes, Phys. Lett. **84B**, 368 (1979).
- [77] J. M. Akkermans and H. Gruppelaar, Phys. Lett. **157B**, 95 (1985).
- [78] S. Matsuyama *et al.*, Jour. of Nucl. Sci. and Technology **27**, 601 (1990).
- [79] M. Blann, Phys. Rev. **C54**, 1341 (1996).
- [80] M. Blann, Phys. Rev. Lett. **27**, 337 (1971).

- [81] M. Blann and A. Mignerey, Nucl. Phys. A **186**, 245 (1972).
- [82] M. Blann, Phys. Rev. Lett. **28**, 757 (1972).
- [83] M. Blann, Nucl. Phys. A **213**, 570 (1973).
- [84] J. Bisplinghoff, Phys. Rev. C **33**, 1569 (1986).
- [85] A. V. Ignatyuk, G. N. Smirenkin, and A. S. Tishin, Sov. J. Nucl. Phys. **21**, 255 (1975).
- [86] A. Gilbert and A. G. W. Cameron, Can. J. Phys. **43**, 1446 (1965).
- [87] P. G. Young *et al.*, Trans. Amer. Nucl. Soc. **60**, 271 (1989).
- [88] A. Iljinov *et al.*, Nuclear Physics A **543**, 517 (1992).
- [89] A. V. Ignatyuk, Technical Report INDC(CCP)-233, IAEA, Vienna, Austria (unpublished).
- [90] A. V. Ignatyuk, K. K. Istekov, and G. N. Smirenkin, Sov. J. Nucl. Phys. **29**, 450 (1979).
- [91] G. Hansen and A. Jensen, Nuclear Physics A **406**, 236 (1983).
- [92] E. Rastopchin, M. Svirin, and G. Smirenkin, Sov. J. Nucl. Phys. **52**, 799 (1990).
- [93] A. Junghans *et al.*, Nucl. Phys. **A629**, 635 ((1998)).
- [94] O. Grudzevich, A. Ignatyuk, V. Plyaskin, and A. Zelenetsky, in *Proceedings of the International Conference on Nuclear Data for Science and Technology, 30 May-3 June 1988, Mito, pp. 767-770*, edited by S. Igarashi (JAERI, Tokai, Ibaraki, 1988).
- [95] A. D'Arrigo *et al.*, J. Phys. **G20**, 365 (1994).
- [96] A. R. Junghans *et al.*, Nucl. Phys. **A629**, 635 (1998).
- [97] P. Moller and J. R. Nix, At. Data Nucl. Data Tables **26**, 165 (1981).
- [98] S. E. Vigdor and H. J. Karwowski, Phys. Rev. **C26**, 1068 (1982).
- [99] G. Andersson *et al.*, Nucl. Phys. **A268**, 205 (1976).
- [100] S. Goriely, M. Samyn, and J. M. Pearson, Phys. Rev. C **75**, 064312 (2007).
- [101] S. Hilaire, J. Delaroche, and M. Girod, Eur. J. Phys. A **12**, 169 (2001).
- [102] S. Goriely, Journal of Nuclear Science and Technology **Supplement 2**, 536 (2001).
- [103] G. Audi, A. Wapstra, and C. Thibault, Nucl. Phys. **A729**, 337 (2003).

- [104] R. Capote, A. Ventura, F. Cannata, and J. M. Quesada, Phys. Rev. C **71**, 064320 (2005).
- [105] J. M. Blatt and V. Weisskopf, *Theoretical Nuclear Physics* (John Wiley and Sons, Inc., New York, 1952).
- [106] V. M. Kolomietz, V. A. Plujko, and S. Shlomo, Phys. Rev. C **54**, 3014 (1996).
- [107] J. Kopecky, M. Uhl, and R. E. Chrien, Phys. Rev. C **47**, 312 (1993).
- [108] V. A. Plujko, Acta Phys. Pol. **B 31**, 435 (2000).
- [109] V. A. Plujko, in *9<sup>th</sup> International Conference for Nuclear Reaction Mechanisms*, edited by E. Gadioli (Universita degli Studi di Milano, Varenna, Italy, 2000), Vol. Suppl. 115, p. 113.
- [110] V. A. Plujko, S. N. Ezhov, and M. O. Kavatsyuk, in *International Conference on Nuclear Data for Science and Technology*, edited by K. Shibata (Atomic Energy Society of Japan, Tsukuba, Japan, 2001), Vol. 1, p. 811.
- [111] S. F. Mughabghab and C. L. Dunford, Phys. Lett. **B 487**, 155 (2000).
- [112] D. M. Brink, Ph.D. thesis, Oxford University, 1955.
- [113] S. S. Dietrich and B. L. Berman, Atom. Nucl. Data Tables **38**, 199 (1998).
- [114] D. R. Chakrabarty *et al.*, Phys. Rev. C **36**, 1886 (1987).
- [115] J. Speth and A. van de Woude, Rep. Prog. Phys. **44**, 719 (1981).
- [116] W. V. Prestwich, Z. Phys. **A315**, 103 (1984).
- [117] M. Sin and R. Capote, Phys. Rev. C **77**, 054601 (2008).
- [118] A. Ignatyuk and V. Maslov, Sov. J. Nucl. Phys. **54**, 647 (1991).
- [119] S. Bjornholm and J. E. Lynn, Rev.Mod.Phys. **52**, 725 (1980).
- [120] B. S. Bhandari, Phys.Rev. C **19**, 1820 (1979).
- [121] B. B. Back, O. Hansen, H. C. Britt, and J. D. Garrett, Phys. Rev. C **9**, 1924 (1974).
- [122] U. Brosa, S. Grossmann, and A. Muller, Phys. Rep. **197**, 167 (1990).
- [123] S. Goriely and J. M. Pearson, Int. Conf. on Nuclear Data for Science and Technology, 22 - 27 April 2007, Nice, France .

- [124] S. Bjornholm, A. Bohr, and B. Mottelson, in *Proc. Third IAEA Symp. on Physics and Chemistry of Fission, Rochester, New York, 13 - 17 August, 1973, Rep. STI/PUB/347* (International Atomic Energy Agency, Vienna, Austria, 1974), Vol. I, pp. 367–372.
- [125] S. Goriely, S. Hilaire, and A. J. Koning, *Phys. Rev. C* **78**, 064307 (2008).
- [126] N. Froman and P. O. Froman, *JWKB Approximation, Contributions to the Theory* (North-Holland, Amsterdam, ADDRESS, 1965).
- [127] N. Fröman and O. Dammert, *Nucl. Phys.* **A147**, 627 (1970).
- [128] M. Sin *et al.*, Int. Conf. on Nuclear Data for Science and Technology, 22 - 27 April 2007, Nice, France .
- [129] S. Goriely and S. Hilaire, Int. Conf. on Nuclear Data for Science and Technology, 22 - 27 April 2007, Nice, France .
- [130] W. D. Myers and W. J. Swiatecki, *Phys. Rev.* **C60**, 014606 (1999).
- [131] P. Grange and H. A. Weidenmüller, *Phys. Lett.* **B96**, 26 (1980).
- [132] E. M. Rastopchin *et al.*, *Sov. J. Nucl. Phys.* **53**, 741 (1991).
- [133] H. Kramers, *Physica* **7**, 284 (1940).
- [134] P. Talou *et al.*, *Phys. Rev. C* **83**, 064612 (2011).
- [135] D. G. Madland and J. R. Nix, *Nucl. Sci. and Eng.* **81**, 213 (1982).
- [136] V. Weisskopf, *Phys. Rev.* **52**, 295 (1937).
- [137] N. V. Kornilov, A. B. Kagalenko, and F.-J. Hambsch, *Phys. At. Nucl.* **62**, 173 (1999).
- [138] V. V. Malinovskii *et al.*, Technical report, IAEA (unpublished).
- [139] S. F. Mughabghab, *Atlas of Neutron Resonances: Thermal Cross Sections and Resonance Parameters* (Elsevier, Amsterdam, 2006).
- [140] Y.-S. Cho *et al.*, in *Proc. of Int. Conf. on Nuclear Data for Science and Technology*, edited by O. Bersillon (CEA, Nice, France, 2007), p. 1159.
- [141] M. Herman *et al.*, *Nuclear Data Sheets* **109**, 2752 (2008).
- [142] S. Y. Oh, J. H. Chang, and S. F. Mughabghab, Technical report, BNL-NCS-67469 (unpublished).
- [143] T. Kawano and K. Shibata, *Covariance Evaluation System, JAERI Data/Code*, Japan Atomic Energy Research Institute, Tokai, Japan, 1997.

- [144] D. Smith, Technical report ANL/NDM-159, Argonne National Lab (unpublished).
- [145] R. Capote *et al.*, Nuclear Data Sheets **110**, 3107 (2009).
- [146] D. Muir, A. Mengoni, and I. Kodeli, Nuclear Data Sheets **109**, 2874 (2008).
- [147] Tcl/Tk software package, available free of charge from <http://dev.scripatics.com/software/tcltk/>.
- [148] S. H. S. Goriely and A. Koning, Phys. Rev. **C78**, 064307 (2008).
- [149] H. Leeb, D. Neudecker, and T. Srdinko, Nuclear Data Sheets **109**, 2762 (2008).
- [150] M. Herman *et al.*, Nuclear Data Sheets **109**, 2752 (2008).
- [151] G. D. Agostini, Nuclear Instruments and Methods **A 346**, 306 (1994).

# Appendix A

## EMPIRE optional input keywords

The optional input allows modifications to the default model parameters. Optional input consists of an arbitrary number of records, entered in any order and closed with the GO record, which indicates the end of the input. In the simplest case (all defaults), only the GO record must be entered.

Each optional record starts with an alphanumeric keyword **NAME**. If the first character of the line (i.e. **NAME(1:1)**) is \*, # or !, then this line contains comments and is ignored by the code. There might be an arbitrary number of comments line in the optional input. If the first character of the line **NAME(1:1)** is @, then this line contains a title, which will be printed in EMPIRE outputs; obviously the title is not used in any calculations. Multiple titles are allowed. Users are strongly encouraged to use titles and comments in EMPIRE inputs; that will be a significant step toward a better documentation of our theoretical calculations and evaluations.

The optional-input keyword **NAME** is followed by the value VAL and four positional parameters I1, I2, I3, I4. The keyword indicates a physical quantity, such as the binding energy or level density parameter or scaling parameter. VAL takes the numerical value of the given quantity or scaling parameter.

The positional parameters are typically used to specify to which nucleus the quantity should be applied (generally if these are omitted the value is applied to all nuclei in the given calculation). Positional parameters may be also used to indicate the estimated uncertainty of the quantity defined by the input keyword (except optical model parameters for which the uncertainty is defined by VAL). Each record must be in the FORTRAN format:

FORMAT (A6,G10.5,4I5) **NAME**,VAL,I1,I2,I3,I4

Fixed format allows to avoid typing zeros if no input is needed for some positional parameters.

The GO record indicates end of the optional input and starts calculations. It may be followed by an unlimited list of incident energies (and titles or comments) (one per record)

terminated with a record containing a negative value. Anything below this line will be ignored by the code.

## Calculation control

<b>NEX</b>	Maximum number of energy steps in the integration set to VAL (default: min(50, NDEX)). NDEX parameter is defined in the <i>dimension.h</i> file.
<b>ENDF</b>	<p>Controls output for ENDF formatting and exclusive/inclusive emission</p> <p>= 0 no ENDF formatting (default).</p> <p>&gt; 0 output for the full ENDF formatting will be created (including double differential MF=6) as shown in the two examples below</p> <p style="padding-left: 40px;">= 2 means all reactions emitting 2 or less particles are exclusive the rest are inclusive (lumped into MT=5)</p> <p style="padding-left: 40px;">= 3 means all reactions emitting 3 or less particles are exclusive the rest are inclusive (lumped into MT=5)</p>
<b>RECOIL</b>	<p>Controls calculation of recoils,</p> <p>= 0 recoils are not calculated (default if ENDF = 0, no ENDF formatting)</p> <p>= 1 recoils are calculated (default if ENDF &gt; 0, ENDF formatting)</p> <p>If keyword ENDF=0 is given in the input, then recoils are not calculated independently of the keyword RECOIL.</p>
<b>PRGAMM</b>	<p>Controls calculation of primary gammas</p> <p>= 0 Primary gammas are not printed (default)</p> <p>&gt; 1 Primary gammas are printed</p> <p>If keyword ENDF=0 is given in the input, then primary gammas are not printed independently of the keyword PRGAMM.</p>
<b>GAMPRN</b>	<p>Controls printing of gamma production cross sections (n,xng)</p> <p>= 0 Gamma production cross sections are not printed (default)</p> <p>&gt; 0 Gamma production cross sections files and plots are produced.</p>
<b>HRTW</b>	<p>Controls HRTW calculations (width fluctuation correction)</p> <p>= 0 no HRTW</p> <p>&gt; 0 HRTW width fluctuation correction up to the energy set by VAL.</p>



<b>FISSPE</b>	Controls calculation of prompt fission neutron spectra (PFNS). = 0 PFNS are not calculated (default) = 1 PFNS are calculated using Los Alamos model [135] = 2 PFNS are calculated using Kornilov parameterization [137]
<b>CNANGD</b>	Controls calculation of CN angular distribution. = 0 Compound nucleus (CN) angular distribution assumed isotropic (default) > 0 Compound nucleus (CN) angular distribution assumed anisotropic; collective levels must be present and DIRECT > 0.
<b>INTERF</b>	Controls calculation of interference effects between direct and compound decay. = 0 Compound nucleus (CN) and direct cross section are added incoherently (default) = 1 Compound nucleus (CN) and direct interference considered by Engelbrecht-Weidenmuller transformation (see Phys.Rev. C8(1973)859-862). Collective levels must be present and DIRECT > 0.
<b>FISSPE</b>	Controls calculation of prompt fission neutron spectra (PFNS). = 0 PFNS are not calculated (default) = 1 PFNS are calculated using Los Alamos model [135] = 2 PFNS are calculated using Kornilov parameterization [137]
<b>BENCHM</b>	Controls if benchmark calculation is requested. = 0 no benchmark calculation (default), > 0 benchmark calculation requested. Energies do not need to be in increasing order.
<b>KALMAN</b>	Controls calculation of a sensitivity matrix, = 0 no sensitivity matrix calculations (default), = 1 sensitivity matrix is calculated.
<b>RANDOM</b>	Controls randomization of input parameters that were input with uncertainty = 0 no random sampling is allowed (default) > 0 random sampling based on normal (Gaussian) distribution with the given 1-sigma parameter uncertainty

< 0 random sampling based on uniform distribution with the given 1-sigma parameter uncertainty

**ISOMER** The minimum isomer half life (in seconds) set to VAL  
This keyword defines minimum half-life of the state to be considered an isomer (default 1. = 1 second)

## Output control

**IOUT** Main output control set to VAL

- = **1** input data and essential results (all cross sections) (default),
- = **2** as IOUT=1 plus fusion spin distribution, yrast state population,  $\gamma$ -transition parameters, fusion barrier, inclusive spectra,
- = **3** as IOUT=2 +  $\gamma$  and particle spectra + discrete levels' decay + double differential cross sections (if MSD>0),
- = **4** as IOUT=2 + ORION output + residual nuclei continuum population (up to spin 12),
- = **5** as IOUT=2 + ORION output + transmission coefficients (up to l=12),
- = **6** as IOUT=2 + ORION output + level densities (up to spin 12). Should be used to get ZVV level density plots.

**NOUT** MSC calculation output control set to VAL (default: 0).

## Optical Model Potential

**OMPOT** Selects optical model parameters for outgoing particle

The value of I1 selects the outgoing particle as follows:

- =1 neutrons,
- =2 protons,
- =3 alphas,
- =4 deuterons,
- =5 tritons,
- =6 He-3;

VAL must be set to a RIPL catalog number (e.g. 2408 for Capote et al OMP) of the potential as it appears in the empire/RIPL/optical/om-data/om-index.txt file or in Help => 'RIPL omp' when using GUI. For backward compatibility this number can be entered with a negative sign.

<b>DIRPOT</b>	Optical model parameters to be used in DWBA or coupled-channels calculations by ECIS/OPTMAN codes. Parameters are the same as above, except that I1 need not be specified (always refers to the incident channel).
<b>RELKIN</b>	Override the RIPL defined kinematics used in a given optical model potential, = 0 classical (default), = 1 relativistic.
<b>TRGLEV</b>	Excited level of the target is set to VAL (e.g., VAL=3 for the 2 <sup>nd</sup> excited state; default: 1 (ground state)).
<b>UOMPab</b>	<p>Uncertainty of the parameters defining the potential strength of the optical model potential. The letter a can be V (real potential strength) or W (imaginary potential strength). The letter b can be V (volume) or S(surface). Thus the combinations VV (real volume), WV (imaginary volume), and WS (imaginary surface) specify 3 different terms in the RIPL optical potential described in Refs. [35, 145]. The combination VS is not allowed, as parameters of the real surface potential (VS) are usually not used in deriving phenomenological potentials. The exception is for dispersive potentials, but in this case the VS uncertainty is fully determined by the uncertainty of the imaginary surface potential (WS). The uncertainty of the spin-orbit potential is also not considered as its influence on calculated cross sections is small.</p> <p>The relative uncertainty in % of the corresponding parameter (defined by letters <i>a</i> and <i>b</i>) is given by VAL, target's Z and A numbers are defined by I1 and I2, respectively. I3 defines the outgoing particle, i.e., the incident particle for the inverse reaction (I3=1 for neutron, I3=2 for protons, etc). Some examples of potential strength uncertainties are given below.</p> <pre> * The three lines below define 1.5% uncertainty of the real * volume potential strength and 10% uncertainty of the real * and imaginary surface potential strength for neutron and * proton emission channels from the 56-Mn compound nucleus UOMPVV  1.50000  25    55    1 UOMPWV  10.0000  25    55    1 UOMPWS  10.0000  25    55    1 * The same for the proton emission channel UOMPVV  1.50000  24    55    2 UOMPWV  2.5000   24    55    2 UOMPWS  10.0000  24    55    2 </pre>
<b>UOMPcd</b>	Defines the uncertainty of the geometry component of the optical model potential. The letter c can be R (radius) or A (diffuseness). The letter d

can be V (real volume), W (imaginary volume) or S (imaginary surface). Thus the following six combinations are possible: RV and AV (real volume radius and diffuseness), RW and AW (imaginary volume radius and diffuseness), and RS and AS (surface radius and diffuseness).

The relative uncertainty of the corresponding parameter (defined by letters c and d) is given by VAL (in percent), target's Z and A are defined by I1 and I2, respectively. I3 defines the outgoing particle, i.e. the incident particle for the inverse reaction (I3=1 for neutron, I3=2 for protons, etc). It is recommended to avoid variations of potential strength (e.g. VV,WV) and corresponding potential radius (e.g. RV, RW) in the same run, as those parameters are strongly correlated within the optical model. Some examples of geometry uncertainties of the optical model parameters are given below.

```
* The two lines below define 1.5% uncertainty of the
* imaginary volume radius, and 2.5% uncertainty of the
* imaginary volume diffuseness for a neutrons incident
* on 55Mn nucleus
UOMPRW  1.50000  25    55    1
UOMPAW  2.5000  25    55    1
* The same for the proton emission channel
* corresponding to the surface potential.
UOMPRS  1.50000  24    55    2
UOMPAS  2.5000  24    55    2
```

## Scattering on collective levels

EMPIRE includes two coupled-channels codes: ECIS and OPTMAN[7, 8, 9]. ECIS is the default optical model solver, but OPTMAN should be used for selected potentials, when soft-rotor couplings are desired, as well as for actinide potentials that couple levels beyond the ground state rotational band.

**DIRECT** Controls use of coupled-channel calculations (ECIS and OPTMAN)

**=0** spherical OM used (default)

**=1** Coupled Channel (CC) method used for calculation of inelastic scattering to collective levels in the incident channel. If a selected OM potential is of CC type, the elastic and reaction cross sections are also taken from ECIS/OPTMAN calculations. Otherwise, spherical OM results are used. Transmission coefficients for all outgoing channels are calculated with spherical OM.

- =2** as above but transmission coefficients for the inelastic outgoing channels are calculated within Coupled Channel approach (longer calculation time).
- =3** as DIRECT=1 but DWBA is used instead of CC for calculation of inelastic scattering to collective levels in the incident channel. All transmission coefficients calculated with spherical OM.

NOTE: OM potential to be used by ECIS/OPTMAN might be different from the one used in the rest of the calculations and can be specified with the DIRPOT option.

**CALCTL** Controls use of calculated transmission coefficients for both projectile and ejectiles.

- = 0** Transmission coefficients calculated during the first run are stored, and reused in subsequent EMPIRE runs (default),
- > 0** Transmission coefficients are calculated for each run even if they were calculated before and respective files exist. This option is useful to calculate some quantities that are only used if TL are not already present (e.g. Bass fusion barrier in HI induced reactions).  
NOTE: this option slows down the execution of the code in subsequent runs by up to a factor of 10 (additional time is needed to calculate TLs again; reading them is much faster).

**EcDWBA** Automatically selects all discrete levels to be used in DWBA calculations for uncoupled collective levels.  
The default cut-off energy is  $3 * 30/A^{2/3}$ , and the default maximum spin 4. With these defaults all levels ( $J < 5$ ) with excitation energy less than 2.4 MeV for  $^{238}\text{U}$ , and less than 6.2 MeV for  $^{56}\text{Fe}$  are considered.  
The default selection rules could be modified by the VAL parameter that redefines the cut-off energy, and the parameter I1 that sets the maximum spin.

**RESOLF** Energy resolution in MeV used to spread calculated collective cross sections in the continuum set to VAL.  
This parameter is used if there are collective levels (in the \*-lev.col file) that are located in the continuum (see the *cont* flag). The scattering cross sections on these levels will be calculated by DWBA (if keyword DIRECT > 0).

**DEFNUC** Deformation of the target nucleus set to VAL.  
The threshold value to assume that the nucleus is deformed is 0.1 If you

want to force the assumption of sphericity for a given nucleus you can use this parameter with a value less than 0.1 this parameter also affects the deformation used in MSD calculations.

**ECONT** The energy continuum for the nucleus with Z=I1 and A=I2 starts at energy given by VAL in MeV.  
This parameter overwrites the continuum cut-off energy defined in the default RIPL levels for a given nucleus (or even the value given in the local LEVELS file). If not nucleus is given, then the value is ignored.

## Scaling parameters correcting for model deficiencies

These parameters are non-physical parameters designed to be used in nuclear data evaluation to correct for reaction model deficiencies, and to define model parameters' uncertainties. They are also used for covariance calculations by providing a straightforward way to calculate sensitivities (required as input for KALMAN), and to allow for random sampling of model parameters within defined uncertainties (required for Monte Carlo generation of theoretical model covariances).

**TUNE** The equilibrium decay width  $\Gamma_i^{EQ}$  of the ejectile  $i$  given by I3, for the nucleus with Z=I1 and A=I2 will be multiplied by VAL.  
Estimated relative uncertainty in % of this parameter can be given by I4.

**TUNEFI** The fission decay width  $\Gamma_F$  will be multiplied by VAL for the nucleus with Z=I1 and A=I2.  
Estimated uncertainty of this parameter can be given by I3.

**TUNEPE** The preequilibrium decay width  $\Gamma_i$  of the ejectile  $i$  given by I1 will be multiplied by VAL. It applies only to the PE decay from the compound nucleus calculated by PCROSS (exciton model), input keyword PCROSS > 0.  
Estimated relative uncertainty in % of this parameter can be given by I2.

**PFNNIU** Used in prompt fission neutron (PFN) calculations. The evaluated total prompt neutron multiplicity  $\tilde{\nu}$  (read from NUBAR-EVAL.ENDF) will be multiplied by VAL (default: 1.). The relative uncertainty of the scaling factor in % could be given by I1.

**PFNTKE** Used in prompt fission neutron (PFN) calculations. The total kinetic energy (TKE) of the fission fragments will be multiplied by VAL (default: 1.). The TKE enters the energy balance equation defining the total excitation energy of the fissioning system  $U_{exc} = E_{rel} - TKE + E_{incid} + B_n$ . This parameter could be interpreted as the uncertainty of the measured

fission kinetic energy.

The relative uncertainty of the scaling factor in % could be given by I1.

#### PFNALP

Used in prompt fission neutron (PFN) calculations. The default parameter  $\alpha$  ( $\alpha_0 = 1$  for Madland-Nix (LA) model [135] and  $\alpha_0 = 0.9$  for Kornilov parameterization [137]) will be multiplied by VAL (default: 1.). The values  $E_f^L$  and  $E_f^H$  of the average kinetic energy per nucleon of the average light fragment AL and average heavy fragment AH are scaled by  $\alpha$ . The effect of this parameter on PFNS calculations is strongly correlated with TKE (see keyword PFNTKE above). // Physically, this parameter allows for a reduction of the kinetic energy of the fragment due to neutron emission during Coulomb acceleration.

The relative uncertainty of the scaling factor in % could be given by I1.

#### PFNRAT

Used in prompt fission neutron (PFN) calculations. The default parameter  $r = T_f^L/T_f^H$  ( $r_0 = 1$  for Madland-Nix (LA) model [135] and  $r_0 = 1.248$  for Kornilov parameterization [137]) will be multiplied by VAL (default: 1.). This parameter defines the ratio of temperatures of the light to heavy fragment. Experimental evidence strongly supports 20% higher temperature of the light fragment.

The relative uncertainty of the scaling factor in % could be given by I1.

#### PFNERE

Used in prompt fission neutron (PFN) calculations. The total fission energy release ( $E_{rel}$ ) will be multiplied by VAL (default: 1.). The  $E_{rel}$  enters the energy balance equation defining the total excitation energy of the fissioning system  $U_{exc} = E_{rel} - TKE + E_{incid} + B_n$ . The relative uncertainty of the scaling factor in % could be given by I1.

#### TMAXW

Used in prompt fission neutron (PFN) calculations. PFNS plots are scaled by a Maxwellian function with  $T = VAL$  (default: 1.32) MeV.

#### DEFSTA

The static deformation needed in rigid-rotor CC calculations will be multiplied by VAL (default: 1.).

The relative uncertainty of the scaling factor in % could be given by I1. It is recommended not to vary dynamical deformation above 10 MeV (i.e. set its uncertainty to zero) to avoid numerical instabilities.

#### DEFDYN

Dynamical deformations of uncoupled levels for DWBA calculations will be multiplied by VAL (default: 1.).

Dynamical deformations are listed for all collective levels in the collective file (\*-col.lev).

The relative uncertainty of the scaling factor in % could be given by I1.

It is recommended not to vary dynamical deformation above 10 MeV (i.e. set its uncertainty to zero) to avoid numerical instabilities.

- ELARED** The shape elastic cross section will be multiplied by VAL (default: 1.). The change is also reflected in the total cross section. The relative uncertainty of the scaling factor in % could be given by I1.
- FUSRED** The fusion (reaction) cross section will be multiplied by VAL (default: 1.). The change is also reflected in the total cross section. The relative uncertainty of the scaling factor in % could be given by I1.
- FCCRED** The calculated direct cross section for discrete collective levels will be multiplied by VAL (default: 1.). Cross sections of both coupled and uncoupled discrete levels are scaled. The uncertainty of the scaling factor in % could be given by I1. It has no effect if DIRECT keyword is set to zero in the input (default).
- FCORED** The DWBA calculated direct cross section for collective levels in the continuum will be multiplied by VAL (default: 1.). Giant multipole resonances are also scaled if specified in the collective level file (flagged with negative deformation). The uncertainty of the scaling factor in % could be given by I1. It has no effect if DIRECT keyword is set to zero in the input (default). A value of zero could be used to suppress DWBA collective levels in the continuum, without recalculating the transmission coefficients (TLs).
- TOTRED** The total cross section will be multiplied by VAL (default: 1.). The relative uncertainty of the scaling factor in % can be given by I1. TOTRED is applied through other scaling factors, namely ELARED, FUSRED, FCCRED and FCORED. If those factors are present, then the final scaling will be a product of them (e.g., if both TOTRED and FUSRED are specified, then the fusion (reaction) cross section will be multiplied by FUSRED\*TOTRED. This parameter is recommended to be used to correct small deficiencies (3%) of your optical model calculated total cross sections. It is not recommended to be used for simulation of the experimental fluctuations of total cross section.
- CELRED** The compound elastic cross section will be multiplied by VAL (default: 1.). The relative uncertainty of the scaling factor in % can be given by I1. This parameter may be used to simulate the CN resonances (obviously not included in the optical model), or to simulate physical effects arising from



the compound-direct processes interference (Engelbrecht-Weidenmuller transformation). The interference increases the compound inelastic cross sections, reducing others compound channels (incl. the compound elastic). If you use CELRED and CINRED at the same energy please note that some interference will result as they affect the same quantities.

- CINRED** The compound inelastic cross section to discrete levels will be multiplied by VAL (default: 1.).  
 The discrete level number can be given by I1.  
 The relative uncertainty of the scaling factor in % can be given by I2.  
 This parameter may be used to simulate physical effects arising from the compound-direct processes interference (Engelbrecht-Weidenmuller transformation). The interference increases the compound inelastic cross sections, reducing others compound channels (incl. the compound elastic).
- DXSRED** The calculated deuteron pick-up/stripping cross section for incident deuteron on the target nucleus will be multiplied by VAL). It has no effect on other incident particles.
- > 0 deuteron pick-up/stripping parameterization of Kalbach used for incident deuterons (default: 1.),  
 = 0 deuteron pick-up/stripping suppressed.

## Optical model fitting

- FITOMP** Controls fitting of optical model potential in the incident channel,
- =0 No fit (default)  
 =1 GUI assisted manual fitting; independently of what is specified in the input only total, elastic, capture and inelastic scattering are calculated. If plots with 'List names' ompR1 and eventually ompR2 are set they will be updated and reproduced after each run.  
 =2 Automatic fit. See default EMPIRE input (../scripts/skel.inp) or the description of the parameter FITabc below for keywords to be placed in the input.
- FITabc** Selects an optical model parameter for adjustment. The letter a can be R (real) or I (imaginary) and the letter b can be V (volume), S (surface) or O (spin-orbit). Thus the combinations RV, IV, RS, IS, RO and IO specify the 6 different terms in the RIPL optical potential described in Refs. [35, 145]. The letter c can be V (potential strength), R (radius) or D (diffuseness). The initial shift in the parameter is given by VAL and

the maximum allowed variation is given by  $0.01 \cdot I1$ .  $I2$  specifies which of the parameters in the potential strength, radius or diffuseness is to be adjusted.

Some examples are given below.

FITRVV	0.	500	1	!fit real volume depth (+- 5 MeV)
FITIVV	0.	100	1	!fit imag. volume depth (+- 1 MeV)
FITISV	0.	100	1	!fit imag. surface depth (+- 1 MeV)
FITVR	0.	10	1	!fit real volume radius (+- 0.1 fm)
FITIVR	0.	10	1	!fit imag. volume radius (+- 0.1 fm)
FITRVD	0.	10	1	!fit real volume diffus. (+- 0.1 fm)
FITISD	0.	5	1	!fit imag. surf. diffus. (+- 0.05 fm)

**FITDEF** Selects the deformation parameter of multipole  $I2$  for adjustment. The initial shift in the parameter is given by VAL and the maximum allowed variation is given by  $0.01 \cdot I1$ . The value of  $I2$  can be 2 or 4 for rotational nuclei and 2 or 3 for vibrational nuclei, e.g.,

FITDEF	0.	10	2	!fit l=2 (quadrupol) defor. (+- 0.1)
--------	----	----	---	--------------------------------------

**FITWT** Multiplies weights of experimental data of type MF= $I1$  and MT= $I2$  in  $\chi^2$  by VAL.

**FITWT0** Multiplies weights of natural element experimental data in  $\chi^2$  by VAL.

**FITITR** Sets the number of iterations in the gradient  $\chi^2$  minimization to VAL=maxitr+0.01\*itmax, where maxitr is the number of times the gradient is calculated and itmax is the number of iterations along each gradient (default is 3.05).

**FITEMX** Maximum incident energy of experimental data used in fitting set to VAL (default is 30 MeV).

**FITGRD** Defines the initial grid of incident energies of nuclear model calculations used to obtain  $\chi^2$ . When set, the first interval is VAL, the second VAL+0.001\* $I1$ , the third VAL+0.002\* $I1$ , etc. (The default incident energy grid is the one given in the input file.)

## Fusion

These input parameters are typically used for heavy ion induced reactions.

<b>CSREAD</b>	Controls HI fusion cross section determination, $> 0$ HI fusion cross section is set to VAL [in mb], $= -1$ distributed barrier model used , $= -2$ simplified coupled-channel treatment CCFUS-code (default for HI). Note: CSREAD has no effect if <i>.fus</i> file ( <i>FUSION</i> in manual mode) exists.
<b>BFUS</b>	Fusion barrier height in the distributed barrier model (Eq. 1.2) set to VAL (default: $B_{fus}$ calculated by CCFUS).
<b>SIG</b>	SIGMA in the distributed barrier model (Eq. 1.2) set to VAL (default: $0.05B_{fus}$ ).
<b>TRUNC</b>	Truncation in the distributed barrier model (Eq. 1.2) set to VAL (default: 2.).
<b>EXPUSH</b>	Extra-push energy set to VAL (default: 0.).
<b>CRL</b>	Critical $l$ -value for HI fusion (Eq. 1.5) set to VAL (default: 0).
<b>DFUS</b>	Diffuseness in the transmission coefficients for HI fusion (Eq. 1.5) set to VAL (default: 1.).

## Photo-absorption

<b>E1</b>	$= 0$ E1 photo-absorption blocked $= 1$ E1 photo-absorption selected
<b>M1</b>	$= 0$ M1 photo-absorption blocked $= 1$ M1 photo-absorption selected
<b>E2</b>	$= 0$ E2 photo-absorption blocked $= 1$ E2 photo-absorption selected
<b>QD</b>	Quasideuteron photo-absorption cross section normalized by a factor VAL

## CCFUS input

CCFUS code provides a simplified coupled-channel treatment to obtain the reaction cross section in near-barrier heavy ion reactions. It is not recommended for reactions with light incident particles ( $A < 5$ ).

<b>DV</b>	DV barrier parameter in CCFUS set to VAL. This parameter can be used to adjust the fusion barrier. Typical range for changes $-10 < DV < 10$ . (default: 10).
<b>FCC</b>	FCC parameter in CCFUS set to VAL  <b>=0</b> diagonalization of the coupling is performed at the barrier position $r_b$ , <b>=1</b> exponential character of the form factor is taken into account. A second order estimation of the position and height of the effective barriers is carried out within a one-Fermi distance from $r_b$ . This option is recommended for strong coupling (default).
<b>NSCC</b>	Number of inelastic surface channels in CCFUS set to VAL (default: 4).
<b>NACC</b>	Number of additional channels set to VAL (default: 0).
<b>BETCC</b>	Deformation of the $I2^{th}$ collective mode set to VAL.
<b>FLAM</b>	Multi-polarity of the $I2$ -th collective mode set to VAL (entered with positive sign for target modes and negative sign for projectile modes) (default: 2, 3, -2, -3, needs NSCC numbers).
<b>QCC</b>	Q-value of the $I2^{th}$ collective channel set to VAL - excitation energy of the collective level adopted with a negative sign (default: - energies of the first 2+ and 3- levels in the target and the projectile).
<b>FCD</b>	Strength of the coupling at the barrier for $I2^{th}$ collective mode set to VAL. For FCC=1 the characteristic radial dependence of the one-particle transfer form factor is assumed. Used only if NACC > 0 (no default).

## Multi-step Direct

<b>MSD</b>	Controls Multi-step Direct calculations,  <b>= 0</b> no MSD calculations (default), <b>= 1</b> MSD calculations selected - ORION + TRISTAN will be executed, <b>= 2</b> MSD calculations selected including the MSD contribution to discrete levels. This option should be used with care if coupled channel optical model potentials are employed. Since MSD gives the vibration component of the direct cross section it sometimes it might be summed with the rotational CC contribution but summing it with the vibrational CC one would be an obvious double-counting.
------------	---

<b>MSDMIN</b>	The minimum energy to start MSD calculations set to VAL (default: 5.).
<b>DEFMSD</b>	Deformation $\beta_2$ of the Nilsson Hamiltonian set to VAL (default: 0.). The Nilsson hamiltonian is used to obtain single-particle levels employed in MSD calculations.
<b>WIDEX</b>	Experimental energy resolution set to VAL (default: 0.2).
<b>GAPP</b>	Proton pairing gap for target set to VAL (default: $12/\sqrt{A}$ ).
<b>GRANGP</b>	Energy window around the $E_F^p$ for proton pairing calculations for target set to VAL (default: 5.).
<b>GAPN</b>	Neutron pairing gap for target set to VAL (default: $12/\sqrt{A}$ ).
<b>GRANGN</b>	Energy window around the $E_F^n$ for neutron pairing calculations for target set to VAL (default: 5.).
<b>HOMEGA</b>	$\hbar\omega$ oscillator energy (default: $41.47/A^{1/3}$ MeV ).
<b>EFIT</b>	Coupling constants of multi-polarity I1 fitted to the level at energy VAL (defaults: -1 for $\lambda = 0$ , $E_{GDR}$ for $\lambda = 1$ , energies of the first low-lying 2+, 3-, and 4+ levels for $\lambda = 2, 3, 4$ , respectively).
<b>RESNOR</b>	Response function for multi-polarity I1 will be normalized by factor VAL (default: 1).
<b>ALS</b>	spin-orbit coupling strength in the harmonic oscillator (default: 1.5).

## Multi-step Compound

<b>MSC</b>	Controls Multi-step Compound calculations, = 0 no MSC calculations (default), = 1 MSC calculations selected.
<b>XNI</b>	Initial exciton number set to VAL (default set internally depending on the case, 3 for nucleon induced reactions).
<b>GDIV</b>	Single particle level densities in preequilibrium models (MSC, DTRANS, PCROSS) set to A/VAL (default: 13.0).
<b>TORY</b>	Ratio of unlike to like nucleon-nucleon interaction cross section set to VAL. Used for the determination of the relative share between neutron and protons in the exciton configurations (default: 4.).

<b>EX1</b>	Initial number of excitons that are neutrons set to VAL (default set internally depending on the case and on TORY).
<b>EX2</b>	Initial number of excitons that are protons set to VAL (default set internally depending on the case and on TORY).
<b>D1FRA</b>	Ratio of the spreading GDR width to the total GDR width set to VAL (default: 0.8).
<b>GST</b>	Controls $\gamma$ -emission in MSC, = 0 no $\gamma$ -emission in MSC (default), = 1 $\gamma$ -emission in MSC selected.
<b>STMRO</b>	=0 closed form $p$ - $h$ state densities selected (default)

## Monte Carlo pre-equilibrium model (HMS)

<b>HMS</b>	Controls Monte Carlo pre-equilibrium calculations, = 0 HMS disabled (default), = 1 HMS enabled.
<b>NHMS</b>	Number of events in HMS set to VAL
<b>CHMS</b>	Default damp rate in HMS multiplied by VAL
<b>FHMS</b>	Transition densities used in HMS set by VAL = 0 Exciton densities are used, = 1 Fermi gas densities are used, = 2 Exact NR Fermi gas densities are used, = 3 Exact rel. Fermi gas densities are used.

## PCROSS exciton model with Iwamoto-Harada cluster emission (PCROSS)

<b>PCROSS</b>	Controls calculations with PCROSS: = 0 PCROSS disabled (default) > 0 PCROSS enabled with mean free path multiplier set to VAL. VAL must be greater than 0.5 and lower than 3. Estimated relative uncertainty in % of this parameter can be given by I1.
---------------	---

<b>PEDISC</b>	Controls how discrete levels are treated in PCROSS: = 0 Preequilibrium contribution to discrete levels neglected (default). > 0 Preequilibrium contribution to discrete levels considered.
<b>PESPIN</b>	Controls how preequilibrium spin cut-off parameter is calculated in the exciton model (PCROSS): = 0 Exciton model spin cut-off parameter taken as $2 \cdot 0.26 \cdot A^{2/3}$ (default). This is equivalent to the assumption that spin-distribution is equal to the spin-distribution of the $n=2$ ( $p=h=1$ ) exciton states independent of the emission energy and of the exciton number $n$ . > 0 Exciton model spin cut-off parameter taken as $(p+h) \cdot 0.26 \cdot A^{2/3}$ (default). This produces higher-spin states at lower emission energies, changing the spin-distribution of the pre-equilibrium emission. If MSD model is active, then PESPIN is reset to the default value of zero.
<b>PEPAIR</b>	Controls how pairing is treated in PCROSS. > 0 Pairing corrections included in PCROSS calculations (default). = 0 Pairing corrections not considered in PCROSS calculations.
<b>GTILNO</b>	Single particle level density parameter $g$ (in PCROSS) multiplied by VAL for the nucleus with $Z=I1$ and $A=I2$ . Estimated relative uncertainty in % of this parameter can be given by I3.
<b>MAXHOL</b>	Coefficient defining the equilibrium exciton number (in PCROSS) given by VAL. VAL must be greater than 0.1 and lower than 1.5 (Default coefficient 0.54). If the coefficient is bigger than 0.54 means that the preequilibrium contribution is bigger, as contribution from higher exciton states will be considered. Coefficient lower than 0.54 will produce smaller preequilibrium contribution.

## Selection of Level density model

<b>LEV DEN</b>	Selects level density approach, = 0 EMPIRE-specific level densities, adjusted to RIPL-3 experimental $D_{obs}$ and to discrete levels (default), = 1 Generalized Superfluid Model (GSM, Ignatyuk et al), adjusted to RIPL experimental $D_{obs}$ and to discrete levels,
----------------	--

- = **2** Gilbert-Cameron level densities (parametrized by Ijnov et al), , adjusted to RIPL experimental  $D_{obs}$  and to discrete levels,
- = **3** RIPL-3 microscopic HFB level densities.

**FITLEV** Option for adjusting range of discrete levels used in the calculations. Plots of cumulative number of discrete levels along with the integrated level densities are created and calculations stop at this point.

- > 0 cumulative plots of discrete levels will be displayed. If LEVDEN=0 the energy range of the plot will extend VAL MeV above the last discrete level,
- = **0** no cumulative plots (default).

**LDSHIF** Excitation energy shift in the BCS region set to VAL for the nucleus with Z=I1 and A=I2 (default 1.).  
The input value is being reduced by 1, allowing for positive or negative energy shift. The default value of 1 means that the resulting energy shift is zero.  
This parameter is applicable for GSM type of LD models (LEVDEN < 2).

**ATILNO** Value of the level density parameter  $\tilde{a}$  will be multiplied by VAL for the nucleus with Z=I1 and A=I2. Estimated relative uncertainty in % of this parameter can be given by I3.  
This parameter is applicable if keyword LEVDEN < 3 (i.e. for all level density models but HFB).

## Gilbert and Cameron level density model

- GCROA** Level density parameter  $a$  in Gilbert-Cameron approach  
 > 0 parameter  $a$  in nucleus Z=I1, A=I2 set to VAL ,  
 = 0 parameter  $a$  in all nuclei according to Ignatyuk systematics,  
 = -1 parameter  $a$  in all nuclei according to Arthur systematics,  
 = -2 parameter  $a$  in all nuclei according to Ilijnov systematics (default).
- GCROUX** Level density parameter  $U_x$  in Gilbert-Cameron approach for nucleus Z=I1, A=I2 set to VAL (default calculated internally).
- GCROD** Pairing shift  $\Delta$  in Gilbert-Cameron approach for nucleus Z=I1, A=I2 set to VAL (default determined internally according to Gilbert-Cameron table, for  $Z > 98$  and/or  $N > 150$   $\Delta = 12/\sqrt{A}$  is taken).



<b>GCROE0</b>	Level density parameter $E_0$ in Gilbert-Cameron approach for nucleus $Z=I1$ , $A=I2$ set to VAL (default calculated internally).
<b>GCROT</b>	Level density parameter $T$ in Gilbert-Cameron approach for nucleus $Z=I1$ , $A=I2$ set to VAL (default calculated internally).

## RIPL-3 HFB level density model

<b>ROHFBP</b>	HFB pairing-like parameter to shift in energy numerical HFB level densities for nucleus $Z=I1$ , $A=I2$ set to VAL. Default is taken from the internal file ( <i>empire/RIPL/densities/total/level-densities-hfb/xxxx.cor</i> ) estimated in RIPL-3. This value is overwritten by ROHFBP thus the change in the calculations is with respect to the zero-shift case rather than to the default calculations. Estimated uncertainty of this parameter can be given by I3.
<b>ROHFBA</b>	HFB pseudo $a$ parameter to adjust numerical HFB level densities for nucleus $Z=I1$ , $A=I2$ set to VAL. Tabulated HFB level densities are multiplied by the factor $\exp(ROHFBA)\sqrt{(U)}$ , which is proportional to the dominant energy dependence of the Fermi gas level densities. Positive values of ROHFBA increase level densities while negative decrease them. The default value is taken from the RIPL-3 file ( <i>empire/RIPL/densities/total/level-densities-hfb/xxxx.cor</i> ). ROHFBA overwrites the default thus the change in the calculations is with respect to the no-adjusted case rather than to the default calculations that use default adjustment if available in the <i>xxxx.cor</i> file. Estimated uncertainty of this parameter can be given by I3.

## Fission

<b>FISSHI</b>	Controls treatment of the fission channel for nucleus $Z=I1$ , $A=I2$  = <b>0</b> advanced low-energy fission treatment with multi-humped barriers. Recommended for light particle or photon induced fission (default). = <b>1</b> high energy fission over single-humped barrier with dynamical effects. Recommended for heavy ion reactions when fission channel is important. = <b>2</b> fission ignored.
---------------	--

**The following options are valid only when FISSHI = 0**

<b>FISBAR</b>	Controls origin of fission barrier data for nucleus $Z=I1, A=I2$
---------------	--

	<p>= <b>0</b> internal EMPIRE fission barrier library (/data/EMPIRE-fisbar)</p> <p>= <b>1</b> RIPL-3 empirical fission barriers (/RIPL/fission/empirical-barriers.dat) (default)</p> <p>= <b>2</b> Parabolic approximation derived from numerical RIPL-3 HFB barriers (/RIPL/fission/HFB-parab-fisbar.dat)</p> <p>= <b>3</b> One-dimensional non-parabolic numerical RIPL-3 HFB barriers (/RIPL/fission/HFB2007/z0xx.dat, <math>79 &lt; xx &lt; 99</math>)</p>
<b>FISDEN</b>	<p>Controls level densities at saddle points for nucleus <math>Z=I1</math>, <math>A=I2</math></p> <p>= 0 EGSM (low K limit)</p> <p>= 3 HFB microscopic calculations</p>
<b>FISOPT</b>	<p>Controls subbarrier effects for nucleus <math>Z=I1</math>, <math>A=I2</math></p> <p>= 0 no subbarrier effects</p> <p>= 1 subbarrier effects considered</p> <p>= 2 subbarrier effects considered including isomeric fission and gamma emission inside the wells (under development)</p> <p>= 3 the same as 2; but the phases are calculated assuming the barrier (or well) is represented by uncoupled parabola (under development)</p>
<b>FISDIS</b>	<p>Controls discrete transitional states</p> <p>= 0 no discrete states above fission barrier for nucleus <math>Z=I1</math>, <math>A=I2</math></p> <p>= 1 discrete states above fission barrier for nucleus <math>Z=I1</math>, <math>A=I2</math></p>
<b>FISMOD</b>	<p>Controls multi-modality of fission for nucleus <math>Z=I1</math>, <math>A=I2</math></p> <p>= 0 single-modal fission</p> <p>= 1 multimodal fission (2 modes)</p> <p>= 2 multimodal fission (3 modes)</p>
<b>FISATn</b>	<p>The fission level-density parameter <math>\tilde{a}_F</math> at the saddle point <math>n</math> will be multiplied by VAL for the nucleus with <math>Z=I1</math> and <math>A=I2</math> (default 1.).</p> <p>The letter n take values 1,2,3 according to the barrier number. Estimated uncertainty of the level density parameter at saddle <math>n</math> can be given by I3.</p>
<b>FISVEN</b>	<p>The vibrational enhancement parameter of fission level-density at the saddle point <math>n</math> will be multiplied by VAL for the nucleus with <math>Z=I1</math> and <math>A=I2</math> (default 1.).</p> <p>The letter n take values 1,2,3 according to the barrier number. Estimated uncertainty of the vibrational enhancement parameter at saddle <math>n</math> can be given by I3.</p>

<b>FISDLn</b>	<p>The fission level density at the saddle point <math>n</math> will be shifted by VAL for the nucleus with <math>Z=I1</math> and <math>A=I2</math> (default 1.).</p> <p>The letter <math>n</math> take values 1,2,3 according to the barrier number. Estimated uncertainty of the fission pairing parameter <math>DEL</math> at saddle <math>n</math> can be given by I3.</p>
<b>FISVFn</b>	<p>The height of the fission barrier <math>n</math> will be multiplied by VAL for the nucleus with <math>Z=I1</math> and <math>A=I2</math> (default 1.).</p> <p>The letter <math>n</math> take values 1,2,3 according to the barrier number. Estimated uncertainty of the barrier height can be given by I3.</p>
<b>FISHOn</b>	<p>The width of the fission barrier <math>n</math> will be multiplied by VAL for the nucleus with <math>Z=I1</math> and <math>A=I2</math> (default 1.).</p> <p>The letter <math>n</math> take values 1,2,3 according to the barrier number. Estimated uncertainty of the barrier width can be given by I3.</p>
<b>FISTGA</b>	<p>Gamma transition probability for the isomeric gamma cascade in the second well.</p> <p><b>The following options are valid only when FISSHI = 1</b></p>
<b>QFIS</b>	Liquid drop fission barriers multiplied by VAL (default: 1).
<b>BETAV</b>	Viscosity parameter in Eqs. 4.181, 4.182 and 4.183 set to VAL ( $10^{-21}s^{-1}$ ) (default: 4).
<b>SHRJ</b>	Shell correction to fission barrier damped (Eq. 4.180) to 1/2 at spin VAL (default: 24).
<b>SHRD</b>	Diffuseness of the shell correction damping (Eq. 4.180) set to VAL (default: 2.5).
<b>TEMPO</b>	Temperature at which shell correction fade-out (Eq. 4.179) space starts set to VAL (default: 1.65).
<b>SHRT</b>	Parameter in the temperature shell correction fade-out (Eq. 4.179) set to VAL (default: 1.066).
<b>DEFGA</b>	$d$ (amplitude) in the Gaussian term of Eq. 4.180 set to VAL (default: 0. - no correction).
<b>DEFGW</b>	$\Delta J_G$ (width) in the Gaussian term of Eq. 4.180 set to VAL (default: 10).
<b>DEFGP</b>	$J_G$ (position) in the Gaussian term of Eq. 4.180 set to VAL (default: 40).

## Gamma-ray strength functions

<b>GSTRFN</b>	Controls modeling of the $\gamma$ -ray strength function = 0 EGLO enhanced generalized Lorentzian (Uhl-Kopecki) as in 2.18 and earlier = 1 MLO1 modified Lorentzian version 1 (Plujko, RIPL) (default) = 2 MLO2 modified Lorentzian version 2 (Plujko, RIPL) = 3 MLO3 modified Lorentzian version 3 (Plujko, RIPL) = 4 EGLO enhanced generalized Lorentzian (RIPL) = 5 GFL (Mughabghab) = 6 SLO standard Lorentzian
<b>WEDNOR</b>	Weisskopf single particle estimates for E1 $\gamma$ transitions will be multiplied by VAL for the nucleus with Z=I1 and A=I2 (ATTENTION default: 0.01). In the table of GDR parameters in *.lst file this quantity is referred to as CE1.
<b>WEQNOR</b>	Weisskopf single particle estimates for E2 $\gamma$ transitions will be multiplied by VAL for the nucleus with Z=I1 and A=I2 (ATTENTION default: 0.1). In the table of GDR parameters in *.lst file this quantity is referred to as CE2.
<b>WEMNOR</b>	Weisskopf single particle estimates for M1 $\gamma$ transitions will be multiplied by VAL for the nucleus with Z=I1 and A=I2 (ATTENTION default: 0.1). In the table of GDR parameters in *.lst file this quantity is referred to as CM1.

## GDR parameters

<b>GDRGFL</b>	Selects source of GDR parameters = 0 Messina systematics = 1 experimental or systematics of RIPL (default)
<b>GDRDYN</b>	Controls GDR treatment, = 0 GDR shape depends on the ground state deformation (default), = 1 GDR shape dependence accounts for the rotation induced deformation (spin dependent, Eq. 4.84).
<b>EGDR1</b>	GDR energy of first peak set to VAL (default calculated internally from systematics).

<b>GGDR1</b>	GDR width of first peak set to VAL (default calculated internally from systematics).
<b>CSGDR1</b>	GDR cross section of first peak set to VAL (default calculated internally from systematics).
<b>EGDR2</b>	GDR energy of second peak set to VAL (default calculated internally from systematics).
<b>GGDR2</b>	GDR width of second peak set to VAL (default calculated internally from systematics).
<b>CSGDR2</b>	GDR cross section of second peak set to VAL (default calculated internally from systematics).
<b>GDRWP</b>	Factor $c$ in the energy increase of the GDR width (Eq. 4.117) set to VAL (default: 0.0026).
<b>GDRWA1</b>	GDR width of first peak increased by VAL (default: 0).
<b>GDRWA2</b>	GDR width of second peak increased by VAL (default: 0).
<b>GDRESH</b>	GDR position shifted by VAL (default: 0).
<b>GDRSPL</b>	Splitting of GDR peaks increased by VAL (default: 0).
<b>GDRST1</b>	GDR cross section of first peak multiplied by VAL (default: 1).
<b>GDRST2</b>	GDR cross section of second peak multiplied by VAL (default: 1).
<b>MIXGDR</b>	relative contributions of the GDR and Weisskopf estimates to the E1- $\gamma$ -strength set to $VAL \cdot GDR + (1 - VAL) \cdot Weiss$ . Note that the condition $0 \leq VAL \leq 1$ must be fulfilled (allowed from 0 to 1. default = 1 means pure GDR).
<b>MIXGMR</b>	relative contributions of the GDR and Weisskopf estimates to the M1- $\gamma$ -strength set to $VAL \cdot GDR + (1 - VAL) \cdot Weiss$ . Note that the condition $0 \leq VAL \leq 1$ must be fulfilled (allowed from 0 to 1. default = 1 means pure GMR).
<b>MIXGQR</b>	relative contributions of the GDR and Weisskopf estimates to the E2- $\gamma$ -strength set to $VAL \cdot GDR + (1 - VAL) \cdot Weiss$ . Note that the condition $0 \leq VAL \leq 1$ must be fulfilled (allowed from 0 to 1. default = 1 means pure GQR).

**GCASC** Controls calculation of the  $\gamma$ -cascade in the first compound nucleus  
 = 0 no  $\gamma$ -cascade (only primary transitions),  
 = 1 full  $\gamma$ -cascade (primary and secondary transitions)  
 (default: full  $\gamma$ -cascade in the first Compound Nucleus if the initial excitation energy is less or equal to 20 MeV, otherwise primary transitions only).

## Miscellaneous

**BNDG** Binding energy of ejectile I3 in nucleus Z=I1, A=I2 set to VAL (default calculated internally from RIPL nuclear masses).  
 Uncertainty of the binding energy in % may be given by I4.

**SFACT** The removal of the s-wave Coulomb barrier transmission probability and the 1/E dependence of the cross section.  
 = 1 outputs the S-factor for (x, $\gamma$ )  
 = 2 outputs the S-factor for (x,n)  
 = 3 outputs the S-factor for (x,p)

**SHELNO** Shell correction read from RIPL database will be multiplied by VAL for the nucleus with Z=I1 and A=I2.  
 Uncertainty of the shell correction value in % may be given by I4 (default 1.0).  
 The default value corresponds to the use of RIPL Myers-Swiatecki shell corrections assuming a negligible uncertainty.

**JSTAB** Rotation stability limit with respect to spin for the nucleus Z=I1 and A=I2,  
 = 0 spin at which fission barrier (incl. shell correction) disappears (default),  
 > 0 set to VAL.

# Appendix B

## Description of test cases

In EMPIRE-3.2 system there are two types of tests: benchmarks and test cases. The benchmarks (subdirectory *benchmarks*) are intended for the verification of the local installation, and most of them are single-energy calculations. About 15 benchmarks are currently included with the system. The test cases (subdirectory *test-cases*) are intended to contain real physical show cases, a few of them are provided. This directory will ideally expand in the future to include the best cases of successful applications of EMPIRE-3.2 submitted by users.





# Appendix C

## ChangeLog

### Changes in version 3.1 with respect to 2.19

Sao Jose dos Campos, June 2011

1. PREPRO2007 updated to PREPRO2010
2. Merging resonance parameters into the final ENDF file
3. GUI assisted OMP fitting
4. Prompt fission neutron spectra including post-fission neutrons emitted from fully accelerated fragments (Los Alamos or Kornilov model) (M. Sin, R. Capote)
5. DWBA calculations on odd nuclei (discrete levels embedded in the continuum only) (R. Capote)
6. ECIS subroutine modified to allow use of dispersive potentials with different geometry of the imaginary and real parts (R. Capote)
7. MSD-model extended to deformed nuclei (H. Wienke)
8. Recursive treatment of transmission through multi-hump fission barrier (M. Sin, R. Capote)
9. Library of neutron resonances updated to ENDF/B-VII.1
10. Library of nubar evaluations for most actinides from all major libraries included
11. Checking codes updated
12. Calculation, formatting and plotting of isomers
13. Options are partially implemented to use average radiation width, neutron width, and resonance spacing, to create fake resonance file (MF=2).

14. EXFOR library updated to January 2011 version
15. MySQL based EXFOR retrieval system moved to more robust FORTRAN implementation
16. Moments of inertia (spin distribution parameter) controlled from the input
17. Resonance module added
  - Parameters from Atlas of Neutron Resonances => MF2
  - Parameter uncertainties => MF32
  - Reproducing thermal cross section uncertainties
  - Inclusion of arbitrary correlations among gamma-widths and among neutron-widths
18. New parametrization of EGSM level densities (EGSM = Enhanced/EMPIRE Generalized Superfluid Model)
19. New fission model implemented (Phys. Rev. C 77 (2008) 054601)
20. RIPL-3 updates
  - Discrete levels library
  - Optical model parameters
  - Microscopic level densities (HFB) with parity dependence
21. ECIS-2006 implemented
22. OPTMAN implemented
23. Covariance generation capabilities using Monte Carlo approach or Kalman filter
24. Accounting for model uncertainties in covariance generation
25. Correlated sampling in Monte Carlo
26. Scaling factor in Kalman filter
27. Six ejectiles (n, p, alpha, g, d, t, 3He) + arbitrary light ion; includes ENDF-6 formatting (Capote, Trkov)
28. Upgrade of ZVView package with 2-D and 3-D plotting of covariance matrices (Zerkin)
29. DDHMS preequilibrium model extended to produce exclusive spectra
30. KERCEN code incorporated in the EMPIRE system (not linked through GUI)
31. Primary capture gammas isolated and printed separately

## Changes in version 2.19 with respect to 2.18

### Brookhaven, March 2005

1. Error in the Wilmore-Hodgson omp corrected. VOM(4, Nejc, Nnuc) set to -0.0018 instead of -0.00018. This coefficient was also found to be wrong in the preliminary version of RIPL-2 (M. Herman).
2. MSD is automatically turned off for non-nucleon incident reactions (M. Herman).
3. Internal conversion coefficients included in the gamma cascade between discrete levels (ICC data from RIPL)(M. Herman).
4. Bug in reading branching ratios from the RIPL file corrected (emission probabilities instead of branching ratios were used in the previous RIPL-2 versions) (R. Capote).
5. Bug in DEGAS resulting in lack of the preequilibrium population in the Compound Nucleus continuum corrected (bug has been introduced in version 2.18) (E. Betak).
6. ENDRES code and BNL-325 file with resonance parameters added in order to merge resonance parameters into the final ENDF file (also dxsend.f has been updated) (A. Trkov).
7. LINEAR and RECENT utility codes added in order to reconstruct cross sections from the resonance parameters and enable plotting (M. Herman & A. Trkov).
8. Some potentially empty files removed if actually empty (M. Herman).
9. run, runE, format and plot scripts modified to avoid double coding (M. Herman).
10. Processing with FIXUP split into two runs to avoid redundant data in the final ENDF file (reconstruction of 203 and 207 postponed to the second run) (M. Herman).
11. Last energy point in the gamma spectra from capture included in the file \*.out with energy of the CN excitation energy and respective cross section scaled to preserve spectrum integral.
12. Option for manual OMP fitting added to the new GUI (M. Herman).
13. PSYCHE added to the chain of utility codes (M. Herman).
14. Spectral energies for ENDF formatting printed in F10.5 instead of F9.4 format to improve accuracy (M. Herman).
15. EMPEND revised to eliminate some undesired entries in the ENDF file (A. Trkov).
16. Fission with under-barrier effects in terms of optical model for fission implemented (R. Capote, M.Herman, M. Sin, and A. Ventura).

17. Reactions on excited targets (M. Herman).
18. PostScript (and eps) files produced from within ZVV viewer are stored in the work directory with a name following standard convention (M. Herman).
19. 'mb' printed after gamma emission intensity of discrete transitions in order to be able to plot respective excitation functions directly from the EMPIRE output (\*.lst) (M. Herman).
20. 'zvpl' script for direct plotting from the EMPIRE output modified. Additional window to paste a pattern is being opened. A bit more cumbersome than before but more reliable. Before, many patterns were misunderstood due to skipping blanks in the pattern and garbage plot was produced (M. Herman).
21. Maximum number of aliases in c4sort.f increased to 200.
22. 'reaction' and 'titles' files used by X4TOC4 corrected and extended to cover proton induced reactions (still needs a consistent check) (M. Herman).
23. On-line retrieval of the EXFOR data from the remote database implemented. At the moment works only at nuclear data centers but will be extended to reading from the EXFOR CD-ROM (V. Zerkin & M. Herman).
24. Spectra for the ENDF formatting printed also for the proton induced reactions (M. Herman).
25. File 'titles' in x4toc4 modified to treat properly min and max bin energies in the emission spectra (M. Herman).
26. Correction to DEGAS regarding flux conservation (E. Betak)
27. X4TOC4 replaced with the version available from ENDVER (version 2001-8) (A. Trkov).
28. sixtab.f and dxsend.f modified to enable processing of more advanced formatting used in the recent LANL evaluations (discrete gamma's are still not processed correctly in such cases) (A. Trkov).
29. Archives directories moved from inside 'work' to 'empire' to make 'work' more manageable (change inside Xrun.tcl) (M. Herman).
30. Retrieval of EXFOR data from the relational MySQL database - opens access to the periodically updated EXFOR library issued by the IAEA-NDS on CD-ROMs (V. Zerkin, M. Herman).
31. Preequilibrium emission of clusters (Iwamoto-Harada) coded by R. Capote (PCROSS module).

32. Xrun.tcl GUI updated: selective delete, access to fission input, and generation of three piece-wise input templates (M. Herman).
33. ZVView updated to the zvv97l.exe version (V. Zerkin).
34. Spectra of recoils calculated using 'ENDF=2 prescription' instead of a rough approximation used before (M. Herman).
35. Pre-fission spectra of particles printed in \*.out for ENDF formatting (M. Herman)
36. Zerkin's GUI allowing for customized EXFOR retrieval can be started from the EMPIRE GUI (M. Herman)
37. Confirmation dialogs added to GUI for all 'delete' buttons (M. Herman)
38. CHECKR added to the chain of utility codes (M. Herman).
39. FIZCON added to the chain of utility codes (M. Herman).
40. STANEF added to the chain of utility codes (M. Herman).
41. Printing particle spectra in the \*.out output of EMPIRE rearranged so that transitions to the discrete levels are printed first with negative energies and end points of the spectra are indicated by repeating the line.
42. EMPEND adjusted to accept format of p.41 above - improves energy balance above reaction thresholds (A. Trkov).
43. Suite of gamma-strength functions from RIPL coded by Plujko and implemented by R. Capote and M. Herman.
44. Reaction/MT-number conversion table for X4TOC4 updated to include gammas in the incident channel (A. Trkov & M. Herman).
45. Ordering error in ENDF/MF12 corrected in EMPEND (A. Trkov)
46. Quasideuteron photoabsorption added by B. Carlson
47. Formating of photonuclear reactions added to EMPEND (A. Trkov)
48. X4TOC4 updated by A. Trkov.
49. Fixed energy balance in exclusive spectra by including missing gamma-ray transitions in the ENDF file (levels without branching ratio assumed to decay to the ground state) (M. Herman).
50. Scripts moved to the empire/scripts/ directory allowing for multiple working directories (M. Herman)

51. Run section in the GUI redesigned to allow for free selection of modules to run (M. Herman)
52. Comparison plots including an arbitrary ENDF-6 file possible also for spectra and double-differential cross sections (M. Herman)
53. Numerical procedure for determining experimental coupling constants, used for construction of QRPA response functions, in MSD-tristan/inelas modified in order to avoid fluctuations with incident energy (H. Wienke)
54. ECIS06 converted into subroutine by R. Capote
55. SCAT2 replaced by ECIS06 (R. Capote)
56. ENDRES updated by A. Trkov

## Changes in version 2.18 with respect to 2.17.1 (Vienna, September 2002)

1. Bug fixed in reading levels file when preparing collective levels for ECIS (R. Capote).
2. Bug fixed in reading Coulomb parameters of o.m.p. from the RIPL-2 file (affects charged particle channels) (R. Capote).
3. Relativistic correction in tl.f removed ( $\gamma=1$ ). It is not needed since SCAT2 and ECIS take care of it (R. Capote).
4. Bug in EMPEND, which caused skipping the last but one energy point fixed (A. Trkov).
5. EMPEND formats branching ratios in the ENDF file (A. Trkov).
6. xterm closes when calculations are done as it was in versions 2.17 and earlier (p.3.iii below removed) since it was inconvenient for running piece-wise and multiple calculations (M. Herman).
7. gamma-strength function uses a temperature consistent with the current level densities for the final state (not for the initial one as erroneously coded before) (M. Herman).
8. Beta version of the new GUI (Xrun.tcl) added (M. Herman).
9. Corrected renormalization of the absorption cross section in DEGAS (E. Betak).
10. Corrected way of restricting exciton configurations used in DEGAS (E. Betak).

11. Maximum number of excitons used in DEGAS set to 5 (3 configurations) (M. Herman).
12. PLOT4 updated to produce  $\gamma$ -spectra (continuum contribution from the capture reaction has not yet been included) (A. Trkov).
13. Bugs in PLOT4 fixed. PLOT4 tested on Linux with g77 and Absoft90 ver. 7.0 compilers and on Ms Windows with Lahey 75 (A. Trkov).
14. If discrete levels are inconsistent with Gilbert-Cameron level densities and LEVFIT is non-negative calculations are continued using nuclear temperature taken from the systematics. Appropriate message is printed and cumulative plot displayed (without blocking further calculations) (M. Herman).
15. Bug in empire-specific level densities at very high energies (close to 200 MeV) when level density exceeds capacity of the 32-bit word has been fixed by ignoring fit to the discrete levels (unfortunately in all nuclei) (M. Herman).
16. File Ko in tl.f is rewound to avoid messages that particular omp is not found in the local file (M. Herman).
17. Number of iterations when fitting discrete levels with Gilbert-Cameron level densities limited to 300 to avoid the possibility of infinite loop (M. Herman).
18. Z=105 name changed to 'Db'; thanks to Erik Strub for pointing it out (M. Herman).
19. Problem with the discontinuity of neutron capture cross section when incident energy becomes lower than the integration bin width has been solved. Capture cross sections, even at very low energies ( $< 10$  keV) can now be calculated even with as few as 50 energy bins (tested on  $^{193}\text{Ir}$ ) (M. Herman).
20. All collective levels are used in ECIS calculations with DIRECT=1,2, even if they can not be excited because of the too low incident energy. In the previous versions only open channels were taken into consideration and coupling to the closed ones was ignored (R. Capote).
21. Minor corrections of nuclear masses in EMPEND (avoid potentially infinite loop while the ENDF formatted file is processed by SIXTAB) (A. Trkov).
22. Thresholds for particle emission channels corrected in EMPEND (A. Trkov).
23. Discrete level library updated to the RIPL-2 version of September 24, 2002 (M. Herman).
24. LSTTAB corrected to allow for plotting spectra at  $90^\circ$  with ZVView (A. Trkov).

## Changes in version 2.17.1 with respect to 2.17 (Vienna, April 2002)

1. Bug in reading RIPL discrete levels fixed by R. Capote.
2. All scripts modified: (i) all links made symbolic to allow for using network drives, (ii) ./ added in front of calls (thus ./ is no longer needed in the PATH), (iii) xterm remains open after calculations are completed so that runtime messages can be inspected (M. Herman).
3. GUI background color changed to gray (M. Herman).
4. guizvv.tcl for graphical comparison of up to three calculations/evaluations (already present in 2.17) modified (nonstandard Tcl/Tk widget replaced) (M. Herman).

## Changes in version 2.17 with respect to 2.17beta (Vienna, February 2002)

1. Bug corrected: adding CN contribution to angular distributions for discrete levels. Gammas were added to CSAlev(.,.,0) in HFcomp.f with 0 being out of dimension. Adding of gammas is now blocked. Thanks to V. Plujko for pointing this out.
2. PLOT4 updated by A. Trkov to produce spectra (including double-differential) for outgoing protons and alphas. Structure of the PostScript files improved.
3. RIPL files placed in the empire/RIPL-2 directory following RIPL-2 structure and naming convention (compatibility with the RIPL-2 CD-ROM).
4. Optical model database updated to the preliminary RIPL-2 version.
5. EXFOR library updated to version of 18.05.2001 (NOTE: previous EXFOR database will NOT work with EMPIRE-2.17 due to a different directory structure).
6. Case specific file with extracted discrete levels (file 14) closed at the end of calculations.
7. The new script “*setup-emp*” assists installation procedure and allows to use EXFOR library and/or HFB level densities directly from the installation CD-ROM without copying them onto hard disk.



## **Changes in version 2.17beta with respect to 2.16.2 (Vienna, November 2001)**

1. Dispersive optical model potential implemented (SCAT2, ECIS, ORION3) (R. Capote)
2. Optical model database updated to the preliminary version from RIPL2 (including 4 dispersive omp) (R. Capote)
3. Discrete levels database updated to the preliminary version of RIPL2 (R. Capote)
4. Number of discrete levels constituting a complete scheme taken from the preliminary version of RIPL2 (R. Capote)
5. Elastic is calculated in all cases on the  $2.5^\circ$  grid, while all the rest are on the  $10^\circ$  grid. Previous inconsistency removed (transfer of elastic when  $\text{DIRECT} > 0$  was used) (M. Herman)
6. GUI starts with gvim editor selected by default (M. Herman)
7. Two compilation warnings in tl.f fixed (M. Herman)
8. Cumulative plots of discrete levels created as a PostScript file rather than being dumped onto the screen. The file is stored as \*cum.ps and available through GUI (M. Herman)
9. Damping of the rotational level density enhancement below BCS critical energy made consistent with the one above critical energy. Removes discontinuity at critical energy for perfectly spherical nuclei ( $\beta=0$ ) (M. Herman)
10. List of warnings available through the GUI (M. Herman)
11. Tabulated HFBCS levels densities, as provided to RIPL-2 by S. Goriely, included as additional level density option (M. Herman)

## **Changes in version 2.16.2 with respect to 2.16 (Vienna, 21 August 2001)**

1. Implementation of the HMS model completed
2. New version of V. Zerkov viewer (zvv94l.exe) provides eps format and interaction with plot titles (use A + right shift)
3. Duplicate use of file 33 removed (36 used in levdens.f)

## Changes in version 2.16 with respect to 2.15 (Vienna, July 2001)

1. EXFOR retrieval using FORTRAN instead of UNIX 'grep'.
2. Fission barrier set to 1000 MeV for  $Z < 19$ .
3. GDR second peak energy set to 0 for spherical nuclei.
4. Temperature in the generalized Lorentzian protected against 0 excitation energy.
5. Plotc4.f improved (A. Trkov) to allow for up to 23 data sets to be drawn on a single plot. Plotc4 input modified to include whole energy range.
6. Orion calculations performed up to 99% of the maximum energy loss (instead of 90% that cause problems with extrapolation to low outgoing energies).
7. Plotc4.f improved (A. Trkov) to allow for energy spectra and angular distributions plots.
8. Legend and lsttab added for future improvements but not fully implemented yet.
9. ENDF=2 option added (lumped channel representation MT=10 or 5). SO FAR DDX ARE NOT SUPPORTED BY EMPEND!!!!
10. Exact treatment of recoil spectra with ENDF=2 option.
11. Call to Monte Carlo preequilibrium model HMS coded by M.B. Chadwick. NO TRANSFER OF THE RESULTS!!!!
12. Exciton model code DEGAS implemented by P. Oblozinsky
13. Fixed bug in flux conservation when GST option selected but MSC gamma channel closed.
14. New version of SCAT2 introduced by R. Capote
15. Link to ECIS for calculation of the elastic, absorption and cross sections to discrete collective levels within rotational and vibrational CC model. Includes automatic selection of collective levels (R. Capote).
16. Link to the omp segment of RIPL introduced by R. Capote. NOTE: change in the format and name of the local file with internal omp. New name is \*omp.int and two columns are added in definition of om potentials (just before radii). RIPL potentials are stored in the file \*omp.ripl.
17. New version of V. Zerkin viewer (zvv93l.exe)

18. List of RIPL omp added to the GUI under Help menu
19. DWBA option with ECIS added by R. Capote
20. pol20, pol21 and pol22 variables in SCAT2 initialized with 0.
21. Bug fixed in ACCUMSD when MSD transitions to continuum were energetically closed (seems to have had no effect on the results).
22. Total cross section added to EXFOR retrieval, and together with fission to the MT list for ZVView plotting.
23. “zvpl” script added for plotting excitation function for any cross section from the main EMPIRE output (\*.lst).
24. “runpiecewise” script added for running up to 3 different inputs for the same case in the 3 non-overlapping energy ranges (incident energies inside and among the 3 ranges must increase monotonically).
25. Division by 0 in fitting field parameters in MSD tristan.f protected.
26. GUI modified to include 'zvpl' script and allow for merging ZVV plots.
27. Form factor for the  $l=0$  transitions in MSD controlled from the optional input (default: standard surface form factor).
28. Provision for use of combined preequilibrium models in a single run.
29. “zvcomb” script added to combine various existing ZVView plots.
30. Utility code manuals and Frequently Asked Questions (FAQ) added to the GUI under Help menu.
31. Utility code inputs accessible from the GUI Options menu.
32. Utility code c4sort added to sort \*.c4 file in ascending energy. Actually, disabled (commented) in run and runE scripts as sorting takes too long for large files.

## **Changes in version 2.15 with respect to 2.14.1 (Vienna, November 2000)**

1. Adding of plotting of double differential cross sections for neutron production using PLOT4 (modified by A. Trkov). This involves modification of EXFOR retrieval (new REAC\\_SIG.TXT file, changes in the 'sel' script and input.f), as well as modifications in the util/x4toc4/reaction file.

2. Activated printout of total and shape elastic cross sections, shape elastic angular distributions, strength functions, and scattering radius from SCAT2.
3. Minimum Tl set to 1.0E10 to avoid underflow in the calculations. This limit might be changed in line 761 of tl.f

## **Changes in version 2.14.1 with respect to 2.14 (Vienna, October 2000)**

1. Bugs fixed:
  - (a) flux conservation at very low incident energies (in HRTW),
  - (b) mismatch of elastic channels for negative parity targets (in HRTW),
  - (c) division by zero 1p0h level density in MSC gamma emission,
  - (d) undefined variables in MSC NVWY.f and MSD tristan.f defined (KASE in MSD orion.f still remains undefined, Z1 and Z2 are not problems since they are unused).
2. MATIN1 replaced by MTXINV in MSC gamma emission.
3. VMS specific statements marked with \*IF VMS in input.f and io.h
4. Print of C.M. incident energy to standard output added in main.f

## **Changes in version 2.14 with respect to 2.13 (Vienna, September 2000)**

1. Second chance preequilibrium emission applying Chadwick model to the result of the MSD.
2. Bug fixed in clearing the population of discrete levels when using ENDF option.
3. Bug fixed in writing optical model parameters for the incident channel on the ompar file.
4. SHC(2)=SHC(1) bug fixed in main.f
5. Misprint for 95Zr in data/ldp.dat(7676) fixed by setting the value to 0.
6. Removed redundant FLOAT in ORION2.
7. Collective level densities with  $a=A/\text{LEV DEN}$  used whenever  $\text{LEV DEN} \geq 2.0$

8. Star format for recoil mass replaced by fixed format.
9. Alphanumeric branching ratios in orsi.liv replaced by numbers and input.f changed appropriately (BCDNUM removed).
10. HRTW formulation of the statistical model included (width fluctuation correction).
11. Bug fixed that caused use of Weisskopf estimates for gamma strength at all incident energies except the first one.
12. Bug removed in passing GDR parameters through input.
13. Zerkin's zvd plotting capability added (through zvd script and tcl/tk GUI).
14. EXFOR entries for neutron capture coded as SIG,,AV (averaged cross sections) included in plots.

## **Changes in version 2.13 with respect to 2.12.2 (Vienna, March 2000 )**

1. General cleanup of the FORTRAN source.
2. New organization of modules that reflects physical contents.
3. Check whether MSD cross section is not larger than the fusion cross section.
4. Gamma cascade in the first CN is default if CN excitation energy is below 20 MeV and can be controlled with GCASC in optional input.
5.  $l=0$  transfer strength in MSD-orion set to the self-consistent value by default (rather than to GMR energy as before).
6. Fusion cross sections read from the file name.fus are treated as fusion cross sections at subsequent  $l$  values (starting with  $l=0$ ) rather than fusion cross sections to a given spin of CN. Transmission coefficients are calculated from the read values and a proper angular momentum and parity coupling is performed to obtain Compound Nucleus spin distribution.
7. Error removed in BCS blocking in TRISTAN.
8. BCS blocking in TRISTAN made automatic (no input required).
9. pipe.c replaced with coding by Capote.
10. Automatic retrieval of EXFOR data.
11. Link to EMPEND to create ENDF formatted file.

12. Link to X4TOC4 and PLOT4 to produce plots at the end of the run.
13. Fission barriers for  $Z > 102$  according to Myers&Swiatecki, Phys. Rev. C60 1999.
14. FITLEV creates a whole set of cumulative plots without interaction.
15. Fusion barrier can be read from input (BFUS).
16. Bass option for fusion disabled.
17. Distributed fusion barrier mode now relies on the CCFUS fusion barrier.
18. OMPAR (.omp) file with optical model parameters produced and used for input.

### **Changes in version 2.12.2 with respect to 2.12.1 (Vienna, 11 April 1999)**

1. Energy shift used to fit low-energy discrete levels gradually decreased between  $E_{cut}$  and neutron binding to recover agreement with Dobs.
2. Entire code checked with FTNCHEK and some errors corrected (undefined variables, unreferenced variables removed).
3. All DO loops given separate endings (END DO, no labels).
4. Entire code consistently indented.

### **Changes in version 2.12.1 with respect to 2.12 (Vienna, 07 Dec. 1998)**

1. Dsource directory added with explicit double precision source (no compiler -r8 option required).
2. roign.f routine replaced by roemp.f. Fits dynamic level densities (BCS approach below critical energy) to discrete levels by applying an energy shift. ATTENTION: these shifts destroy agreement with Dobs at neutron binding.

### **Changes in version 2.12 with respect to 2.11 (Vienna, 15 Sept. 1998)**

1. Error removed in the determination of pairing corrections in readnix.f (for Gilbert-Cameron).

2. Errors removed in coding of the dynamic level densities.
3. New, EMPIRE-specific systematics of level density parameter  $a$  for dynamic level densities introduced and set as default if dynamic level density chosen. This systematics fits Ilijnov-Mebel  $D_{obs}$  using EMPIRE formulae for level densities. If an experimental value for a given nucleus is present in the *ldp.dat* file, this value is adopted. The average normalization factor is calculated from these cases and applied to those for which there are no experimental data. All nuclei are treated as deformed as far as collective enhancement is concerned. Damping of the collective effects has been temporarily removed, i.e. level densities are calculated by means of an adiabatic approach.

# Index

- BCS, 27, 28, 58, 213
- C4SORT, 8, 132
- CCFUS, 13, 14, 139, 140, 209, 267, 268
- CHECKR, 9
- Coupled-Channels, 8, 13, 15, 17, 18, 37, 47, 140, 176, 184, 201, 202, 210
- distributed fusion-barrier, 14
- Doppler, 133
- DWBA, 8, 18, 24, 140, 176, 184, 200, 207, 210, 261
- ECIS, 47, 49, 140, 184, 199–201, 210, 260
- EMPEND, 8, 125, 132, 184
- ENDRES, 8
- FIXUP, 8, 132, 184
- Hauser-Feshbach, 7, 17, 18, 30, 31, 51, 69, 141, 142, 200, 201
- HFB, 134, 142, 203, 212, 213
- Hill-Wheeler, 14, 91
- HMS, 20, 43, 47, 49, 50, 145, 270
- HYBRID, 7, 47
- isomeric fission, 83, 87
- LEGEND, 8, 132, 184
- level densities, 51, 53, 55, 56, 59, 63, 64, 134, 142, 187, 195, 203, 207–209, 212–214, 258
- level density, 22, 29–31, 52, 139, 174, 195, 197, 198, 273
- LINEAR, 184
- LSTTAB, 8, 132
- MSC, 7, 21, 29–36, 47, 49, 50, 141, 145, 211, 212, 258, 269, 270
- MSD, 8, 21, 22, 24–29, 35–37, 47, 49, 50, 120, 140, 141, 145, 195, 208, 211, 258, 268
- NVWY, 7, 29, 30, 34, 35, 141
- ORION, 21, 28, 36, 140, 141, 174, 258, 268
- p-h level densities, 34, 35, 43, 46, 141, 212
- p-h level density, 34
- PCROSS, 20, 47, 49, 50, 270
- PLOT4, 9, 132, 135, 150, 190
- QRPA, 141
- RECENT, 184
- RIPL, 139, 140, 176, 183, 184, 199–202, 210, 213, 215
- RIPLomp, 199
- RPA, 26–28
- SIGMA1, 184
- SIXTAB, 8, 132, 184
- TRISTAN, 27–29, 139–141, 174, 268
- TUL, 8, 140
- X4TOC4, 8, 132, 135, 186, 187
- ZVView, 9, 132, 133, 154, 155, 188, 190, 191